ENHANCEMENT OF SPATIALLY-CONTROLLED MSC RESPONSES IN A MULTI-COMPARTMENT CG SCAFFOLD FOR TENDON-BONE JUNCTION REGENERATION

BY

WILLIAM KANE GRIER

DISSERTATION

Submitted in partial fulfillment of the requirements
for the degree of Doctor of Philosophy in Chemical Engineering
in the Graduate College of the
University of Illinois at Urbana-Champaign, 2017

Urbana, Illinois

Doctoral Committee:

Associate Professor Brendan Harley, Chair
Associate Professor Marni Boppart
Associate Professor Mary Kraft
Associate Professor Charles Schroeder

ABSTRACT

There have been many advancements in the field of tissue engineering for the repair or regeneration of single tissues. However, orthopedic injuries often occur at the interface between soft tissues and bone. The tendon-bone junction (TBJ) is a classic example of such an interface, containing overlapping patterns of growth factors, extracellular matrix (ECM) proteins and structure, and mineral content that serve to dissipate stress concentrations and effectively transfer force between contracting muscles and bone for locomotion. Current clinical strategies to treat common TBJ injuries, such as in the rotator cuff, prioritize mechanical reattachment, forsaking biological reintegration and recapitulation of the native structure. As a result, TBJ repairs are plagued by high failure rates, and new tissue engineering solutions are necessary for improved patient outcomes. Modern efforts in tissue engineering have focused on the design of new instructive biomaterials that present combinations of compositional, microstructural, mechanical, and biochemical cues, with the potential to control stem cell fate decisions and promote enhanced tissue regeneration. This thesis describes a series of studies undertaken to better comprehend the impact of biomaterial cues and mechanical stimulation on cell bioactivity and the application of this knowledge to the design of spatially-graded biomaterials and culture techniques for engineering the TBJ. The studies herein utilize collagen-glycosaminoglycan (CG) scaffolds, a set of regulatory compliant analogs of the native ECM that have been previously applied to the regeneration of dermis, peripheral nerves, and osteochondral tissues. Here, we show how scaffold microstructure and mechanical properties are critical regulators of the maintenance of tenocyte phenotype and bioactivity in *in vitro* culture. We also describe the design and fabrication of a custom cyclic tensile strain (CTS) bioreactor system for the examination of the effects of mechanical stimulation on cell-material interactions and stem cell differentiation for tendon

regeneration. The knowledge gained in this study was then applied to a spatially graded scaffold to selectively bias stem cell differentiation for TBJ applications. These results represent the first application of CTS across a spatially graded material with variations in microstructural alignment, mineral content, and mechanical properties. Finally, we adapt the CG scaffold system to selectively sequester and display growth factor content through the promotion of guest-host interactions. The growth factors presented by the scaffolds are sufficient to drive enhanced stem cell responses. Together, these studies present the framework for designing instructive biomaterials to regulate stem cell fate in a spatially-dependent manner in the context of musculoskeletal interface repair.

To my wife and family, for their unending support.

Also, to Mrs. Wichers, my high school biology teacher, who's mentorship and guidance fostered my early appreciation for science and research.

ACKNOWLEDGMENTS

This thesis would not have been possible without the contributions and support of many friends, family, and colleagues. First, I would like to acknowledge all of the individuals who contributed directly to the research that is covered in this thesis: Professor Steven Caliari, who was an incredible mentor during my first year of study and who spearheaded the initial work to develop the multi-compartment scaffolds for TBJ repair, Martins Iyoha (Chapter 2), Ashley Moy (Chapter 3), Jordan Meyer (Chapter 4), Michael Foley (Chapters 4-5), and Matthew Ramsey (Chapters 4-5). Many others also contributed to this work: Professors Matt and Allison Stewart provided tendon cells, Dr. Sandra McMasters prepared media, Drs. Scott Robinson and Cate Wallace assisted with critical point drying and electron microscopy, and Professor Marni Boppart and Dr. Koyal Garg and Ziad Mahmassani generously shared their laboratory's equipment and expertise with mouse models and muscle development that will be a focus of future work.

I would also like to thank all of my lab mates for their support and assistance over the last five years. Rebecca, Dan, Jackie, and Laura all shared office space with me for most of my time here, and were great to bounce ideas off and helped to make things light. Also, Sunny, Bhushan, Sara, Seema, Emily, Mai, Aidan, Raul, Alec, and Marley, and everyone else who has passed through the lab over the last five years.

I've also been fortunate to interact with some incredible faculty and staff here at the University of Illinois. Professors Wilfred van der Donk and Paul Hergenrother and Nan Holda and Sam Tarter were great mentors during my time in the CBI training program. Thank you to Christy Bowser, Cathy Paceley, Kay Moran, Jadii Rogers, and Maggie Metzger Chappell for always helping with paperwork and reimbursements. Professors Deborah Leckband and Joon Kong for allowing me to spend time rotating through their labs during my first few months. Professors Jon Higdon, Dave

Flaherty, and Charles Sing for always being available for discussion. I'd especially like to thank my thesis committee: Professors Marni Boppart, Mary Kraft, Charles Schroeder, and my advisor Brendan Harley. When I came to Illinois five years ago I had some idea of what I wanted to pursue, but I can honestly say that I couldn't imagine things working out any better than they did, and that is in large part due to the people I've been fortunate enough to interact with since I came here.

The work described here was funded by the Chemistry-Biology Interface Training Program NIH T32GM070421, National Institute of Arthritis and Musculoskeletal and Skin Diseases of the National Institutes of Health under Award Numbers R03 AR062811 and R21 AR063331, the National Science Foundation (NSF) Science and Technology Center Emergent Behavior of Integrated Cellular Systems (EBICS) Grant CBET-0939511. Additional support was provided by the Chemical and Biomolecular Engineering Dept., the Imaging Technology Group within the Beckman Institute for Advanced Science and Technology, and the Carl R. Woese Institute for Genomic Biology (BACH) at the University of Illinois at Urbana-Champaign.

Finally, I am grateful and blessed to have an unbelievable group of family and friends who have stayed by my side throughout this journey. I would like to thank my Mom, Dad, and my sister Annie for their support. Lastly, I would especially like to recognize my new wife, Jill, who has always been there and put up with weekly four hours commutes and weekend visits over the last five years. Your continued love, patience, and support has been key to help me get through this journey. I love you.

TABLE OF CONTENTS

SYMBOLS AND ABBREVIATIONS

Abbreviation	Term, Definition
ACAN	Aggrecan
ACL	Anterior cruciate ligament
ALP	Alkaline phosphatase
ANOVA	Analysis of variance
ASC	Adipose-derived stem cell
BMP-x	Bone morphogenetic protein; relevant isoforms include BMP-2 and BMP-7
BSA	Bovine serum albumin
BSP	Bone sialoprotein
CaP	Calcium phosphate
cDNA	Complementary DNA (deoxyribonucleic acid)
CG	Collagen-glycosaminoglycan co-precipitate
CGCaP	Collagen-glycosaminoglycan-calcium phosphate triple co-precipitate
CGCyclo	Collagen-glycosaminoglycan with β-cyclodextrin co-precipitate
COL1A1	Collagen I alpha 1
COL3A1	Collagen III alpha 1
COMP	Cartilage oligomeric matrix protein
COOH	Carboxyl group
DCN	Decorin
DHT	Dehydrothermal crosslinking
DMEM	Dulbecco's modified Eagle's media
DNA	Deoxyribonucleic acid
ECM	Extracellular matrix
E_s	Elastic modulus of individual scaffold strut
E^*	Elastic modulus of the entire cellular material
E_sI	Scaffold strut flexural rigidity
ε	Tensile strain
EDC	1-Ethyl-3-(3-dimethylaminopropyl) carbodiimide hydrochloride
EDTA	Ethylenediaminetetraacetic acid
ERK 1/2	Extracellular signal-related protein kinase
FBS	Fetal bovine serum
FGF	Fibroblast growth factor
GAGs	Glycosaminoglycans
GAPDH	Glyceraldehyde 3-phosphate dehydrogenase; used as housekeeping gene
GDF-x	Growth/differentiation factor; relevant isoforms include GDF-5, 6, and 7
MAPK	Mitogen-activated protein kinase
MCL	Medial cruciate ligament
MKX	Mohawk; a transcription factor highly expressed in mature tendon
MMP	Matrix metalloproteinase
MRI	Magnetic resonance imaging
MSC	Mesenchymal stem cell or marrow stromal cell
NHS	N-hydroxysulfosuccinimide

OC	Osteocalcin
OP	Osteopontin; late marker of bone formation
PBS	Phosphate-buffered saline
PCR	Polymerase chain reaction
PDGF-BB	Platelet-derived growth factor-BB
PDMS	Poly(dimethylsiloxane)
PTFE	Poly(tetrafluoroethylene)
$\rho^*/\rho_{s\rho}$	Scaffold relative density
RhoA	Ras homolog gene family, member A
RIPA	Radio immunoprecipitation assay
RNA	Ribonucleic acid
ROCK	Rho-associated protein kinase
RUNX2	Runt-related transcription factor 2
SCXB	Scleraxis; a transcription factor highly expressed in tendon
SE	Secondary electron
SEM	Scanning electron microscopy
SIS	Small intestine submucosa
SMAD	Portmanteau of SMA and MAD (mothers against decapentaplegic) genes
SOX9	Sry-related homeobox gene 9; transcription factor involved in chondrogenesis
TBJ	Tendon-bone junction
TC	Tendon cell
$\mathbf{T_f}$	Freezing Temperature
TGF-βx	Transforming growth factor-βx; relevant isoforms include TGF-β1, TGF-β2, and TGF-β3
TNC	Tenascin-C

CHAPTER 1: INTRODUCTION AND BACKGROUND: BIOMATERIAL STRATEGIES TO ENGINEER MULTI-TISSUE JUNCTIONS AND REGULATE STEM CELL FATE[1]

1.1 Thesis overview

This chapter will introduce the concept of biomaterials as regenerative templates for tissue engineering applications and review the latest work in the field of tendon-bone junction (TBJ) engineering and stem cell fate regulation through the controlled presentation of material and biological cues. The remainder of the thesis will focus on the development of a collagen-GAG (CG) scaffold material system for TBJ engineering, including the influences of local scaffold microstructure, supplemental mechanical stimulation, and biomolecule presentation on spatially-defined lineage specification of mesenchymal stem cells (MSCs). Some of the materials used in this thesis were initially developed as part of separate projects, including a geometrically anisotropic CG scaffold that mimics the microstructure of native tendon (Caliari and Harley 2011) as well as a multi-compartment CG scaffold with distinct, but continuous, regions of structural anisotropy and mineral content as seen in the native TBJ (Caliari, Weisgerber et al. 2015). For more information of these fundamental studies, please reference the cited manuscripts.

In this thesis, Chapter 2 will describe the influence of scaffold pore structure, as determined by freezing temperature, and scaffold stiffness, as a function of covalent crosslinking density, on the maintenance of a tendon phenotype in equine tenocytes. Chapter 3 introduces the design and use of a custom cyclic tensile strain (CTS) bioreactor system to promote the robust tenogenic differentiation of human MSCs on aligned CG scaffolds. Chapter 4 expands on the use of the bioreactor system to evaluate the effects of CTS on multi-compartment CG scaffolds designed for

[1] This chapter has been adapted from the following publication:
Grier, W.K. and B. A. C. Harley (in preparation). "Biomaterial strategies to engineer multi-tissue junctions and regulate stem cell fate."

TBJ regeneration and the resultant compartment-specifics effects of mechanical stimulation on MSC differentiation. Chapter 5 explores the next generation of instructive biomaterials, incorporating β-cyclodextrin into CG scaffolds, as a means to sequester and control the presentation of selected growth factors, for the preferential differentiation of MSCs. Finally, Chapter 6 will then conclude this thesis with a summary of the findings and recommendations for ongoing and future work.

1.2 Chapter overview

To date, the bulk of tissue engineering research has focused on the repair of individual tissues. This has led to many advances in the field, with a number of products being successfully introduced into clinical settings. Despite these advances, many orthopedic injuries often occur at tissue interfaces, such as the tendon-bone junction. The nature of these interfacial tissues motivates new approaches to expand current, regenerative strategies to address unique challenges associated with such multi-tissue structures. The current clinical approaches to repair these interfaces are generally inadequate and prioritize simple surgical reattachment over biological reintegration of the tissues. As a result, the intricate patterns of extracellular matrix structure and composition at these interfaces are rarely recapitulated, leading to a loss of function. In this review, we will highlight emerging technologies to develop spatially stratified biomaterials for the regulation of stem cell fate for the regeneration of complex multi-tissue structures. We will first introduce the unique challenges inherent in engineering the interface between tendon and bone and the regulation of stem cell fate in a spatially-dependent manner. We will summarize the current strategies available for the development of spatially-stratified biomaterial systems for multi-tissue repair applications. We will then review approaches to leverage the applications of mechanical stimulation and biochemical supplementation in cell culture, specifically for the regeneration of

the tendon-bone junction. Lastly, we will conclude with a perspective on how to potentially integrate the knowledge gleaned from new understandings of native tissue development for the design of next-generation tissue engineering systems.

1.3 Introduction

The fields of tissue engineering and regenerative medicine have seen major advancements over the last 25 years (Langer and Vacanti 1993). Early biomaterial systems focused on passive materials which permitted and supported biological responses. Normally, the adult wound healing process results in the formation of hypertrophic scar tissue that is characterized by a disorganized, mechanically-inferior extracellular matrix (ECM) and general loss of function (Rhett, Ghatnekar et al. 2008). Evidence has shown that the use of biomaterials to aid in wound healing can fundamentally alter this process. Materials specifically designed to block the initial wound contraction have already been successfully introduced into the clinic for dermal and peripheral nerve applications (Yannas, Lee et al. 1989; Soller, Tzeranis et al. 2012). By blocking the initial contraction of the wound site and providing a base material to support new tissue growth, these biomaterials can promote the enhanced regeneration of the natural tissue over simple wound closure.

More recently, there has been an increased focus on the development of instructive biomaterials that have the ability to facilitate and guide tissue repair or regeneration through microstructural, mechanical, and biochemical means. Cells naturally exist within locally-defined regions of ECM which display complex and tissue-specific properties. All tissues display a unique combination of characteristics based on their composition, microstructural organization, mechanical properties, and biomolecule content/availability. It has been shown that these local cues are critical to promote early tissue development and regeneration *in vivo* (Blitz, Viukov et al. 2009; Pryce, Watson et al.

2009; Schweitzer, Zelzer et al. 2010), and that mechanical cues, such as substrate stiffness, are sufficient to control MSC differentiation *in vitro* (Engler, Bacakova et al. 2004; Allen, Cooke et al. 2012). The incorporation of these instructive cues that are specific to the tissue of interest is a critical component of new biomaterial systems.

While designing materials for the regeneration of a single tissue type is already a daunting task, many injuries occur at the interface between two dissimilar tissue types, particularly in orthopedics. These multi-tissue structures commonly contain distinct regions or specific architectural, mechanical, and compositional cues that, together, are critical in order to maintain tissue and organ integrity and function. Therefore, any biomaterial strategy to regenerate these multi-tissue structures must at least be able to incorporate the prominent features of these disparate tissues.

This review will focus on the development of biomaterial systems and supplementation strategies specifically for the regeneration of tendon-bone, or osteotendinous, junctions (TBJ). While a number of reviews have focused on material systems to engineer orthopedic interfaces (Lu and Thomopoulos 2013; Lee, Robinson et al. 2016), or specific strategies to regenerate either tendon (Voleti, Buckley et al. 2012) or bone (Porter, Ruckh et al. 2009), this review will serve as a bridge between those two communities while focusing on applications for osteotendinous repair. This review will begin with an overview of the tendon-bone junction organization and biology in an effort to understand critical components to be considered for biomaterial design. It will continue with a discussion of the various biomaterial strategies that have recently been employed in this field. We will then discuss various mechanical stimulation and biochemical supplementation strategies to control stem cell differentiation and tissue development. Finally, we will conclude

with a perspective on how the combination of biomaterial design, stem cell biology, and external factors can be used to pursue optimal regenerative strategies for the TBJ moving forward.

1.4 Tendon-bone junction organization and biology

The tendon joins muscle to bone, allowing for force generated in muscle fibers to be translated into motion (Wang 2006). Tendons are hierarchical, and mechanically and geometrically anisotropic tissues composed primarily of type I collagen fiber bundles. These fiber bundles show a characteristic crimp pattern that helps the tissue adapt to normal loading. Collagen fiber bundles are bound together by the endotenon, which in turn is integrated with the peritenon, surrounding the whole tissue (Gross and Hoffmann 2013). The peritenon is composed of an inner layer called the epitenon and an outer layer called the paratenon. Some tendons, especially in the hands and feet, are enclosed by synovial sheaths to enable smooth gliding during movement (Gross and Hoffmann 2013). Tendons can be up to an order of magnitude stiffer in the plane longitudinal to collagen fiber alignment compared to the transverse plane (Quapp and Weiss 1998). Tendon tissue is 70% water, with collagen comprising 75-85% of the dry weight, of which 95% is type I with the remainder being types III and V (Wang 2006). Elastin composes less than 3% of the tendon tissue and proteoglycans constitute about 2%, although this amount varies widely and is typically higher in tendons that must withstand significant compressive stress (Martin, Burr et al. 1998). Type III collagen is typically localized to the endotenon and epitenon, although it can also appear in mechanically dynamic regions such as the supraspinatus (Duance, Restall et al. 1977). Tendons are populated primarily by fibroblastic cells, called tenocytes, which are interspersed throughout the collagen fibers in the tissue (James, Kesturu et al. 2008).

The junction between tendon and bone, or the enthesis, is where the tendon inserts into subchondral bone through a fibrocartilage insertion region. This tissue interface is structurally continuous but

consists of compositionally and microstructurally distinct regions of tendon, non-mineralized fibrocartilage, mineralized fibrocartilage, and bone (Blevins, Djurasovic et al. 1997; Genin, Kent et al. 2009; Genin and Thomopoulos 2017). The transition zone between tendon and bone tissues is fairly well conserved between different joints and generally span a total distance between 250-800 μm, with approximately half of that span consisting of calcified fibrocartilage (Lee, Robinson et al. 2016). The TBJ is an emerging tissue engineering target as injuries frequently occur right at this interface due to the high stress concentrations that develop between the two mechanically mismatched tissues (Saadat, Deymier et al. 2016). Rotator cuff injuries for example, account for more than 4.5 million physician visits and 250,000 repair surgeries each year in the United States (Galatz, Sandell et al. 2006; Colvin, Egorova et al. 2012). These rotator cuff injuries commonly present at the supraspinatus-humerus junction. Current clinical repair strategies typically involve mechanical fixation of tendon to the bone, but tendon detachment remains a primary cause for surgical failure. Rotator cuff repairs generally fail at a rate of 27% within 2 years of surgery with rates as high as 94% in older demographics (Lorbach, Baums et al. 2015). Poor surgical outcomes are attributed to the very poor innate healing response and general inability to recapitulate the native complexities of the interface (Lorbach, Baums et al. 2015).

In order to facilitate the design of adequate solutions for regeneration of the tendon enthesis, many groups have looked to inspiration from the embryonic development of the tendon (Okech and Kuo 2016). In vertebrates, the tendon enthesis begins to develop when a subset of mesenchymal cells amass and begin to form a cartilaginous template for the future bone. However, unlike primary cartilage, where progenitor cells only express *SOX9*, the progenitor cells at the sites of the tendon enthesis co-express *SOX9* and the tendon marker scleraxis (*SCX*) (Blitz, Sharir et al. 2013). SCX is a transcription factor that is highly expressed throughout both progenitor and mature tendinous

tissues and is known to regulate differentiation (Schweitzer, Chyung et al. 2001). Currently, there are two lines of thought how the final connection between bone, fibrocartilage, and tendon is formed. The connection may form following differentiation, which would require signaling to direct the tendon to the correct insertion site, or the tissues may be derived from a common pool of progenitors that undergo divergent differentiation (Zelzer, Blitz et al. 2014). The use of a common pool of progenitors, in combination with directed differentiation, is attractive for tissue engineering applications as it would require just a single cell isolation to regenerate this spatially-defined tissue structure. A single cell source would also reduce the number of specific cell isolations required and associated donor site morbidity, as well as issues associated with the difficulty of culturing and maintaining terminally-differentiated primary cells, like tenocytes, *in vitro* (Yao, Bestwick et al. 2006).

The maturation of the TBJ is primarily regulated by a combination of TGF-β and BMP-4 signaling (Blitz, Sharir et al. 2013). Ablation of the TGF-β type II receptor in mouse embryos results in the complete loss of all tendon tissue (Pryce, Watson et al. 2009) and is suggested to regulate the development of both cartilage and bone in limb development (Lorda-Diez, Montero et al. 2009). As the tendon matures, a gradient of mineral gradually moves into the developing transition zone of the TBJ and begins to mineralize the fibrocartilaginous progenitors, through a process known as endochondral ossification (Schwartz, Pasteris et al. 2012). Mechanical loading is also known to play an important role in TBJ development. Once the tendon is sufficiently anchored into the bone, muscle forces can be transmitted across the interface and have been linked to the regulation of growth and mineralization (Thomopoulos, Kim et al. 2007; Schwartz, Lipner et al. 2013; Song, Jiang et al. 2017). Altogether, the combination of cells, local microstructural cues, biochemical

signals, and mechanical force are crucial for the development of the TBJ, and these relationships must be taken into consideration when designing regenerative medicine solutions.

1.5 Technologies for fabricating multi-phase biomaterials

The majority of materials designed for TBJ regeneration fall into two categories, stratified scaffolds with distinct regions of specific biomimetic cues and gradient materials that are able to recapture some of the organization of native transitional zones (Lee, Robinson et al. 2016).

An attractive method to try and mimic the natural biomimetic cues of the TBJ is to use spatially stratified materials with regions of distinct characteristics. One of the first stratified constructs designed specifically for tendon-bone regenerations, Xie *et al*. fabricated PLGA nanofiber scaffolds with discrete areas of randomly distributed and highly aligned fibers (Xie, Li et al. 2010). Mechanical testing showed significantly higher tensile modulus and ultimate stress in mats composed of the aligned fibers compared to randomly oriented fibers. When seeded with tendon fibroblasts, the aligned region of the scaffolds promoted increased cell elongation and alignment and upregulated expression of collagen type I. Font Tellado *et al*. has recently produced a silk fibroin scaffold with separate regions of aligned and isotropic porosity which were suitable to induce spatial patterns in tenogenic and chondrogenic gene expression (Font Tellado, Bonani et al. 2017). Dickerson *et al*. produced a biphasic scaffold by demineralizing a portion of a cancellous bone explant (Dickerson, Misk et al. 2013). When implanted into an ovine rotator cuff wound model, the groups treated with scaffolds showed better tissue integration and histological evidence of a preliminary fibrocartilaginous interface development when compared to standard suture repair. Our lab has also previously developed a bi-phasic collagen-GAG scaffold with distinct, but continuous, regions of microstructural alignment and mineral content by combining a directional solidification approach with liquid-phase co-synthesis (Caliari, Weisgerber et al. 2015).

Another class of biomaterials developed for the tendon-bone junction repair are those containing explicit gradient properties. Phillips *et al*. produced collagen scaffolds with a gradient of retroviral vectors encoding the osteogenic transcription factor *RUNX2* (Phillips, Burns et al. 2008). Primary fibroblasts seeded onto the materials showed a graded response with regards to osteogenic differentiation and mineral deposition. There have also been a number of studies on materials with gradients of mineral content. Li *et al*. produced a gradient of calcium phosphate on an electrospun PLGA mats. This gradient of mineral content resulted in spatially-graded stiffening of the material and variations in the adhesion and proliferation of murine preosteoblast cells (Li, Xie et al. 2009). Similar scaffold materials were later used by Lipner *et al*. and implanted into a rat rotator cuff model along with adipose-derived stem cells that had been engineered to overexpress BMP-2 (Lipner, Liu et al. 2014; Lipner, Shen et al. 2015). In this case, it was noted that the scaffold alone, and groups seeded with cells, resulted in delayed healing and inferior mechanical properties when compared to standard suture repair. Zou *et al*. developed a similar electrospun scaffold composed of poly(DL-lactide) with gradients of hydroxyapatite and plasmid DNA which resulted in gradients of cellular proliferation, osteogenic differentiation, and collagen deposition (Zou, Liu et al. 2012). Recently, Liu *et al*. used an ultrasound treatment to develop decellularized tendon matrix scaffolds with gradients in structural alignment for a ligament-to-bone junction application (Liu, Yang et al.). These scaffolds demonstrated increased chondrogenic and osteogenic differentiation of MSCs on the randomly-oriented regions of the scaffold and improved bone and fibrocartilage formation at the interface in an *in vivo* model.

These studies have demonstrated that biomaterials that mimic the natural characteristics of the TBJ with spatially distributed mineral content, composition, and microstructural alignment are crucial for the reestablishment of the fibrocartilaginous interface. Most of this previous work has focused

on the development of gradients of biomimicry of a single factor (i.e mineralization or anisotropy). This presents an emerging need to develop multi-functional biomaterial strategies which resemble the compositional and structural heterogeneity that makes up the native TBJ.

1.6 Targeted mechanical stimulation for tendon-bone junction engineering

As previously discussed in section 1.4, biomechanical loading is a crucial factor during the development and maturation of the tendon and enthesis (Thomopoulos, Kim et al. 2007; Killian, Cavinatto et al. 2012; Schwartz, Lipner et al. 2013; Song, Jiang et al. 2017). Additionally, variations in tension and compressive loading paradigms have been shown to play a role in the differentiation of MSCs towards a fibrocartilage or tendon-like phenotype (Connelly, Vanderploeg et al. 2010; Thomopoulos, Das et al. 2011). Thus, it will be critical to design mechanical loading paradigms and systems to impart physiologically relevant loads onto materials for TBJ regeneration. This would potentially include applications and materials which experience spatially graded strain profiles as are normally seen in mechanically mismatched tissues like orthopedic interfaces.

Early work evaluating the effect of tensile strain on tendon regeneration was performed in 2D systems, such as the Tissue Train culture plate in conjuction with the Flexcell Loading Station (Flexcell international, Hillsborough, NC). In these systems, a vacuum is used to stretch a flexible membrane over a loading post, exposing any cells or materials on the membrane to tensile strain. Kuo *et al*. seeded MSCs into a collagen gel on a Flexcell membrane to show that cyclic stretching at 1 Hz and 1% elongation for 30 minutes per day was required to maintain the expression of the tendon-marker *SCX* over the course of a 7 day study (Kuo and Tuan 2008). More recent work has involved the use of custom bioreactor systems to impart a defined tensile strain onto 3D biomaterials. These systems generally consist of either loading posts, which string-like materials

can be tied to (Qiu, Lei et al. 2014) or clamps to grip the ends of the biomaterial (Burk, Plenge et al. 2016).

While the systems mentioned above have been used successfully to demonstrate that MSCs can differentiate towards a fibroblast or tendon-like state on a variety of compatible materials, such as electrospun mats (Xu, Wang et al. 2015), decellularized tendon matrix (Burk, Plenge et al. 2016) or collagen fiber bundles (Qiu, Lei et al. 2014), there has been a demonstrated need to develop systems to apply strain to alternative materials such as porous scaffolds or hydrogels, which are not amenable to these attachment methods. In order to address this issue, Doroski *et al*. and Connelly *et al*. developed a system in which fibrin gels could be formed between two solid end blocks, which could be hooked onto loading posts within a bioreactor system (Connelly, Vanderploeg et al. 2010; Doroski, Levenston et al. 2010). Paxton *et al* used a similar method by forming a fibrin gel between two brushite anchors in order to optimize loading paradigms designed to promote increased collagen production (Paxton, Hagerty et al. 2012). We have also recently expanded on this method by embedding the ends of porous collagen-GAG scaffolds into hollow end blocks (Grier, Moy et al. 2017).

Cells sense various mechanical stimuli via a network of mechanotransduction pathways. These pathways, activated through microstructural cues and applied mechanical stimulation, can influence stem cell activation and differentiation. Substrate alignment and stiffness have been shown to activate canonical RhoA/ROCK1 and FAK pathways to promote MSC differentiation towards musculoskeletal lineages (Sarasa-Renedo, Tunç-Civelek et al. 2006; Xu, Song et al. 2011; Allen, Cooke et al. 2012; Xu, Song et al. 2012; Andalib, Lee et al. 2013; Kanazawa, Furumatsu et al. 2014). The application of cyclic tensile strain can also promote the phosphorylation of ERK 1/2 via RhoA activation (Laboureau, Dubertret et al. 2004), and the upregulation of procollagen

mRNA (Papakrivopoulou, Lindahl et al. 2004). As a result, some studies have focused on identifying strain profiles to prolong ERK 1/2 activation to promote cell-mediated ECM biosynthesis (Paxton, Hagerty et al. 2012). The p38 mitogen-activated protein kinase pathway is known to inhibit ERK 1/2 activation (Papakrivopoulou, Lindahl et al. 2004; Weinbaum, Schmidt et al. 2013), suggesting an alternate target for promoting ECM biosynthesis. A better understanding of how mechanical stimulation and resultant mechanotransduction signaling affect stem cell differentiation would help to identify more robust tissue engineering culture systems.

One thing that must be noted is that the overwhelming majority of published work has been limited to the application of cyclic tensile strain for the development of just tendon or fibroblastic tissues (Govoni, Muscari et al. 2016). Despite evidence that loading is crucial for the development and healing the of TBJ (Thomopoulos, Kim et al. 2007; Schwartz, Lipner et al. 2013; Song, Jiang et al. 2017), there has yet to be any comprehensive study on the application of loading on spatially-graded materials designed for TBJ applications.

1.7 Biochemical strategies for tendon-bone junction engineering

Another key area to consider for tendon enthesis regeneration is the use of biologics, such as growth factors, that are known to play a role during tissue development. The primary growth factors involved in tendon and enthesis development interact with cells via TGF-β signaling (Pryce, Watson et al. 2009). There are two main sub-groups within the TGF-β superfamily, the TGF-β and bone morphogenic protein (BMP) subfamilies, which activate the Smad 2/3 and Smad 1/5/8 intracellular pathways, respectively. In general, BMP signaling and Smad 1/5/8 activation is associated with osteogenic differentiation while TGF-β signaling, and Smad 2/3 activation is associated with the development of connective tissues, such as tendon, ligament, and cartilage (Towler and Gelberman 2006; Maeda, Sakabe et al. 2011; Shen, Gelberman et al. 2013). Smad 3

has been shown to interact directly with the transcription factor *SCX* and regulate tendon matrix organization (Berthet, Chen et al. 2013). However, BMP-12, BMP-13, and BMP-14 (also known as GDF-7, GDF-6, and GDF-5, respectively) are also shown to be expressed in developing tendons and ligaments and have been used to promote tendon healing (Wolfman, Hattersley et al. 1997; Shen, Gelberman et al. 2013). While critical for development of the tendon enthesis, TGF-β treatment for tendon repair has generally been unsuccessful, leading to increased collagen production, but also fibrosis and scar formation (Beredjiklian, Favata et al. 2003).

In addition to TGF-β, there are several other growth factors that have demonstrated efficacy, particularly in tendon healing. Basic fibroblast growth factor (bFGF) and platelet-derived growth factor-BB (PDGF-BB) have been used to promote accelerated wound closure and matrix synthesis (Chan, Chan et al. 1997; Thomopoulos, Das et al. 2010). Fibrin gels designed for the sustained release of active bFGF were used in a canine model to promote neovascularization and cell proliferation but failed to produce improvements in functional or mechanical properties. Instead, the increased cellular activity resulted in increased scar formation and reduced range of motion (Thomopoulos, Kim et al. 2010). In a comparable manner to the bFGF work, fibrin or heparin-based delivery systems of PDGF-BB were able to improve collagen remodeling and cell proliferation but also resulted in improved range of motion (Thomopoulos, Zaegel et al. 2007; Thomopoulos, Das et al. 2009; Manning, Schwartz et al. 2013). More recently, the use of connective tissue growth factor (CTGF) has shown promising results in the ability to induce tenogenic, fibroblastic, and chondrogenic differentiation of MSCs (Fukunaga, Yamashiro et al. 2003; Lee, Shah et al. 2010; Liu, Tao et al. 2015). In a similar manner to BMP-12, CTGF increased the expression of tenocyte lineage markers, like *SCX*, *in vitro* (Liu, Tao et al. 2015).

A few select studies have examined the patterned display of growth factors to control cellular responses in a spatially-dependent manner. Inkjet printing has been used to establish gradients of BMP-2 and FGF onto 2D fibrin surfaces to preferentially drive osteogenic differentiation of C2C12 myogenic precursor cells (Miller, Phillippi et al. 2009). Ker *et al*. has investigated a similar method to print FGF and BMP-2 onto both fibrin-coated substrates and polymer fiber mats, showing spatially localized differentiation of C2C12 cells with myogenic differentiation on unprinted regions and tenogenic and osteogenic differentiation in regions patterned with FGF and BMP-2, respectively (Baselga, Rothenberg et al. 2008; Ker, Chu et al. 2011; Ker, Nain et al. 2011). Benzophenone photochemistry has also been used to selectively pattern CG substrates of varying stiffness with BMP-2 and PDGF-BB to regulate adipose-derived stem cell bioactivity and, proliferations, and gene expression (Banks, Mozdzen et al. 2014).

In addition to growth factors, some groups have started to use materials derived from native tendon to provide many of the innate cues for enthesis development (Schulze-Tanzil, Al-Sadi et al. 2012). The deceulluarized tendon matrix matches the biomechanical and structural properties of the native tendon and can include growth factors entrapped within the ECM (Hoganson, O'Doherty et al. 2010). Zhang *et al*. used a decellularized tendon matrix coating on tissue culture plastic to promote the maintenance of tendon stem cells *in vitro* and then implanted a tendon stem cell and matrix composite into rat models where the combination led to increased tendon-like tissue formation (Zhang, Li et al. 2011). ECM derived from tendon tissue was also shown to induce TGF-β dependent differentiation of adipose-derived stem cells (Yang, Rothrauff et al. 2016). When looking across the full TBJ, Schulze-Tanzil *et al.* implanted a decellularized tendon-bone graft into a rat model and found that animals treated with the composite graft showed increased mechanical properties with a more organized matrix structure after 12 weeks (Farnebo, Woon et al. 2014).

While the use of native EMC can provide many of the necessary cues to influence stem cells and regenerate these complex tissues, decellularized tissues face many obstacles in reaching the clinic. It can be difficult to adequately characterize explants and ensure uniformity from one graft to the next. Additionally, there are always limitations based on limited donor availability and potential disease transmission or immunogenic responses. Thus, ideal tissue engineering solutions should be fabricated from commercially available materials.

1.8 Overall summary and future perspective

The fields of tissue engineering and regenerative medicine have grown substantially over the last two decades. Current research has expanded to focus on the design of spatially organized materials to regenerate complex multi-tissue structures, like the tendon-bone junction and other common injury sites in orthopedics. In parallel, a great amount of work has focused on the fundamental understanding of the microstructural, mechanical, and biochemical cues that drive stem cell differentiation, looking to developmental biology as a guide. Moving forward, the integration of these two areas of study is likely to yield new breakthroughs in clinical applications to repair tissues.

Many of the materials outlined in this review have focused on spatial distributions of singular components of the native TBJ, primarily mineral content or structural alignment. Additionally, gradient materials have only been developed at non-physiological scales on the order of centimeters, while the native enthesis is normally less than 1 millimeter in length (Lee, Robinson et al. 2016). Disparate spatially-stratified materials may appear to mimic the overall scale of the TBJ, but the hard interfaces used in their fabrication can lead to issues, such as excess shear and inadequate transport and cellular crosstalk at the interface. The use of decellularized tissues, that match the native structure, overcomes many of these issues; however, there remains complications

due to donor availability and potential host immune response. The previous work from our lab (Caliari, Weisgerber et al. 2015), along with the work presented here, aims to address this need by the fabrication of a continuous natural ECM material with distinct regions of structural anisotropy and mineral content.

In addition to heterogenous material systems, a variety of supplemental factors, such as mechanical stimulation or growth factor supplementation have been shown to play crucial roles in the regeneration of the tendon enthesis. However, for the most part their use has so far been limited to singular applications of growth factor supplementation or mechanical stimulation. Comprehensive studies of the combined influence of growth factors with mechanical stimulation and the combined influence of material properties are still lacking, despite evidence of the importance of these interactions in musculoskeletal development (Mei, Nguyen et al. 2013; Rys, Monteiro et al. 2016).

To conclude, the future of multi-tissue engineering is exciting. Substantial advancements have been made in the development of intricate material systems and supplementation strategies to regulate stem cell fate. This provides realistic opportunities for multi-disciplinary approaches to leverage combinatorial products for the improved repair and regeneration of complex orthopedic interfaces.

CHAPTER 2: THE INFLUENCE OF PORE SIZE AND STIFFNESS ON TENOCYTE BIOACTIVITY AND TRANSCRIPTOMIC STABILITY IN COLLAGEN-GAG SCAFFOLDS[2]

2.1 Chapter overview

The focus of this chapter will be on the evaluation of CG scaffold microstructural properties on the phenotypic maintenance in equine tenocytes. The scaffold pore size and strut stiffness were independently by controlling freezing temperatures during lyophilization and crosslinking density. The effects of scaffold microstructure on cell-mediated scaffold contraction and resultant tenocyte bioactivity, viability, and gene expression were assessed in an effort to inform the design of biomaterials for tendon repair.

2.2 Introduction

The field of tissue engineering faces a unique set of challenges with geometrically and mechanically anisotropic tissues. The functional capacity of tendon derives from its extracellular matrix (ECM) composed of type I collagen that is arranged in highly aligned cross-linked fibrils (Towler and Gelberman 2006; James, Kesturu et al. 2008; Liu, Ramanath et al. 2008). The cellular component of tendon is primarily composed of tendon fibroblasts, or tenocytes, distributed throughout a hierarchical organization of aligned type I collagen fibers (James, Kesturu et al. 2008; Liu, Ramanath et al. 2008). Tendon and ligament injuries plague individuals from all walks of life, from elite athletes to the elderly, with more than 32 million occurrences every year in the US alone (James, Kesturu et al. 2008; Liu, Ramanath et al. 2008; Xu and Murrell 2008; Breidenbach, Gilday et al. 2013). While small tendon injuries heal spontaneously via regeneration, larger defects

[2] This chapter has been adapted from the following publication:
Grier, W.K. E.M. Iyoha, et al. (2017). "The influence of pore size and stiffness on tenocyte bioactivity and transcriptomic stability in collagen-GAG scaffolds." J. Mech. Behav. Biomed. Mater **65**: 295-305.

undergo a repair-mediated process generating fibrocartilagenous scar tissue with inferior structural and biomechanical properties. The resulting misaligned ECM leads to losses in range of motion and strength along with high rates of injury recurrence (James, Kesturu et al. 2008; Liu, Ramanath et al. 2008; Xu and Murrell 2008). Inadequate healing after surgical repair remains a primary clinical challenge. Because the musculoskeletal system depends on a balance of contributions from multiple tissues to maintain joint patency, ineffective tendon repair has both short-term (i.e. slowed rehabilitation) and long-term (*i.e.* chronic, degenerative joint pathologies) consequences (Butler, Juncosa-Melvin et al. 2008; Liu, Ramanath et al. 2008). Due to an ageing US population with increasing rates of underlying chronic conditions (*i.e.* obesity, diabetes), injury volume and complexity are only expected to increase (Fox, Bedi et al. 2011).

A primary challenge to improving tendon regeneration is poor understanding of how tenocytes respond to the dynamic structural microenvironment within the tendon. Tendon fibroblasts, or tenocytes (TCs) are responsible for tendon homeostasis, remodeling, and repair. However, tenocytes exhibit rapid de-differentiation when cultured in 2D or within hydrogels (Clegg, Strassburg et al. 2007; Taylor, Vaughan-Thomas et al. 2009). While tensile loading and aligned topographical cues on two-dimensional substrates can partially abrogate this effect (Caporali, Kapoor et al. 2009; Maeda, Shelton et al. 2009; Paxton, Hagerty et al. 2011), 3D platforms for stable expansion of tenocytes represent an important advance for the field. A crucial effort in the development of tissue engineering and regenerative medicine approaches for a range of tissues is the design of an appropriate biomaterial platform. Often these approaches are inspired by the native extracellular matrix (ECM) in order to provide an environment to speed healing or regeneration (Yannas, Lee et al. 1989; Spilker, Asano et al. 2001; Yannas 2001).

Collagen-glycosaminoglycan (CG) scaffolds have been used in a wide variety of in vivo applications for skin, peripheral nerve, and cartilage tissue engineering, as well as 3D environments for *in vitro* studies of cell-matrix interaction (cell, migration and contraction) behaviors (Yannas, Lee et al. 1989; Schulz Torres, M. Freyman et al. 2000; Harley, Spilker et al. 2004; O'Brien, Harley et al. 2005; Farrell, O'Brien et al. 2006; Harley, Freyman et al. 2007; Harley, Kim et al. 2008). The vast majority of past efforts using CG scaffolds have primarily been focused on the regeneration of soft tissues. However, those scaffold variants were unsuitable for tendon repair applications due to their inability to withstand TC-mediated contraction (Schulz Torres, M. Freyman et al. 2000; Caliari and Harley 2011) leading to rapid tenocyte de-differentiation. We have recently developed a fabrication method to produce anisotropic CG scaffolds composed of an aligned ellipsoidal pore structure (Caliari and Harley 2011). This anisotropic scaffold geometry promotes preferential tenocyte alignment along the long axis of the ellipsoidal pores. Surprisingly, increasing the scaffold relative density while maintaining the aligned pore geometry was shown to reduce TC-mediated scaffold contraction, maintain an aligned morphology, and reduce TC de-differentiation (Caliari and Harley 2011; Caliari, Ramirez et al. 2011; Caliari, Weisgerber et al. 2012). The potential to tailor scaffold anisotropy and its resistance to adverse (contraction-based) remodeling events offers an exciting platform to control long-term maintenance of tenocyte bioactivity. Here, we look at two different means to alter the local scaffold environment experienced by individual tenocytes: *pore size* and *crosslinking density*. For a low-density, open-cell foam such as the CG scaffold, changing scaffold pore size does not affect the macro-scale mechanical properties, such as scaffold elastic modulus (Harley, Leung et al. 2007; Gibson, Ashby et al. 2010). However, changing the pore size for a series of scaffolds with constant relative density does alter the length and thickness (hence, flexural rigidity) of individual struts which define the

pore structure of the scaffold (Harley, Freyman et al. 2007). Alternatively, increasing scaffold crosslinking density via either dehydrothermal (DHT) (Olde Damink, Dijkstra et al. 1996; Schulz Torres, M. Freyman et al. 2000; Harley, Leung et al. 2007; Gibson, Ashby et al. 2010) or chemical (1-ethyl-3-[3-dimethylaminopropyl] carbodiimide hydrochloride, EDC; N-hydroxysulfosuccinimide, NHS) (Olde Damink, Dijkstra et al. 1996) means can increase scaffold and individual strut stiffness, independent of pore size. Both modifications alter the local strut properties but via different means, opening the door to questions exploring how strut stiffness versus pore size affects TC-mediated contraction and resultant maintenance of TC-phenotype.

The work presented here seeks to describe the relationship between scaffold pore size and crosslinking with scaffold mechanical properties and its ability to resist TC-mediated contraction. We hypothesized that a scaffold's ability to resist TC-mediated contraction would increase with increasing crosslinking density and decreasing pore size. Moreover, more mechanically robust scaffolds with smaller pore sizes and higher crosslinking densities were hypothesized to be more supportive of the maintenance of a tendon-like phenotype through the resistance to TC-mediated contraction and preservation of a permeable open-cell pore structure that allows for efficient nutrient transport and cell spreading. While our group and others have investigated the impact of initial scaffold pore size and crosslinking on cell attachment and tenocyte contraction (Schulz Torres, M. Freyman et al. 2000; Caliari and Harley 2011; Caliari, Weisgerber et al. 2012), this previous work did not examine long-term cell-mediated contraction of the scaffold network, nor the effect of EDC crosslinking density on scaffold pore size and TC-mediated contraction and subsequent bioactivity.

2.3 Materials and Methods

Preparation of CG suspension

Type I microfibrillar collagen from bovine tendon (Sigma-Aldrich, St. Louis, MO) and chondroitin-4,6-sulfate from shark cartilage (Sigma-Aldrich, St. Louis, MO) were homogenized in 0.05M acetic acid. The concentration of the collagen suspension made was 1.0%, and the ratio of the collagen to glycosaminoglycan was kept at 11.25:1 (Yannas, Lee et al. 1989; O'Brien, Harley et al. 2004; Caliari and Harley 2011).

Aligned CG scaffold fabrication

The scaffolds were fabricated through directional solidification as previously described (Caliari and Harley 2011). Degassed CG suspension was pipetted into a polytetrafluoroethylene (PTFE) - copper mold (8mm diameter, 15mm deep), and placed on a pre-cooled freeze-dryer shelf (VirTis, Gardner, NY). The mismatch in thermal conductivity between the PTFE body and copper base of the mold promotes unidirectional heat transfer through the more conductive copper, resulting in anisotropic ice crystal formation when cooled (Caliari and Harley 2011). In order to control pore size, the CG suspension was frozen at three different temperatures (T_f): -10°C, -40°C, and -60°C. These freezing temperatures have been previously shown to produce scaffolds with aligned pore geometries of 243, 152, and 55 μm diameters respectively (Caliari and Harley 2011). The CG suspensions were frozen for 2 hours, and then sublimated at 0°C and 200mTorr to remove the ice crystals, resulting in a dry, porous scaffold.

Aligned CG scaffold crosslinking

Following lyophilization, the scaffolds were DHT crosslinked in a vacuum oven (Welch, Niles, IL) (105°C, <25 torr) for 24 hours, and then stored in a desiccator until use. Before use, scaffolds were immersed in 200-proof ethanol for 6 hours, followed by washing with phosphate-buffered

saline (PBS) overnight. Solutions of 1-ethyl-3-[3-dimethylaminopropyl] carbodiimide hydrochloride (Sigma-Aldrich, St. Louis, MO) and N-hydroxysulfosuccinimide (Sigma-Aldrich) were used to further crosslink each of the three scaffolds groups at three different molar ratios: 1:1:5 (low), 5:2:5 (medium), and 5:2:1 (high) EDC:NHS:COOH that correspond with increasing collagen strut and overall scaffold stiffness (Olde Damink, Dijkstra et al. 1996; Harley, Leung et al. 2007).

Equine tenocyte isolation and culture

Equine tenocytes were isolated as previously described (Caliari and Harley 2011) from horses, aged 2–3 years, euthanized for reasons not related to tendinopathy, and in a manner consistent with protocols approved by the University of Illinois IACUC. Digital flexor tendons were extracted, diced, and incubated in a collagenase solution at 37◦C, under constant shaking. Digest solution was filtered (40 μm pore size) to isolate tenocytes (Kapoor, Caporali et al. 2010). Tenocytes were plated at a density of $1x10^4$ cells/cm^2, and cultured in high glucose Dulbecco's modified Eagle's medium (DMEM, Fisher, Pittsburgh, PA) with 1% L-glutamine (Invitrogen, Carlsbad, CA) supplemented with 10% fetal bovine serum (FBS, Invitrogen, Carlsbad, CA), 1% penicillin/streptomycin (Invitrogen, Carlsbad, CA), 1% amphotericin-B (MP Biomedical, Solon, OH), and 25μg/mL ascorbic acid (Wako, Richmond, VA) (Caliari and Harley 2011). The tenocytes were cultured at 37°C and 5% CO_2, and fed every 3 days. Cells were used at passage 3.

Scaffold seeding

Each cylindrical CG scaffold (8mm diameter, 15mm length) was cut into ~5mm long plugs (8mm dia.) and placed in ultra-low attachment, 6-well plates (Corning Life Sciences, Lowell, MA). Confluent tenocytes were trypsinized and resuspended at a concentration of $5x10^5$ cells/20μL media. Scaffolds were seeded, with tenocytes using a previously validated static seeding method

(O'Brien, Harley et al. 2005; Caliari and Harley 2011), with 10μL of cell suspension ($2.5x10^5$ cells) pipetted directly onto each scaffold. The scaffolds were then incubated at 37°C for 15 minutes, turned over, and seeded with an additional 10 μL of cell suspension, for a total of $5x10^5$ cells seeded per scaffold. The cell-seeded scaffolds were then incubated at 37°C with 5% CO_2 and fed complete DMEM every 3 days (Caliari and Harley 2011).

Quantification of cell metabolic activity

The mitochondrial metabolic activity of the tenocytes within each scaffold was determined through the use of non-destructive AlamarBlue® assay as previously described (Caliari and Harley 2011). Healthy, viable cells continuously convert the active ingredient in AlamarBlue® (resazurin) to a fluorescent byproduct (resorufin), allowing comparison of the gross metabolic activity of each cell-seeded construct. Cell-seeded scaffolds were incubated at 37°C in AlamarBlue (Invitrogen, Carlsbad, CA) solution with gentle shaking for 2 hours (Tierney, Jaasma et al. 2009). Resorufin fluorescence was measured (excitation: 540 nm, emission: 590 nm) via a fluorescent spectrophotometer (Tecan, Switzerland). Relative cell metabolic activity was determined from a standard curve generated from known cell numbers prior to seeding the scaffolds and reported as a percentage of the total number of seeded cells.

Measurement of cell-mediated scaffold contraction

At days 1, 4, 7, and 14, the diameter of each scaffold disk was measured using a standard drafting template. The measurements were then normalized against the diameter of each scaffold at day 0 to determine cell-mediated contraction of each scaffold disk (Spilker, Asano et al. 2001; Caliari, Weisgerber et al. 2012).

Quantification of cell number

The total number of cells on each scaffold was assayed via DNA quantification (Caliari and Harley 2011). Scaffolds were rinsed in PBS and placed in a papain solution (Sigma-Aldrich, St. Louis, MO) (60°C, 24 hours) to digest the scaffolds and lyse the cells. Hoechst 33258 dye (Invitrogen, Carlsbad, CA) was used to fluorescently label double-stranded DNA (Kim, Sah et al. 1988). Fluorescence was read (excitation: 360nm; emission: 465nm) via a fluorescent spectrophotometer (Tecan, Switzerland). Experimental readings were normalized to the scaffolds with crosslinking density of 5:2:1 and T_f of -10°C in order to serve as a comparison to previous work (Kim, Sah et al. 1988).

RNA isolation and real-time PCR

RNA from the tenocytes in the scaffolds was extracted at days 1, 4, 7 ,and 14, using an RNeasy Plant Mini kit (Qiagen, Valencia, CA) and was then reverse transcribed to cDNA in a Bio-Rad S1000 thermal cycler using the QuantiTect Reverse Transcription kit (Qiagen, Valencia, CA), as previously described (Caliari and Harley 2011). Real-time PCR reactions were carried out in triplicate, using 10ng of cDNA and QuantiTect SYBR Green PCR kits (Qiagen, Valencia, CA) in a 7900HT Fast Real-Time PCR system (Carlsbad, CA). The primers used were consistent with previous studies (**Table 2.1**; collagen type I alpha 2; collagen type III alpha 1; cartilage oligomeric matrix protein; decorin; scleraxis; tenascin-c, C; matrix metalloproteinases 1, 3, and 13; glyceraldehyde 3-phosphate dehydrogenase, housekeeping) (Caliari and Harley 2011; Caliari, Weisgerber et al. 2012), and were synthesized by Integrated DNA Technologies (Coralville, IA). Results were generated using the ΔΔCt method, and all results were expressed as fold changes normalized to the expression levels of cells on the -10°C/5:2:1 scaffold group at day 1 for comparison to previous studies (Caliari and Harley 2011; Caliari, Ramirez et al. 2011; Caliari,

Weisgerber et al. 2012; Caliari and Harley 2013). The expression levels of the MMP genes are shown relative to the normalized scaffold contraction for each group, at each time point, in order to better elucidate the interplay of cell-mediated contraction forces and cell-mediated remodeling (Gotoh, Hamada et al. 1997; Lo, Marchuk et al. 2004; Jones, Corps et al. 2006; Clegg, Strassburg et al. 2007).

Statistical Analysis

One-way analysis of variance (ANOVA) was performed on all data sets within each group to examine differences with time. Two-way ANOVAs (independent factors: crosslinking density, T_f) were applied to data sets for each time point. For scaffold contraction, significant changes from the day 0 time point were determined by Dunnett's post-hoc test. Statistical significance for all other measurements were determined by Tukey-HSD post-hoc tests. Significance was set at $p < 0.05$. Cell metabolic activity (n=6), scaffold diameter (n=6), and gene expression (n=3) were analyzed at each time point. For MMP gene expression, relative to normalized scaffold diameter, linear or exponential regression models were used to fit the data and corresponding R^2 values (n = 27) were reported. Error was reported in figures as the standard error of the mean, unless otherwise noted.

2.4 Results

Tenocyte viability in CG scaffolds

Tenocytes remained viable in all scaffold variants across the fourteen day experiment. While the metabolic activity of the tenocyte-seeded scaffolds was consistent for all scaffold groups at day 1 after seeding, by day 14, significant expansion in overall metabolic activity and cell number was observed. Here, cell number and construct metabolic activity increased significantly ($p < 0.01$)

with crosslinking density, with the largest increases in cell number and metabolic activity seen for the most strongly crosslinked (EDC:NHS:COOH 5:2:1) variants (**Figure 2.1A, 2.1B**). A significant effect of both crosslinking density ($p < 0.001$) and scaffold pore size (T_f, $p < 0.001$) was observed on tenocyte mediated scaffold contraction (**Figure 2.1C)**. Scaffolds crosslinked at the lightest (1:1:5) density started showing signs of contraction as early as day 1, Then, they showed significantly ($p < 0.01$) greater contraction (smaller, normalized diameter) than scaffolds crosslinked at higher densities on all following days. Scaffolds crosslinked at a middle (5:2:5) density began to show signs on contraction by day 4, and on all following days, they were significantly more contracted than the scaffolds crosslinked at the highest (5:2:1) density. These scaffolds at the highest crosslinking density exhibited little-to-no contraction throughout the 14-day experiment. For crosslinking densities that yielded significant contraction (1:1:5, 5:2:5), there was also a significant ($p < 0.01$) effect of scaffold pore size on contraction. Scaffolds with larger pore sizes (higher T_f) showed greater contraction when compared to scaffolds with the same crosslinking density but smaller pore sizes.

Tenocyte gene expression within CG scaffolds

Subsequently, we examined the gene expression profiles of the cells remaining in each construct after 14 days in culture. Three distinct sub-sets of genes were examined: structural proteins associated with tendon ECM (*COL1A2*, *COL3A1*, *COMP*, *DCN*; **Figure 2.2**); genes associated with tendon phenotype (*SCXB*, *TNC*; **Figure 2.3**); and genes associated with matrix remodeling (*MMP1*, *MMP3*, *MMP13*; **Figure 2.4**).

Structural protein gene expression

Gene expression levels of *COL1A1*, *COL3A3*, *COMP*, and *DNC* showed some global changes in expression for earlier time points (days 1, 4, and 7; **Figures 2.5, 2.6**). By day 4, the scaffolds least

resistant to contraction (1:1:5 crosslinking density) showed significant increases in *COL3A1*, *COMP*, and *DCN*. The scaffolds moderately able to resist contraction (5:2:5 crosslinking density) showed significantly higher expression of all four structural protein markers. Scaffolds most resistant to contraction (5:2:1 crosslinking density) only showed increased expression of *DCN*. More interestingly, we examined changes in structural genes at day 14, at which point significant cell-mediated contraction had occurred (**Figure 2.2**). Notably, scaffolds most resistant to contraction (5:2:1 crosslinking density; -40°C and -60°C T_f) showed significantly higher expression of *COL1A2* compared to scaffolds with lower crosslinking densities and the same T_f (**Figure 2.2**). While not always significant, an overall change in expression profiles for all genes were observed, with crosslinking groups less resistant to contraction (1:1:5, 5:2:5) showing a decrease in expression with decreasing pore size; while the crosslinking groups most resistant to contraction (5:2:1) showed an increase in expression with decreasing pore size. Finally, while there were no significant differences in expression of *DCN*, the scaffold with the smallest pores, most resistant to contraction (-60°C T_f; 5:2:1 crosslinking) showed significantly higher expression of *COMP* than all other scaffold groups at day 14 **(Figure 2.2)**.

Tendon phenotype gene expression

Expression of the transcription factor *SCXB* increased initially in all scaffold variants (through day 4). However, significant cell-mediated contraction began to affect the expression profile for subsequent days for the scaffold groups least resistant to contraction (1:1:5 and 5:2:5 crosslinking density), while the scaffold group resistant to contraction (5:2:1 crosslinking density) maintained the elevated *SCXB* expression through days 14 (F**igure 2.7**). Comparing scaffold pore size and crosslinking at day 14, we observed the scaffold variant most resistant to contraction (5:2:1 crosslinking density, -60°C T_f) showed significantly higher expression of *SCXB* than all other

groups. Further, scaffolds with reduced resistance to contraction (1:1:5 crosslinking density, -40° T_f) showed significantly lower expression of *SCXB* than all other groups **(Figure 2.3)**. *TNC* expression followed a similar trend to *SCXB*, with all groups showing increasing expression though day 7 (**Figure 2.7**). While not significant by day 14, an increasing trend in *TNC* expression was observed for scaffolds most resistant to contraction (5:2:1 crosslinking density; -40 and -60°C T_f).

MMP gene Expression

All three MMP genes examined (*MMP1, MMP3*, and *MMP13*) showed similar trends regarding expression between groups over time (**Figure 2.8**). In general, MMP expression levels increased with each time point and were significantly higher in the scaffolds least resistant to contraction (warmer T_f, lower crosslinking densities). We subsequently examined MMP expression profiles against the normalized (versus starting diameter) diameter of each scaffold, collapsing the effect of time, pore size, and crosslinking density onto a single plot (**Figure 2.4**). With the exception of day 1, at which point minimal contraction had taken place ($R^2 = 0.25$), we observed very strong correlation between increasing MMP expression profiles and increased scaffold contraction. This correlation resulted in $R^2 \geq 0.84$ for day 14 results. *MMP1* and *MMP3* showed effectively linear increases in expression with scaffold crosslinking and time, while *MMP13* showed an exponential increase in expression with time. Scaffolds least resistant to contraction (1:1:5 density, -10°C T_f) showed more than a 600 fold increase in *MMP13* over the course of 14 days **(Figure 2.4C)**.

2.5 Discussion

Biomaterial scaffold mechanical properties, at both the macro and micro-scales, have been widely reported to influence cellular behaviors such as adhesion, migration, proliferation, and differentiation (Pelham and Wang 1997; Freyman, Yannas et al. 2001; Grinnell, Ho et al. 2003;

Engler, Bacakova et al. 2004; Peyton and Putnam 2005; Yeung, Georges et al. 2005; Zaman, Trapani et al. 2006). The motivation for this work is the significant de-differentiation often observed with tenocytes when cultured in vitro, as well as the observation that structural alignment in two-dimensions and application of tensile strain may reduce this de-differentiation (Taylor, Vaughan-Thomas et al. 2009). Future tendon tissue engineering efforts require the expansion of primary tenocytes in order to address large injuries, necessitating approaches that use three-dimensional biomaterial constructs for cell culture and eventual in vivo implantation. If a microstructurally-aligned material is unable to maintain a high degree of anisotropy, due to contractile forces, the microstructural cues that guide cell-fate decisions will be significantly altered as the cells remodel the local microenvironment.

Here, we describe the production and analysis of a series of anisotropic CG scaffolds fabricated at different T_f and a range of crosslinking densities for the in vitro culture of primary equine tenocytes. Our group recently described an approach where the relative density of a series of CG scaffolds was varied in order to prevent TC-mediated contraction, resulting in reduced scaffold contraction. Maintenance of the aligned structural cues, provided by the scaffold and resultant, increased maintenance of TC-associated gene expression profiles for cells within the scaffold (Caliari, Weisgerber et al. 2012). However, changes in the relative density of the scaffold result in changes in scaffold pore size as well as in the mechanical properties of the scaffold. This is at the scale of the overall construct and at the level of an individual cell within the scaffold. This observation therefore motivated our effort here to generate a wider library of CG scaffolds to more specifically examine the effect of scaffold architecture on resultant TC-mediated contraction and phenotypic stability.

Low-density open-cell foams such as the CG scaffold demonstrate a unique set of structure-mechanic relationships (Gibson, Ashby et al. 2010). For these materials, it is essential to consider the mechanical property at the scale of the overall construct (bulk properties), as well as at the level of the individual fibers (termed struts) that make up the scaffold architecture and to which individual cells attach. The bulk mechanical properties of the scaffold critically depend on the crosslinking density and relative density (1 – porosity), not pore size, of the scaffold. For example, the elastic modulus of the bulk scaffold (E^*) depends on the crosslinking density of the collagen (defining E_s, the modulus of the individual strut) along with the relative density (ρ_*/ρ_s) of the scaffold: $E^* \sim E_s \cdot (\rho_*/\rho_s)^2$ (Harley, Leung et al. 2007). However, the modulus is insensitive to scaffold pore size (Gibson and Ashby 1997; Harley, Leung et al. 2007). Cell-mediated contraction is mediated not by the bulk elastic properties, but rather the mechanical properties of the individual struts to which they attach. Previous studies have shown that contractile cells possess the ability to generate sufficient contractile forces to buckle individual struts and deform the local pore structure around them (Freyman, Yannas et al. 2001). These local contractions, when compounded throughout the entire scaffold, result in a macroscopic deformation of the overall scaffold. Furthermore, the magnitude of contractile forces generated by individual cells can be estimated via the flexural rigidity of the strut, depending on crosslinking density (E_s) and the length and thickness of the strut (Harley, Freyman et al. 2007). Here, increasing the pore size for a series of scaffolds with a set relative density increases the length of individual struts (Harley, Leung et al. 2007). Therefore, selective modification to both scaffold crosslinking and pore size provides a wider platform to consider the influence of local strut mechanical properties, resistance to TC-mediated contraction, and subsequent maintenance of tenogenic gene expression profiles within the scaffold.

For this project, we employed a previously defined set of scaffold fabrication techniques, altering the freezing temperature during lyophilization to generate a series of anisotropic scaffolds within decreasing pore size (-10°C, -40°C, -60°C; 243, 152, and 55 μm pore size) (Caliari and Harley 2011). We subsequently employed a series of three discrete carbodiimide crosslinking densities (1:1:5, 5:2:5, 5:2:1) that span a 3.6-fold increase in stiffness (Harley, Leung et al. 2007). TC-mediated contraction, metabolic activity and cell number, and resultant changes in gene expression profiles for a diverse set of tendon-associated structural proteins, tenocyte markers, and matrix-remodeling genes were then traced across the full set of 9 experimental scaffold groups. Here, we observed scaffold pore size and crosslinking density were able to elicit differential responses during long-term cell culture.

In general, an increase in the number and metabolic activity of primary equine tenocytes was observed with culture time. However, we noted a significant effect of both crosslinking density and scaffold pore size on cell-mediated contraction of the scaffolds **(Figure 2.1A)**. Increasing scaffold crosslinking density resulted in reduced cell-mediated contraction; however, we also noted a significant effect of pore size on contraction, with scaffolds containing smaller pores more able to resist cellular contractile forces over time (**Figure 2.1C**). The loss of structural stability via contraction has a significant, negative effect on cell metabolic activity due with time, likely due to reduced biotransport through the denser scaffold. This finding is consistent with previous findings showing reduced scaffold permeability with the application of compressive strain (Weisgerber, Kelkhoff et al. 2013). While we observed a significant reduction in metabolic activity and cell number after 14 days of culture in scaffolds that exhibited significant contraction **(Figure 2.1A, 2.1B**), it was important to also establish the effect on the phenotype of the resultant cells.

We subsequently examined the effects of cell-mediated contraction on the maintenance of a healthy tendon-like phenotype via transcript levels of ECM proteins associated with native tendon (*COL1A2*, *COL3A1*, *COMP*, *DCN*) (Lui, Rui et al. 2011), as well as transcription factors and matricellular markers of tenocytes (*SCXB*, *TNC*) (Blitz, Viukov et al. 2009; Pryce, Watson et al. 2009; Doroski, Levenston et al. 2010; Schweitzer, Zelzer et al. 2010) **(Figures 2.2-2.3)**. Lastly, we also examined a series of matrix metalloproteinases (*MMP1*, *MMP3*, *MMP13*) important for cell migration, wound healing, and matrix remodeling, but also those that showed reduced expression levels, indicative of healthy tendon (Gotoh, Hamada et al. 1997; Jones, Corps et al. 2006; Clegg, Strassburg et al. 2007). Transcript levels at each time point were normalized against expression levels of tenocytes in scaffolds with a -10°C T_f and 5:2:1 crosslinking density to compare to previous studies investigating the influence of the CG scaffold microenvironment on the transcriptomic stability of tenocytes (Caliari and Harley 2011; Caliari, Weisgerber et al. 2012; Caliari and Harley 2013). Importantly, by day 14, *COL1A2*, *COL3A1*, *COMP*, and *DCN* all showed decreased expression in scaffolds with reduced crosslinking density (1:1:5 and 5:2:5) and scaffolds with the largest pore size (least resistant to contraction). Expression levels were increased in scaffolds most resistant to contraction (T_f -60; 5:2:1 crosslinking density). Expression of *SCXB* was significantly higher in scaffolds most resistant to contraction (T_f -60; 5:2:1 crosslinking density), while *TNC* expression follows a similar, but not significant, trend. Heightened *MMP1*, *MMP3*, and *MMP13* expression all followed nearly identical and dramatic trends. By plotting the results, not as a function of scaffold pore size or crosslinking density, but rather versus overall resistance to TC-mediated contraction, these data collapse onto clear trends of reduced TC-associated markers with increasing cell-mediated contraction (**Figure 2.4**).

While earlier results suggested reduced TC-associated markers with increasing scaffold contraction results in changes in overall scaffold relative density(Caliari, Weisgerber et al. 2012), changes in relative density masked our ability to determine whether the stiffness of the scaffold strut versus the flexural rigidity of the strut was the primary design consideration that could be used in subsequent biomaterial variants. Here, by selectively modifying scaffold pore size and crosslinking density, we are able to independently tune strut length versus strut stiffness. We found that the overall ability to resist contraction was the best predictor of maintenance of tenocyte-associated gene expression profiles. However, examining the effect of pore size versus crosslinking in more detail, we noted that crosslinking density provides a primary means to resist TC-mediated contraction. For lower crosslinking densities (1:1:5, 5:2:5) where significant contraction was observed, the poorest response was seen in the smallest pore size variants. Likely due to the significant contraction, not only destroying the aligned structure signals provided by the pore, but also significantly reducing biotransport. However, in the highest crosslinking density (5:2:1) where limited contraction was observed, the scaffold with the smallest pore size, more resistant to contraction, demonstrated the highest level of TC-associated genes. Together, these results suggest that while scaffold ability to resist TC-mediated contraction forces play a significant role in regulating tenocyte gene expression, scaffold crosslinking, not necessarily changes in pore size, provides the primary means to optimize culture conditions for expansion and maintenance of primary tenocytes.

2.6 Conclusions

This work describes the evaluation of the ability for a series of anisotropic CG scaffolds to promote the expansion of primary tenocytes in vitro. In general, equine tenocytes showed increased proliferation and metabolic activity, as well as less cell-mediated contraction in scaffolds with

higher crosslinking densities and smaller pore sizes. Gene expression analysis showed scaffolds most resistant of cell-mediated contraction were able to maintain a tendon-like-phenotype over the course of the experiment. Importantly, the high expression levels of MMPs 1, 3, and 13 in scaffolds that showed more contraction indicate a high degree of scaffold remodeling and loss of tendon-like phenotype. This suggests that the structural stability of biomaterials for tissue engineering applications is of particular importance when considering clinical translation.

2.7 Table

Table 2.1 PCR primer sequences.

Transcript	Sequence	Reference
COL1A2	Forward: 5'- GCACATGCCGTGACTTGAGA -3' Reverse: 5'- CATCCATAGTGCATCCTTGATTAGG -3'	(Taylor, Vaughan-Thomas et al. 2009)
COL3A1	Forward: 5'- GTCCACCTGAGGAACTGTCT--3' Reverse: 5'- TGATCAGGACCACCAACATCA-3'	(Taylor, Vaughan-Thomas et al. 2009)
COMP	Forward: 5'- GGTGCGGCTGCTATGGAA -3' Reverse: 5'- CCAGCTCAGGGCCCTCAT -3'	(Taylor, Vaughan-Thomas et al. 2009)
DCN	Forward: 5'- CATCCAGGTTGTCTACCTTCATAACA-3' Reverse: 5'- CCAGGTGGGCAGAAGTCATT -3'	(Taylor, Vaughan-Thomas et al. 2009)
SCXB	Forward: 5'- TCTGCCTCAGCAACCAGAGA -3' Reverse: 5'- TCCGAATCGCCGTCTTTC-3'	(Taylor, Vaughan-Thomas et al. 2009)
TNC	Forward: 5'- GGGCGGCCTGGAAATG -3' Reverse: 5'- CAGGCTCTAACTCCTGGATGATG-3'	(Taylor, Vaughan-Thomas et al. 2009)
MMP1	Forward: 5'- GGTGAAGGAAGGTCAAGTTCTGAT -3' Reverse: 5'- AGTCTTCTACTTTGGAAAAGAGCTTCT -3'	(Garvican, Vaughan-Thomas et al. 2008)
MMP3	Forward: 5'- GCACATGCCGTGACTTGAGA-3' Reverse: 5'- CCTATGGAAGGTGACTCCATGTG -3'	(Garvican, Vaughan-Thomas et al. 2008)
MMP13	Forward: 5'- CTGGAGCTGGGCACCTACTG -3' Reverse: 5'- ATTTGCCTGAGTCATTATGAACAAGAT-3'	(Garvican, Vaughan-Thomas et al. 2008)
GAPDH	Forward: 5'- GCATCGTGGAGGGACTCA -3' Reverse: 5'- GCCACATCTTCCCAGAGG-3'	(Taylor, Vaughan-Thomas et al. 2009)

2.8 Figures

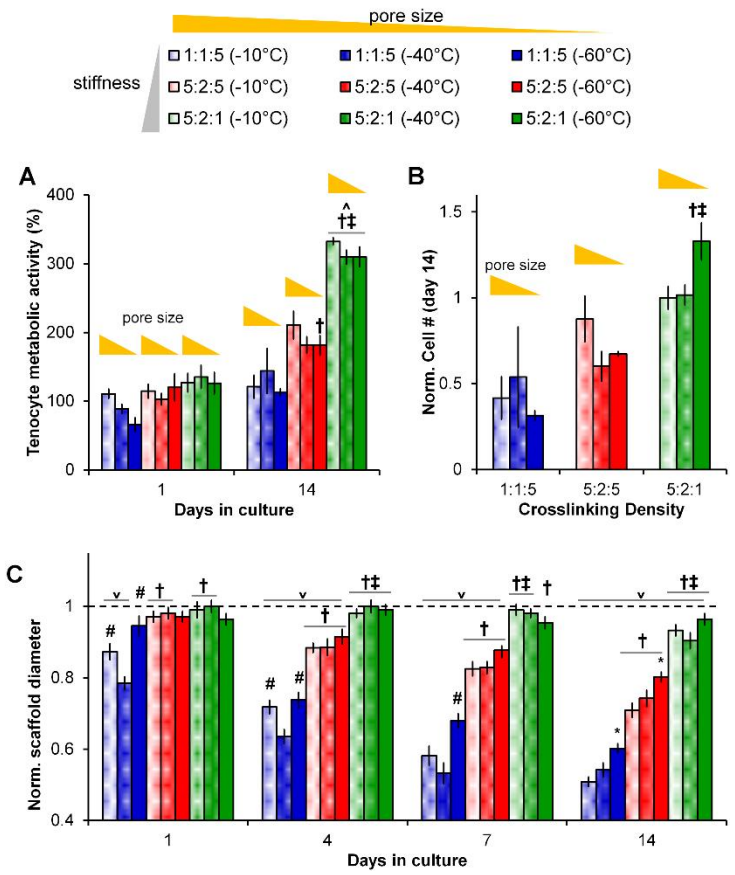

Figure 2.1 Tenocyte viability and contraction of CG scaffolds. (A) Metabolic activity of tenocytes at days 1 and 14 for all nine CG scaffold groups. **(B)** Normalized number of cells (relative to number initially seeded) at day 14 for all nine CG scaffold groups. **(C)** Scaffold contraction, normalized to the initial scaffold diameter, at days 1, 4, 7, and 14 for all nine CG scaffold groups. Data expressed as mean ± SEM (n=6). ∨: significantly ($p < 0.01$) lower than initial scaffold diameter. †: significantly ($p < 0.01$) different than scaffolds of same pore size with lowest (1:1:5) crosslinking density. ‡: significantly ($p < 0.01$) different than scaffolds of same pore size with middle (5:2:5) crosslinking density. *: significantly ($p < 0.01$) different from scaffolds of same crosslinking density with largest pore size (-10°C T_f). #: significantly ($p < 0.01$) different from scaffolds of same crosslinking density with middle pore size (-40°C T_f).

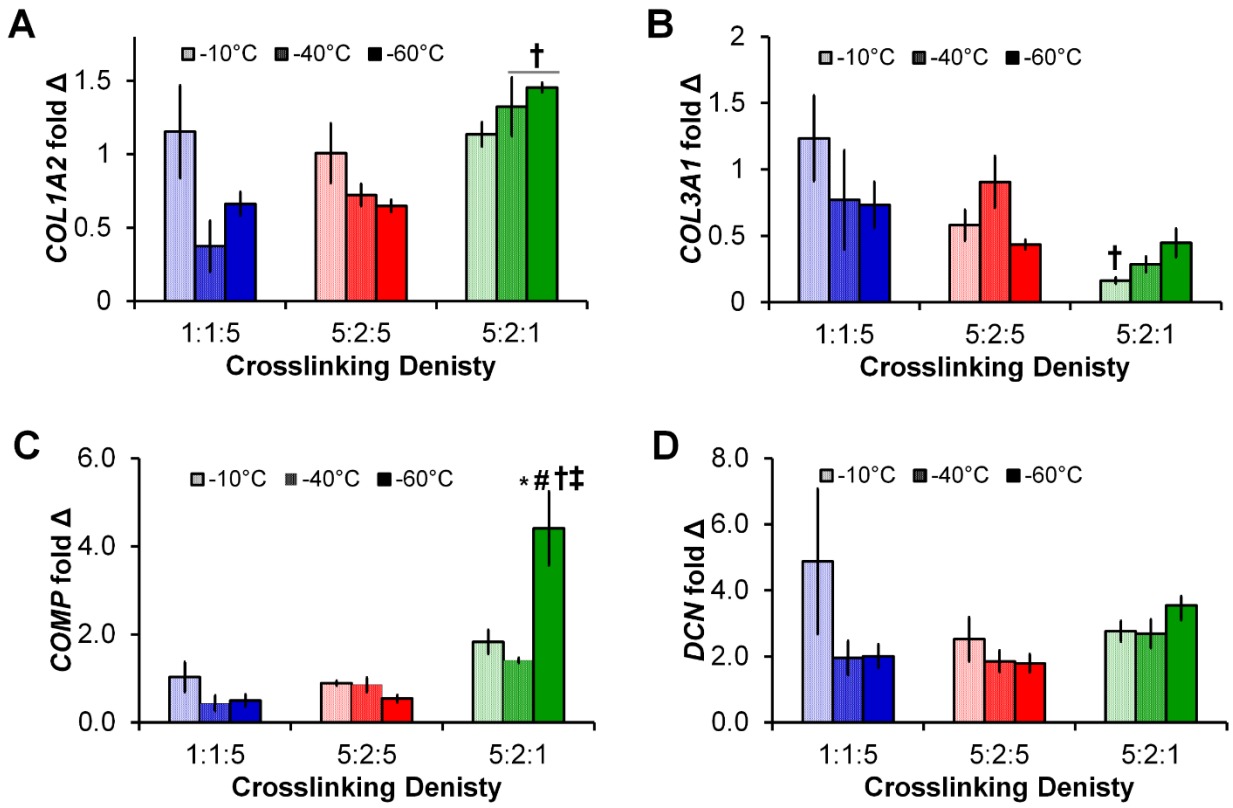

Figure 2.2 Structural protein gene expression. Expression levels of **(A)** *COL1A2*, **(B)** *COL3A1*, **(C)** *COMP*, and **(D)** *DCN* after 14 days in all 9 scaffold groups. Data expressed as mean ± SEM (n=3). †: significantly ($p < 0.01$) different than scaffolds of same pore size with lowest (1:1:5) crosslinking density. ‡: significantly ($p < 0.01$) different than scaffolds of same pore size with middle (5:2:5) crosslinking density. *: significantly ($p < 0.01$) different from scaffolds of same crosslinking density with largest pore size (-10°C T_f). #: significantly ($p < 0.01$) different from scaffolds of same crosslinking density with middle pore size (-40°C T_f).

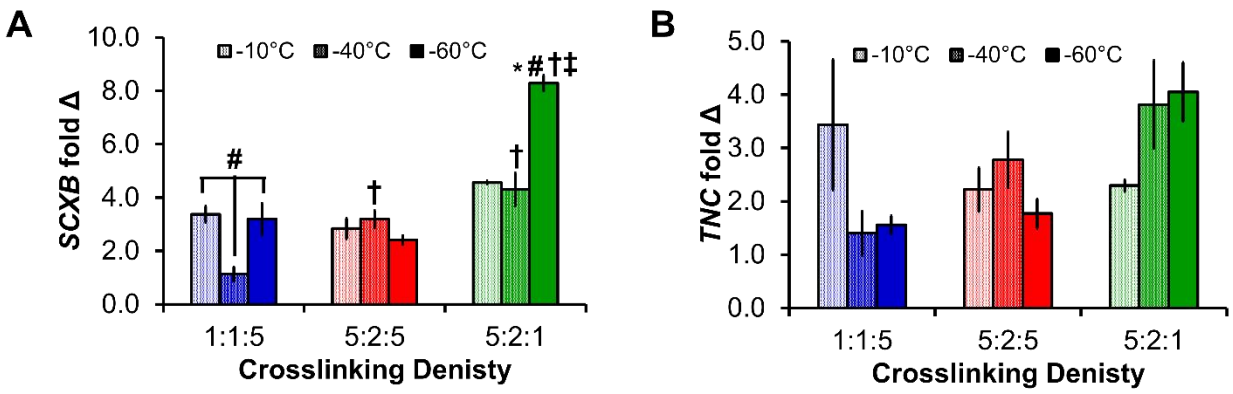

Figure 2.3 Tendon phenotype gene expression. Expression levels of **(A)** *SCXB* and **(B)** *TNC* after 14 days in all 9 scaffold groups. Data expressed as mean ± SEM (n=3). †: significantly ($p < 0.01$) different than scaffolds of same pore size with lowest (1:1:5) crosslinking density. ‡: significantly ($p < 0.01$) different than scaffolds of same pore size with middle (5:2:5) crosslinking density. *: significantly ($p < 0.01$) different from scaffolds of same crosslinking density with largest pore size (-10°C T_f). #: significantly ($p < 0.01$) different from scaffolds of same crosslinking density with middle pore size (-40°C T_f).

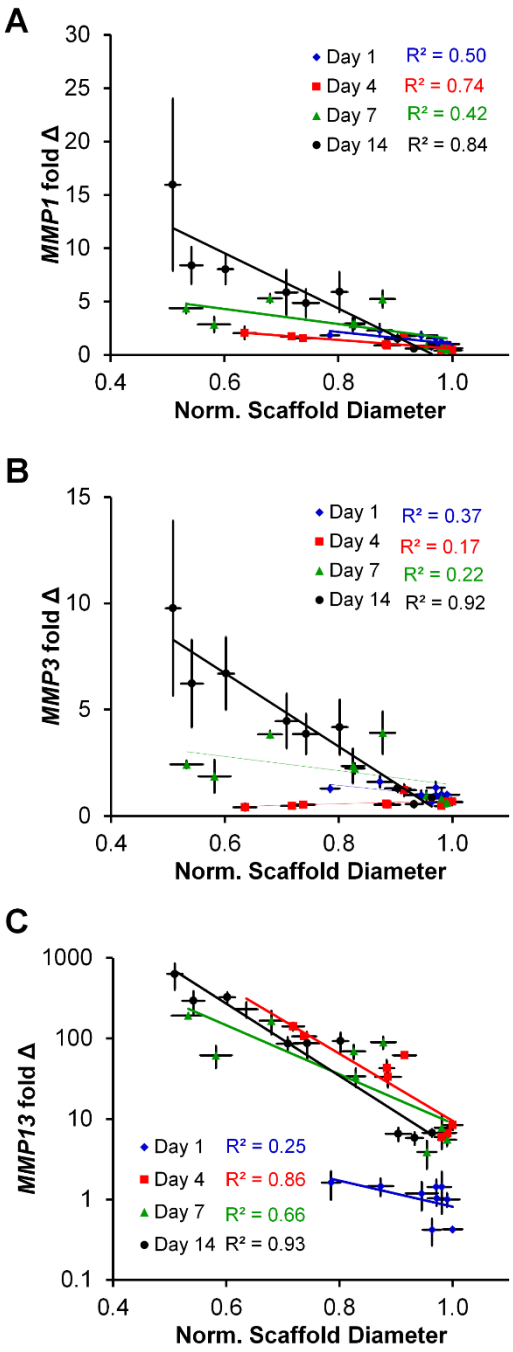

Figure 2.4. MMP gene expression. (A) MMP 1, **(B)** MMP3, and **(C)** MMP13 expression levels at days 1, 4, 7, and 14 relative to normalized scaffold diameter for all 9 scaffold groups. Data expressed as mean ± SEM (n=3). The degree of correlation (R^2) was between gene expression and scaffold contraction was determined as a function of experimental time point (day 1, 4, 7, and 14).

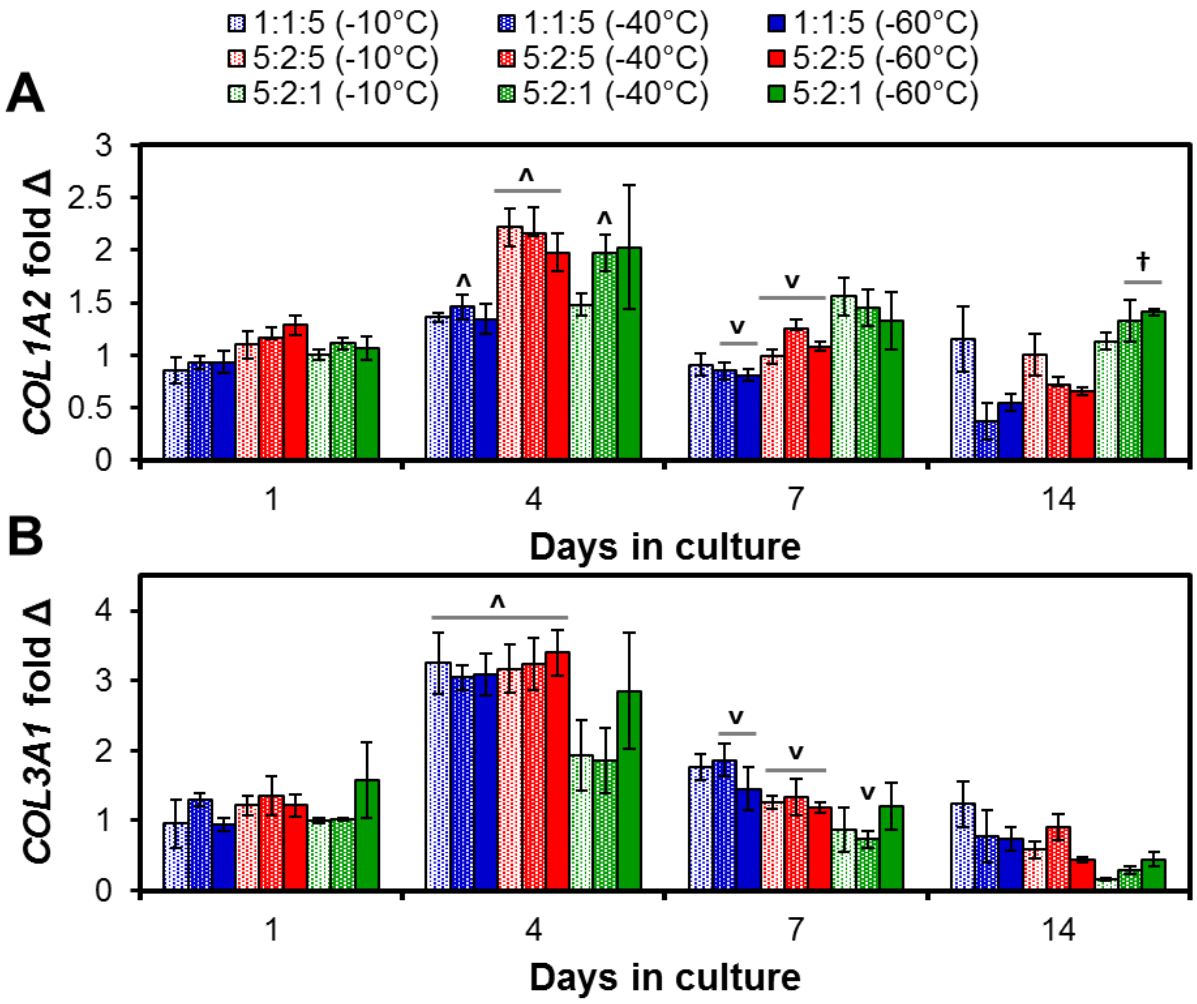

Figure 2.5: **Structural protein gene expression (1)**. Expression levels of **(A)** *COL1A2* and **(B)** *COL3A1* in all 9 scaffold groups at days 1, 4, 7, and 14. Data expressed as mean ± SEM (n=3). †: significantly ($p < 0.01$) different than scaffolds of same pore size with lowest (1:1:5) crosslinking density. ‡: significantly ($p < 0.01$) different than scaffolds of same pore size with middle (5:2:5) crosslinking density. *: significantly ($p < 0.01$) different from scaffolds of same crosslinking density with largest pore size (-10°C T_f). #: significantly ($p < 0.01$) different from scaffolds of same crosslinking density with middle pore size (-40°C T_f). ∨: significantly ($p < 0.01$) lower than expression at previous time point within group. ^: significantly ($p < 0.01$) than expression at previous time point within group.

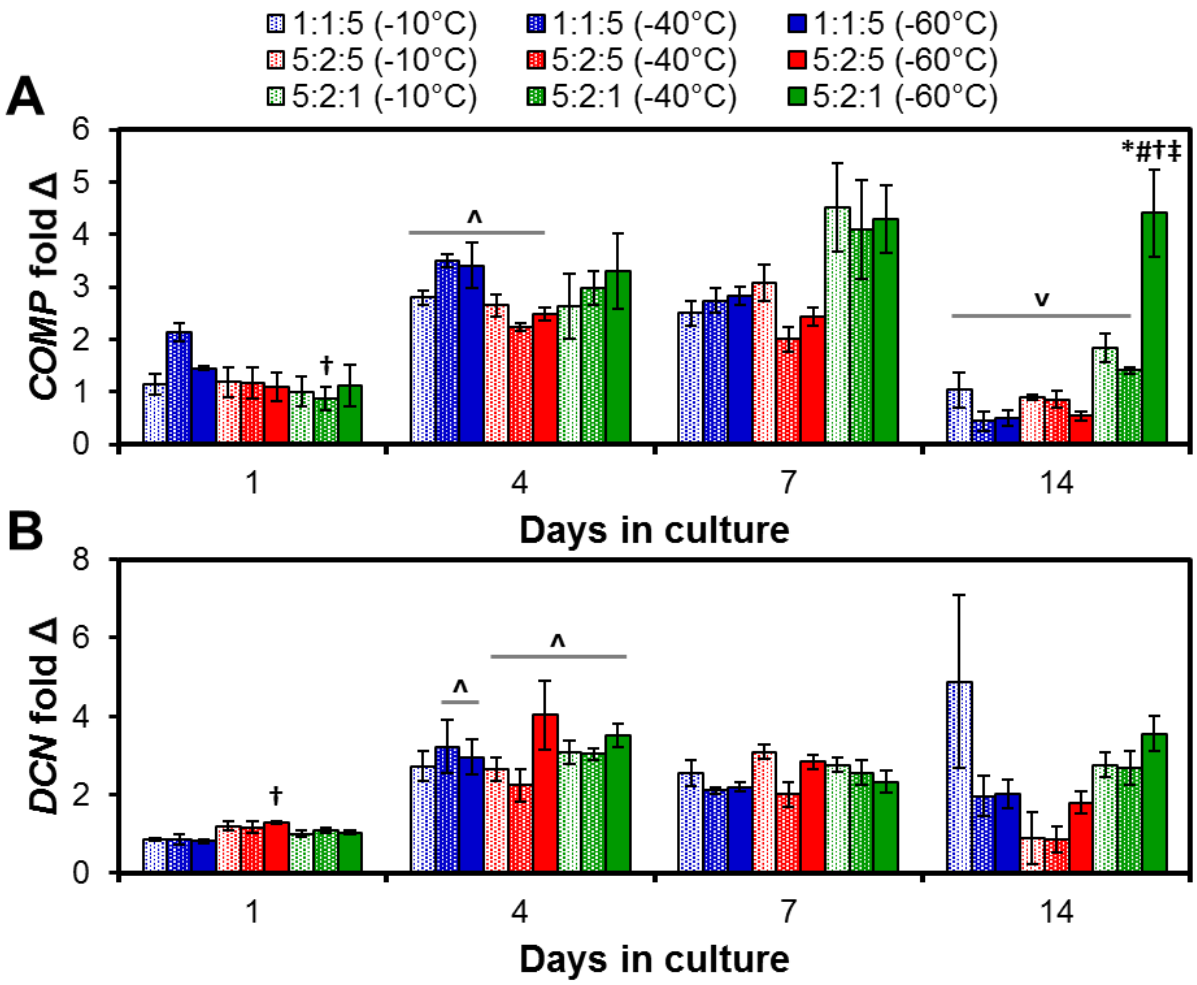

Figure 2.6: **Structural protein gene expression (2)**. Expression levels of **(A)** *COMP*, and **(B)** *DCN* in all 9 scaffold groups at days 1, 4, 7, and 14. Data expressed as mean ± SEM (n=3). †: significantly ($p < 0.01$) different than scaffolds of same pore size with lowest (1:1:5) crosslinking density. ‡: significantly ($p < 0.01$) different than scaffolds of same pore size with middle (5:2:5) crosslinking density. *: significantly ($p < 0.01$) different from scaffolds of same crosslinking density with largest pore size (-10°C T_f). #: significantly ($p < 0.01$) different from scaffolds of same crosslinking density with middle pore size (-40°C T_f). ∨: significantly ($p < 0.01$) lower than expression at previous time point within group. ^: significantly ($p < 0.01$) than expression at previous time point within group.

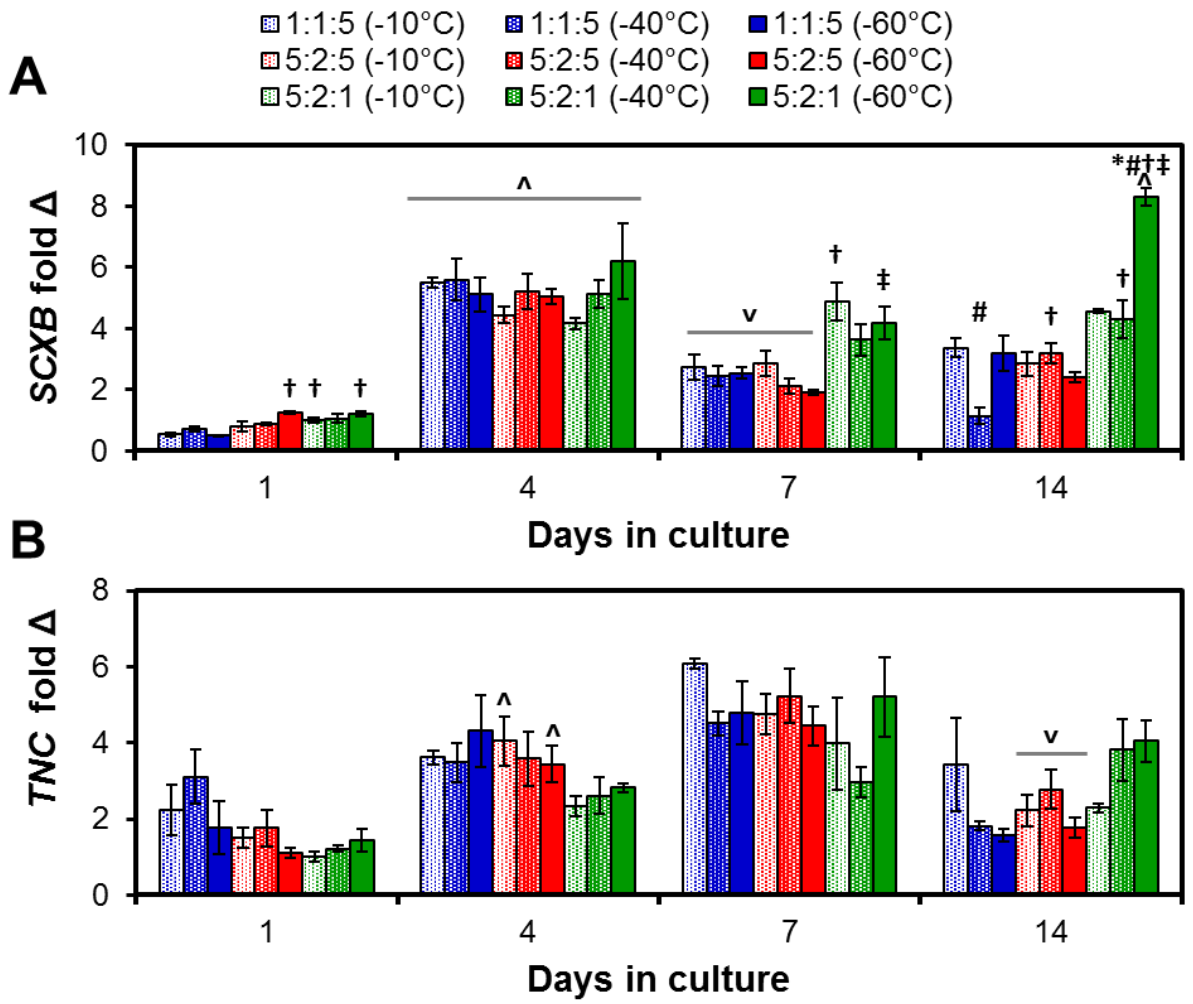

Figure 2.7: **Tendon phenotype gene expression**. Expression levels of **(A)** *SCXB* and **(B)** *TNC* in all 9 scaffold groups at days 1, 4, 7, and 14. Data expressed as mean ± SEM (n=3). †: significantly ($p < 0.01$) different than scaffolds of same pore size with lowest (1:1:5) crosslinking density. ‡: significantly ($p < 0.01$) different than scaffolds of same pore size with middle (5:2:5) crosslinking density. *: significantly ($p < 0.01$) different from scaffolds of same crosslinking density with largest pore size (-10°C T_f). #: significantly ($p < 0.01$) different from scaffolds of same crosslinking density with middle pore size (-40°C T_f). ∨: significantly ($p < 0.01$) lower than expression at previous time point within group. ^: significantly ($p < 0.01$) than expression at previous time point within group.

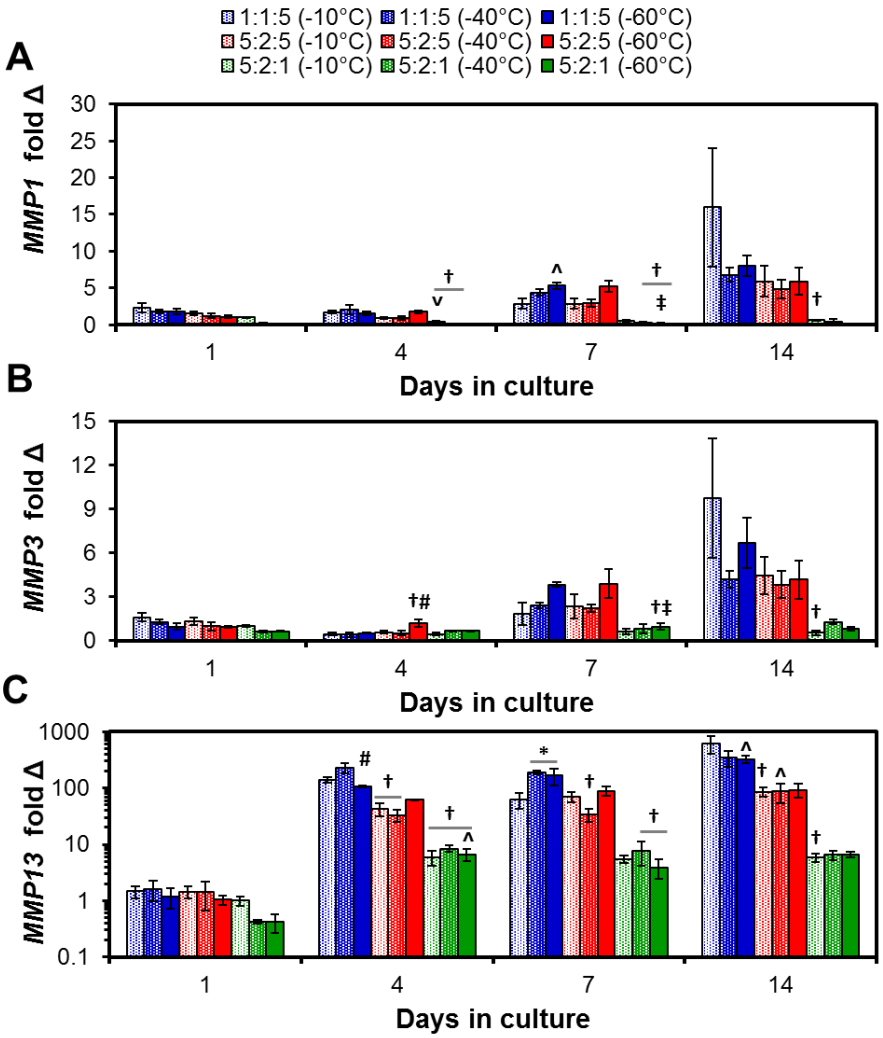

Figure 2.8: **MMP gene expression.** Expression levels of **(A)** *MMP1*, **(B)** *MMP3*, and **(C)** *MMP13* in all 9 scaffold groups at days 1, 4, 7, and 14. Data expressed as mean ± SEM (n=3). †: significantly ($p < 0.01$) different than scaffolds of same pore size with lowest (1:1:5) crosslinking density. ‡: significantly ($p < 0.01$) different than scaffolds of same pore size with middle (5:2:5) crosslinking density. *: significantly ($p < 0.01$) different from scaffolds of same crosslinking density with largest pore size (-10°C T_f). #: significantly ($p < 0.01$) different from scaffolds of same crosslinking density with middle pore size (-40°C T_f). ∨: significantly ($p < 0.01$) lower than expression at previous time point within group. ^: significantly ($p < 0.01$) than expression at previous time point within group.

CHAPTER 3: CYCLIC TENSILE STRAIN ENHANCES HUMAN MESENCHYMAL STEM CELL Smad 2/3 ACTIVATION AND TENOGENIC DIFFERENTIATION IN ANISOTROPIC COLLAGEN-GLYCOSAMINOGLYCAN SCAFFOLDS[3]

3.1 Chapter overview

In this chapter, the influence of intermittent cyclic tensile strain on the tenogenic differentiation potential of MSCs in aligned CG scaffolds is explored using a custom bioreactor system. The initial work focused on the design and fabrication of a bioreactor that is suitable for the use with porous 3D materials. Then, the immediate impact of cyclic tensile strain on MSC-scaffold interactions and mechanotransduction pathway activation were evaluated in order to validate an appropriate loading paradigm for extended culture. The validated loading paradigm was then applied over the course of a 7-day experiment and the resulting impact on cellular activity, tenogenic differentiation, and Smad pathway activation are assessed.

3.2 Introduction

Tendon and ligament injuries pose a significant challenge for medical professionals, affecting a wide range of individuals, from athletes to the elderly, with more than 32 million occurrences every year in the US alone (James, Kesturu et al. 2008; Liu, Ramanath et al. 2008; Xu and Murrell 2008; Breidenbach, Gilday et al. 2013). While not all injuries require surgical intervention, many classes of these injuries, such as rotator cuff and Achilles tendon tears, account for more than 100,000 surgeries per year in the US (Vitale, Vitale et al. 2007; Pedowitz and Kirwan 2013) and can show wide ranges of re-failure rates based on patient demographics (Galatz, Sandell et al. 2006). Tendon and ligament defects generally display poor intrinsic healing properties, requiring

[3] This chapter has been adapted from the following publication:
Grier, W. G., A. S. Moy, et al. (2017). "Cyclic tensile strain enhances human mesenchymal stem cell Smad 2/3 activation and tenogenic differentiation in anisotropic collagen-glycosaminoglycan scaffolds." European cells & materials 33: 227-239.

surgical intervention. These result in fibrous scar tissue formation with misaligned extracellular matrix (ECM) and inferior mechanical properties, leading to high rates of injury recurrence (James, Kesturu et al. 2008; Liu, Ramanath et al. 2008; Xu and Murrell 2008). As a result, tissue engineering solutions, particularly those that are able to address the geometrically aligned and mechanically dynamic nature of these tissues, are becoming researched at an increasing rate in order to address the shortcomings of current surgical procedures and to improve outcomes from injury.

Collagen-glycosaminoglycan (CG) scaffolds have been used in a wide variety of tissue engineering applications for skin, peripheral nerve, and cartilage tissue engineering, as well as 3D environments for *in vitro* studies of cell-matrix interactions (cell, migration and contraction) behavior (Yannas, Lee et al. 1989; Schulz Torres, M. Freyman et al. 2000; Harley, Spilker et al. 2004; O'Brien, Harley et al. 2005; Farrell, O'Brien et al. 2006; Harley, Freyman et al. 2007; Harley, Kim et al. 2008). We have recently developed a fabrication method to produce anisotropic CG scaffolds composed of an aligned ellipsoidal pore structure for applications in tendon repair (Caliari and Harley 2011). The anisotropic scaffold microstructure promotes cell alignment along the long axis of the ellipsoidal pores (Caliari and Harley 2011), resists tenocyte-mediated contraction and loss of tenogenic gene expression profiles (Caliari, Weisgerber et al. 2012; Grier, Iyoha et al. 2017), and promotes mesenchymal stem cell (MSC) elongation and differentiation towards a tenogenic phenotype in the absence of applied cyclic strain or exogenous growth (Caliari and Harley 2011; Caliari and Harley 2014). While promising, these initial findings suggested the need to improve the structural mechanics of the materials. By incorporating structural reinforcement elements, one can make the scaffold more mechanically robust for in vivo applications (Mozdzen, Rodgers et al. 2016; Mozdzen, Vucetic et al. 2017). As a result, there is a

specific need to identify culture conditions to enhance tenogenic differentiation and promote extracellular matrix remodeling in order to ensure the scaffold would remain structurally competent and fully integrate into a wound repair site.

Mechanical stimulation has shown significant value in musculoskeletal tissue engineering applications. Matrix mechanical cues have shown to be important tools for altering stem cell differentiation profiles (Engler, Bacakova et al. 2004; Janmey and McCulloch 2007; Hao, Zhang et al. 2013). Of particular interest to tendon applications, mechanical force has been shown to be a critical element during development in the recruitment of scleraxis-expressing cells to the tendon-bone-junction enthesis (Schweitzer, Zelzer et al. 2010; Chen, Yin et al. 2012) as well as to promote rehabilitative healing of the enthesis after injury (Thomopoulos, Zampiakis et al. 2008; Galloway, Lalley et al. 2013). In addition to playing a role in development, mechanotransduction pathways activated through microstructural cues and applied mechanical stimulation can influence stem cell activation and differentiation. Substrate alignment and stiffness can activate canonical RhoA/ROCK1 and FAK pathways to promote MSC differentiation towards musculoskeletal lineages (Sarasa-Renedo, Tunç-Civelek et al. 2006; Xu, Song et al. 2011; Allen, Cooke et al. 2012; Xu, Song et al. 2012; Andalib, Lee et al. 2013; Kanazawa, Furumatsu et al. 2014). As a result of this increased focus on mechanical cues, bioreactors capable of providing mechanical strain to cell-seeded biomaterials are of particular interest in recent tendon and ligament tissue engineering applications. Here, applied cyclic tensile strain can promote the phosphorylation of ERK 1/2 via RhoA activation (Laboureau, Dubertret et al. 2004) and the upregulation of procollagen mRNA (Papakrivopoulou, Lindahl et al. 2004). As a result, many studies have focused on identifying strain profiles to prolong ERK 1/2 activation to promote cell-mediated ECM biosynthesis (Paxton, Hagerty et al. 2012). The p38 mitogen-activated protein kinase pathway inhibits ERK 1/2

activation (Papakrivopoulou, Lindahl et al. 2004; Weinbaum, Schmidt et al. 2013), suggesting an alternate target for promoting ECM biosynthesis. In the related area of biomaterial for ligament repair, *Paxton et al.* demonstrated that MSCs in fibrin hydrogels showed increased ERK 1/2 activation when exposed to an intermittent cyclic tensile strain paradigm where the constructs were subjected to 10% strain at 1 Hz for just 10 minutes every 6 hours (Paxton, Hagerty et al. 2012). Maximal re-activation and sustained activation of ERK 1/2 required 6 hour periods of rest after the initial application of strain, thought to be a mediated by residual phosphorylated p38 inhibiting ERK 1/2 re-phosphorylation.

The Smad 2/3 and Smad 1/5/8 pathways play a crucial role in the development of musculoskeletal tissues, primarily through regulating the action of the TGF-β and BMP family of growth factors on cell differentiation and activity (Miyazono 2000; Shi and Massague 2003; Maeda, Sakabe et al. 2011; Allen, Cooke et al. 2012). Activation of Smad 1/5/8 by BMP-2 plays an important role in MSC osteogenic differentiation while the activation of Smad 2/3 by TGF-β plays a critical role in tendon and ligament development (Towler and Gelberman 2006; Maeda, Sakabe et al. 2011; Shen, Gelberman et al. 2013). Recent work by *Berthet et al.* also showed activated Smad 3 binds to the Scleraxis (SCXB) and Mohawk (MKX) transcriptional regulators during tendon matrix development (Berthet, Chen et al. 2013). Efforts by the Alliston lab also reported that crosstalk between mechanical stimuli and growth factor supplementation could both activate Smad 1/5/8 as well as drive a feedback loop driven by subsequent endogenous growth factor production to enhance musculoskeletal differentiation (Allen, Cooke et al. 2012). And while the vast majority of this body of work has primarily employed 2D culture environment, it motivates new efforts to define linkages between the mechanical microenvironment of the cell, smad activation and

endogenous growth factor production, as well as subsequent stem cell differentiation and tissue development.

Here we describe the development of a bioreactor system to facilitate the culture and analysis of MSC-seeded collagen-GAG scaffolds under physiological levels of cyclic tensile strain (CTS). Based on a design previously described by *Levenston et al.* (Vanderploeg, Wilson et al. 2008; Doroski, Levenston et al. 2010), this bioreactor allows parallel culture of 24 distinct biomaterial constructs in individually isolated wells. Many early bioreactor systems employed clamps to grip and pull on the ends of cell-seeded materials (Bosworth, Rathbone et al. 2014), though many clamping approaches require the ends of the substrate to be crushed or significantly deformed to prevent slippage, which is not suitable for extended culture of porous biomaterial scaffolds. As a result, recent efforts have focused on the use of yarn or textile style biomaterials that show less deformation from clamps or can be looped or tied around loading posts (Paxton, Hagerty et al. 2012; Bosworth, Rathbone et al. 2014). Unfortunately, neither of these approaches lend themselves to use with porous biomaterials. *Temenoff et al.* recently described a potentially translatable approach where a hydrogel substrate was infiltrated into porous polymeric end blocks that could be securely griped within a bioreactor (Doroski, Levenston et al. 2010). Here, we used Polydimethylsiloxane (PDMS) to infiltrate both the ends of the CG scaffolds as well as porous, polymeric end blocks to facilitate immobilization of the porous CG scaffold within the bioreactor. We report the effect of cyclic tensile strain on activation of MSC mechanotransduction pathways as well as subsequent MSC proliferation and pro-tenogenic differentiation in extended culture in vitro.

3.3 Materials and Methods

All materials were purchased from Sigma-Aldrich (St Louis, MO) unless otherwise specified.

Fabrication of collagen-GAG scaffolds

Type 1 microfibrillar collagen from bovine tendon (Collagen Matrix Inc. Oakland, NJ) and chondroitin sulfate from shark cartilage (Sigma-Aldrich, St. Louis, MO) were homogenized in 0.05M acetic acid at a ratio of collagen to glycosaminoglycan at 11.25:1 (Yannas, Lee et al. 1989; Madaghiele, Sannino et al. 2008). Anisotropic scaffolds were fabricated via lyophilization using a previously described directional solidification approach (O'Brien, Harley et al. 2004; Caliari and Harley 2011). Briefly, degassed CG suspension was pipetted into wells (6mm diameter, 30mm deep) within in a polytetrafluoroethylene (PTFE) mold with a copper bottom that was then placed on a pre-cooled (-10^{o}C) freeze-dryer shelf (VirTis, Gardner, NY). The mismatch in thermal conductivity between the PTFE body and copper base of the mold promotes unidirectional heat transfer through the more conductive copper (Caliari and Harley 2011). The CG suspension was frozen at -10°C for 2h, and then sublimated at 0°C and 200mTorr to remove the ice crystals, resulting in a dry porous scaffold. Following lyophilization, scaffolds crosslinked via dehydrothermal (DHT) crosslinking in a 105°C oven (Welch, Niles, IL) under vacuum (<25torr) for 24 hours and then stored in a desiccator until use.

Bioreactor design

Inspired by a previous design from the Levenston lab (Doroski, Levenston et al. 2010), the cyclic tensile strain bioreactor system consisted of a sliding rake system that was controlled by a linear motor actuator and controller (**Fig. 3.1A**) (Pololu Corp. Las Vegas, NV). The motor was controlled using a custom C# program. A total of 24 modular wells were constructed with a static loading post at one end. The modular nature of the wells allows for easy adaptation to various scaffold

sizes and geometries. For static controls, a separate set of wells of identical geometry with two posts at a fixed distance was constructed. The ends of dry CG scaffolds were embedded into hollow end blocks fabricated via additive manufacturing that could be affixed to the static and loading posts within the bioreactor. In order to measure scaffold strain as a function of bioreactor settings, dry scaffolds were marked with black India Ink (Dick Blick Art Materials, Galesburg, IL) (**Fig. 3.1B**). Video was then taken while the bioreactor was in motion using a Canon EOS-5D Mark II SLR 21.1MP Digital Camera (Canon, Tokyo, Japan). Individual frames were then converted to grayscale image sequences and imported into ImageJ where the distance between each mark was then measured using the Object Tracker plugin. Overall strain was calculated by normalizing the distance between each point to the initial length and then averaging across the entire scaffold (**Fig. 3.1C**). Due to tolerances required to insert the scaffolds into the bioreactor, a discrepancy in applied system strain (movement of the sliding rake system) and resultant scaffold deformation was observed. Throughout the experiment, we will refer to the magnitude of applied strain as the movement of the sliding rake system.

Embedding scaffolds into loading blocks

Hollow end blocks were fabricated from acetyl-butyl-styrene (ABS) using a Makerbot Replicator 2X 3D printer (MakerBot Industries, Brooklyn, NY). One side of the end blocks was designed to fit over the loading posts of the bioreactor system (5 mm dia.) while the other end was open to allow for the ends of the scaffolds to be inserted (6 x 6 mm). End blocks were filled with a 5:1 solution of polydimethylsiloxane (PDMS): catalyst (Hisco Inc. Houston, TX). After allowing the PDMS to cure at 37°C for 45 minutes, 5 mm of one end of 25mm long CG scaffolds was inserted into the PDMS in the end block, then allowed to cure overnight at 37°C. This was then repeated with the opposite side of the scaffold, resulting in a 15 mm gauge length (**Fig 3.1B**).

Scaffold crosslinking

After embedding, scaffolds were immersed in 200-proof ethanol for 6 hours, followed by washing with phosphate-buffered saline (PBS) overnight. The scaffolds were then crosslinked via carbodiimide chemistry. Scaffolds were soaked in a solution of 1-ethyl-3-[3-dimethylaminopropyl] carbodiimide hydrochloride (EDC) and N-hydroxysulfosuccinimide (NHS) at a molar ratio of 5:2:1 EDC:NHS:COOH in PBS for 2hr at room temperature (Olde Damink, Dijkstra et al. 1996; Harley, Leung et al. 2007). After crosslinking, the scaffolds were washed twice in sterile PBS before seeding.

Critical point drying and SEM analysis

Scaffold microstructure was examined after carbodiimide crosslinking. First, each scaffold was dehydrated using a series of washes with ethanol from 10% to 100% concentration followed by subjection to critical point drying (CPD) using a Samdri-PVT-3D (Tousimis, Rockville, MD). The CPDD process replaces the ethanol with liquid CO_2, and held above 1072 PSI and 31°C allowing the CO_2 to be gently removed from the system as a gas with minimal structure deformation. The samples were then sectioned by cutting and mounted on carbon tape before sputter coating with a gold/palladium mixture. Imaging was then carried out with a Philips XL30 ESEM-FEG (FEI Company, Hillsboro, OR) at 5 kV with a secondary electron detector.

Human mesenchymal stem cell culture

Human bone marrow-derived MSCs were purchased from Lonza (Walkersville, MD). Cells from multiple lots originating from separate donors were combined to account for any donor-specific responses. The MSCs were cultured in a complete MSC growth medium, consisting of low-glucose Dulbecco's Modified Eagle Medium with 10 vol% MSC fetal bovine serum and 1 vol% antibiotic-

antimitotic (Thermo Fisher, Waltham, MA), at 37°C and 5% CO_2, fed twice a week, and used at passage 6 for all experiments.

Culture of MSC-seeded CG scaffolds

CG scaffolds embedded in end blocks (6 mm diameter, 15 mm gauge length) were seeded with MSCs using a previously validated static seeding method (O'Brien, Harley et al. 2005). Briefly, scaffolds were partially dried with Kimwipes and seeded with 3.0×10^5 MSCs per 60 μL media (3x20 μL drops along scaffold length) in the individual wells of the bioreactor system. Cells were allowed to attach for 1 hour before submerging in media; constructs were given an additional 24 hours before application of CTS to ensure cell attachment. Cell-seeded scaffolds in the CTS groups were subjected to continuous cyclic tensile strain (10% strain at 1 Hz) for 10 – 120 minutes to demonstrate the activation of mechanotransduction pathways. For extended culture examining MSC differentiation, scaffolds were subjected to intermittent CTS (10% strain, 1 Hz) for 10 minutes every 6 hours for up to 6 days using a protocol inspired by *Paxton et al.* (Paxton, Hagerty et al. 2012) to allow for sufficient cellular refractory period to ensure prolonged effects. Cell-seeded scaffolds were cultured at 37°C and 5% CO_2 and fed twice a week with complete MSC growth medium. For static controls, scaffolds were placed into a separate set of wells of identical geometry to the bioreactor but which contained two posts at a fixed distance equal to that of the bioreactor at rest. During the experiment, scaffolds were collected for further analysis immediately after the conclusion of a strain cycle by physically separating them from the end blocks by cutting.

Protein Extraction, gel electrophoresis, and immunoblotting

Following stretch, scaffolds were briefly washed in warm phosphate-buffered saline, blotted dry, and then submerged in RIPA buffer with 1/100 dilutions of protease and phosphatase II and III inhibitor cocktails and kept on ice for 30 minutes with regular agitation. Total protein

concentration was determined by the BCA assay kit (Pierce). For gel electrophoresis, 10 µg of protein from each sample was solubilized in an equal volume Laemmli sample buffer and heated to 90°C for 10 minutes. Total lysates were separated by tris-glycine gel electrophoresis on 4-20% gradient gels using a constant 150V for 90 minutes. Following electrophoresis, a semi-dry transfer was used to transfer proteins to a nitrocellulose membrane (GE Healthcare) at 15 V for 15 min. Membranes were then blocked for 1 hour in 5% milk in Tris-buffered-saline + 0.1% Tween (TBST). Membranes were incubated overnight at 4°C with the appropriate primary antibody in 5% bovine serum albumin in TBST. The membrane was then washed three times in TBST before incubation for 1 hour at room temperature with HRP-linked goat anti-rabbit IgG secondary antibody (1:5,000. Cell Signaling) in TBST. Antibody binding was then detected using SuperSignal West Pico or Femto Chemiluminescent Substrate (Thermo Fisher, Waltham, MA). After probing, membranes were stripped with OneMinute® Western Blot Stripping Buffer (GM Biosciences, Rockville, MD) and re-probed up to two times following the same protocol. Antibodies were purchased from Cell Signaling (Danvers, MA): ROCK1 (4035), FAK (3285), pFAK (3283), p38 (8690), p-p38 (9215), ERK 1/2 (4695), pERK 1/2 (4370), Smad 2/3 (8685), pSmad 2/3 (8828), Smad 1 (6944), pSmad 1/5/8 (9511), β-actin (4967). Imaging was carried out using an Imagequant LAS 4010 system (GE Healthcare) and ImageJ was used for band intensity quantification.

Quantifying cell number and metabolic activity

A previously described DNA quantification assay was used to determine the number of cells attached to the scaffold (Kim, Sah et al. 1988). Briefly, scaffolds were washed in PBS to remove unattached cells, placed in a papain solution to digest the scaffold and lyse the cells in order to expose their DNA, then incubated with a Hoechst 33258 dye (Invitrogen, Carlsbad, CA) to

fluorescently label double-stranded DNA. Fluorescence intensities (352/461 nm excitation/emission) from each sample were read using a fluorescence spectrophotometer (Tecan, Männedorf, Switzerland) and then compared to a standard curve created from known numbers of MSCs.

The mitochondrial metabolic activity of the MSCs within each scaffold was determined through the use of non-destructive alamarBlue® assay as previously described (Tierney, Duffy et al. 2013). Cell-seeded scaffolds were incubated in the alamarBlue solution (Invitrogen, Carlsbad, CA) with gentle shaking for 1 h. The reduction of resazurin in the solution by metabolically active cells to the fluorescent by-product resorufin was measured on a fluorescent spectrophotometer. Relative cell metabolic activity was determined from a standard curve generated from known cell numbers prior to seeding the scaffolds and reported as a percentage of the total number of seeded cells.

RNA isolation and real-time PCR

RNA was extracted from the MSC-seeded scaffolds at days 1, 4, 7, and 14, using an RNeasy Plant Mini kit (Qiagen, Valencia, CA). RNA was then was reverse transcribed to cDNA in a Bio-Rad S1000 thermal cycler using the QuantiTect Reverse Transcription kit (Qiagen, Valencia, CA) as previously described (Duffy, McFadden et al. 2011; Caliari, Weisgerber et al. 2012). Real-time PCR reactions were carried out in triplicate, using 10ng of cDNA and QuantiTect SYBR Green PCR kit (Qiagen, Valencia, CA) in a 7900HT Fast Real-Time PCR system (Carlsbad, CA). The primers used were consistent with previous studies, and were synthesized by Integrated DNA Technologies (Coralville, IA). The expression level of the following markers was quantified: collagen type I alpha 2 (*COLIA2*), collagen type III alpha 1 (*COL3A1*), cartilage oligomeric matrix protein (*COMP*), decorin (*DCN*), scleraxis (*SCXB*), tenascin-c (*TCN*), Mohawk homeobox (*MKX*), and glyceraldehyde 3-phosphate dehydrogenase (*GAPDH*) which was used as a house keeping

gene (**Table 3.1**). Results were generated using the ΔΔCt method and all results were expressed as fold changes normalized to the expression levels of MSCs at the time of seeding the scaffolds.

Statistical analysis

One-way analysis of variance (ANOVA) was performed on the western blot, metabolic activity, cell number, and gene expression data sets (independent variable: strain condition) followed by Tukey-honest significant difference *post hoc* tests. Significance was set at $p < 0.05$. All statistical analysis was performed in R. Scaffolds from three independent experiments were analyzed at each time point for all metrics. Error is reported in figures as the standard error of the mean unless otherwise noted.

3.4 Results

Identifying the duration of tensile strain required to activate MSC mechanotransduction pathways within CG scaffolds

We first examined whether the level of applied strain (5, 10, 15% strain) altered the activation of MSC mechanotransduction pathway, and found no significant difference in activation with level of tensile strain (data not shown). As a result, and inspired by previous studies showing optimal ligament cell response to 10% strain (Paxton, Hagerty et al. 2012), all subsequent studies were performed at 10% CTS. Initial activation of MSC mechanotransduction pathways in response to 10% CTS at 1 Hz were monitored for up to two hours of continuous strain application. ROCK1 expression was significantly reduced within 10 minutes of application of cyclic strain, and remained reduced for up to 2 hours of CTS (**Fig. 3.2A**). Maximal activation of ERK 1/2 was seen after 10 minutes of CTS stimulation, but was significantly reduced when CTS was maintained for longer time periods (30m – 2 h). The reduction in ERK 1/2 activation was associated with an increase in p38 activity starting by 30 minutes of CTS (**Fig. 3.2B**). In order to maximize ERK 1/2

activation for long-term, subsequent experiments used an intermittent strain paradigm with 10 minutes of CTS followed by 5 hours 50 minutes rest to facilitate recovery of baseline ERK 1/2 and p38 expression (Paxton, Hagerty et al. 2012).

Intermittent tensile strain alters MSC proliferation and metabolic activity

MSC metabolic activity and cell number were monitored over the course of 6 days of culture with and without CTS (10% strain, 1Hz, for 10 minutes every 6 hours). While not statistically significant ($p = 0.12$), MSCs subjected to CTS trended towards increased metabolic activity during the first three days of culture. However, by the end of the 6 days, there was no noticeable increase or decrease in the metabolic activity of the cell populations with or without CTS (**Fig. 3.3A**). While there were no significant changes in total cell number in the scaffolds between days 1 and 6 within either the Static or CTS cultures, Static cultures showed significantly greater total number of cells compared to CTS at day 6 (**Fig. 3.3B**) ($p < 0.01$), suggesting the metabolic activity per cell is enhanced in response to CTS throughout the experiment.

Cyclic tensile strain promotes activation of tendon-related genes

We subsequently examined expression levels of a series of tendon-phenotype related genes *TNC, MKX,* and *SCXB* over the course of the experiment. The tenogenic transcription factor *SCXB* was significantly upregulated as rapidly as 24 hours ($p = 0.017$) in response to CTS and was found to be more strongly expressed in CTS culture for the remainder of the experiment (**Fig. 3.4A**). Expression levels of the transcription factor *MKX* and tendon-associated glycoprotein *TNC* showed little difference between CTS and static groups at days 1 and 3 (**Fig. 3.4B,C**). While not always significant, expression levels for all three genes trended towards being increased after 6 days with CTS when compared to expression levels at day 1 with the effect of time significant for *MKX*.

Cyclic tensile strain promotes activation of ECM biosynthesis related genes

We subsequently examined the effect of CTS on the expression of tendon-associated matrix biosynthesis genes. Expression levels of the primary tendon matrix component *COL1A2* was similarly expressed between CTS and static culture throughout the duration of the 6-day culture (**Fig. 3.5A**). However, levels of *COL3A1*, a critical element of tendon healing due to its ability to catalyze formation of rapid crosslinks to stabilize the repair site (Liu, Yang et al. 1995), increased significantly after days 3 and 6 with CTS. By day 6 *COL3A1* expression was significantly higher in response to CTS versus static culture ($p = 0.024$) (**Fig. 3.5B**). *DCN*, a regulator of the assembly of collagen fibrils during tendon development (Zhang, Ezura et al. 2006), was found to increase at each time point in the anisotropic scaffolds, and expression was significantly higher after day 6 with CTS. (**Fig. 3.5C**). CTS also promoted higher expression levels of the tendon-associated matrix gene *COMP* at all three time points, especially at day 6 (**Fig. 3.5D**), where expression levels in the static control group were almost completely lost ($p < 0.001$).

Smad 2/3 pathway is activated in the presence of cyclic tensile strain

The activation of the Smad 2/3 and Smad 1/5/8 pathways in MSCs within the CG scaffold was evaluated after 24 hours of CTS and again after 6 days of culture. At day 6, expression levels of Smad 2/3 were significantly increased for MSCs within scaffolds cultured under CTS conditions (**Fig. 3.6A**). However, activation of the Smad 1/5/8 pathway was not significantly altered by the application of cyclic strain at the time points examined (**Fig. 3.6B**).

3.5 Discussion

Mechanical stimulation, in the form of cyclic tensile strain, has been shown to be a critical regulator in the development of the tendon enthesis and in the regulation of stem cell fate decisions (Murchison, Price et al. 2007; Blitz, Viukov et al. 2009; Pryce, Watson et al. 2009; Schweitzer,

Zelzer et al. 2010). Our group has recently described an approach to fabricate CG scaffolds with an anisotropic pore geometry that is suitable for tendon tissue engineering applications (Caliari and Harley 2011). While the porous anisotropic CG scaffolds have been previously shown to support both the stable culture of differentiated tenocytes (Caliari, Weisgerber et al. 2012; Grier, Iyoha et al. 2017) as well as to induce tenogenic differentiation of MSCs (Caliari and Harley 2014), this work focused on the development of a custom bioreactor system to facilitate studies on mechanical stimulation of human MSCs in porous anisotropic CG scaffolds. Previous work using a variety of 2D and 3D constructs has shown that a number of protein kinases are activated in mesenchymal stem cells in response to tensile strain (Banes, Tsuzaki et al. 1995; Wang, Miyazu et al. 2001; Arnoczky, Tian et al. 2002). In particular, ERK 1/2 is believed to play an important role in the stretch-activated increase in collagen production (Papakrivopoulou, Lindahl et al. 2004), making it an important target for development of tendon repair biomaterial. To examine the effect of CTS on MSC response within the CG scaffold, we developed a 24-well tensile strain bioreactor inspired by previous work of *Vanderploeg et al.* (Vanderploeg, Wilson et al. 2008) that allows us to isolate individual samples and/or media at intermediate time-points to evaluate a range of different metrics. The programmable nature of the linear actuator further allows for easily tunable culture conditions (strain amplitude, rate, durations; refractory period), and the modular design enables adaptation to fit a wide range of scaffold geometries. In order to facilitate attachment of scaffolds within the bioreactor, a method inspired by the Temenoff lab's procedure using end blocks to fix hydrogels between two posts was employed (Doroski, Levenston et al. 2010). By embedding the scaffold ends into hollow end blocks with PDMS, we were able to avoid scaffold deformation, tearing, or slippage as commonly seen with the traditional use of clamps.

This work concentrates on initial metrics of MSC response to applied cyclic strain for up to 6 days. While not long enough to demonstrate extensive matrix remodeling in response to CTS, it did allow us to define MSC protein kinase response to applied cyclic tensile strain, with results here using CG scaffolds consistent with the antagonistic roles of ERK1/2 and p38 seen in 2D and 3D biomaterials (Banes, Tsuzaki et al. 1995; Wang, Miyazu et al. 2001; Arnoczky, Tian et al. 2002). Indeed, our examination of MSC response within porous collagen scaffolds within a tensile bioreactor showed time-resolved activation of ERK1/2 and p38 on a time scale of 10 to 30 minutes, consistent with previous result for Achilles tendon fibroblasts in fibrin hydrogels as reported by *Paxton et al.* (Paxton, Hagerty et al. 2012). More significantly, we showed the combination of CTS and an anisotropic CG scaffold is sufficient to establish critical cellular signatures of early tendon development in MSCs. CTS did not lead to negative effects on cell proliferation, and in fact increased metabolic activity per cell. Further, gene expression levels of markers of early tenogenic development (*SCXB*, *TNC*, *MKX*) as well as tendon-associated extracellular matrix proteins (*COL3A1*, *COMP*, *DCN*) were all generally elevated after 6 days in culture with mechanical stimulation. Indeed, the significant drop in *COMP* expression in static culture suggests that not only can CTS provide significant positive influence on remodeling associated genes, but that a lack of tensile stimulation has significant negative effects on cell activity and remodeling potential over time. This upregulation of traditional tendon markers, when taken in combination with the increase in metabolic activity on a per cell basis, demonstrates that CTS promotes robust differentiation of metabolically active MSCs towards an early tendon phenotype on aligned CG scaffolds.

While previous work in our lab showed that an anisotropic microstructure was sufficient to drive initial tenogenic differentiation of MSCs within 7 days (Caliari and Harley 2014), the biomaterial

alone did not provide an adequate environment to promote robust expression of remodeling associated genes. With the development of this bioreactor system we show that intermittent cyclic tensile strain, when applied in an appropriate manner, can be used to improve MSC metabolic activity, enhance tenogenic differentiation, and show enhanced expression levels of key tendon-associated ECM compounds (*DCN*, *COMP*, *COL3A1*). However, the lack of increases in other matrix remodeling genes such as COL1A2 after 7 days suggest the need for longer bioreactor cultures in future experiments. Findings here also suggest opportunities to continue to explore the canonical vs. non-canonical activation of Smad2/3. While previous efforts have largely concentrated on 2D cell cultures, our efforts using anisotropic CG scaffolds also demonstrate preferential activation of Smad 2/3 and enhanced tenogenic differentiation within 6 days of CTS, a finding well-aligned with previously reported responses. Cytoskeletal tension and matrix mechanical signals are known critical factors for Smad activation and TGF-β production (Skutek, van Griensven et al. 2001; Allen, Cooke et al. 2012; Rys, Monteiro et al. 2016). Further, heightened ERK 1/2 activity is a known element of non-canonical Smad pathway activation (Hayashida, Decaestecker et al. 2003). Together, this suggests that CTS applied to MSC-seeded CG scaffolds may drive non-canonical Smad activity via enhanced ERK 1/2 activation, leading to tenogenic differentiation as well as the endogenous production of TGF-β family growth factors which may then lead to canonical Smad2/3 activation and enhanced tenogenic differentiation. While the presence of such an autocatalytic feedback loop is not the subject of this project, ongoing efforts are now employing the bioreactor system developed and validated here to better elucidate the relationship between CTS, TGF-β associated growth factor signaling, Smad activation, and the role that these pathways play in the regulation of musculoskeletal tissue development. Such efforts

will also allow for a more focused approach to develop long-term culture systems to study in vitro scaffold remodeling and more mature tendon development.

3.6 Conclusions

This work demonstrates the use of a custom-designed cyclic tensile strain bioreactor to mechanically stimulate human MSCs in anisotropic CG scaffolds as a means to enhance proliferation and tenogenic differentiation. Intermittent CTS (10% applied strain, 1Hz, 10 minutes every 6 hours) was found to rapidly, stably upregulate mechanosensitive protein kinase activity. MSCs showed increased gene expression profiles of a range of tendon-related ECM proteins and phenotypic markers in response to CTS over the course of the experiment in the presence of applied CTS. Interestingly, we also found that Smad 2/3, but not Smad 1/5/8, was preferentially activated in MSCs exposed to extended CTS. This work demonstrates a pathway to refine mechanical stimulation protocols to enhance tenogenic differentiation and matrix biosynthesis for tendon repair applications. Given the design of the bioreactor that affords separate culture of each specimen, these findings also highlight significant opportunities to further define the role played by CTS on the endogenous production of growth factors that may further refine MSC differentiation and matrix biosynthesis.

3.7 Table

Table 3.1 PCR primer sequences.

Transcript	Sequence	Reference
COL1A2	Forward: 5'- TGACCTCAAGATGTGCCACT -3' Reverse: 5'- ACCAGACATGCCTCTTGTCC -3'	(Pauly, Klatte et al. 2010)
COL3A1	Forward: 5'- GCTGGCATCAAAGGACATCG -3' Reverse: 5'- TGTTACCTCGAGGCCCTGGT -3'	(Pauly, Klatte et al. 2010)
COMP	Forward: 5'- GCAACACGGACGAGGACAAG -3' Reverse: 5'- CGCCATCACTGTCCTTCTGG -3'	(Klatte-Schulz, Pauly et al. 2013)
DCN	Forward: 5'- CGCCTCATCTGAGGGAGCTT -3' Reverse: 5'- TACTGGACCGGGTTGCTGAA -3'	(Pauly, Klatte et al. 2010)
SCXB	Purchased from Qiagen (sequence unavailable)	(Caliari and Harley 2014)
MKX	Forward: 5'- CGTATTGGAAGGAGATCAACG -3' Reverse: 5'- GGACGACTTCTGGATGATGC -3'	(Lorda-Diez, Canga-Villegas et al. 2013)
TNC	Forward: 5'- TTCACTGGAGCTGACTGTGG -3' Reverse: 5'- TAGGGCAGCTCATGTCACTG -3'	(Pauly, Klatte et al. 2010)
GAPDH	Forward: 5'- CCATGAGAAGTATGACAACAGCC -3' Reverse: 5'- CCTTCCACGATACCAAAGTTG -3'	(Pauly, Klatte et al. 2010)

3.8 Figures

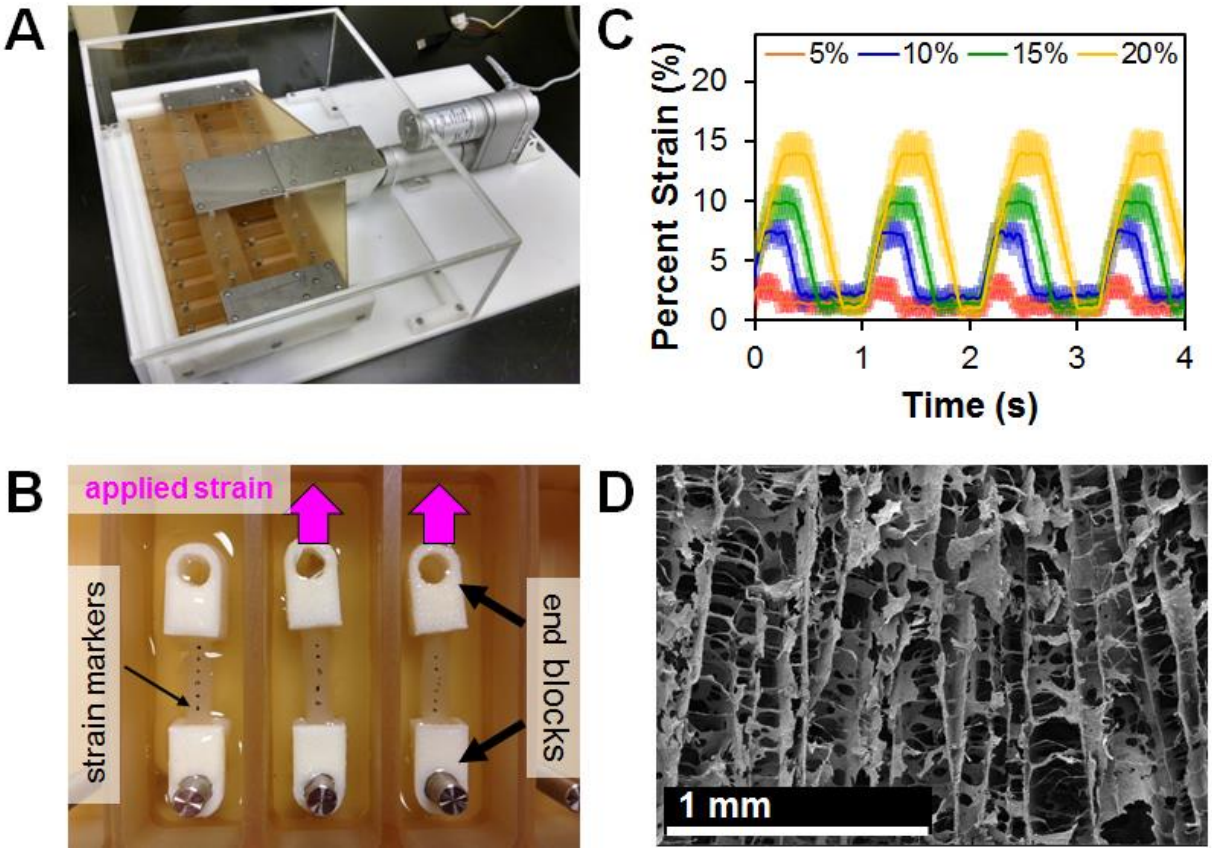

Fig. 3.1 Custom cyclic strain bioreactor. (A) Custom bioreactor designed with 24 individual wells with static loading posts and moveable rake controlled by a programmable linear actuator. **(B)** Scaffolds (with fiduciary marks) embedded into hollow PLA end-blocks that can be attached on either end to the static loading post and movable rake within the bioreactor. **(C)** Superimposition of measured scaffold deformation in response to a range of system applied cyclic strain amplitudes (5 – 20%, all 1 Hz). Scaffold deformation is shown as mean ± SEM. **(D)** SEM image of aligned scaffold pore microstructure. Scale bar: 1 mm.

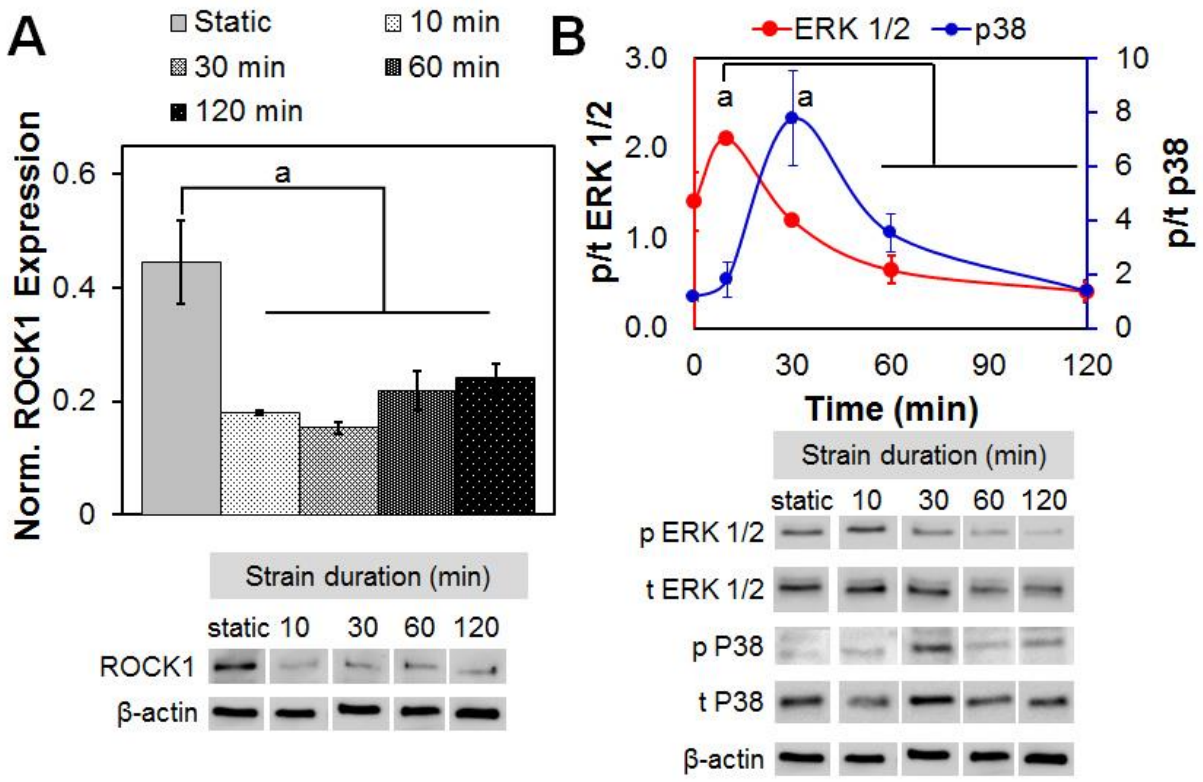

Fig. 3.2 Rapid activation of mechanotransduction pathways with applied cyclic tensile strain. **(A)** Expression of ROCK1 normalized to β-actin expression as a function strain cycle duration is rapidly down regulated in response to CTS (all at 10% strain, 1 Hz). **(B)** MSCs in CG scaffolds showed a sequential increase in the ratio of active (phosphorylated) to total protein for ERK 1/2 (p/t ERK1/2) and then p38 MAPK (p/t p38), normalized to the ratio seen under static conditions, as a function of increasing time of applied CTS (10% applied system strain, 1 Hz). Data expressed as mean ± SEM (n = 3). [a] Significantly higher expression ($p < 0.05$) than other time points.

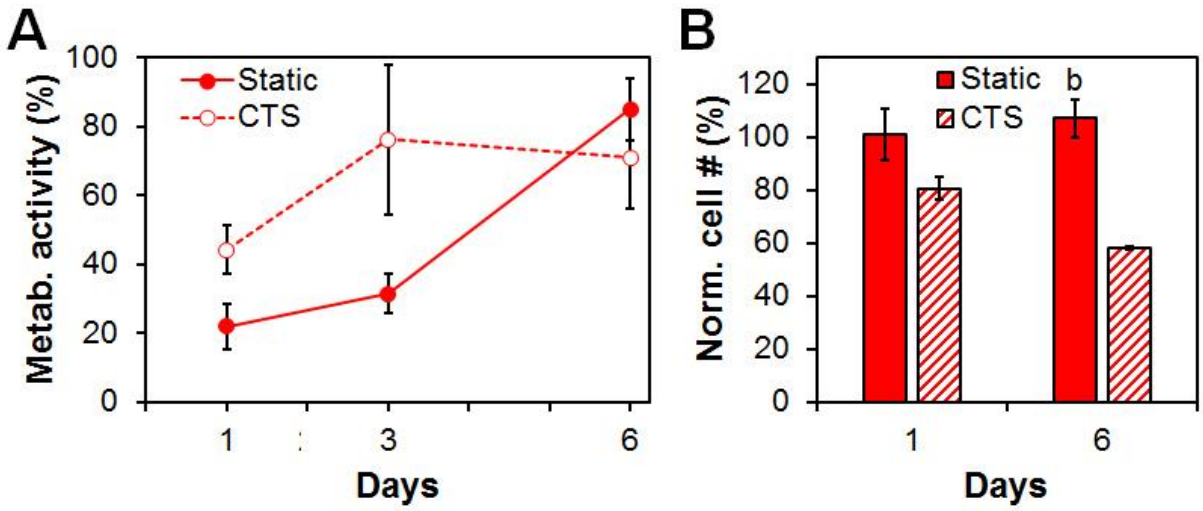

Fig. 3.3 MSC viability in CG scaffolds undergoing CTS. (A) Metabolic activity of MSCs in CG scaffolds in either static culture or exposed to repeated cycles of CTS (10min at 10% strain and 1 Hz) followed by 5 hours 50 minutes recovery at days 1, 3, and 6. **(B)** Normalized number of cells (relative to number initially seeded) at days 1 and 6 in both static and CTS groups. Data expressed as mean ± SEM (n = 3). [b] Significantly higher ($p < 0.05$) than CTS group at same day.

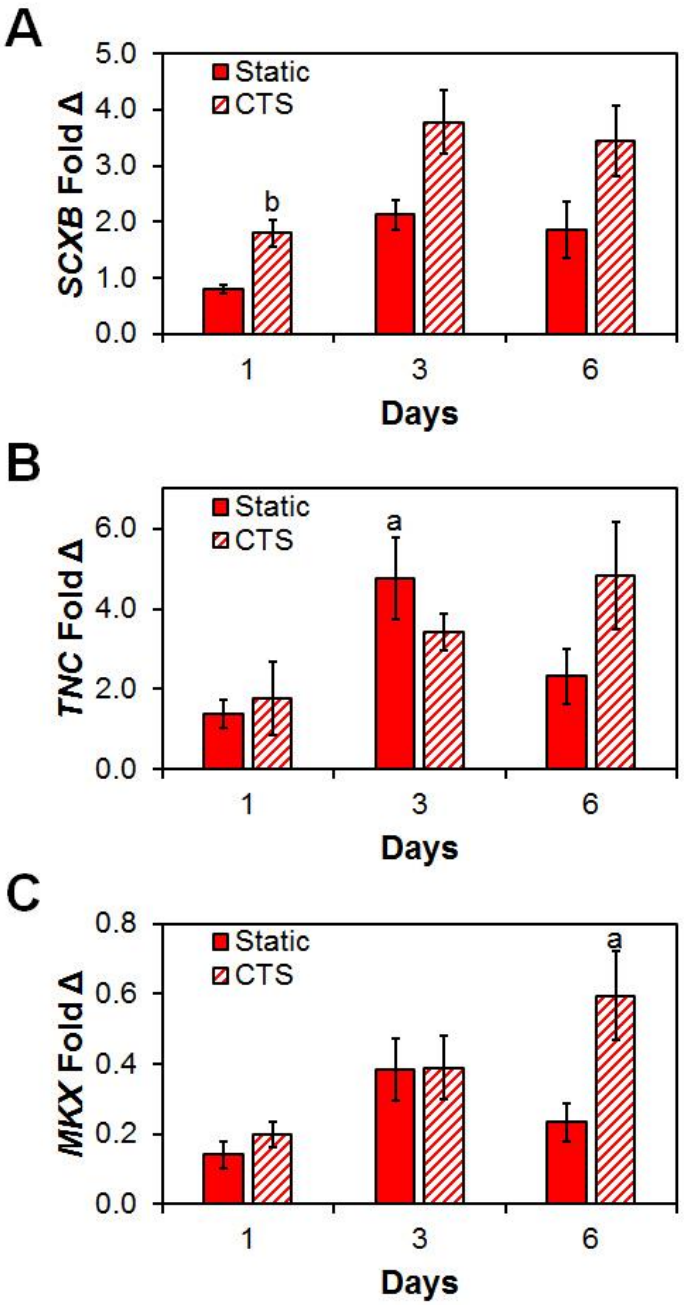

Fig. 3.4 Changes on pro-tenogenic gene expression profiles in response to CTS. Expression levels of **(A)** *SCXB*, **(B)** *TNC*, and **(C)** *MKX* at days 1, 3, and 6 relative to cells at the time of seeding in both static and CTS groups. Data expressed as mean ± SEM (n = 3). [b] Significantly higher ($p < 0.05$) than static group at same day. [a] Significantly higher expression ($p < 0.05$) than day 1 within the same group.

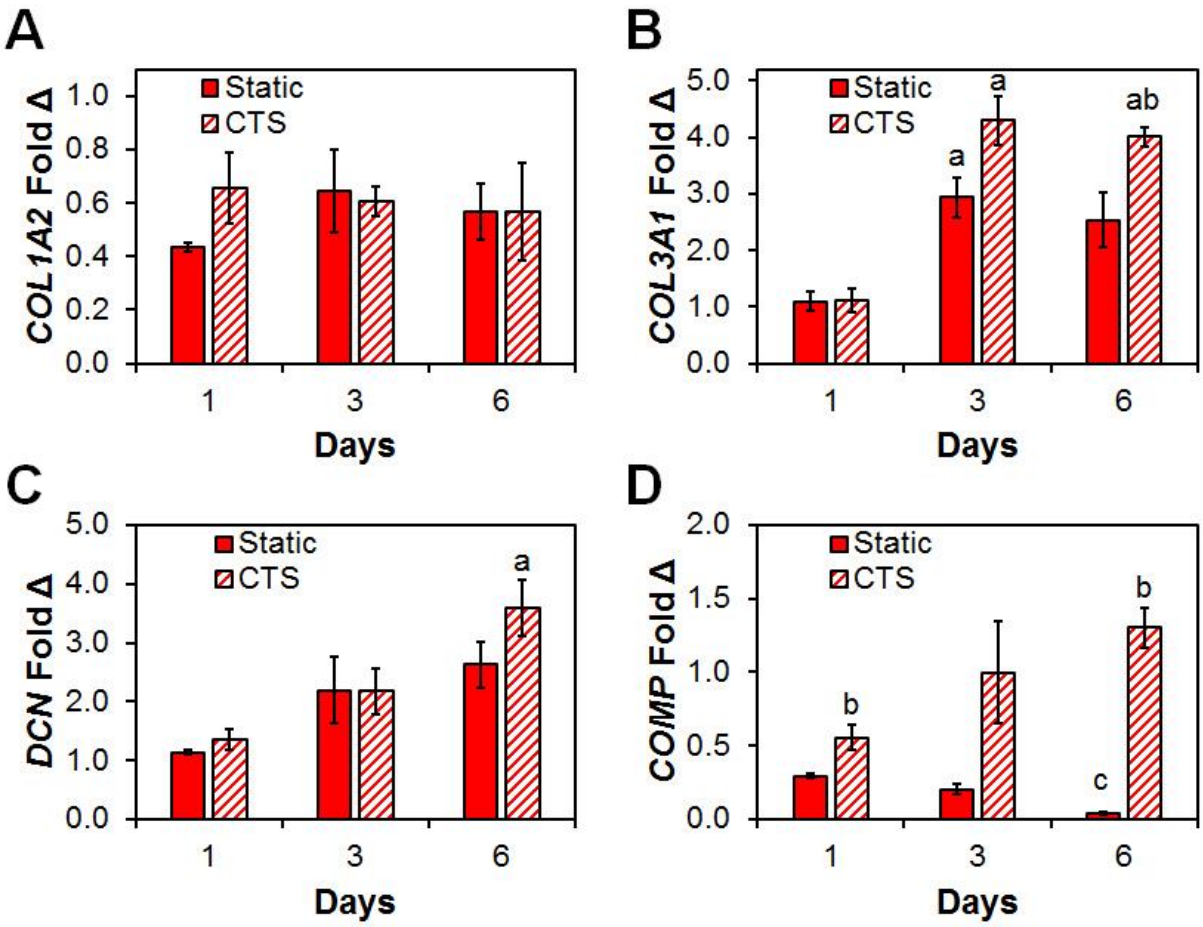

Fig. 3.5 Changes in structural protein gene expression in response to CTS. Expression levels of **(A)** *COL1A2*, **(B)** *COL3A1*, **(C)** *DCN*, and **(D)** *COMP* at days 1, 3, and 6 relative to cells at the time of seeding in both static and CTS groups. Data expressed as mean ± SEM (n = 3). [b] Significantly higher ($p < 0.05$) than static group at same day. [a] Significantly higher expression ($p < 0.05$) than day 1 within the same group. [c] Significantly lower expression ($p < 0.05$) than both day 1 and day 3 within the same group.

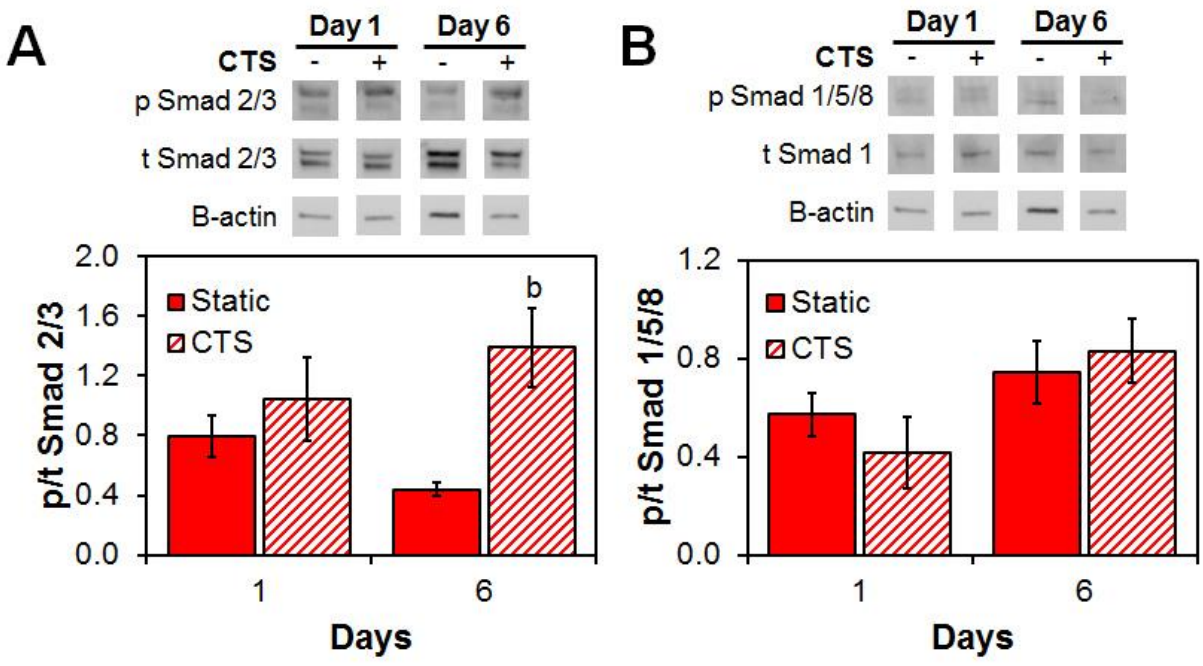

Fig. 3.6 Differences in the activation of canonical vs. non-canonical Smad pathways for MSCs within the CG scaffold in response to CTS. Relative phosphorylation of **(A)** the non-canonical Smad 2/3 and **(B)** the canonical Smad 1/5/8 at days 1 and 6 as determined by immunoblot. Data expressed as mean ± SEM (n = 3). [b] Significantly higher ($p < 0.05$) than static group at same day.

CHAPTER 4: THE INFLUENCE OF CYCLIC TENSILE STRAIN ON MULTI-COMPARTMENT COLLAGEN-GAG SCAFFOLDS FOR SPATIAL CONTROL OF MSC LINEAGE SELECTION[4]

4.1 Chapter overview

In chapters 2 and 3, we evaluated the use of single-compartment CG scaffolds with anisotropic pore structures for applications in tendon tissue engineering. Here, we apply the knowledge gained regarding cyclic tensile strain to multi-compartment scaffolds with distinct regions of structural anisotropy and mineral content designed for tendon-bone junction regeneration. The application of strain across a spatially-graded material results in variations in local strain profiles corresponding to the mechanics of each compartment. The local effects of strain in combination with local material properties are evaluated for alterations in the differentiation potential of MSCs in an effort to reproduce the organization of the native tendon-bone junction.

4.2 Introduction

The tendon-bone junction (TBJ), or enthesis, is a complex stratified region that functionally integrates tendon to bone to provide a smooth transition between the two dissimilar tissues (Moffat, Wang et al. 2009; Yang and Temenoff 2009). The aligned and elastic structure of tendon makes it very strong under tensional loads while the increased stiffness and mineral content of bone are more optimized for compressive loading. As a result, the interface between these two tissues are sites of high stress concentrations (Shaw and Benjamin 2007). In order to effectively dissipate these high stress concentrations while maintaining structural integrity, the TBJ displays opposing gradients in structural organization via collagen alignment and mineralization (Genin, Kent et al.

[4] This chapter has been adapted from the following publication:
Grier, W.K. M.D. Ramsey et al. (submitted). "The influence of cyclic tensile strain on multi-compartment collagen-GAG scaffolds for tendon-bone junction regeneration."

2009; Lu and Thomopoulos 2013). Nevertheless, certain TBJs, such as in the rotator cuff, are prone to a variety of chronic and acute injuries. Unfortunately, the intricate nature of the enthesis is not naturally regenerated following surgical repair, which is characterized by the formation of disorganized scar tissue, resulting in high rates of recurrence (Lu and Thomopoulos 2013; Font Tellado, Balmayor et al. 2015). Improved techniques for the regeneration of the full spectrum of tendon-to-bone need to be developed with the future potential for the regeneration of a functional interface.

Tissue engineering is an attractive strategy to improve on current standards for tissue interface regeneration. The extracellular matrix (ECM) environment in which a cell resides has been shown to be critical for tissue development by influencing cell proliferation, morphology, adhesion, and differentiation (Engler, Bacakova et al. 2004; Dalby, Gadegaard et al. 2014). Thus, many groups have developed biomaterial systems that mimic components of the native ECM across various orthopedic interfaces. The Gibson Group has previously developed a layered scaffold with distinct regions of mineral content and porous microstructure for osteochondral repair. (Harley, Lynn et al. 2010; Harley, Lynn et al. 2010; Lynn, Best et al. 2010). A number of groups have developed polymeric biomaterial systems specifically for the tendon-bone interface with either gradients of mineral content (Lipner, Liu et al. 2014), or multiphase materials with separate regions for tendon, bone, and interface regeneration (Spalazzi, Dagher et al. 2008; Font Tellado, Bonani et al. 2017).

Collagen-glycosaminoglycan (CG) materials are composed of natural ECM components and have shown great promise as tissue engineering scaffolds. Initially developed for a clinical dermal regeneration template, porous CG scaffolds are fabricated by freeze-drying acidic suspensions of type I collagen and glycosaminoglycans (Yannas, Lee et al. 1989). CG scaffolds have since been developed for a wide range of applications, including nerve (Chamberlain, Yannas et al. 2000),

cartilage (Vickers, Gotterbarm et al. 2010), and tendon (Caliari and Harley 2011; Caliari, Weisgerber et al. 2012). Calcium phosphate-mineralized variants have also been employed for bone applications (Harley, Lynn et al. 2010; Lee, Pereira et al. 2015; Ren, Bischoff et al. 2015; Weisgerber, Caliari et al. 2015; Ren, Tu et al. 2016; Ren, Weisgerber et al. 2016). By combining directional solidification and liquid cy-synthesis techniques we have previously developed a multi-compartment CG scaffold with distinct regions of structural anisotropy and mineral content with a continuous interface for TBJ regeneration (Caliari, Weisgerber et al. 2015). This material system was shown to promote the initial signs of spatially-selective tenogenic and osteogenic differentiation of human mesenchymal stem cells (MSCs), indicating that would be a promising candidate for future studies to regenerate the full spectrum from tendon to bone.

While CGCaP scaffold variants alone have been shown to be sufficient for the robust regeneration of bone tissue (Ren, Bischoff et al. 2015), structural anisotropy can only drive an initial tenogenic response from MSCs. Generally, soluble growth factors have been required in order to induce a strong tenogenic response (Caliari and Harley 2014; Holladay, Abbah et al. 2014; Jiang, Gao et al. 2016). Growth factors present complications for clinical applications due to their prohibitive cost, dosage requirements, and off-target effects (Lyons, Gleeson et al. 2014; Quinlan, Thompson et al. 2015). As an alternative, many groups have explored the use of alternate treatment strategies, such as the application of low-amplitude cyclic tensile strain (CTS), in order to reproduce the unique mechanical environment of tendons for a more robust differentiation profile (Doroski, Levenston et al. 2010; Paxton, Hagerty et al. 2012; Bosworth, Rathbone et al. 2014; Govoni, Muscari et al. 2016).

Mechanical force has been shown to be important during the development of the TBJ (Schweitzer, Zelzer et al. 2010; Chen, Yin et al. 2012), as well as to promote rehabilitative healing of the

enthesis after injury (Thomopoulos, Zampiakis et al. 2008; Galloway, Lalley et al. 2013). Exposure to mechanical strain has been shown to lead to the phosphorylation of ERK 1/2 mitogen-activated protein kinase (MAPK) pathway via the activation of RhoA (Laboureau, Dubertret et al. 2004). The increased activity of ERK 1/2 has been shown to lead to the upregulation of procollagen mRNA (Papakrivopoulou, Lindahl et al. 2004). As a result, a number of tissue regeneration studies have focused on identifying strain paradigms to maximize ERK 1/2 activation in order to promote cell-mediated ECM deposition and remodeling (Paxton, Hagerty et al. 2012). The p38 MAPK pathway is known to inhibit ERK 1/2 activation after extended exposure to strain (Papakrivopoulou, Lindahl et al. 2004; Weinbaum, Schmidt et al. 2013), suggesting the need to use an intermittent strain paradigm to best promote ECM biosynthesis. *Paxton et al.* have previously demonstrated that tendon fibroblasts seeded in fibrin hydrogels showed increased ERK 1/2 activation when exposed to an intermittent cyclic tensile strain paradigm (10% strain at 1 Hz for just 10 minutes every 6 hours) for ligament engineering applications (Paxton, Hagerty et al. 2012). We have recently reported on the use of a CTS bioreactor system with a similar strain paradigm to promote increased tenogenic differentiation through the activation of growth factor-associated pathways and upregulation of tendon-specific gene markers of MSCs on anisotropic CG scaffolds (Grier, Moy et al. 2017).

Here, we integrate our previous work in multi-compartment CG biomaterials and CTS bioreactor systems to show that the application of an intermittent strain paradigm can elicit compartment-specific cellular responses. The discrepancy in stiffness between the anisotropic and mineralized compartments results in the total scaffold strain being primarily distributed over the softer non-mineralized region. Thus, it is expected that the effects of the CTS will be more pronounced in the regions with higher local strain. Additionally, the application of a dynamic loading profile may

lead to the preliminary development of an enthesis phenotype at the interface between the two compartments. We report the combined effects of cyclic tensile strain and scaffold microstructure and composition on spatially-selective MSC proliferation, mechanotransduction pathway activation, and differentiation in extended *in vitro* culture.

4.3 Materials and Methods

All materials were purchased from Sigma-Aldrich (St Louis, MO) unless otherwise specified.

Preparation of collagen suspensions

Two types of collagen suspensions were prepared. The first CG suspension consisted of 1 w/v% type 1 microfibrillar collagen from bovine tendon (Collagen Matrix Inc. Oakland, NJ) and heparin from porcine intestinal mucosa (Sigma-Aldrich, St. Louis, MO) were homogenized in 0.05M acetic acid at a ratio of collagen to glycosaminoglycan at 11.25:1 (Yannas, Lee et al. 1989; Madaghiele, Sannino et al. 2008). Next, a collagen-glycosaminoglycan-calcium phosphate (CGCaP) suspension was made by adding calcium salts ($Ca(OH)_2$, $Ca(NO_3)_2{\cdot}4H_2O$) to the collagen and heparin and by substituting phosphoric acid as the solvent (Harley, Lynn et al. 2010; Lynn, Best et al. 2010). Both suspensions were homogenized at 12000 rpm and 4°C to prevent collagen denaturation as previously described (Yannas, Lee et al. 1989; O'Brien, Harley et al. 2004). Following homogenization suspensions were stored overnight at 4°C and degassed prior to use.

Multi-compartment scaffold fabrication via freeze-drying

Multi-compartment scaffolds were fabricated by combining a previously described directional solidification approach (O'Brien, Harley et al. 2004; Caliari and Harley 2011) with a liquid-phase co-synthesis method (Harley, Lynn et al. 2010). First, degassed CG suspension was pipetted into wells (6mm diameter, 30mm deep) within in a polytetrafluoroethylene (PTFE) mold with a copper

bottom. Then, CGCaP suspension was carefully layered on top of the CG suspension in the mold in a 1:1 volume ratio **(Fig. 4.1A)**. The mold was then placed on a freeze-dryer shelf (VirTis, Gardiner, NY) precooled to -10°C and maintained at this temperature for 2 h to complete freezing. The mismatch in thermal conductivity between the PTFE body and copper base of the mold promotes unidirectional heat transfer through the more conductive copper (Caliari and Harley 2011). Following the freezing step, the frozen suspensions were then sublimated at 0°C and 200mTorr to remove the ice crystals, resulting in a dry porous scaffold with a distinct mineralized CGCaP and aniostropically-aligned CG compartments with a continuous interfacial region **(Fig. 4.1B)**. Following lyophilization, a guide was used to trim the ends of each scaffold equidistant from the interface to a total length of 25 mm. The scaffolds were then stored in a desiccator until use.

Embedding scaffolds into loading blocks

As previously described (Grier, Moy et al. 2017), hollow end blocks were fabricated from acetyl-butyl-styrene (ABS) using a Makerbot Replicator 2X 3D printer (MakerBot Industries, Brooklyn, NY). One side of the end blocks was designed to fit over the loading posts of the bioreactor system (5 mm dia.) while the other end was open to allow for the ends of the scaffolds to be inserted (6 x 6 mm). End blocks were filled with a 5:1 solution of polydimethylsiloxane (PDMS): catalyst (Hisco Inc. Houston, TX). After allowing the PDMS to cure at 37°C for 45 minutes, 5 mm of one end of 25mm long CG scaffolds was inserted into the PDMS in the end block, then allowed to cure overnight at 37°C. This was then repeated with the opposite side of the scaffold, resulting in a 15 mm gauge length. A group of 6 scaffolds was set aside and marked with black India Ink (Dick Blick Art Materials, Galesburg, IL) to be used for strain analysis.

Scaffold hydration and crosslinking

Scaffolds were immersed in 200-proof ethanol for 6 hours, followed by washing with phosphate-buffered saline (PBS) overnight. The scaffolds were then crosslinked via carbodiimide chemistry. Scaffolds were soaked in a solution of 1-ethyl-3-[3-dimethylaminopropyl] carbodiimide hydrochloride (EDC) and N-hydroxysulfosuccinimide (NHS) at a molar ratio of 5:2:1 EDC:NHS:COOH in PBS for 2 hours at room temperature (Olde Damink, Dijkstra et al. 1996; Harley, Leung et al. 2007). After crosslinking, the scaffolds were washed twice in sterile PBS. Scaffolds designated for cell-seeding were soaked in complete MSC growth media, consisting of low-glucose Dulbecco's Modified Eagle Medium with 10 vol% MSC fetal bovine serum and 1 vol% antibiotic-antimitotic (Thermo Fisher, Waltham, MA), for 72 hours prior to seeding.

Critical point drying and SEM analysis

Scaffold microstructure was examined after crosslinking. First, each scaffold was dehydrated using a series of brief washes with ethanol from 10% to 100% concentration followed by subjection to critical point drying (CPD) using a Samdri-PVT-3D (Tousimis, Rockville, MD). The CPD process first replaces the ethanol with liquid CO_2, and then holds the sample above 1072 PSI and 31°C allowing the CO_2 to be gently removed from the system as a gas, minimizing any structural deformation. The samples were then sectioned and mounted on carbon tape prior to sputter coating with a gold/palladium mixture. Imaging was then carried out with a Philips XL30 ESEM-FEG (FEI Company, Hillsboro, OR) at 5 kV with a secondary electron detector.

Bioreactor design

The cyclic tensile strain bioreactor used in this study was previously described for use with monolithic anisotropic CG scaffolds for tendon regeneration (Grier, Moy et al. 2017). Inspired by a previous design from the Levenston lab (Doroski, Levenston et al. 2010), the main system

consists of 24 loading and 24 stationary wells, a moveable rake, and a linear actuator and controller that are integrated with a custom C# program (**Fig. 4.2A**) (Pololu Corp. Las Vegas, NV). One end block on each scaffold was placed over the stationary loading post in each well while the other end block was interfaced with the rake. The high stiffness of the end blocks compared to the hydrated scaffolds allowed for the strain to be completely distributed along the length of the scaffold (Grier, Moy et al. 2017). For static controls, a separate set of wells with identical geometry to the bioreactor was constructed. These wells contained two posts at a fixed distance equal to that of the bioreactor at rest (**Fig. 4.2B**). In order to measure local scaffold strain as a function of bioreactor settings, the scaffolds that had been marked with India Ink were placed into the system. Video was then taken while the bioreactor was set to a 5% system strain at 1 Hz using a Canon EOS-5D Mark II SLR 21.1MP Digital Camera (Canon, Tokyo, Japan). Individual frames were then converted to grayscale image sequences and imported into ImageJ where the distance between each mark was then measured using the Object Tracker plugin. Overall strain was calculated by normalizing the distance between each point to the initial length and then averaging across the entire scaffold. Groups of points within each compartment were analyzed in order to determine compartment specific strain (**Fig. 4.2C**). Due to tolerances required to insert the scaffolds into the bioreactor, a discrepancy in applied system strain (movement of the sliding rake system) and resultant scaffold deformation was observed. A system setting of 5% strain translated to a 3.44 ± 0.05% overall strain with 5.69 ± 0.04% and 1.90 ± 0.11% strain in the CG and CGCaP compartments, respectively. Throughout the experiment, we will refer to the magnitude of applied strain as the movement of the sliding rake system.

Human mesenchymal stem cell culture

Human bone marrow-derived MSCs were purchased from Lonza (Walkersville, MD). Cells from multiple lots originating from separate donors were combined to account for any donor-specific responses. The MSCs were cultured in a complete MSC growth medium, at 37°C and 5% CO_2, fed twice a week, and used at passage 6 for all experiments.

Culture of MSC-seeded CG scaffolds

CG scaffolds embedded in end blocks (6 mm diameter, 15 mm gauge length) were seeded with MSCs using a previously validated static seeding method (O'Brien, Harley et al. 2005). Briefly, scaffolds were partially dried with Kimwipes and seeded with 3.0×10^5 MSCs per 60 μL media (3x20 μL drops along scaffold length) in the individual wells of the bioreactor and static well systems. Cells were allowed to attach for 2 hours before submerging in media; constructs were given an additional 24 hours before application of CTS to ensure cell attachment. Cell-seeded scaffolds in the CTS groups were subjected to continuous cyclic tensile strain (5% overall strain at 1 Hz) for 10 minutes every 6 hours, for up to 6 days, using a protocol inspired by *Paxton et al.* (Paxton, Hagerty et al. 2012; Grier, Moy et al. 2017), to allow for sufficient cellular refractory period to ensure prolonged effects. Cell-seeded scaffolds were cultured at 37°C and 5% CO_2 and fed twice a week with complete MSC growth medium. During the experiment, scaffolds were collected for further analysis at designated times, or immediately after the conclusion of a strain cycle, by physically separating them from the end blocks by cutting with a razor blade. A cutting guide was then used to cut the scaffolds into three sections for compartment-specific analysis, one each from the CG compartment, CGCaP compartment, and the middle third of the scaffold containing the interface.

Protein Extraction, gel electrophoresis, and immunoblotting

Following stretch cycles, scaffold sections were briefly washed in warm phosphate-buffered saline, blotted dry, and then submerged in RIPA buffer with 1/100 dilutions of protease and phosphatase II and III inhibitor cocktails. The scaffold sections were then kept on ice for 30 minutes with regular agitation. Total protein concentration was determined by the BCA assay kit (Pierce). For gel electrophoresis, 10 μg of protein from each sample was solubilized in an equal volume Laemmli sample buffer and heated to 90°C for 10 minutes. Total lysates were separated by tris-glycine gel electrophoresis on 4-20% gradient gels using a constant 150V for 90 minutes. Following electrophoresis, a semi-dry transfer was used to transfer proteins to a nitrocellulose membrane (GE Healthcare) at 15 V for 15 minutes. Membranes were then blocked for 1 hour in 5% milk in Tris-buffered-saline + 0.1% Tween (TBST). Membranes were incubated overnight at 4°C with the appropriate primary antibody in 5% bovine serum albumin in TBST. The membrane was then washed three times in TBST before incubation for 1 hour at room temperature with HRP-linked goat anti-rabbit IgG secondary antibody (1:5,000. Cell Signaling) in TBST. Antibody binding was then detected using SuperSignal West Pico or Femto Chemiluminescent Substrate (Thermo Fisher, Waltham, MA). After probing, membranes were stripped with OneMinute® Western Blot Stripping Buffer (GM Biosciences, Rockville, MD) and re-probed up to two times, following the same protocol. Antibodies were purchased from Cell Signaling (Danvers, MA): p38 (8690), p-p38 (9215), ERK 1/2 (4695), pERK 1/2 (4370), Smad 2/3 (8685), pSmad 2/3 (8828), Smad 1 (6944), pSmad 1/5/8 (9511), β-actin (4967). Imaging was carried out using an Imagequant LAS 4010 system (GE Healthcare) and ImageJ was used for band intensity quantification.

Quantifying cell number and metabolic activity

The mitochondrial metabolic activity of the MSCs within each scaffold section was determined through the use of non-destructive alamarBlue® assay as previously described (Tierney, Duffy et al. 2013). Cell-seeded sections were incubated in the alamarBlue solution (Invitrogen, Carlsbad, CA) with gentle shaking for 1 hour. The reduction of resazurin in the solution by metabolically active cells to the fluorescent by-product resorufin was measured on a fluorescent spectrophotometer. Relative cell metabolic activity was determined from a standard curve generated from known cell numbers prior to seeding the scaffolds and reported as a percentage of the total number of seeded cells.

RNA isolation and real-time PCR

RNA was extracted from the MSC-seeded scaffold sections at days 1, 3, and 6 using an RNeasy Plant Mini kit (Qiagen, Valencia, CA). RNA was then was reverse transcribed to cDNA in a Bio-Rad S1000 thermal cycler using the QuantiTect Reverse Transcription kit (Qiagen, Valencia, CA) as previously described (Duffy, McFadden et al. 2011; Caliari, Weisgerber et al. 2012). Real-time PCR reactions were carried out in triplicate, using 10ng of cDNA and QuantiTect SYBR Green PCR kit (Qiagen, Valencia, CA) in a 7900HT Fast Real-Time PCR system (Carlsbad, CA). The primers used were consistent with previous studies, and were synthesized by Integrated DNA Technologies (Coralville, IA). The expression level of the following markers was quantified: collagen type III alpha 1 (*COL3A1*), cartilage oligomeric matrix protein (*COMP*), scleraxis (*SCXB*), Mohawk homeobox (*MKX*), aggrecan (ACAN), SRY Box 9 (SOX9), alkaline phosphatase (*ALP*), bone sialoprotein (*BSP*), osteopontin (*OP*), runt-related transcription factor 2 (*RUNX2*), and glyceraldehyde 3-phosphate dehydrogenase (*GAPDH*), which was used as a house keeping gene (**Table 4.1**). Results were generated using the ΔΔCt method, and all results were

expressed as fold changes normalized to the expression levels of MSCs at the time of seeding the scaffolds.

Statistical analysis

Two-way analysis of variance (ANOVA) was performed on the western blot, metabolic activity, and gene expression data sets to evaluate the effects of scaffold compartment and strain conditions (independent variables: scaffold compartment, strain condition). One-way ANOVA was performed within each group to evaluate temporal effects (independent variable: time). ANOVA was followed by Tukey-honest significant difference *post hoc* tests. Significance was set at $p < 0.05$. A minimum of three independent scaffolds were analyzed at each time point for all metrics. Error is reported in figures as the standard error of the mean unless otherwise noted. All statistical analysis was performed in Microsoft Excel using the Real Statistics Resource Pack.

4.4 Results

The effects of intermittent cyclic tensile strain on compartment-specific cellular metabolic activity.

MSC metabolic activity was monitored in each scaffold compartment over the course of 6 days of culture with and without CTS (5% total strain, 1 Hz, for 10 minutes every 6 hours) **(Fig. 4.3)**. In general, higher levels of cellular metabolic activity were observed in the CG compartment compared to the CGCaP compartment, and within the CG compartment, metabolic activity was higher with CTS compared to static conditions. Initially, cells in the CG compartment subjected to CTS show significantly higher metabolic activity ($p < 0.05$) compared to all other groups. By day 3, cells in the static CG show higher activity compared to day 1 ($p < 0.05$), and cells in both CG compartments, with and without CTS, are significantly more active than in the CGCaP compartments ($p < 0.05$). At the end of the culture on day 6, cells in the static CG compartment and CGCaP compartment with CTS display an increased metabolic activity in comparison to day

1 ($p < 0.05$). However, the cells in the CG compartment with CTS show increased metabolic activity levels compared to both days 1 and 3 as well as all other groups on day 6 ($p < 0.05$).

Mechanotransduction pathway activation

Samples were analyzed immediately prior to and at the conclusion of the first (0-10 minutes) and second (360-370 minutes) strain cycles in culture in order to evaluate compartment-specific mechanotransduction pathway activation as a result of the intermittent CTS paradigm. While not significant, ERK 1/2 activation tended to be higher in the CGCaP compartment compared to the CG compartment at all timepoints ($p = 0.18$) **(Fig. 4.4A)**. Additionally, immediately after the second strain cycle, ERK 1/2 activation is significantly upregulated in the CGCaP compartment ($p < 0.05$). The activation of p38 MAPK displays an inverse trend compared to ERK 1/2 with slightly lower activation levels in the CGCaP compartment compared to the CG compartment, and significantly reduced activation in the CGCaP compartment after the second strain cycle ($p < 0.05$) **(Fig. 4.4B)**.

Smad pathway activation

The compartment-specific activation of the Smad 2/3 and Smad 1/5/8 pathways was evaluated after 1 and 3 days in culture. While not significant, the activation of Smad 1/5/8 tended to be higher in the CGCaP compartment compared to the CG compartment and with strain compared to static condition **(Fig. 4.5A)**. The activation of Smad 2/3 on the other hand did not show much effect of strain condition or compartment on day 1, but did trend higher in the CG compartment with CTS after 3 days **(Fig. 4.5B)**.

The impact of CTS on compartment-specific gene expression

The gene expression profiles for the cells in each scaffold section were examined throughout the 6-day culture. Three sub-sets of genes were examined: tendon-related genes (*COL3A1*, *COMP*, *SCX*, *MKX*, **Fig. 4.6**); osteogenic-related genes (*ALP*, *BSP*, *OP*, *RUNX2*, **Fig. 4.7**); and fibrocartilage-related genes that are relevant to the TBJ (*ACAN, SOX9*, **Fig. 4.8**).

Tendon-specific gene expression

After 1 day of culture, gene expression levels of *COMP*, *SCX*, and *MKX* were generally highest in the CG and interface compartments with strain while there was negligible impact of strain on the expression of *COL1A1* **(Fig. 4.9)**. Interestingly, many of differences between groups were not noticeable on day 3. The most relevant comparisons were made at the end of the study, on day 6, between the two main compartments of the scaffolds with and without CTS (**Fig. 4.6**). A significant decrease in *COL1A1* expression is observed in the CGCaP compartment when exposed to CTS, compared to the CG compartment with or without CTS ($p < 0.05$). The expression levels for both *COMP* and *SCX* are significantly upregulated in the CG compartment with CTS, compared to the same compartment under static conditions, and the CGCaP compartment, regardless of strain conditions ($p < 0.05$). Finally, *MKX* expression, while still relatively low, is significantly higher in the CG compartment with CTS compared to the CGCaP compartment under static conditions ($p < 0.05$).

Osteogenic gene expression

In general, CTS had a much smaller impact on osteogenic genes compared to the tenogenic markers over the full course of the experiment (**Fig 4.10**). On the final day of the study, *ALP* expression was significantly higher in the interface region under static conditions compared the other groups ($p < 0.05$). There was no significant impact of CTS, nor scaffold compartment, on

the expression levels of *BSP*. Expression levels for *OP* were higher in the CGCaP compartment with CTS, on day 1, compared to all groups under static conditions, while the interface region in static culture showed significantly lower expression than all other groups and conditions ($p < 0.05$). On days 3 and 6, this trend reversed, and the groups exposed to CTS showed lower expression levels of *OP* compared to those in static culture ($p < 0.05$). *RUNX2* expression levels were higher in the CGCaP compartment with CTS compared to the same compartment in static culture on day 1 ($p < 0.05$) but lower in the static CGCaP compartment compared to the other groups under static conditions on day 6 ($p < 0.05$). Most importantly, we examined the differences between the CGCaP compartment, with and without CTS, at the conclusion of the study (**Fig. 4.7**). Here, it can be seen that there is a minor downregulation of *OP* expression in the CGCaP compartment with CTS ($p < 0.05$). Otherwise, there is no significant impact of CTS on osteogenic gene expression within the CGCaP compartment.

Interface gene expression

The expression levels of both *ACAN* and *SOX9*, while variable, were generally higher in groups exposed to CTS compared to those in static culture (**Fig. 4.8**). All groups in static culture showed significantly lower expression of *ACAN* compared to the interfacial region on day 1 and both the interface and CG compartment on day 3 ($p < 0.05$). *SOX9* expression was also significantly higher in the interface on day 6 and both the interface and CGCaP compartment on day 1 compared to all three compartments under static conditions ($p < 0.05$).

4.5 Discussion

The application of low-amplitude cyclic tensile strain is known to be an important regulator in the development of the native tendon and enthesis, as well as for the regulation of a number of stem cell fate decisions (Murchison, Price et al. 2007; Blitz, Viukov et al. 2009; Pryce, Watson et al.

2009; Schweitzer, Zelzer et al. 2010). Our group has recently described the development of a multi-compartment CG scaffold material system with distinct regions of structural anisotropy and mineral content for tendon-bone-junction engineering (Caliari, Weisgerber et al. 2015). While this work was able to demonstrate the ability to tailor material properties in order influence stem cell fate in a spatially-dependent manner, there is a distinct need to drive a more robust tenogenic response in the structurally anisotropic region of the scaffold for more complete tissue development. Separately, we have also described the use of a custom bioreactor system in conjunction with monolithic anisotropic CG scaffolds which showed a more robust upregulation of tenogenic markers and activation of mechanotransduction and TGF-β growth factor pathways known to be vital in the development of native tendon (Grier, Moy et al. 2017). This work focused on the integration of these two technologies to demonstrate the use of CTS within a multi-compartment CG scaffold for spatially-selective augmentation of tenogenic development for the regeneration of the full tendon-bone-junction.

The primary focus on this work was to examine how the application of CTS within a multi-compartment material may impact the initial determinants of tenogenic and osteogenic differentiation in a spatially-dependent manner. While the timeframe of the work did not allow for the demonstration of extensive matrix remodeling and *de novo* tissue development, it has allowed us to show that MSCs seeded on a spatially graded material with gradations in microstructural alignment, mineral content, and bulk mechanics, will display disparate responses to tensile stimulation depending on the location within the material. Specifically, the cells within the CG compartment displayed responses that were consistent with our previous work in single-compartment CG scaffolds (Grier, Moy et al. 2017). When exposed to CTS on an anisotropic CG material, MSCs exhibited higher cellular metabolic activity, increased expression levels of

tenogenic markers COMP, SCX, and MKX, and generally increased activation of the Smad 2/3 pathway.

Additionally, it was important to evaluate the effect of CTS on cells within the CGCaP compartment of the scaffold. This compartment is about 20-fold stiffer than the CG compartment and thus subject to minimal levels of local strain (Weisgerber, Kelkhoff et al. 2013). With that being said, the very low amplitude strain that was observed along with fluid flow in dynamic culture could have implications on MSC responses. Indeed, previous work has shown that both CTS (Jiang, Wang et al. 2016) and shear flow (Yourek, McCormick et al. 2010) could be drivers of osteogenic differentiation of MSCs. In this case, there was little-to-no impact of CTS on MSCs within the CGCaP compartment. This was not altogether surprising. As we have previously shown, the CGCaP material alone is sufficient to drive a robust osteogenic response. MSCs seeded on CGCaP scaffolds show increased mineral deposition and matrix remodeling along with upregulation of osteogenic markers *BSP*, *OP*, and osteocalcin (Lee, Pereira et al. 2015; Weisgerber, Caliari et al. 2015). This increase in osteogenic activity has been demonstrated to be a result of the innate activation of the Smad 1/5/8 pathway in MSCs seeded on the CGCaP material (Ren, Bischoff et al. 2015; Ren, Tu et al. 2016). Any potential impact of the comparatively low amplitude strain that was observed in this stiffer compartment was likely overshadowed by the response to the material properties.

While not the primary goal of this study, the evaluation of fibrocartilaginous markers at the intersection of the two compartments does provide intriguing insight for future studies. When evaluating the expression levels of *ACAN* and *SOX9* across each scaffold, a clear trend of increased expression when exposed to CTS was observed. This trend was especially apparent for *SOX9* in the middle third of each scaffold which contained the interface between the two materials. This is

promising for next generation approaches to specifically regenerate the tendon enthesis. Previous work from *Spalazzi et al*. demonstrated the use of used a tri-culture system on a tri-phasic material with osteoblasts, chondrocytes, and fibroblasts seeded on bone, interface, and tendon specific regions (Spalazzi, Dagher et al. 2008). *He et al.* also developed a similar tri-lineage co-culture with MSCs seeded between osteoblasts and fibroblasts on a uniform silk scaffold for the development of a partially mineralized fibrocartilaginous interfacial zone (He, Ng et al. 2012). Recently, *Liu et al.* investigated the use of decellularized tendon matrix treated with ultrasound in order to influence rabbit MSCs towards an fibrocartilaginous-like state (Liu, Yang et al.). While these previous works do show the potential for these multipotent MSCs to develop into enthesis tissue, there has yet to be any in depth evaluation of a full tendon-bone-junction model that incorporates a physiologically relevant and competent enthesis. In this case, the combination of CTS along with the unique material properties at the intersection of two distinct, but continuous compartments, may be sufficient to drive that initial fibrocartilaginous response.

In order to comprehensively evaluate the impact of CTS on multi-compartment scaffolds for TBJ regeneration, we plan to address three critical components. First, a better understanding of the interplay between CTS and compartment-specific Smad activation should be explored. We have demonstrated Smad 2/3 activation on CG scaffolds after exposure to CTS, but the mechanism of this activation is not yet understood. There are two possible modes of Smad activation. Canonical activation could result from the endogenous production of TGF-β growth factors after initial differentiation. Non-canonical methods of activation could also play a role as mechanotransduction pathways like ERK 1/2 and p38 have been shown to influence Smad activity (Ren, Weisgerber et al. 2016). It is also possible that the initial non-canonical activation of Smad 2/3 by mechanical stimulation could drive an autocatalytic cycle of differentiation and endogenous

growth factor production resulting in more robust Smad activation and MSC differentiation as postulated by *Allen et al*. (Allen, Cooke et al. 2012). There is also a need for extended studies to evaluate long-term matrix remodeling and *de novo* tissue development. We have shown that this scaffold model is capable of driving spatially-distinct initial tenogenic and osteogenic responses, but the long-term effects of this treatment have yet to be verified. A final consideration needs to be for the specific development of a function enthesis zone between the tendon and bone. This requires higher resolution methods to evaluate cellular activity and gene expression at the narrow region, which is generally less than 1 mm, between the bulk of the two compartments (Weisgerber, Kelkhoff et al. 2013; Caliari, Weisgerber et al. 2015).

4.6 Conclusions

This work demonstrated the use of multi-compartment scaffolds, with distinct but continuous regions of structural anisotropy and mineral content, in combination with intermittent cyclic tensile strain to drive spatially-controlled MSC responses for the regeneration of the tendon-bone-junction. The strain paradigm (5% strain, 1 Hz, for 10 minutes every 6 hours) was found to have very little effect on the osteogenic capacity of MSCs in the stiffer, mineralized CGCaP region of the scaffold, while there was significant upgregulation of tenogenic markers and cellular metabolic activity in the anisotropic non-mineral CG region when subjected to CTS. These results provide the basis for future work to define the role of the interplay between cellular local microenvironment and external mechanical stimuli on the development of multi-tissue structures such as the TBJ.

4.7 Table

Table 4.1 PCR primer sequences.

Transcript	Sequence	Reference
COL3A1	Forward: 5'- GCTGGCATCAAAGGACATCG -3' Reverse: 5'- TGTTACCTCGAGGCCCTGGT -3'	(Pauly, Klatte et al. 2010)
COMP	Forward: 5'- GCAACACGGACGAGGACAAG -3' Reverse: 5'- CGCCATCACTGTCCTTCTGG -3'	(Klatte-Schulz, Pauly et al. 2013)
SCXB	Purchased from Qiagen (sequence unavailable)	(Caliari and Harley 2014)
MKX	Forward: 5'- CGTATTGGAAGGAGATCAACG -3' Reverse: 5'- GGACGACTTCTGGATGATGC -3'	(Lorda-Diez, Canga-Villegas et al. 2013)
ACAN	Forward: 5'- TGCATTCCACGAAGCTAACCTT -3' Reverse: 5'- GACGCCTCGCCTTCTTGAA -3'	(Zhou, Xu et al. 2011)
SOX9	Forward: 5'- AGCGAACGCACATCAAGAC -3' Reverse: 5'- GCTGTAGTGTGGGAGGTTGAA -3'	(Zhou, Xu et al. 2011)
ALP	Forward: 5'- AGCACTCCCACTTCATCTGGAA -3' Reverse: 5'- GAGACCCAATAGGTAGTCCACATTG -3'	(Zhou, Xu et al. 2011)
BSP	Forward: 5'- TGCCTTGAGCCTGCTTCC -3' Reverse: 5'- GCAAAATTAAAGCAGTCTTCATTTTG -3'	(Frank, Heim et al. 2002)
OP	Forward: 5'- CTCAGGCCAGTTGCAGCC -3' Reverse: 5'- CAAAAGCAAATCACTGCAATTCTC -3'	(Frank, Heim et al. 2002)
RUNX2	Forward: 5'- AGAAGGCACAGACAGAAGCTTGA -3' Reverse: 5'- AGGAATGCGCCCTAAATCACT -3'	(Zhou, Xu et al. 2011)
GAPDH	Forward: 5'- CCATGAGAAGTATGACAACAGCC -3' Reverse: 5'- CCTTCCACGATACCAAAGTTG -3'	(Pauly, Klatte et al. 2010)

4.8 Figures

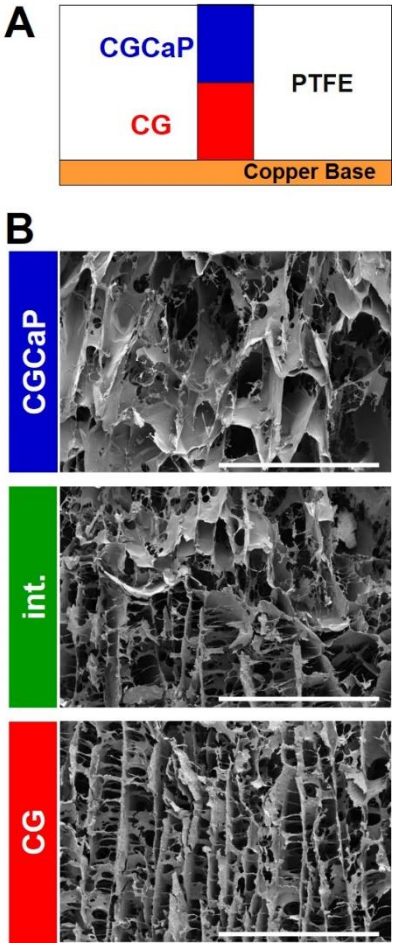

Figure 4.1 CG scaffold fabrication. (A) Schematic of scaffold mold with layered collagen suspensions. **(B)** Scanning electron micrographs of individual multi-compartment CG scaffold regions and interface. Scale bars = 1 mm.

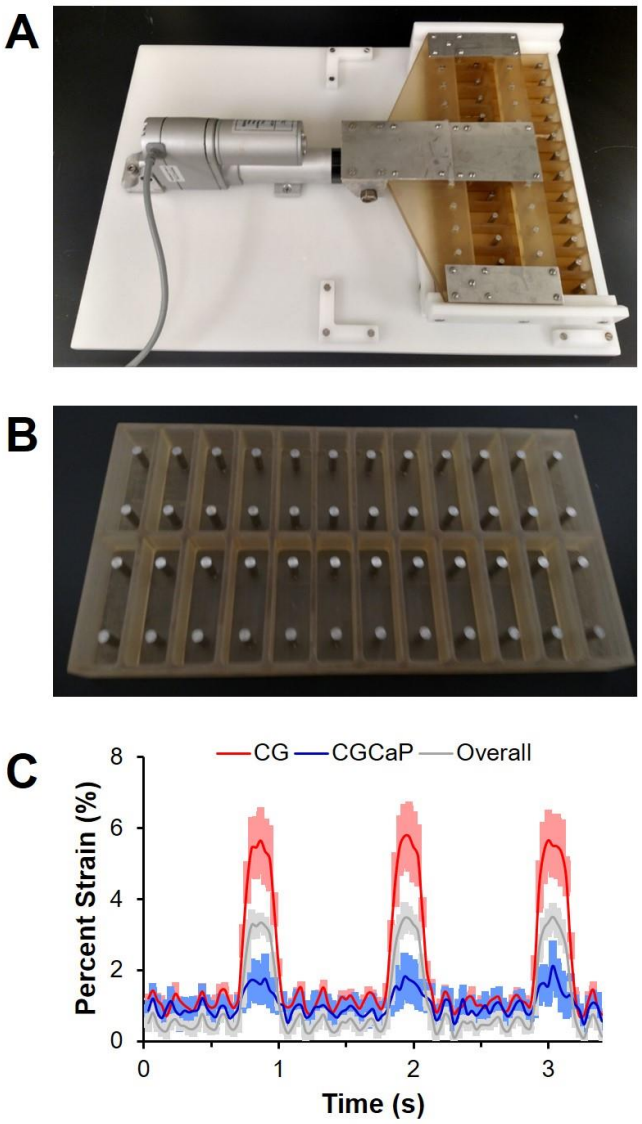

Fig. 4.2 Custom cyclic strain bioreactor. (A) Custom bioreactor designed with 24 individual wells with static loading posts and moveable rake controlled by a programmable linear actuator. **(B)** Static well system for control cultures run in parallel to bioreactor. **(C)** Compartment-specific measured scaffold deformation in response to cyclic tensile strain (5%, at 1 Hz). Scaffold deformation is shown as mean ± SEM.

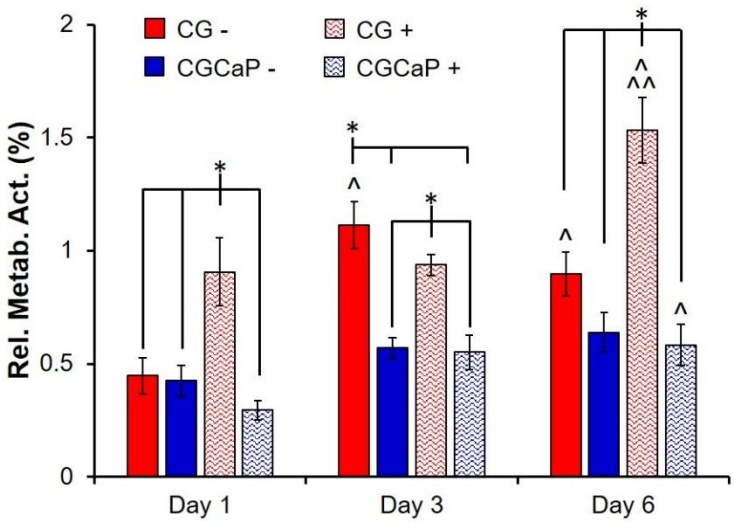

Fig. 4.3 MSC metabolic activity in multi-compartment scaffolds undergoing CTS. Compartment-specific metabolic activity of MSCs in CG scaffolds in either static culture or exposed to repeated cycles of CTS (10min at 5% strain and 1 Hz) followed by 5 hours 50 minutes recovery at days 1, 3, and 6. Data expressed as mean ± SEM (n = 6). * Significantly higher (p < 0.05) than indicated groups at same day. $^{\wedge}$ Significantly higher (p < 0.05) than same group on day 1. $^{\wedge\wedge}$ Significantly higher (p < 0.05) than same group on day 3.

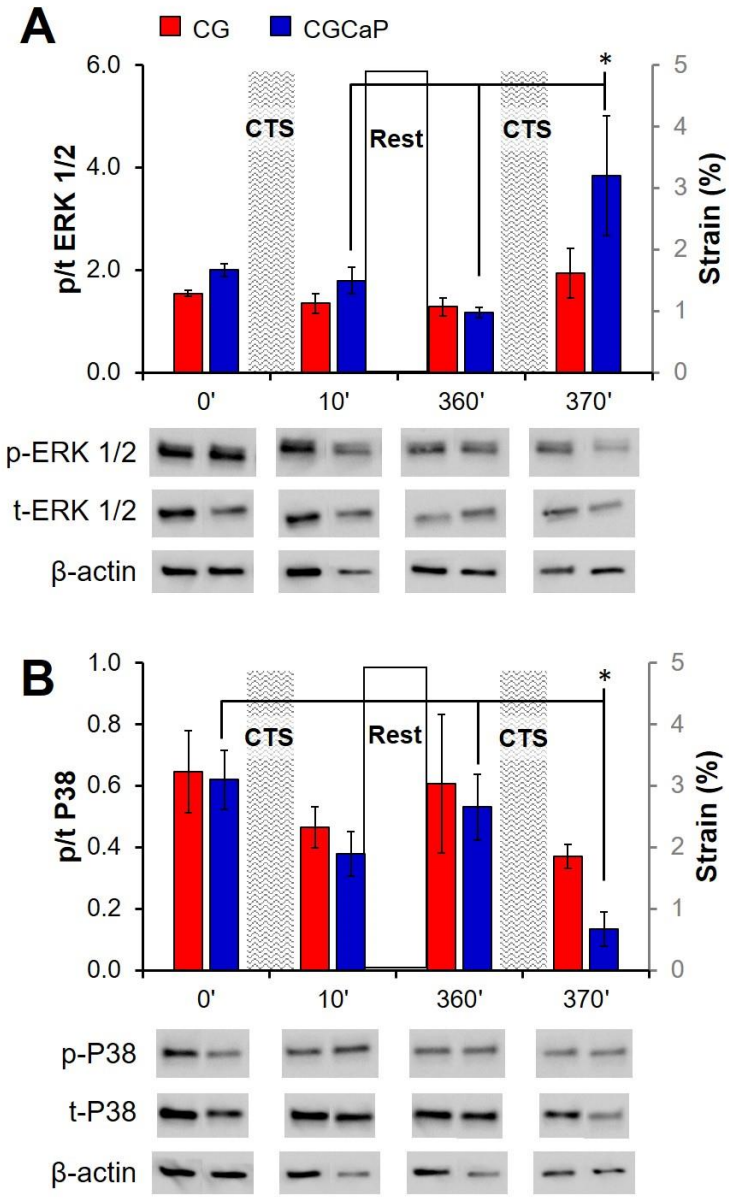

Fig. 4.4 Compartment-specific mechanotransduction pathway activation with CTS. Relative levels of phosphorylated : total **(A)** ERK 1/2 and **(B)** p38 MAPK in each compartment of CG scaffolds with and without CTS as determined by immunoblot immediately prior to and following the first and second strain cycles. Data expressed as mean ± SEM (n = 3). *: $p < 0.05$.

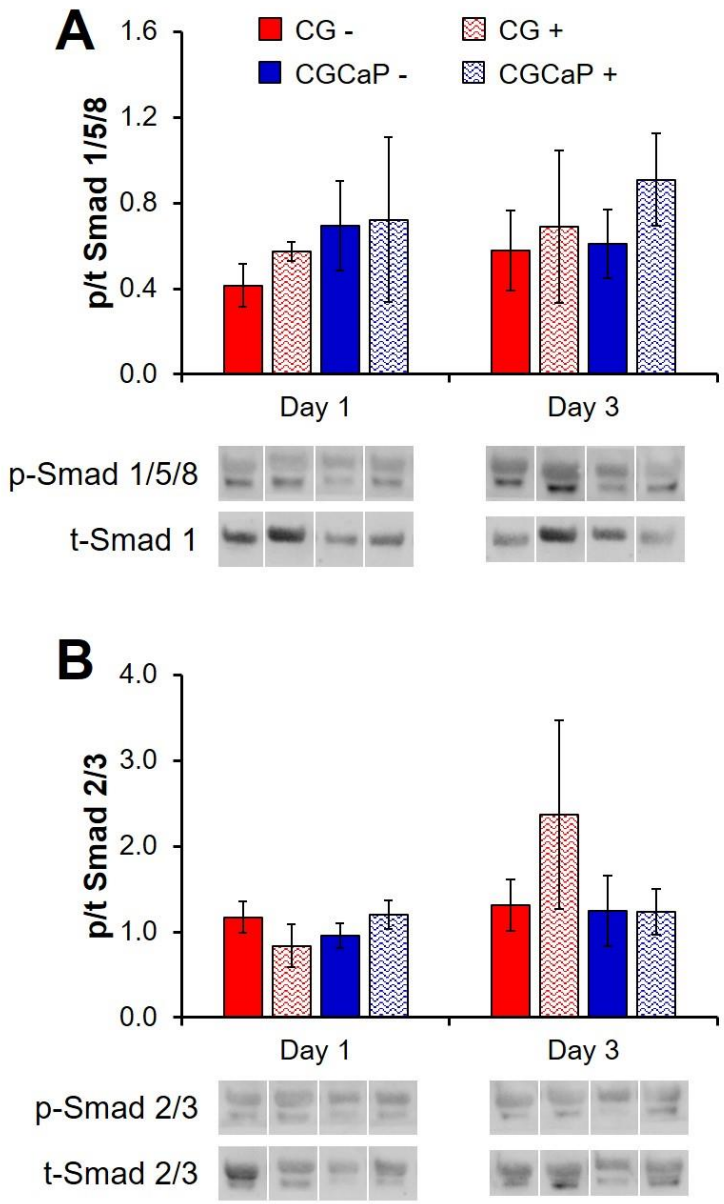

Fig. 4.5 Compartment-specific Smad pathway activation with CTS. Relative levels of phosphorylated : total **(A)** Smad 1/5/8 and **(B)** Smad 2/3 in each compartment of CG scaffolds with and without CTS as determined by immunoblot on days 1 and 3. Data expressed as mean ± SEM ($n = 3$). *: $p < 0.05$.

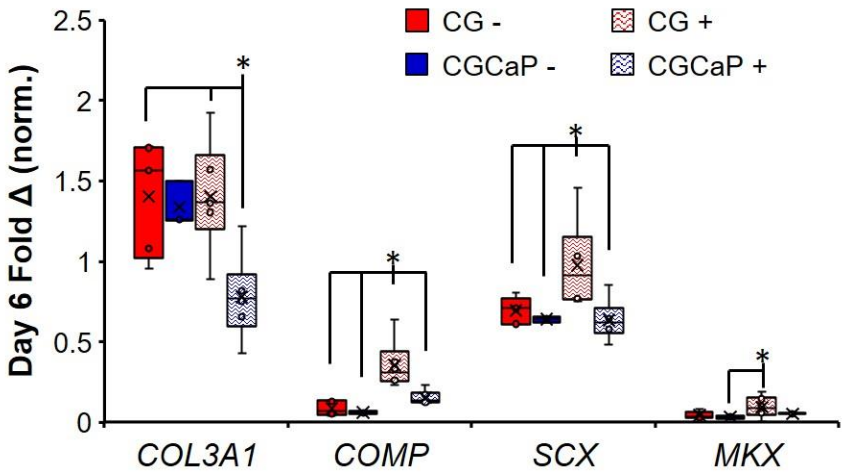

Fig. 4.6 Changes in pro-tenogenic gene expression in response to CTS. Compartment-specific expression levels of *COL1A1*, *COMP*, *SCX*, and *MKX* with and without CTS on day 6. Data expressed as mean ± SEM (n = 6). *: $p < 0.05$.

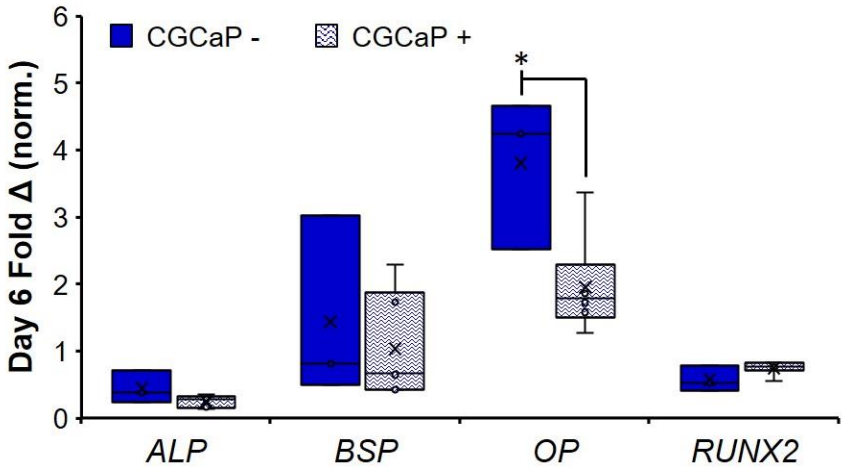

Fig. 4.7 Changes in pro-osteogenic gene expression in response to CTS. CGCaP **c**ompartment-specific expression levels of *ALP*, *BSP*, *OP*, and *RUNX2* with and without CTS on day 6. Data expressed as mean ± SEM (n = 6). *: $p < 0.05$.

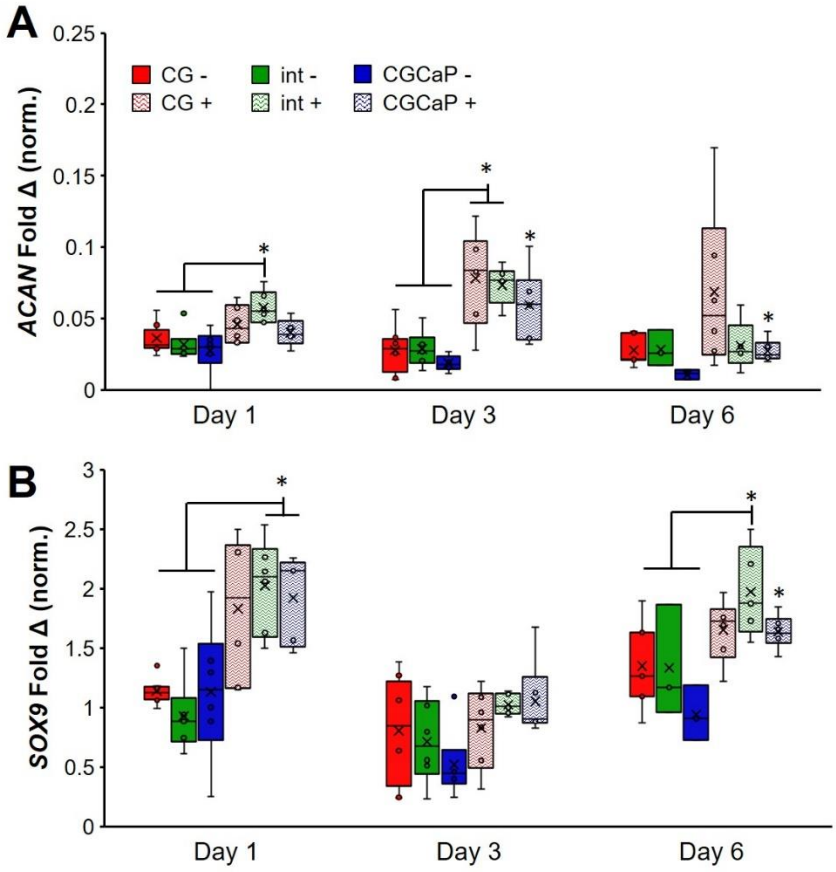

Fig. 4.8 Changes in pro-chondrogenic gene expression in response to CTS. Compartment-specific expression levels of **(A)** *ACAN* and **(B)** *SOX9* with and without CTS on days 1,3, and 6. Data expressed as mean ± SEM (n = 6). *: $p < 0.05$.

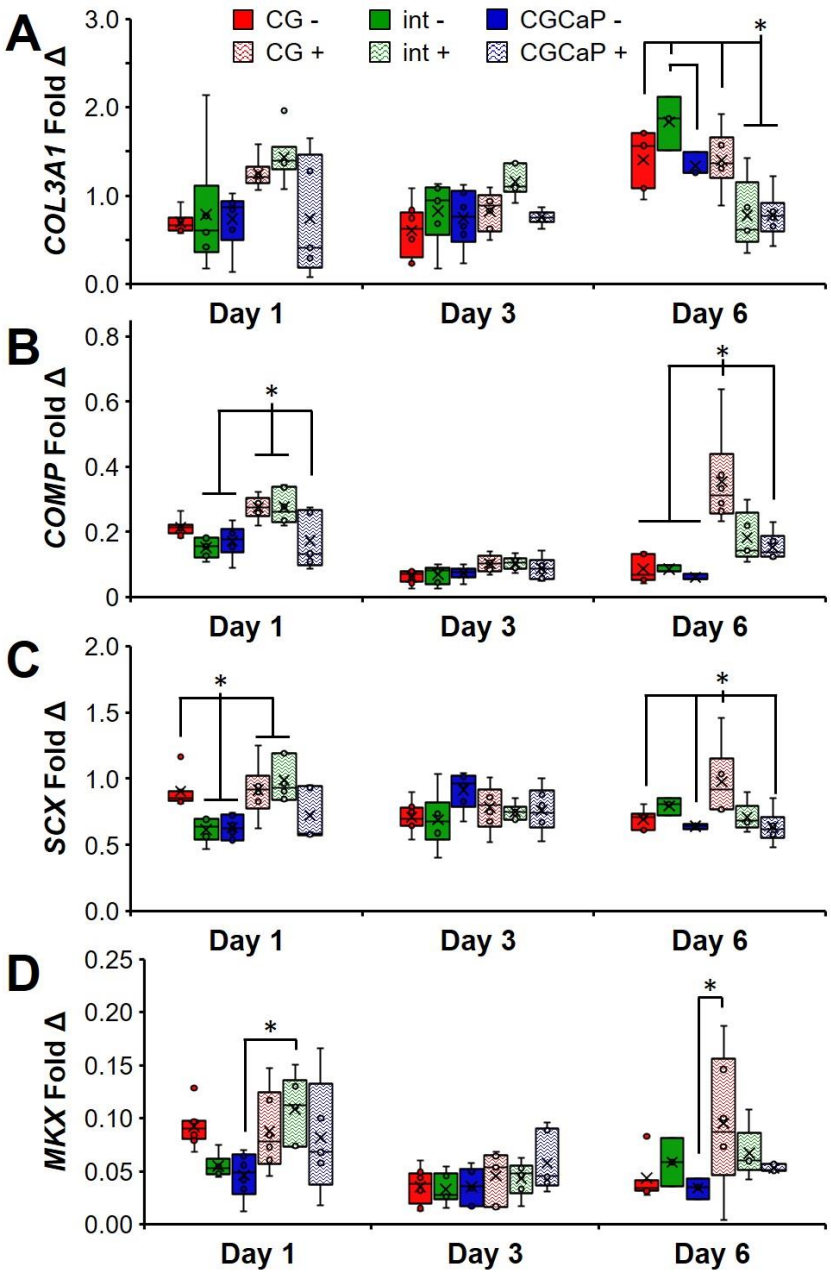

Fig. 4.9 Changes in pro-tenogenic gene expression in response to CTS. Compartment-specific expression levels of **(A)** *COL1A1*, *COMP*, **(C)** *SCX*, and **(D)** *MKX* with and without CTS on days 1, 3, and 6. Data expressed as mean ± SEM (n = 6). *: $p < 0.05$.

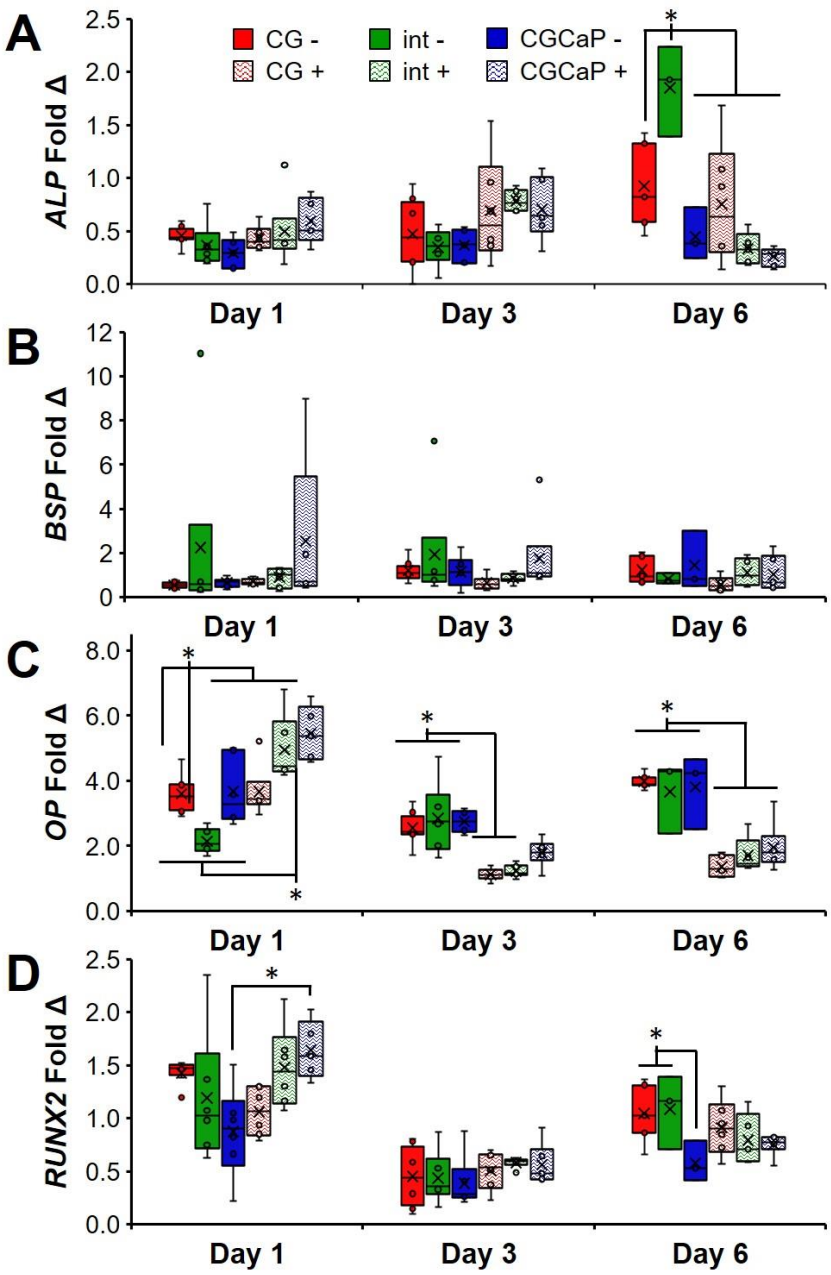

Fig. 4.10 Changes in pro-osteogenic gene expression in response to CTS. Compartment-specific expression levels of **(A)** *ALP*, **(B)** *BSP*, **(C)** *OP*, and **(D)** *RUNX2* with and without CTS on days 1, 3, and 6. Data expressed as mean ± SEM (n = 6). *: $p < 0.05$.

CHAPTER 5: INCORPORATION OF β-CYCLODEXTRIN INTO COLLAGEN-GAG SCAFFOLDS FOR THE SELECTIVE SEQUESTRATION AND PRESENTATION OF GROWTH FACTORS TO GUIDE MSC FATE[5]

5.1 Chapter overview

The preceding three chapters focused on the development of biomaterials and culture systems for specific tissue engineering applications. In this chapter, a novel method for the incorporation and presentation of growth factors in CG scaffolds to direct stem cell responses. B-cyclodextrin is incorporated into CG slurry prior to lyophilization allowing for the passive pull-down of growth factors from solution and subsequent controlled release via guest-host interactions. The effects of growth factor release from the scaffolds is then evaluated on MSC responses through cellular metabolic activity, proliferation, the activation of growth factor signaling pathways, and differentiation.

5.2 Introduction

Collagen-glycosaminoglycan (CG) materials are composed of natural extracellular matrix (ECM) components and have shown great promise as tissue engineering scaffolds. Initially developed for skin regeneration applications, these porous CG scaffolds are produced by the lyophilization of an acidic suspension of type I collagen and glycosaminoglycans (Yannas, Lee et al. 1989). One of the major advantages of CG scaffolds is the ease in which the microstructure, composition, or bioactivity can be adapted to meet the functional demands of a wide variety of tissue engineering applications. For instance, the freezing kinetics can be manipulated to produce anisotropic scaffolds composed of aligned tracks of ellipsoidal pores for tendon repair applications (Caliari

[5] This chapter has been adapted from the following publication:
Grier, W.K. M.D. Ramsey et al. (submitted). "Incorporation of β-cyclodextrin into collagen-GAG scaffolds for the selective sequestration and presentation of growth factors to guide MSC fate."

and Harley 2011; Caliari, Weisgerber et al. 2012; Caliari and Harley 2013). Calcium phosphate nanocrystallites have be incorporated during lyophilization to enhance mesenchymal stem cell (MSC) osteogenic differentiation and bone regeneration (Harley, Lynn et al. 2010; Quinlan, Lopez-Noriega et al. 2015; Ren, Bischoff et al. 2015; Weisgerber, Caliari et al. 2015; Ren, Tu et al. 2016; Ren, Weisgerber et al. 2016). These structural modifications have also shown to bias MSC differentiation down chondrogenic versus osteogenic lineages in the presence of mixed media supplementation (Caliari and Harley 2014). The desire to promote increasingly specific cell behaviors (e.g., proliferation, MSC lineage specification) has motivated efforts to incorporate design elements that alter the bioavailability of growth factors within the scaffolds network itself. In addition to covalent immobilization of growth factors to the scaffold via carbodiimide (Banks, Mozdzen et al. 2014) and benzophenone (Martin, Caliari et al. 2011) crosslinking chemistries, growth factors have also been covalently bound to polymeric reinforcing cages fabricated by 3D printing that can be incorporated into the scaffold during Lyophilization to generate a composite with enhanced mechanical and biomolecular properties (Mozdzen, Vucetic et al. 2017). However, while covalent immobilization offers benefits in the form of extended bioavailability, this process is only applicable to biomolecular signals that do not require receptor internalization. Exciting opportunities therefore exist in the space of non-covalent presentation of biomolecular signals. Temporal control over growth factor bioavailability is also possible via incorporation of gene delivery motifs (e.g., polyethylenimine-DNA complexes) into the scaffold network (Tierney, Duffy et al. 2013; Hortensius, Becraft et al. 2015). Recently, *Hortensius et al.* adapted charge-based transient sequestration concepts previously demonstrated in heparin-modified hydrogels (Sakiyama-Elbert and Hubbell 2000) and 2D culture surfaces (Hudalla, Kouris et al. 2011), and showed the glycosaminoglycan content of the CG scaffold itself could be manipulated to

transiently sequester and release growth factors from the media (Hortensius and Harley 2013; Hortensius, Ebens et al. 2016). However, the complexity of the glycosaminoglycan components to the CG scaffolds motivates efforts here to examine alternative chemistries to transiently sequester activity-inducing growth factors within the CG scaffold network.

A promising method for the selective incorporation of growth factors into biomaterial constructs is the use of supramolecular interactions such as those found in cyclodextrins. These six, seven, and eight member D-glucopyranose rings (α-cyclodextrin, β-cyclodextrin, and γ-cyclodextrin respectively) (Mura 2014; Radu, Parteni et al. 2016) are more commonly used in pharmaceutical applications to increase drug solubility. Cylcodextrins are known for their ability to form cyclodextrin inclusion complexes (CDIC), where guest-host interactions enable the adsorption of hydrophobic guest molecules into the central cavity **(Fig. 5.1 A)** (Bibby, Davies et al. 2000). Cyclodextrin chemistries have been demonstrated as a means to generate dynamic, adaptable hydrogel environments (Liu, Zhang et al. 2011; Machín, Isasi et al. 2012; Liu, Zhang et al. 2013; Osman, Soliman et al. 2015; Rodell, Highley et al. 2016). Cyclodextrins into porous biomaterials as a means to alter the release of drug molecules (Prabaharan and Jayakumar 2009; Soheilmoghaddam, Sharifzadeh et al. 2014). While cyclodextrins have been shown to have a strong affinity for various growth factors (Yuen, Folkman et al. 1990), the ability for these molecules to regulate growth factor sequestration and display within porous scaffold-based biomaterial has not been deeply exploited.

Here, we describe the incorporation of β-cyclodextrin into a CG scaffold variant under development for musculoskeletal repair applications **(Fig. 5.1 B)**. We hypothesized that incorporation of cyclodextrin into the CG scaffold network would facilitate the formation of CDICs with exogenously added soluble growth factors, leading to growth factor sequestration and

enhanced activity on MSCs within the scaffold. We examine sequestration and subsequent release of a model growth factor, transforming growth factor-beta 1 (TGF-β1), within the scaffold network. We then examine the capacity for cyclodextrin modified CG scaffolds (CGcyclo) to enhance the activity of the chondrogenic growth factor TGF-β1 or the osteogenic growth factor bone morphogenetic protein-2 (BMP-2) to influence MSC fate. We examine MSC osteo-chondral lineage specification via activation of activation of the Smad 1/5/8 and Smad 2/3 pathways as well as changes in gene expression profiles.

5.3 Materials and Methods

All materials and chemicals were purchased from Sigma-Aldrich (St. Louis, MO) unless otherwise specified.

Scaffold fabrication

Type I collagen from bovine Achilles tendon and chondroitin sulphate from shark cartilage were homogenized in 0.05 M acetic acid at a ratio of collagen to glycosaminoglycan of 11.25:1(Yannas, Lee et al. 1989; Madaghiele, Sannino et al. 2008). For the cyclodextrin scaffolds, two variants were produced, CGcyclo 1x and 5x were prepared by adding 3.70 μg/mL 18.52 μg/mL of β-cyclodextrin in deionized water directly to the CG slurry. Briefly, 200 μL of degassed CG suspension was pipetted into wells (6 mm diameter, 7 mm deep), within a polysulfone mold that was subsequently placed on a freeze-dryer shelf (VirTis, Gardner, NY). The CG suspension was frozen at -10°C for 2 hours and then sublimated at 0°C and 200 mTorr to remove the ice crystals, resulting in a dry porous scaffold.

Scaffolds were removed from the molds and cut laterally in half using a 3D printed guide (MakerBot Industries, Brooklyn, NY). Scaffolds were then hydrated by immersion in 200 proof

ethanol overnight followed by a 24 hour rinse in sterile phosphate-buffered saline (PBS) replacing the PBS three times. Each scaffold was then crosslinked using carbodiimide chemistry by immersion in a solution of 1-ethyl-3-[3-dimethylaminopropyl] carbodiimide hydrochloride (EDC) and N-hydroxysulfosuccinimide (NHS) for 2 hours at room temperature in a 5:2:1 molar ratio (EDC:NHS:COOH) in sterile PBS with gentle shaking. After crosslinking, the scaffolds were washed twice with sterile PBS and stored at 4°C.

SEM imaging of the scaffold microstructure

Critical point drying (CPD) was used to prepare hydrated and cell-seeded scaffolds for SEM imaging. CPD was performed using a Samdri-PVT-3D (Tousimis, Rockville, MD), where the aqueous media in the scaffold was sequentially replaced with ethanol and then liquid CO_2. Liquid CO_2 was allowed to infiltrate the scaffolds and was then held above 6.895 kPa and 31°C in order to remove the CO_2 as a gas with minimal structural deformation. Samples were then mounted on carbon tape, sputter coated with a gold/palladium mixture, and imaged with a Philips XL30 ESEM-FEG (FEI Company, Hillsboro, OR) at 5 kV with a secondary electron detector.

Biomolecule sequestration and release

The ability for the conventional CG or CGcylco scaffolds to sequester and release a model biomolecule, TGF-β1, was compared via ELISA. Briefly, scaffolds were incubated in 5ng/mL recombinant TGF-β1 (ProSpec-Tany, Ness-Ziona, Israel) in sterile PBS with 1% bovine serum albumin (BSA) for 1 hour on a gentle shaker; solution without scaffolds were used as controls. Following incubation, scaffolds were removed from the TBF-β1 solution, and the amount of TGF-β1 remaining in the media was determined via DuoSet® ELISA (R&D Systems, Minneapolis, MN) in order to calculate the fraction of TGF-β1 sequestered by the scaffold variants themselves (Hortensius and Harley 2013). Some structural deficiencies of the CGcylo 5x scaffolds were

noticed at this point, likely due to the dilution of the CG slurry, so only the CGcylo 1x variants were used after this point.

The elution of TGF-β1 from the CG and CGcyclo 1x scaffold variants was subsequently traced over 72 hours. Briefly, after incubating the scaffolds in 5ng/mL TGF-β1, scaffolds were transferred to pure PBS and maintained in the incubator (37ºC, 5% CO_2) for 72 hours. Samples of the media were removed after 1, 6, 24, and 72 hours for analysis of TGF-β1 released by the scaffold via DuoSet® ELISA. Results are reported as the fraction of the total TGF-β1 that each scaffold was exposed to that was subsequently retained by the scaffold at each time point.

Human mesenchymal stem cell culture and scaffold seeding

Human bone marrow-derived mesenchymal stem cells were purchased from Lonza (Walkersville, MD). Cells from multiple lots, originating from separate donors, were combined to account for any donor-specific responses. The MSCs were cultured at 37°C and 5% CO_2 in a complete MSC growth medium, consisting of low-glucose DMEM with 10 vol% MSC fetal bovine serum and 1 vol% antibiotic-antimitotic (Thermo Fisher, Waltham, MA), fed every three days and used at passage 6.

Selected CG and CGcyclo scaffolds were incubated in 5 ng/mL human recombinant BMP-2 (ProSpec-Tany, Ness-Ziona, Israel) or human recombinant TGF-β1 (ProSpec-Tany, Ness-Ziona, Israel) for 1 hour in sterile PBS in the same manner as previously described. The scaffolds were then moved into 5% FBS MSC Media for 2 hours as cells were lifted and centrifuged in preparation for seeding using a previously established static method (O'Brien, Harley et al. 2005). Scaffolds were partially dried with Kimwipes and seeded with 1.0×10^5 MSCs per 24 μL medium (1, 10 μL drop on opposite sides of the scaffold) in six well plates, with six scaffolds per well. Cells were

allowed to attach for 1 hour before submerging in 6 mL of low-serum MSC media, containing 5% FBS, per well. Cell-seeded scaffolds were cultured at 37°C and 5% CO_2 and fed every three days with the low-serum media.

Cell number and metabolic activity assays

DNA quantification was performed using a previously described method to determine the number of cells present on each scaffold (Kim, Sah et al. 1988; Grier, Moy et al. 2017). Briefly, scaffolds to be terminated were washed three times in warmed, sterile PBS to remove dead and unbound cells and placed in papain solution (2.4 mg/mL PBS) for digestion of the scaffold overnight at 60°C. Lysates were then incubated with Hoechst 33258 dye (Invitrogen, Carlsbad, CA) to fluorescently label double-stranded DNA. Fluorescent intensity (352/461 nm excitation/emission) from each sample was read using a fluorescent spectrophotometer (Tecan Infinite F200 Pro, Männedorf, Switzerland) and translated in cell counts through a standard curve of known MSC numbers.

Mitochondrial metabolic activity of the MSCs bound to each scaffold was quantified using the non-destructive alamarBlue® assay as previously described (Tierney, Duffy et al. 2013). Cell-seeded scaffolds were incubated in 0.75 mL of alamarBlue (Invitrogen, Carlsbad, CA) (1:20 5% FBS MSC Media) and incubated at 37°C for 90 minutes on a gentle shaker. The reduction of resazurin to resorufin by metabolically active cells was quantified on a fluorescent spectrophotometer through differential absorbance. Relative cell metabolic activity was determined from a standard curve generated with known MSC concentrations and reported as a fraction of initial seeding cell count.

Protein isolation, SDS-PAGE, and immunoblotting

Upon reaching each time point, (day 1, 3, 6) scaffolds to be terminated were washed three times in warmed, sterile PBS to remove dead and unbound cells. The scaffolds were then blotted briefly and placed in a cold 1:100 dilution each of protease inhibitor cocktail, phosphatase inhibitor cocktail II and phosphatase inhibitor cocktail III in RIPA buffer and placed back on ice for thirty minutes with agitation. The scaffolds were then removed and lysates were frozen (Caliari, Weisgerber et al. 2015). Protein concentrations were quantified with the Pierce BCA Protein Assay Kit (Thermo Fisher, Waltham, MA) and prepared for gel electrophoresis by diluting 10 μg of protein from each sample with an equal volume of Laemmli buffer. Samples were heated at 90°C for 10 min and loaded into 4-20% polyacrylamide gels (Bio-Rad Laboratories, Hercules, CA) in duplicate for both Smad 2/3 and 1/5/8 imaging. The gel electrophoresis was run at 150V for 90 minutes in 1 L of tris-glycine running buffer (25mM NaCl, 192mM glycine, 0.1% SDS, pH~8.3 in DI water) and immediately tank transferred onto nitrocellulose membranes (GE Healthcare, Little Chalfont, UK) at 300mV for 2 hours in 1 L of Towbin's transfer buffer (2.5M Tris base, 19.2mM glycine, 20% methanol in DI water). The nitrocellulose membranes were then cut and blocked in 5% milk in tris-buffered-saline + 0.1% tween 20 (TBST). Membranes were incubated in primary antibody at 4°C overnight in 5% BSA in TBST, washed three times in TBST, incubated in secondary antibody at RT for 1 hour, washed and imaged using the SuperSignal West Pico or Femto Chemiluminescent Substrate (Thermo Fisher, Waltham, MA) and an ImageQuant LAS 4010 system (GE Healthcare, Little Chalfont, UK). Primary antibodies were purchased from Cell Signaling (Danvers, MA): pSmad 2/3 (8828), Smad 2/3 (8685), pSmad 1/5/8 (9511), Smad 1 (6944), β-actin (4967). Secondary antibody used was HRP-linked goat anti-rabbit IgG (1:5000 in TBST). Membranes were stripped using the OneMinute® Western Blot Stripping Buffer (GM

Biosciences, Rockville, MD) and re-imaged two additional times, repeating the above procedure. ImageJ was used for band intensity quantification. Results were reported as the ratio of phosphorylated to total protein for each pathway.

RNA isolation and target gene expression characterization

RNA was extracted from the MSC-seeded scaffolds at D1, D3, D6 using an RNeasy Plant MiniKit (Qiagen, Valencia, CA) and frozen. The isolated RNA was then reverse transcribed to cDNA in a Bio-Rad S1000 thermal cycler, using the QuantiTect Reverse Transcription Kit (Qiagen, Valencia, CA) (Duffy, McFadden et al. 2011; Caliari, Weisgerber et al. 2012). Real-time PCR reactions were carried out in triplicate, using 10 ng of cDNA and QuantiTect SYBR Green PCR kit (Qiagen, Valencia, CA) in a 7900HT Fast Real-Time PCR system (Applied Biosystems, Carlsbad, CA). The primers used were consistent with previous studies and were synthesized by Integrated DNA Technologies (Coralville, IA). The expression level of the following markers was quantified: proteoglycan aggrecan (*ACAN*), cartilage oligomeric matrix protein (*COMP*), SRY-Box9 (*SOX9*), and glyceraldehyde 3-phosphate dehydrogenase (*GAPDH*), which was used as a house keeping gene **(Table 5.1)**. Results were generated using the ΔΔCt method and expressed as fold changes, normalized to the expression levels of MSCs at the time of seeding, D0.

Statistical analysis

One-way analysis of variance (ANOVA) was performed on the two ELISA experiments (initial sequestration and elution), and two-way ANOVA was performed on western blot, metabolic activity, cell number and gene expression data sets (independent variables: β-cyclodextrin loading and growth factor incubation), followed by Tukey-honest significant difference *post hoc* tests. Significance was set at $p < 0.05$. For cell experiments, scaffolds at each time point were analyzed

for all metrics, however, no statistical analyses was performed between time points. Error is reported in figures as the standard error of the mean, unless otherwise noted.

5.4 Results

Scaffold morphology

Scaffold morphology was examined by SEM after carbodiimide crosslinking and subsequent CPD. The CG scaffolds showed a distinct porous morphology, consistent with our previous studies (**Fig. 5.2A**). Closer examination shows that the characteristic banding pattern of the collagen is maintained through the fabrication and SEM preparation processes (**Fig. 5.2B**). Additional images were acquired 72 hours after MSC seeding, which show cells spreading out along the struts of the CG scaffolds (**Fig. 5.2C**).

β-cyclodextrin Incorporated Scaffolds Bind TGF-β1 More Efficiently and Exhibit Decreased Elution Profiles

First, the binding equilibrium of β-cyclodextrin was examined in CGcylco 1x and 5x scaffolds relative to CG scaffolds. CG scaffolds sequestered 28.98% of the TGF-β1 from solution while the 1x and 5x CGcylco groups sequestered 43.55% and 48.27% of the TGF-β1, respectively (**Fig. 5.3A**). Due to there being only a minimal difference between the 1x and 5x β-cyclodextrin groups' binding kinetics, and structural deficiencies in the 5x group due to dilution of the initial CG slurry, the 5x group was eliminated from future experiments.

The binding equilibrium was then further explored through characterization of the elution profile of TGF-β1 from blank and CGcylco 1x scaffolds. After just 1 hour, the CG scaffolds eluted significantly more bound growth factor than the CGcylco scaffolds ($p < 0.05$). At the end of 72 hours, just 1.38% of the TGF-β1 was retained in the CG scaffolds, while the CGcyclo scaffolds

retained 15.92%, resulting in a more than a 10-fold increase in TGF-β1 retention over 72 hours (**Fig. 5.3B**).

TGF-β1-β-cyclodextrin inclusion complexes increase metabolic activity and proliferation

After establishing the binding efficacy of CGcyclo scaffolds, the growth factor's presentation and effect on MSC response was explored. Specifically, the effect of TGF-β1 on cell number, metabolic activity and protein expression was examined. TGF-β1 had no effect on cellular proliferation (**Fig. 5.4A**) with all four experimental groups increasing from D1 to D3 and essentially remaining constant to D6. Conversely, there was a significant upregulation in cellular metabolic activity in the CGcyclo group with TGF-β1 at all three time points ($p < 0.05$). Accounting for this equal cell count between all four groups, the distinct upregulation of cellular metabolic activity can be attributed to the complexed growth factor within the CGcyclo scaffolds (**Fig. 5.4B**).

BMP-2-β-cyclodextrin inclusion complexes increase metabolic activity and proliferation

In parallel with TGF-β1, the effect of BMP-2 on cell number and metabolic activity was also examined. It was found that BMP-2 has minor effects on cellular proliferation (**Fig. 5.5A**). Slightly lower cell numbers on the CGcyclo scaffolds with BMP-2 compared to the CG scaffolds with no BMP-2 on day 1, while this trend was reversed on day 6. While significant, ($p < 0.05$) the magnitudes of these changes are small compared to the significantly lower metabolic activity observed in the CGcylco scaffolds with BMP-2 compared to the three other groups at all time points. (**Fig. 5.5B**).

TGF-β1-β-cyclodextrin inclusion complexes activate the Smad 2/3 pathway

The effect of TGF-β1 inclusion into CGcyclo scaffolds on the activation of the Smad 2/3 and Smad 1/5/8 pathways was evaluated by SDS-PAGE and western blot on days 1 and 3. Samples showed an increased activation of the Smad 2/3 pathway on day 3 when exposed to TGF-β1 (**Fig. 5.6A**). The increased activation of Smad 2/3 was significantly higher in the CGcyclo group with TGF-β1 compared to both the CG and CGcyclo groups without growth factor. ($p < 0.05$). The Smad 1/5/8 pathway was also examined to determine the non-targeted MSC cellular response to TGF-β1. No significant effects of the incorporation of β-cyclodextrin or TGF-β1 were observed on the activation of Smad 1/5/8 (**Fig. 5.6B**).

BMP-2-β-cyclodextrin inclusion complexes activate the Smad 1/5/8 pathway

The effect of BMP-2 inclusion into CGcyclo scaffolds on the activation of the Smad 2/3 and Smad 1/5/8 pathways was also evaluated on days 1 and 3. Interestingly, significant upregulation of Smad 2/3 activation was seen in the CGcyclo scaffolds with BMP-2 compared to the other three groups on day 1 (**Fig. 5.7A**) ($p < 0.05$). Additionally, while not significant, there was a general trend of increased activation of the Smad 1/5/8 pathway in the CGcyclo group with BMP-2 compared to the other three groups (**Fig. 5.7B)**.

TGF-β1-β-cyclodextrin inclusion complexes increase tenogenic gene expression

The resultant effect of TGF-β1 inclusion into CGclyco scaffolds on MSC chondrogenic gene expression was evaluated on days 1, 3 and 6 (**Fig. 5.8A-C**). While the expression levels for *ACAN* were quite low, large increases in expression of *COMP* and SOX9 were observed in the CGcyclo group with TGF-β1. The expression levels for *ACAN* were considerably lower throughout the experiment and were found to be significantly downregulated in both the CG and CGcyclo groups

with TGF-β1 on day 6 ($p < 0.05$). Conversely, expression levels for *COMP* were significantly higher in the groups with TGF-β1 compared to the unsupplemented CG and CGcyclo groups on days 1 and 3, while the CGcyclo group with TGF-β1 was significantly higher than all three other groups on day 6 ($p < 0.05$). By day 6, the expression levels of *SOX9* were significantly higher in just the CGcyclo group with TGF-β1 compared to all three other groups ($p < 0.05$).

5.5 Discussion

Previous research from our group has shown that porous CG scaffolds serve as robust supports for both the stable culture of MSCs and their subsequent differentiation to tendon, cartilage, and osteogenic phenotypes (Caliari and Harley 2014; Caliari, Gonnerman et al. 2015; Caliari, Weisgerber et al. 2015; Grier, Moy et al. 2017). Here, the focus was shifted to accelerating this differentiation through the more efficient loading and display of growth factors into the CG scaffolds through β-cyclodextrin sequestration. As previously stated, the driving force for β-cyclodextrin sequestration is hydrophobic interactions. Therefore, it is crucial that the host molecule contains hydrophobic moieties to interact with the interior of β-cyclodextrin. Examination of TGF-β1 reveals exposed hydrophobic regions through β-strands β-8 and β-9 that form the 'bow-tie' link of its two arm domains and through an extended loop connecting α1 and α2 helices rich in proline and aromatic residues (Shi, Zhu et al. 2011). It is this region, directly surrounding the α1 helix, that most likely binds the interior of β-cyclodextrin, as it is more exposed on the tip of the molecule and most extensively hydrophobic in character. BMP-2 has been found to contain hydrophobic residues throughout the molecule and in particular local density at the bottom of the growth factor's central cleft (Scheufler, Sebald et al. 1999). The fundamental mechanism for β-cyclodextrin sequestration is applicable to the two growth factors, as it is also

known that BMPR-II:BMP-2 complex interactions are dominantly hydrophobic in nature, proven through residue mutations, and TGF-β receptor:ligand complexes result from a combination of hydrophobic and electrostatic interactions (Yin, Fu et al. 2008; Hinck 2012).

Elucidating the sequestration mechanism for each growth factor to β-cyclodextrin clarifies the results of the work presented. The additional TGF-β1 initially bound by the CGcyclo scaffolds compared to the CG scaffold can be wholly attributed to β-cyclodextrin incorporation. Not only was more TGF-β1sequestered by the CGcyclo scaffolds, but the TGF-β1 that was sequestered was also retained over a longer period. The controlled release of the TGF-β1from the CGcyclo scaffolds makes them an ideal candidate for the control of MSC fate as we have shown here.

Bone morphogenetic proteins (BMPs) belong to the larger transforming growth factor β (TGF-β) superfamily, which regulate a wide array of cellular functions including cell migration, adhesion, division, and differentiation throughout the human life span (Massague and Chen 2000). Cell metabolic activity and Smad pathway activation, traditionally associated with TGF-β1 and BMP-2 signaling, was consequently employed as the metrics for increased growth factor loading. Previous work has shown that the minimum effective concentrations for TGF-β1 and BMP-2 are 0.02 – 2.0 ng/mL and ~20 ng/mL respectively (Zhang and Laiho 2003; Lysdahl, Baatrup et al. 2014). This difference in threshold concentration can help to explain the data observed in **Fig. 5.4-5.7** and the lower activity of BMP-2 compared to TGF-β1 in this study.

TGF-β1 was found to increase cellular metabolic activity, Smad 2/3 pathway activation, and the expression of chondrogenic markers *COMP* and *SOX9*. This is consistent with previous work where TGF-β1 has been found to stimulate proliferation and self-renewal of MSCs and inhibit differentiation into osteogenic lineages through Smad 3 signaling (Guo and Wang 2009). TGF-β1

has also been found to co-stimulate Smad 2/3 through phosphorylation which collectively associates into a larger transcription factor complex (Massague and Wotton 2000; Xin, Li et al. 2013). Phosphorylated Smad 2/3 has then been shown to stimulate tenogenic lineages in conjunction with *COMP*, *ACAN*, and *SOX9* expression (Caliari and Harley 2014; Grier, Moy et al. 2017; Grier, Iyoha et al. 2017).

Conversely, BMP-2 was found to lead to a slight drop in cellular metabolic activity and simultaneously generally increase Smad 1/5/8 phosphorylation. The BMP II receptor-mediated phosphorylation of Smad 1/5/8 allows the activated isoforms to associate with Smad 4, translocate to the nucleus, and stimulate transcription of target genes related to bone deposition, making the 1/5/8 signaling pathway critical in MSC osteogenic signaling (Soltanoff, Yang et al. 2009; Chen, Uludag et al. 2012; Beederman, Lamplot et al. 2013). The upregulation of one such target gene, runt-related transcription factor 2 (*RUNX2*), has been found to lead to the subsequent expression of alkaline phosphatase (*ALP*) and osteocalcin (*OC*), genes critical for bone formation (Lysdahl, Baatrup et al. 2014). The activation of the Smad 1/5/8 osteogenic pathway strongly correlates with the metabolic activity data presented in **Fig. 5.4**, as mature osteocytes rarely divided compared to the more immature MSCs (Malaval, Liu et al. 1999; Westhrin, Xie et al. 2015).

5.6 Conclusions

The work presented demonstrates the ability for β-cyclodextrins to efficiently bind growth factors from solution prior to cell-seeding through CDIC formation as a means to accelerate MSC differentiation with lineage guidance dependent on growth factor bound. This mechanism can effectively lower the *in vitro* concentration of growth factors needed to induce cellular responses and can be potentially utilized for a variety of growth factors, cell types and applications in the

hope of driving down patient related costs. This work establishes a new method for the successful incorporation and display of growth factors within CG scaffolds which, in combination with previously developed methods, has the potential to allow for more intricate designs for the selective display of multiple factors.

5.7 Table

Table 5.1 PCR primer sequences.

Transcript	Sequence	Reference
ACAN	Forward: 5'- TGCATTCCACGAAGCTAACCTT -3' Reverse: 5'- GACGCCTCGCCTTCTTGAA -3'	(Zhou, Xu et al. 2011)
COMP	Forward: 5'- GCAACACGGACGAGGACAAG -3' Reverse: 5'- CGCCATCACTGTCCTTCTGG -3'	(Klatte-Schulz, Pauly et al. 2013)
SOX9	Forward: 5'- AGCGAACGCACATCAAGAC -3' Reverse: 5'- GCTGTAGTGTGGGAGGTTGAA -3'	(Zhou, Xu et al. 2011)
GAPDH	Forward: 5'- CCATGAGAAGTATGACAACAGCC -3' Reverse: 5'- CCTTCCACGATACCAAAGTTG -3'	(Pauly, Klatte et al. 2010)

5.8 Figures

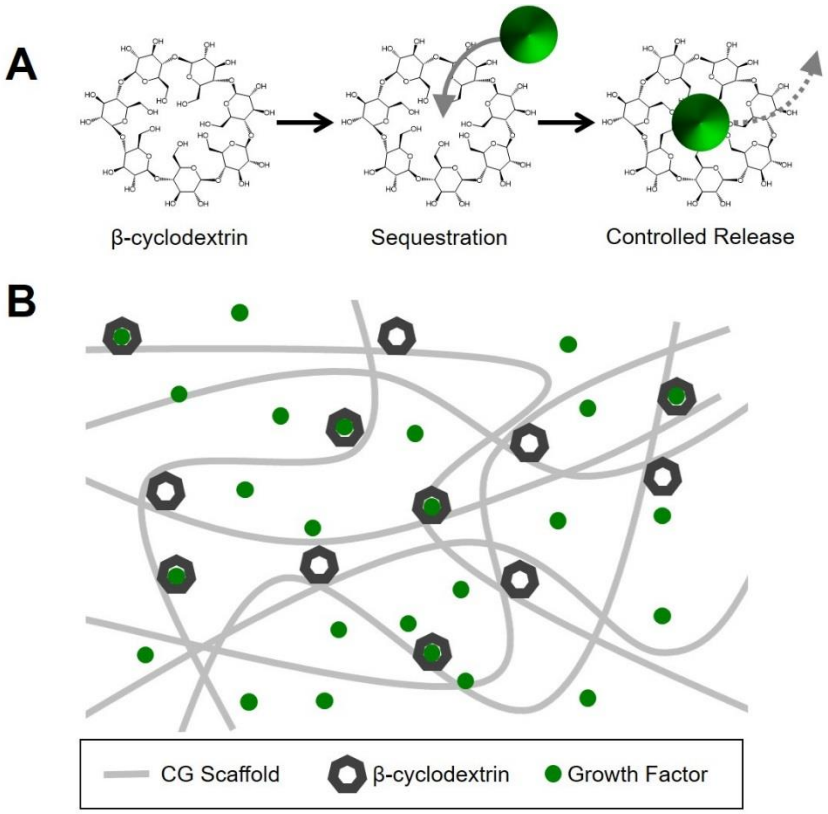

Figure 5.1 β-cyclodextrin guest-host interactions and incorporation into CG scaffolds. (A) Seven-membered ring structure of β-cyclodextrin and the spontaneous process of forming inclusion complexes. **(B)** Representation of β-cyclodextrin incorporation into CG scaffold structure for the pull-down of growth factors from solution.

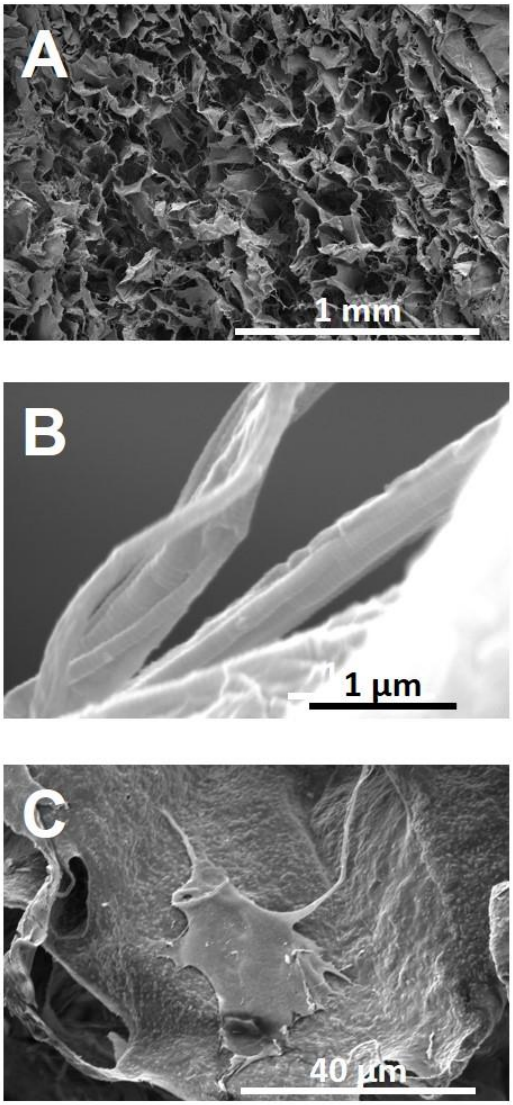

Figure 5.2 CG scaffold microstructure. (A) Cross-section of the porous CG scaffolds. Scale bar: 100µm **(B)** High-magnification image of the individual collagen fiber banding. Scale bar: 1 µm **(C)** hMSC spreading along scaffold surface. Scale bar: 40 µm.

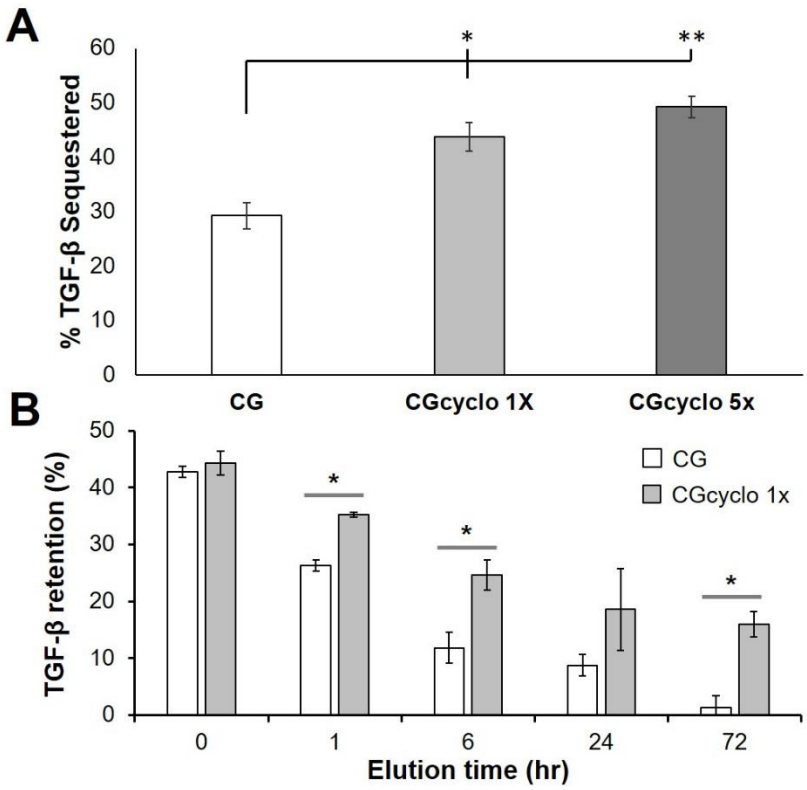

Figure 5.3 TGF-β1 pull-down and controlled release from CG scaffolds with β-cyclodextrin. **(A)** The incorporation of β-cyclodextrin into CG scaffolds in both 1x and 5x concentrations resulted in increased pull-down of TGF-β1 from solution. (**B)** β-cyclodextrin scaffolds showed increased retention of TGF-β1 over 72 hours. *: $p < 0.05$

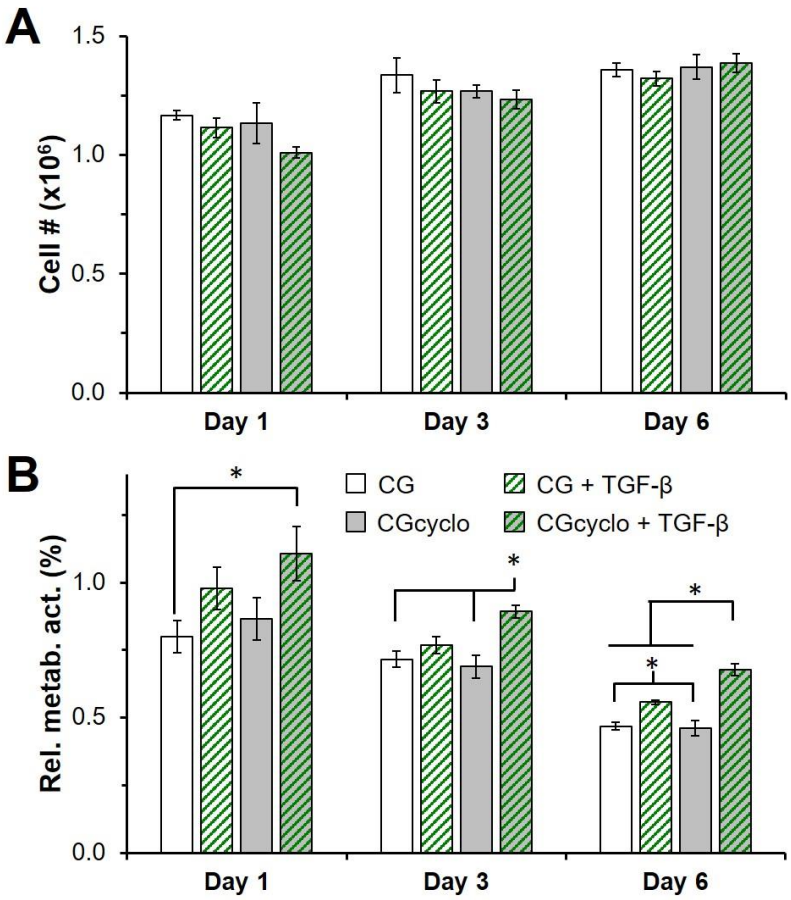

Figure 5.4 MSC viability in CG scaffolds exposed to TGF-β1. (A) Number of cells and **B)** normalized metabolic activity in blank and β-cyclodextrin scaffolds with and without TGF-β1 on days 1, 3, and 6 after seeding. Data expressed as mean ± SEM (n = 6). *: $p < 0.05$.

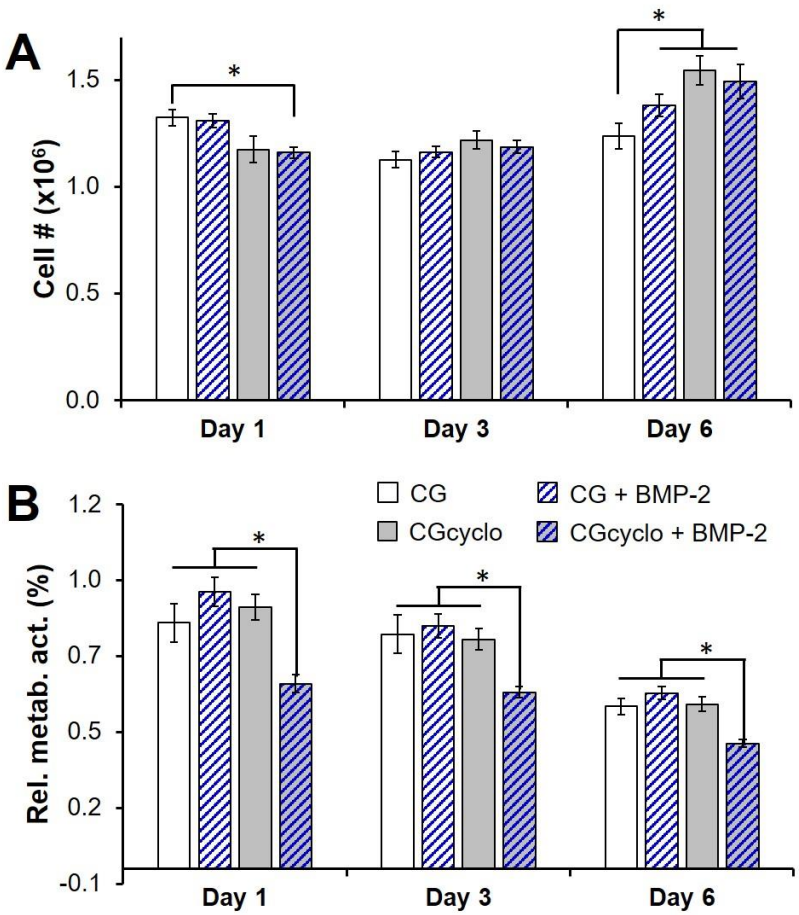

Figure 5.5 MSC viability in CG scaffolds exposed to BMP-2. (A) Number of cells and (**B)** normalized metabolic activity in blank and β-cyclodextrin scaffolds with and without BMP-2 on days 1, 3, and 6 after seeding. Data expressed as mean ± SEM (n = 6). *: $p < 0.05$.

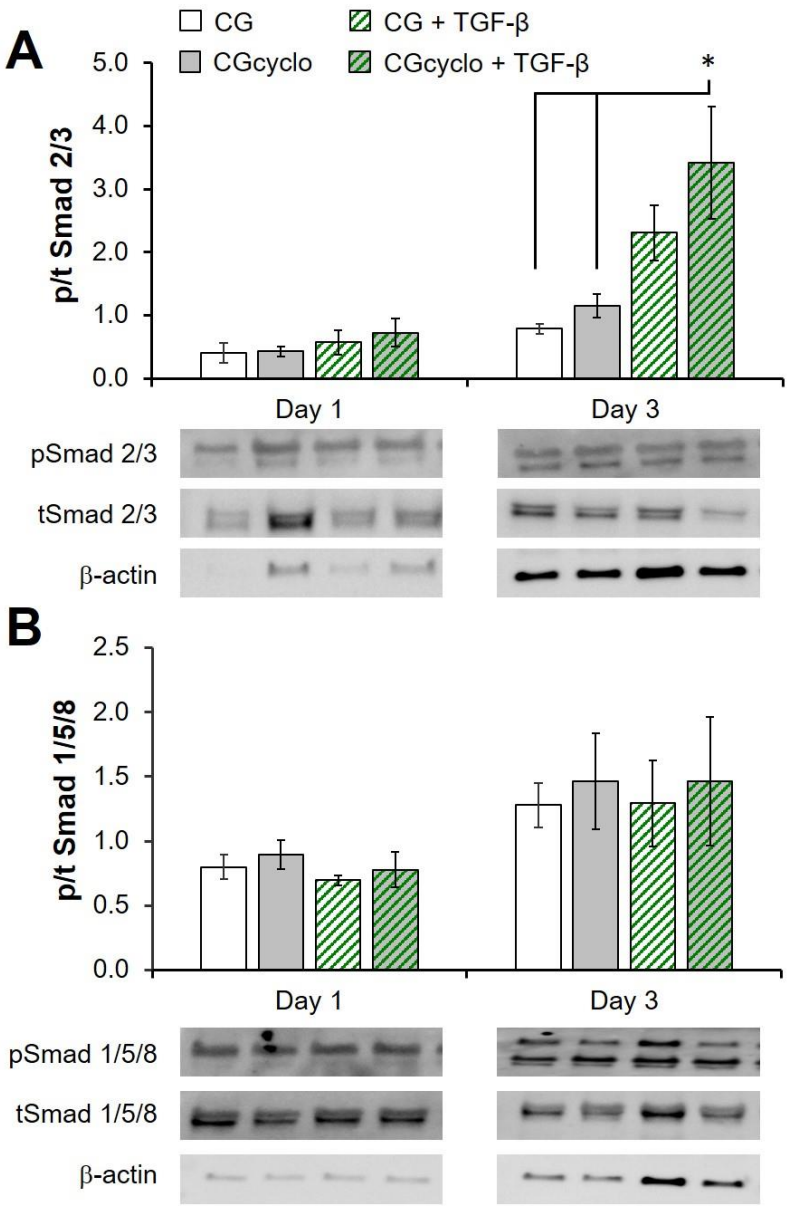

Figure 5.6 Smad pathway activation in CG scaffolds exposed to TGF-β1. Relative levels of phosphorylated : total **(A)** Smad 2/3 and **(B)** Smad 1/5/8 in scaffolds with and without TGF-β1 as determined by immunoblot on days 1 and 3 after seeding. Data expressed as mean ± SEM (n = 3). *: $p < 0.05$.

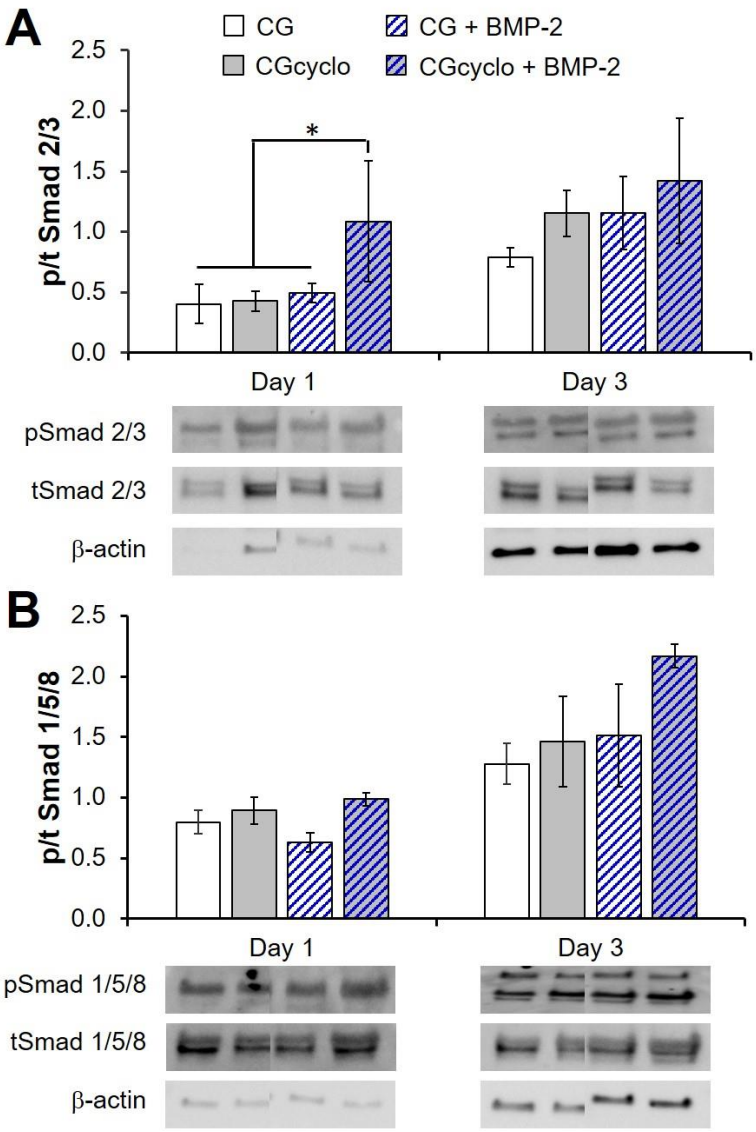

Figure 5.7 Smad pathway activation in CG scaffolds exposed to BMP-2. Relative levels of phosphorylated : total **(A)** Smad 2/3 and **(B)** Smad 1/5/8 in scaffolds with and without BMP-2 as determined by immunoblot on days 1 and 3 after seeding. Data expressed as mean ± SEM (n = 3). *: $p < 0.05$.

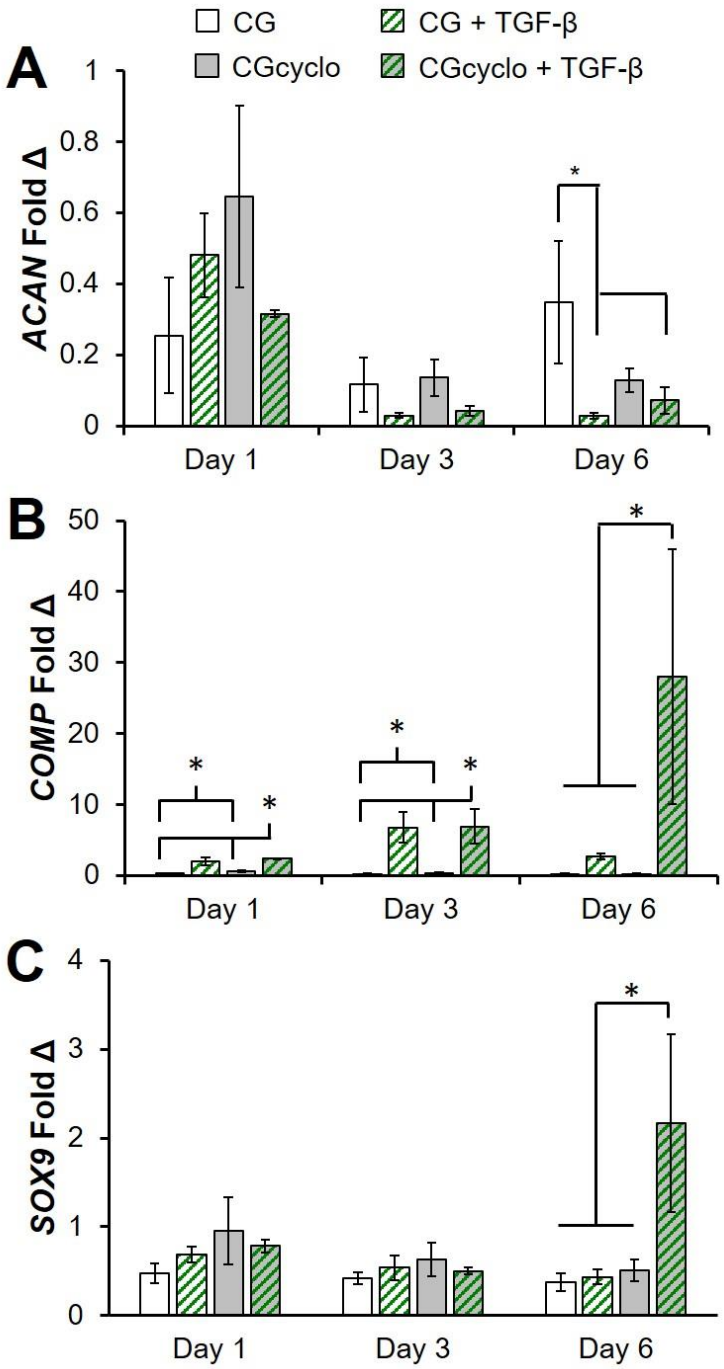

Figure 5.8 Changes in pro-chondrogenic gene expression in response to TGF-β1. Expression levels of **(A)** *ACAN*, **(B)** *COMP*, and **(C)** *SOX9* with and without TGF-β1 exposure on days 1, 3, and 6. Data expressed as mean ± SEM (n = 6). *: $p < 0.05$.

CHAPTER 6: CONCLUSIONS AND FUTURE WORK

6.1 Conclusions

In this work, we sought to develop new biomaterial and culture methods to promote spatial-controlled differentiation of mesenchymal stem cells (MSCs) for tendon-bone junction (TBJ) regeneration applications. We described the development of a collagen-GAG (CG) scaffold system and methods to alter scaffold microstructure and composition in an effort to mimic components of the natural tissue extracellular matrix (ECM) environment to influence MSC differentiation.

Chapter 2 describes the evaluation of scaffold microstructure and mechanics and resultant impacts of tenocyte viability and gene expression profiles for a series of anisotropic CG scaffolds with variable pore size and strut stiffness, as a function of crosslinking density. Equine tenocytes demonstrated considerably less cell-mediated contraction of the more mechanically robust scaffolds with smaller pore sizes (T_f = -60°C) and highest crosslinking density (5:2:1 EDC:NHS:COOH). The tenocytes seeded in these scaffolds that were able to resist contraction showed increased proliferation, metabolic activity, and expression levels of traditional tenogenic ECM and phenotypic markers. This is likely due to the fact that the cell-mediated contraction resulted in constricted pore diameter, limiting nutrient biotransport. Interestingly, the expression levels of matrix metalloproteinases MMP 1, MMP3, and MMP 13 were all significantly upregulated in scaffolds that exhibited the most cell-mediated contraction, a likely indicator of cellular remodeling of the scaffold structure due to losses in contact guidance cues. This work suggests that the scaffold microstructural properties and mechanics are critical design parameters for tendon tissue engineering and the maintenance and development of cellular behavior of long-term culture.

Chapter 3 utilized the optimized anisotropic CG scaffold identified in Chapter 2, in conjunction with a custom bioreactor system to evaluate the potential to use cyclic tensile strain (CTS), as a method to drive tenogenic differentiation of MSCs. The custom bioreactor system was designed with individual wells for sampling and to be adaptable for a wide variety of scaffold geometries and loading paradigms. Additionally, a novel method to embed the ends of porous CG scaffolds into hollow end blocks was developed to enable the loading of scaffolds into the bioreactor without the use of clamps, which can result in crushing or tearing of the scaffold or slippage. The initial effects of CTS on cell-material interactions and mechanotransduction pathways was evaluated and validated that MSCs within our system follow a standard pattern of ERK 1/2 and p38 activation, which led to the development of an intermittent CTS paradigm to promote increased ERK 1/2 activation and resultant collagen production. When exposed to CTS over a 6-day culture period, MSCs showed enhanced tenogenic differentiation as evidenced by increased expression of markers like, *COL3AI*, *COMP*, *SCX*, *TNC*, and *MKX*. By day 6, the application of CTS also resulted in increased activation of the Smad 2/3 pathway, evidence of endogenous TGF-β production which could drive long-term tissue development. Improved understanding of cell-material interactions and responses to CTS here motivated the next generation of work leveraging mechanical stimulation as a means to drive spatially-dependent MSC responses on a graded material.

Chapter 4 then expanded on the work presented in Chapter 3 and investigated the application of CTS on a multi-compartment CG scaffold with continuous, but distinct, regions of mineral content and structural anisotropy, for TBJ regeneration. The variations in mechanical properties across the scaffold compartments resulted in the strain amplitude being primarily localized to the non-mineralized anisotropic compartment of the scaffold. We found that the localization of strain to the CG compartment drove a preferential tenogenic response in that compartment, as evidenced

by expression levels of *COL3A1*, *COMP*, *SCX*, and *MKX*. There were minimal negative effects of CTS on the expression of osteogenic differentiation markers *ALP*, *BSP*, and *RUNX2* in MSCs within the mineralized compartment. These results were supported by evidence of preferential activation of the Smad 2/3 and Smad 1/5/8 pathways in the anisotropic and mineralized compartments, respectively. Interestingly, sections of each scaffold that contained the interfacial zone, along with regions of each compartment, were evaluate for expression levels of fibrocartilaginous interface markers *ACAN* and *SOX9*. These interface-specific genes were generally upregulated with strain and there was some evidence of preferential upregulation specifically in the interfacial region of the scaffold. The low resolution of the sampling techniques used does not allow us to draw any specific conclusions as to how CTS may enhance interface development within a graded biomaterial, but it does motivate future work specifically focused on this region.

While Chapters 2-4 focused on the development of instructive biomaterial cues and cellular interactions with dynamic culture systems, Chapter 5 investigated the potential to alter biomaterial composition for the control of growth factor presentation. Scaffolds with incorporated β-cyclodextrin showed increased pull-down of growth factors, like TGF-β, from solution, followed by controlled release over a number of days. When seeded with MSCs, the β-cyclodextrin scaffolds that had previously been loaded with TGF-β, promoted increased cellular metabolic activity, heightened activity of Smad 2/3, and higher expression of chondrogenic gene markers *COMP* and *SOX9*. Loading β-cyclodextrin scaffolds with BMP-2 resulted in similar results regarding the osteogenic differentiation of MSCs. Cells exposed to extended release of BMP-2 showed lower metabolic activity levels, evidence of osteogenic differentiation, and generally increased activation of Smad 1/5/8. This work provides a new method to selectively sequester and present growth

factors within a biomaterial without the need to chemically modify the scaffold or growth factor. This technology could easily be applied to spatially-graded materials produced by liquid-phase co-synthesis to control the spatial distribution of growth factors with CG scaffolds.

6.2 Future Directions

This thesis provides a foundation for understanding biomaterial design and culture supplementation strategies for the regeneration of complex, structurally heterogeneous, orthopedic interfaces, such as the TBJ. Importantly, this work highlights many key challenges associated with developing comprehensive tissue engineering solution, including:

- Understanding long-term culture dynamics and *de novo* tissue formation or regeneration of structurally competent tissue structures.
- Developing higher resolution techniques to evaluate fibrocartilaginous interface regeneration on a physiologically-relevant sub-millimeter scale through gene expression analysis, cell-matrix interactions, and tissue formation.
- Structural reinforcement of the scaffold structure in order to withstand physiological loading paradigms in order to avoid failure after implantation.
- Evaluation of scaffold performance and healing properties in *in vivo* preclinical animal models.

Long-term culture dynamics

The work presented in this thesis was primarily limited to shorter-duration experiments, up to 6 days of culture, and examined early signs of stem cell differentiation. However, tissue development and healing generally occur over a timespan of weeks to months. It will be important to evaluate how and if this initial MSC differentiation can translate into robust tissue development,

ECM deposition and organization, and augmented mechanical properties over an extended timeline. This will be important for developing *in vitro* culture systems to produce engineered tissue constructs or for understanding the long-term development of implanted biomaterials.

Techniques for interface regeneration

As suggested in Chapter 4, MSCs on spatially-graded CG scaffolds that are exposed to CTS do begin to show initial signs of fibrocartilaginous interface development. This is a particular area of focus that must be explored more thoroughly. Unfortunately, the sub-millimeter scale of the native TBJ limits the available tools to fully and consistently analyze the dynamics in this narrow regime. Emerging statistical and analytical techniques to evaluate gene expression in samples, with small numbers of cells, are becoming more accessible and could be applied in such a situation.

Additionally, it may be prudent to engineer biomaterials with a defined interfacial zone. One may look to design materials with localized distributions of growth factor presentation using a method such as the β-cyclodextrin incorporation discussed in Chapter 5. Alternatively, a distinct fibrocartilage compartment could be incorporated into a CG scaffold. One idea would be to engineer a hydrogel interface that is distributed between the mineralized and anisotropic compartments of the materials used in Chapter 4. While hydrogels lack many of the mechanical properties that are ideal for many orthopedic applications, a number of emerging technologies now exists to print hydrogels with intricate designs and display of factors. Such a hydrogel could be integrated into the scaffold interface to promote fibrocartilage development and relying on the scaffold properties to mitigate many of the mechanical shortcomings of hydrogels.

Scaffold structural reinforcement

One of the main drawbacks of CG scaffolds is an inability for the scaffold material to match the mechanical properties of native tendon tissue. Tendons are dynamic and strong tissues which undergo consistently high levels of strain *in* vivo. The potential for the scaffold to tear or pull out of a defect after implantation is a serious concern before beginning preclinical trials. We have previously demonstrated the use of membrane core-shell composites to improve the mechanical properties of aligned CG scaffolds as well as in incorporation of 3D printed polymer materials to bear high levels of load within a larger composite construct. This type of material could be engineered to work with a multi-compartment material and to promote the spatial distribution of mechanical cues that were seen in Chapter 4.

Animal models

A key step forward for clinical translation of the materials and methods developed in this thesis will be the initialization of animal trials to evaluate their *in vivo* efficacy. Preliminary mouse ectopic models have already been conducted to assess graft durability and capacity to support cellular infiltration ad growth. Eventually, there will be a need for these scaffolds to be implanted into load-bearing wound models. There are early plans to implant miniaturized versions of the multi-compartment scaffolds into either rat or rabbit rotator cuff injury models.

Concluding thoughts

This suite of technologies represents a path towards the development of biomaterials and techniques to control stem cell fate in a spatially-dependent manner for the regeneration of orthopedic interfaces such as the TBJ. The biomaterial systems applied in this thesis still require further development and must be validated through rigorous animal testing before clinical use. This work has helped to answer fundamental questions regarding the influence of material

properties and dynamic culture conditions on MSC differentiation which will inform future studies relating the regeneration of the TBJ and other complex orthopedic tissues and the design of platforms to better understand physiological and pathological states.

APPENDIX A: SCAFFOLD FABRICATION AND CHARACTERIZATION PROTOCOLS

A.1 CG suspension preparation protocol

Reference: (Yannas, Lee et al. 1989; O'Brien, Harley et al. 2004)

Reagents

- Collagen from bovine Achilles tendon (Sigma-Aldrich C9879); store at 4°C
- Chondroitin sulfate sodium salt from shark cartilage (Sigma-Aldrich C4384); store at 4°C
- Glacial acetic acid (Sigma-Aldrich 71251)
- Ethylene glycol (VWR BDH1125-4LP)
- Deionized water

Supplies and equipment

- Recirculating chiller (Fisher Isotemp Model 900)
- Rotor-stator (IKA 0593400)
- Disperser (IKA 3565001)
- Jacketed beaker (Ace Glass 5340-115)
- Freeze-dryer (VirTis Genesis)
- Dual range balance (Mettler Toledo XS105)
- Beakers
- Transfer pipets
- Parafilm

Procedure

*This procedure describes how to make 300 mL of 0.5% CG suspension. Scale collagen and GAG content appropriately to create different volumes of suspension.

1) Fill recirculating chiller with a 50/50 mix of ethylene glycol and deionized water, making sure that the cooling coils are completely immersed in the liquid. Set the recirculating chiller to 4°C.

2) Attach recirculating chiller to jacketed beaker and give 20-30 min for temperature to equilibrate to 4°C. Maintaining this temperature is important, as it will prevent the collagen from denaturing during the blending process.

3) Prepare a 0.05 M solution of acetic acid by adding 0.87 mL of glacial acetic acid to 300 mL of deionized water.

4) Weigh 1.5 g of collagen and add to the jacketed beaker.

5) Pour 250 mL of the 0.05 M acetic acid into the jacketed beaker.

6) Assemble the rotor-stator and attach it to the disperser. Lower the rotor-stator into the suspension. The rotor-stator should be vertical and centered in the beaker.

7) Blend the suspension at 15,000 rpm for 90 min at 4°C. The height of the rotor-stator may need to be adjusted during the blending process: If the rotor-stator is positioned too high, the holes on its side will be visible; if it is too low, the suspension will bubble excessively. Periodically check to see if the rotor-stator is clogged with collagen; remove clogs with a spatula as needed.

8) Add 50 mL of 0.05 M acetic acid to a 50 mL centrifuge tube. Weigh out 0.133 g of chondroitin sulfate (GAG) and add to the centrifuge tube. Keep GAG solution in the refrigerator (4°C) until next step.

9) Mix the GAG solution well and add it drop-wise with a transfer pipet to the collagen suspension while it is being mixed at 15,000 rpm at 4°C. It may be necessary to stop and unclog the rotor-stator with a spatula during this process.

10) Once all of the GAG solution has been added, blend at 15,000 rpm for 90 min at 4°C. Periodically check to ensure the rotor-stator is lowered to the correct depth, as the suspension will gradually become less viscous and creep up the sides of the jacketed beaker. Periodically check to see if the rotor-stator is clogged; remove clogs with a spatula as needed.

11) Store the suspension for 18-22 h at 4°C.

12) Degas the suspension in the freeze-dryer to remove any air bubbles prior to use. Make sure to run the 'Degas' program and let the condenser temperature reach < -50°C to prevent liquid from entering the vacuum pump. Degas suspension in a Parafilm-covered beaker until solution boils. Note that higher density suspensions typically have more trapped bubbles so adjust the degassing volume accordingly.

13) Store the suspension at 4°C. Periodically check the CG suspension; if not homogenous, re-blend at 15,000 rpm for 30 min at 4°C.

A.2 CGCaP suspension preparation protocol

Reference: (Harley, Lynn et al. 2010; Lynn, Best et al. 2010), Process Record No. PR OM-004 Preparation of Mineralized Slurry, BioUetikon and OrthoMimetics, Process Record No. PR OM-001 Preparation of 0.1456M Phosphoric Acid/0.037M Calcium Hydroxide, BioUetikon and OrthoMimetics.

Reagents

- Collagen from bovine Achilles tendon (Sigma-Aldrich C9879); store at 4ºC
- Chondroitin sulfate sodium salt from shark cartilage (Sigma-Aldrich C4384); store at 4ºC
- 0.1456M phosphoric acid / 0.037M calcium hydroxide buffer solution
    - 5.904 mL 85% phosphoric acid (Sigma-Aldrich P5811)
    - 570 mL deionized water
    - 1.644 g calcium hydroxide (Sigma-Aldrich 31219)
    - Add acid to water, then calcium hydroxide. Bring volume to 600 mL and adjust pH to 2.0-2.4. Solution is good for 3 months.
- Calcium hydroxide (Sigma-Aldrich, 31219)
- Calcium Nitrate Tetrahydrate (Sigma-Aldrich, 31218)
- Ethylene glycol (VWR BDH1125-4LP)
- Deionized water

Supplies and equipment

- Recirculating chiller (Fisher Isotemp Model 900)
- Rotor-stator (IKA 0593400)
- Disperser (IKA 3565001)
- Jacketed beaker (Ace Glass 5340-115)
- Freeze-dryer (VirTis Genesis)
- Dual range balance (Mettler Toledo XS105)
- pH meter
- Beakers
- Transfer pipets
- Centrifuge tubes
- Parafilm

Procedure

*This procedure describes how to make 300 mL of 40 wt% CGCaP suspension.

1) Setup the jacketed vessel, setting the water temperature to 4°C.

2) Add 5.7966 g collagen to the jacketed vessel. Then add 242.12mL of phosphate acid / calcium hydroxide buffer to the collagen. Set the blender to 15,000 rpm for 30 min, so that the collagen is submerged prior to hydration. Allow the collagen to hydrate for 18-22 h in the cooled jacketed vessel at 4°C. This mixture will become very viscous and difficult to blend.

3) Measure out 2.515 g of chondroitin sulfate and add it to 42.94mL of phosphate acid / calcium hydroxide buffer in a beaker. Then mix the buffer and the chondroitin (GAG solution), using a magnetic stirring bar, until fully dissolved.

4) Measure out 1.92 g calcium hydroxide and 1.17 g calcium nitrate tetrahydrate and place both in a 50 mL centrifuge tube. Add 15 mL of deionized water to the tube using a pipette. Then mix (vortex/shake) the solution to suspend the salts in the water.

5) Set the blender to 15,000 rpm and blend the hydrated collagen made in step 2 for 60 min.

6) Add the GAG solution prepared in step 3 to the hydrated collagen solution prepared in step 2 in 8 mL steps while mixing at 15,000 rpm. In between each 8 mL step, take care to prevent any clumping of the collagen/GAG with a spatula. With the additional volume, the slurry will mix better.

7) Blend this GAG / hydrated collagen solution at 15,000 rpm for 30 min.

8) Blend the collagen / GAG mixture at 200-800 rpm while adding the salts to maximize dispersion. Using a pipette, add the salt solution at a rate of 8mL/min to the collagen / GAG mixture, allowing time for blending after each volume. Then blend the slurry at 15,000 rpm for 30 min.

9) Stores the slurry for 18-22 h at 2-8°C before use. Periodically check the CG suspension; if not homogenous, re-blend at 15,000 rpm for 30 min at 4^{o}C.

A.3 CG β-cyclodextrin suspension preparation protocol

Reference: (Yannas, Lee et al. 1989; O'Brien, Harley et al. 2004)

Reagents

- Collagen from bovine Achilles tendon (Sigma-Aldrich C9879); store at 4ºC
- Chondroitin sulfate sodium salt from shark cartilage (Sigma-Aldrich C4384); store at 4ºC
- Glacial acetic acid (Sigma-Aldrich 71251)
- β-cyclodextrin (Sigma-Aldrich C4805)
- 1M NaOH
- Ethylene glycol (VWR BDH1125-4LP)
- Deionized water

Supplies and equipment

- Recirculating chiller (Fisher Isotemp Model 900)
- Rotor-stator (IKA 0593400)
- Disperser (IKA 3565001)
- Jacketed beaker (Ace Glass 5340-115)
- Freeze-dryer (VirTis Genesis)
- Dual range balance (Mettler Toledo XS105)
- Beakers
- Transfer pipets
- Parafilm

Procedure

*This procedure describes how to make 150 mL of 1% CG suspension with 3.7 μg/mL β-cyclodextrin. Scale collagen, GAG, and β-cyclodextrin content appropriately to create different volumes of suspension.

1) Fill recirculating chiller with a 50/50 mix of ethylene glycol and deionized water, making sure that the cooling coils are completely immersed in the liquid. Set the recirculating chiller to 4ºC.

2) Attach recirculating chiller to jacketed beaker and give 20-30 min for temperature to equilibrate to 4ºC. Maintaining this temperature is important, as it will prevent the collagen from denaturing during the blending process.

3) Prepare a 0.05 M solution of acetic acid by adding 0.435 mL of glacial acetic acid to 150 mL of deionized water.

4) Weigh 1.5 g of collagen and add to the jacketed beaker.

5) Pour 135 mL of the 0.05 M acetic acid into the jacketed beaker.

6) Assemble the rotor-stator and attach it to the disperser. Lower the rotor-stator into the suspension. The rotor-stator should be vertical and centered in the beaker.

7) Blend the suspension at 15,000 rpm for 90 min at 4°C. The height of the rotor-stator may need to be adjusted during the blending process: If the rotor-stator is positioned too high, the holes on its side will be visible; if it is too low, the suspension will bubble excessively. Periodically check to see if the rotor-stator is clogged with collagen; remove clogs with a spatula as needed.

8) Add 15 mL of 0.05 M acetic acid to a 50 mL centrifuge tube. Weigh out 0.133 g of chondroitin sulfate (GAG) and add to the centrifuge tube. Keep GAG solution in the refrigerator (4°C) until next step.

9) Mix the GAG solution well and add it drop-wise with a transfer pipet to the collagen suspension while it is being mixed at 15,000 rpm at 4°C. It may be necessary to stop and unclog the rotor-stator with a spatula during this process.

10) Prepare a solution of 10 mg/mL β-cyclodextrin in 1 M NaOH.

11) Add 11.1 μL β-cyclodextrin to CG slurry.

12) blend at 15,000 rpm for 15 min at 4°C. Periodically check to ensure the rotor-stator is lowered to the correct depth, as the suspension will gradually become less viscous and creep up the sides of the jacketed beaker. Periodically check to see if the rotor-stator is clogged; remove clogs with a spatula as needed.

13) Store the suspension for 18-22 h at 4°C.

14) Degas the suspension in the freeze-dryer to remove any air bubbles prior to use. Make sure to run the 'Degas' program and let the condenser temperature reach < -50°C to prevent liquid from entering the vacuum pump. Degas suspension in a Parafilm-covered beaker until solution boils. Note that higher density suspensions typically have more trapped bubbles so adjust the degassing volume accordingly.

15) Store the suspension at 4°C. Periodically check the CG suspension; if not homogenous, re-blend at 15,000 rpm for 30 min at 4°C.

A.4 Aligned CG scaffold fabrication protocol

Reference: (Caliari and Harley 2011; Caliari, Ramirez et al. 2011)

Reagents

- CG suspension; store at 4°C
- Welch DirecTorr Gold synthetic pump oil (Fisher 01-184-105)

Supplies and equipment

- Freeze-dryer (VirTis Genesis)
- PTFE-copper freeze-drying mold
- Beakers
- Parafilm
- Aluminum foil

Procedure

*This procedure describes the fabrication of 15 mm tall aligned scaffolds (single and multi-compartment, with and without membrane shells). Check that oil is clean (not yellow) before and after each freeze-dryer run, replacing when necessary.

1) Degas CG suspension in Parafilm-covered beaker by pulling vacuum inside freeze-dryer to remove all air bubbles. Make sure the condenser is at least -50°C or cooler before degassing.

2) Begin to cool freeze-dryer shelves by running 'Tf = xx C shelf cool' program where xx is the desired freezing temperature (-10, -40, or -60°C).

3) If making scaffold-membrane composites, cut membranes to size, roll, and place in PTFE-copper freeze-drying mold holes.

4) Pipette 970 μL (8 mm diameter holes) or 540 μL (6 mm diameter holes) of suspension into each hole in PTFE-copper freeze-drying mold. For scaffold-membrane composites, allow suspension to hydrate membranes for 15-30 min at 4°C.

5) For multi-compartment scaffold fabrication, carefully pipet the first suspension (e.g. CG suspension, 360 μL) into mold wells. Then, add the second suspension (e.g. CGCaP suspension, 180 μL) carefully on top of the first suspension, taking care not to mix the two layers. Following pipetting, place entire mold on Kimwipe and allow to interdiffuse for 15-30 min at 4°C.

6) Cancel shelf cool program and place freeze-dryer mold on the pre-cooled shelf. Shut the freeze-dryer door and run program 'Aligned Tf = xx' where xx is the desired freezing temperature (-10, -40, or -60°C). A typical freeze-drying schedule is shown for the fabrication of an aligned -60°C scaffold:

Step	Temperature °C	Time, min	Ramp/Hold	Vacuum level, torr	PCM
Freezing hold	-60	60	H	~600	N/A
Drying ramp	0	60	R	0.2	150
Drying hold	0	5	H	0.2	1
Extra drying	0	60	H	0.2	0
Storage ramp	20	20	R	0.2	0
Storage hold	20	indefinite	H	0.2	0

PCM refers to the minimum reading difference between the Pirani and capacitance manometer pressure gauges that must be achieved before the program proceeds to the next step. In Pirani gauges, a filament in the gauge is heated so that it is at a constant temperature at a given pressure. As the pressure increases or decreases, the amount of gas molecule collisions with the filament will change accordingly. More collisions remove more heat from the filament, which lowers the temperature and changes the resistance of the filament. This change in resistance is converted to an output pressure. Pirani gauges are accurate to within around 7-8%. Capacitance manometers operate on the principle of a diaphragm held at a very low reference pressure (10^{-7} mbar) that is deflected by changing pressure. This deflection changes the capacitance between the diaphragm and an electrode. This change is converted to pressure. These gauges are extremely accurate (1%). These gauges will read different pressures because they operate on very different principles. The capacitance manometer is more accurate because it reads pressure independent of the type of gas present. In contrast, the temperature of the filament in the Pirani gauge is affected by the thermal conductivity of the colliding gas molecules. For example, the thermal conductivity of water vapor is higher than that of air, so for an equal number of water vapor and air molecules colliding with the filament the water vapor will remove more heat, causing the Pirani gauge to read a higher pressure than the true pressure. Once all of the water vapor is removed the differential between the two gauges should read about the same, indicating that the scaffolds are dry.

7) Once the program has reached the storage hold stage, the program can be cancelled and scaffolds can be removed from the freeze-dryer.

8) Allow scaffolds to sit in mold at room temperature for at least 1 h before carefully removing them with forceps and placing in an aluminum foil pouch. Label pouch with name, collagen type, collagen concentration, freeze date, freeze temperature, and any other relevant notes.

A.5 Isotropic CG scaffold fabrication protocol

Reference: (O'Brien, Harley et al. 2004)

Reagents

- CG suspension; store at 4°C
- Welch DirecTorr Gold synthetic pump oil (Fisher 01-184-105)

Supplies and equipment

- Freeze-dryer (VirTis Genesis)
- Aluminum, polysulfone tray molds (3" x 3")
- Beakers
- Parafilm
- Aluminum foil

Procedure

*This procedure describes the fabrication of 3 mm tall scaffold sheets. Check that oil is clean (clear, not yellowed) before and after each freeze-dryer run, replacing when necessary. It is easiest to replace the oil just after a run, when the oil is still warm.

1) Degas the CG suspension in a beaker (covered in Parafilm with small slits) by pulling vacuum inside freeze-dryer. Degas just to the boiling point to remove all air bubbles. Make sure the condenser is at least -50°C or cooler before degassing.

2) Add 24.25 mL of CG suspension to a 3" x 3" tray mold, ensuring that the suspension reaches the corners. Push any bubbles or unblended collagen to the edge using tweezers.

3) Open freeze- dryer door, place mold on center of shelf. Quickly close the freeze-dryer door and run the program 'Tf-xx No Hold' where xx is the desired freezing temperature (-10, -40, or -60°C). A typical schedule is shown below for the constant cooling fabrication method with a final freezing temperature of -10°C.

Step	**Temperature °C**	**Time, min**	**Ramp/Hold**	**Vacuum level, torr**	**PCM**
Freezing hold	20	5	H	~600	N/A
Freezing ramp	-10	30	R	~600	N/A
Freezing hold	-10	120	H	~600	N/A
Drying ramp	0	10	R	0.2	150
Drying hold	0	5	H	0.2	1
Extra drying	0	60	H	0.2	0
Storage ramp	20	20	R	0.2	0
Storage hold	20	indefinite	H	0.2	0

4) Once the program has reached the storage hold stage, the program can be cancelled and the array can be removed from the freeze-dryer.

5) Gently remove scaffold by lifting from corner with tweezers. Place scaffold in puffed aluminum pouch. Label pouch with name, collagen type, collagen concentration, freeze date, freeze temperature, and any other relevant notes. Clean mold by rubbing with soapy water; use 0.05 M acetic acid to remove collagen residue. Do not use cleaning brushes.

A.6 DHT crosslinking protocol

Reference: (Yannas, Lee et al. 1989; Harley, Leung et al. 2007)

Supplies and equipment

- Sterile air filter (Millipore SLGP033RS)
- Vacuum oven (Welch Vacuum, Fisher 13-262-52)

Procedure

*Note: vacuum pump oil levels and integrity of vacuum fittings should be checked periodically. Also, change sterile air filter on 'Purge' line regularly. Remember that scaffolds containing CGCaP content should be oven treated as this will cause irreversible dehydration of the calcium phosphate phase from brushite to monetite.

1) Turn on vacuum oven and set desired temperature (usually 105°C).

2) Once vacuum oven has reached temperature set point, place CG scaffolds in opened aluminum pouches carefully inside the oven. Close the oven door.

3) Completely open the 'Vacuum' valve on the lower right front face of the vacuum oven while completely closing the 'Purge' valve.

4) Turn on the vacuum pump and make sure vacuum is pulled to a sufficiently low level (< 1 in Hg). Allow scaffolds to crosslink for 24 h.

5) After crosslinking is complete turn off the vacuum pump, close the 'Vacuum' valve, open the 'Purge' valve, carefully remove scaffolds from the oven, and seal the aluminum pouches. Store sealed scaffolds (now sterile) in desiccator until time of use.

A.7 EDAC crosslinking protocol

Reference: (Olde Damink, Dijkstra et al. 1996; Harley, Leung et al. 2007; Caliari, Ramirez et al. 2011)

Reagents

- 1-ethyl-3-[3-dimethylaminopropyl]carbodiimide hydrochloride (EDAC, Sigma-Aldrich E7750); store at -20^{o}C
- N-hydroxysulfosuccinimide (NHS, Sigma-Aldrich H7377); store in desiccator
- Sterile phosphate-buffered saline (PBS)
- 100% ethanol

Supplies and equipment

- 6-well plates (Fisher 08-772-1B)
- 50 mL centrifuge tubes (Fisher 14-432-22)
- Syringe and syringe filter (Fisher 148232A)
- MTS 2/4 digital microtiter shaker (IKA 3208001)
- Dual range balance (Mettler Toledo XS105)
- Razor blades

Procedure

* Note: all steps should be performed in the laminar flow hood unless otherwise noted.

1) Cut scaffold or membrane samples to be crosslinked using a razor blade.

2) Transfer scaffold or membrane pieces to sterile centrifuge tube, remove from laminar flow hood, and weigh pieces on dual range balance.

3) Hydrate pieces in 100% ethanol overnight.

4) Rinse pieces several times in PBS and then let soak in PBS for 24 h before crosslinking.

5) Determine the EDAC and NHS concentrations to be used in crosslinking solution. The sample calculations in this protocol are done with a 5:2:1 EDAC:NHS:COOH molar ratio where COOH is carboxylic acid groups in CG material based on a conversion factor of 1.2 mmol COOH per gram of collagen (Olde Damink, Dijkstra et al. 1996). The mass of EDAC and NHS required can be calculated as follows:

$$M_{EDAC} = M_{scaffold}\left(0.0012\frac{mol_{COOH}}{g_{collagen}}\right)\left(\frac{5mol_{EDAC}}{1mol_{COOH}}\right)\left(\frac{191.7g_{EDAC}}{1mol_{EDAC}}\right) \quad \textbf{(Equation D.1)}$$

$$M_{NHS} = M_{scaffold}\left(0.0012\frac{mol_{COOH}}{g_{collagen}}\right)\left(\frac{2mol_{NHS}}{1mol_{COOH}}\right)\left(\frac{116.0g_{NHS}}{1mol_{NHS}}\right) \quad \textbf{(Equation D.2)}$$

6) Mix the EDAC and NHS in sterile PBS. Approximately 1 mL of solution will be needed per scaffold piece (6-8 mm diameter, 3-5 mm thick).

7) In the laminar flow hood, sterile filter the solution and add to 6-well plates.

8) Add scaffolds in crosslinking solution and place well plate on shaker on bench 6. Allow scaffolds to crosslink under moderate shaking for 1.5 h. Crosslinking time should be increased for less permeable constructs such as membranes and high solids content scaffolds.

9) Remove EDAC/NHS solution and rinse scaffolds in sterile PBS under moderate shaking for 10-15 min.

10) Remove first PBS wash solution and rinse scaffolds in fresh PBS under moderate shaking for an additional 30-45 min. Store in fresh sterile PBS at 4°C until use.

A.8 CG scaffold critical point drying

Reference: (Grier, Moy et al. 2017)

Reagents

- 200 proof (100%) ethanol
- Deionized water
- Carbon dioxide gas

Equipment and Supplies

- 24-well plates (Fisher 08-772-1)
- Pasteur pipettes
- Forceps
- MTS 2/4 digital microtiter shaker (IKA 3208001)
- Samdri-PVT-3D Manual Critical Point Dryer (Tousimis)

Scaffold dehydration procedure

1) Set up step-wise ethanol washes in a 24-well plate on the shaker.

- 20% ethanol – 30 min
- 50% ethanol – 30 min
- 70% ethanol – 30 min
- 90% ethanol – 30 min
- 100% ethanol – over night

Critical point drying protocol

*This procedure describes how to perform manual critical point drying (CPD) on CG scaffolds. Automated methods are available, but are not suitable due to the retention of ethanol by the scaffold.

1) Reserve time on critical point dryer (Samfri-PVT-3D) using calendar on Beckman ITG Microscopy Suite website. The training contact is Cate Wallace.

2) Verify that all knobs on the CPD instrument are closed and set to the zero position (cool, bleed, purge, fill), flip the power switch to "on" and allow the instrument to warm up for ~3 min.

3) Open the chamber and inspect the o-ring for defects or flaws.

4) With a pipette, transfer ~9 mL of 100% ethanol provided at Beckman (in sieves). Note: withdrawal ethanol from the top of the liquid as far as possible from the sieves.

5) Place the scaffold/s into the chamber and close the chamber by evenly tightening the knurled nuts by hand (Do Not Use Tools).

6) Open the valve located on the CO2 tank.

7) Open the cool valve and allow the temperature in the chamber to reach 0 oC. When 0 oC is reached, close the cool valve. This should take ~ 60 seconds. If the cooling seems to be happening too fast, decrease the cool valve position.

8) Slowly open the fill valve and allow CO2 into the chamber and close the valve before the liquid level in the chamber reaches the top. Do not completely fill the chamber at this point. Allow this solution to equilibrate for a few minutes while ensuring that the temperature in the chamber is maintained between 0 oC and 10 oC by opening the cool valve periodically as necessary.

9) With the fill valve closed, open the purge/vent valve and drain the chamber to ~ half level. Ethanol and CO2 will discharge from the tube on the side of the instrument.

10) Repeat steps 7 and 8 until the scaffolds sink to the bottom of the chamber and only solid CO2 discharges from the tube on the side of the instrument. At this point, the ethanol has been completely exchanged with CO2.

11) Open the fill valve and completely fill the chamber. A meniscus will pass across the sight glass when the chamber is full.

12) With the fill valve still open, open the purge/vent valve for ~ 60 seconds to ensure all ethanol has been removed.

13) Close all valves and turn on the heat switch. Allow the chamber to heat/pressurize and allow the chamber to maintain the critical point for at least 5 minutes. Refer to PVT-3D manual for critical point parameters.

14) Leaving the heat switch on, slowly open the bleed valve to exhaust the CO2 from the chamber. Adjust bleed valve accordingly to maintain a pressure release rate of ~ 100 psi/min. This process should take 10-13 minutes.

15) Once the chamber pressure reaches 0 psi, the heat switch can be turned off and samples removed.

16) Turn off the main CO2 valve on the CO2 tank and reattach the chamber lid.

17) Open, in order, the bleed valve, purge/vent valve, fill valve and cool valve to clear all remaining CO2 from the instrument and turn flip the power switch to the off position.

A.9 Scanning electron micrograph imaging of CG scaffolds

Reference: (Grier, Moy et al. 2017)

Equipment and Supplies

- Desk-1 TSC sputter coater (Denton Vacuum)
- FEI Quanta FEG 450 ESEM (FEI Company)
- Carbon tape
- Razor blades
- Forceps

Sputter coating procedure

1) Reserve time on SEM (FEI Quanta FEG 450 ESEM) using calendar on Beckman ITG Microscopy Suite website. The training contact is Cate Wallace

2) Section scaffolds as desired and mount to sample stubs using carbon tape (provided in Beckman ITG Microscopy Suite ESEM room).

3) Place sample stubs into Desk-1 TSC sputter coater (located in wet lab area). The training contact is Scott Robinson.

4) Follow machine instructions located on bench to coat specimens with an Au/Pd mixture.

Sample loading procedure
*This procedure and more information can be found on the Beckman ITG Microscopy Suite website

1) Start xT Microscope Server and log on. Click to hide the Status window. Right click the top of the server window, and choose Show Tiny View.

2) Ensure that live video feed is being displayed to observe all stage movement.

3) Click ‘Vent’ on vacuum mode on the beam control Panel to open the SEM chamber. The color of the chamber icon changes from green to orange. This will take about 1 min.

4) Once vented, slowly pull the chamber door open, taking caution to ensure that any samples left in machine will not hit the pole piece or any detector. Use live video feed to visually confirm this.

5) Load sample stub.

6) Swing the NavCam 90 degrees to activate it.

7) Wait for the stage to move under the NavCam and for the lower-left quadrant to go live.

8) Take a picture with the NavCam by pressing the round silver button located at the base of the NavCam arm. An image of your sample on the stage will appear in quad III. Wait for the light to blink off two times.

9) Swing the NavCam back to its home position.

10) Slowly push the door into the close position. Before initializing pump down, ensure the door is completely closed.

11) Click the radio button to select necessary vacuum mode (high vacuum, low vacuum, or ESEM). For the Low Vacuum mode select the target Chamber Pressure and aperture cone choice before clicking the Pump button. Press the chamber door handle firmly for a few seconds to help seal the chamber at the beginning of pump-down.

SEM imaging procedure
*This procedure and more information can be found on the Beckman ITG Microscopy Suite website

1) While pumping, double click where you want to move the stage to on the NavCam image.

2) Wait until chamber pressure reaches vacuum.

3) Click on Beam On. Either quad I or quad II can be used to perform SEM imaging but only quad I can be fed into EDS. Click on the pause button (or F6) to make that quad go live.

4) Click on the Auto Contrast/Brightness (half black/half white circle) button on the software toolbar.

5) Navigate around to find a distinguishable feature on the sample surface. Focus on your sample by either holding down the right mouse button and dragging the mouse to the left or right or by using the Coarse and Fine knobs on the MUI.
* You can use the Reduced Area icon (or F7) to assist. Focusing at 2x to 3x the magnification needed for the final result will make the lower magnification sharper.

6) To change the magnification, use the + and – buttons on the numpad. This will double and halve the magnification, respectively and will always be a rounded number. You may also use the magnification dial on the MUI. This will change the magnification in smaller increments, but will not be a rounded number. You may use the asterisk (*) button on the numpad to round the number.

7) Link Z by clicking on the icon that looks like a pyramid and a halo with a red question mark in the middle. Working distance can be reduced if necessary by going to the navigation tab on the right and selecting the desired working distance. Usually you want to be at least at 10mm working distance, if not shorter.

8) You can move around the sample by double clicking on the point of interest to center it within the quad, or using arrows on the keyboard, or pressing the scroll wheel on the mouse and dragging the mouse in the direction you want to move.

9) If image moves when changing focus, follow instructions to center aperture.

10) Correct astigmatism by focusing as well as possible at double the magnification used for imaging and hold shift key and right mouse button, moving to the left or right. Repeat as needed.

11) Save the desired image by clicking the Image Acquisition button on upper menu banner, or by selecting F2. The scan will pause after one frame scanned and a save dialog will open. You can also save by going to the File menu and selecting Save As.

Venting chamber and unloading samples
*This procedure and more information can be found on the Beckman ITG Microscopy Suite website

1) Turn the beam off by pressing the Beam On button. The button should turn from yellow to grey.

2) Slowly pull the chamber door open while monitoring the live video feed of the chamber. Ensure that the sample and stage path is clear.

3) Remove sample stubs.

4) Slowly push the chamber door closed and click the Pump button under the Beam Control menu on the right to pump the chamber back to high vacuum.

5) Wait for the vacuum icon to turn green. Hit the Stop button on the server window, and wait for the server to fully unload (the green bar will empty out).

6) Log off.

A.10 Embedding CG scaffolds into end blocks for bioreactor

Reference: (Grier, Moy et al. 2017)

Equipment and Supplies

- Poly(dimethylsiloxane) (PDMS)
- Dual range balance (Mettler Toledo XS105)
- Pipet tips
- 3D printed hollow end blocks
- 3D printed racks and holders
- 25mm Scaffold cutting guides
- Razor blades

Procedure

1) Prepare PDMS for scaffold immobilization. Use a monomer: curing agent ratio of 5:1. About 10 g of PDMS is needed per 36 end blocks.

2) Place end blocks into holders.

3) Using a 1000 μL micropipette tip, fill end blocks with ~200 μL of PDMS. This should fill the end block to slightly below the surface.

4) Briefly allow PDMS to settle, add additional PDMS if needed.

5) Place PDMS-loaded end blocks into 37°C incubator for 45 minutes to begin polymerization.

6) While PDMS is curing, cut scaffolds to length using the 25mm cutting guide.

7) After 45 minutes, remove end blocks in holders from incubator and place racks over top.

8) Push scaffold ends into PDMS in the end blocks, ensuring that the scaffold stays vertically aligned with the rack.

9) Place back into incubator overnight.

10) Repeat steps 1-9 for the other end of the scaffold.

A.11 Ethylene oxide sterilization of CG scaffolds

Reference: (Grier, Moy et al. 2017)

Equipment and Supplies

- Anprolene AN74i benchtop ethylene oxide sterilizer (Anderson Products)
- Large anprolene ampule
- Anprolene bag
- Humidi-chip
- Sterilization pouches
- Vented plastic container

Procedure

1) Place all scaffolds and other items to be sterilized into sterilization pouches. Any pouches containing soft materials, such as scaffolds should then be places into a vented plastic container.

2) Place all pouches into anprolene bag.

3) Turn on sterilizer, it will run through a self-test.

4) Load bag containing samples into sterilizer, place venting apparatus inside bag al of the way to the back.

5) Place humidi-chip in plastic tube and place into bag.

6) Place anprolene ampoule, wrapped in paper in clear back, inside the anprolene bag. Make sure that it can be access from outside the bag later on.

7) Close bag around the large sleeve on the venting tube. Use hook and loop straps to seal closed.

8) Press Start Cycle, the sterilizer will then vent the air from the bag. This takes about 1 min.

9) Once bag is vented, locate anprolene ampoule and break top. The bag will begin to inflate.

10) Close and lock sterilizer door.

11) Select cycle length of either 12 or 24 hours.

A.12 Bioreactor operation protocol

Reference: (Grier, Moy et al. 2017)

Equipment and Supplies

- Bioreactor system
- Linear actuator JRK motor controller (Pololu)
- Computer with Pololu JRK configuration utility
- Variable power supply

Procedure

Configuration utility

1) Connect linear actuator on bioreactor to motor controller using the quick connect cables.

2) Turn on power supply, ensure that it is set to 8V.

3) Open Pololu JRK software.

4) Ensure that controller has open connection to motor.

5) Set target length to starting position (see standard cure for setting for various scaffold lengths).

6) Close Pololu configuration utility.

7) Run 10on5and50off program.

8) Select desired parameters, frequency, rest time, strain amplitude.

9) Click Connect.

10) When removing bioreactor from incubator, click Disconnect, disconnect controller from bioreactor.

Bioreactor operation code

```
using System;
using System.Collections.Generic;
using System.ComponentModel;
using System.Data;
using System.Drawing;
using System.Text;
using System.Windows.Forms;
using Pololu.Jrk;
using Pololu.UsbWrapper;
using System.Threading;
```

```
namespace Pololu.Jrk.JrkExample
{
   public partial class MainWindow : Form
   {
      public MainWindow()
      {
         InitializeComponent();
      }

      #region events
      /// <summary>
      /// When the program starts, this function is called.
      /// It gets the serial number of the first connected Jrk,
      /// since this is probably what you want to connect to.
      /// </summary>
      void MainWindow_Shown(object sender, EventArgs e)
      {
         var deviceList = Jrk.getConnectedDevices();
         if (deviceList.Count > 0)
         {
            SerialNumberTextBox.Text = deviceList[0].serialNumber;
            ConnectButton.Focus();
         }
         else
         {
            SerialNumberTextBox.Focus();
         }
      }

      void ConnectButton_Click(object sender, EventArgs e)
      {
         SerialNumberTextBox.Enabled = false;
         Log("Connecting...");
         UpdateTimer.Start();
         StopConnectingButton.Enabled = true;
         ConnectButton.Enabled = false;
      }

      void StopConnectingButton_Click(object sender, EventArgs e)
      {
         SerialNumberTextBox.Enabled = true;
         TryToDisconnect();
         UpdateTimer.Stop();
         StopConnectingButton.Enabled = false;
         ConnectButton.Enabled = true;
      }
```

```
#endregion

#region logging
void Log(Exception e)
{
   Log(e.Message);
}

void Log(string text)
{
   if (LogTextBox.Text != "")
      LogTextBox.Text += Environment.NewLine;
   LogTextBox.Text += DateTime.Now.ToString() + "\t" + text;
   LogTextBox.SelectionStart = LogTextBox.Text.Length;
   LogTextBox.ScrollToCaret();
}
#endregion

#region the Jrk connection

Jrk jrk = null;

/// <summary>
/// Connects to the device if it is found in the device list.
/// </summary>
void TryToReconnect()
{
   foreach (DeviceListItem d in Jrk.getConnectedDevices())
   {
      if (d.serialNumber == SerialNumberTextBox.Text)
      {
         jrk = new Jrk(d);
         Log("Connected to #" + SerialNumberTextBox.Text + ".");
         jrk.setTarget(MaxTargetConverted);//as soon as connect, go here ASM
         CycleAlreadyStarted = false;
         return;
      }
   }
}

void TryToDisconnect()
{
   if (jrk == null)
   {
      Log("Connecting stopped.");
      return;
```

```
        }

        try
        {
            Log("Disconnecting...");
            jrk.disconnect();
        }
        catch (Exception e)
        {
            Log(e);
            Log("Failed to disconnect cleanly.");
        }
        finally
        {
            // do this no matter what
            jrk = null;
            Log("Disconnected from #" + SerialNumberTextBox.Text + ".");
        }
    }

    int sequenceCounter = 0;

    private const ushort MaxTargetConverted = 850;//scaffold length ASM; switched this from
max to min and mm to weirdunits too

    private const ushort ErrorMargin = 3;

    private double ConvertFromWeirdUnitToMm(ushort value)//used different standard curve
to calc best fit line ASM
    {
        return (value - 148.81) / 82.877;
    }
    //private ushort ConvertFromMmToWeirdUnit(double value)
    //{
    //    return Convert.ToUInt16((value * 82.877) + 148.81);
    //}

    bool CycleAlreadyStarted;

    /// <summary>
    /// Steps through a simple sequence, setting the target to
    /// 1500, 2000, and 2500 with 1 second between frames.
    /// This function is run every 100 ms when the motion sequence
    /// is activated.
    /// </summary>
    void RunSequence()
```

```
    {
        double second=915.0 / UpdateTimer.Interval;
        double workingTime = (360 -
Convert.ToInt32(cmbRestTime.SelectedItem.ToString()))*60*second; //changed for 6 hr//
        if (anothercounter <= workingTime)
        {
            #region setMinTargetConvertedStrain
            string percentStrain = cmbStrain.SelectedItem.ToString();
            ushort MinTargetConverted;
            switch (percentStrain)
            {
                case "2.5":
                    MinTargetConverted = 814;
                    break;
                case "5":
                    MinTargetConverted = 779;
                    break;
                case "7.5":
                    MinTargetConverted = 744;
                    break;
                case "10":
                    MinTargetConverted = 707;
                    break;
                case "12.5":
                    MinTargetConverted = 671;
                    break;
                case "15":
                    MinTargetConverted = 636;
                    break;
                case "20":
                    MinTargetConverted = 565;
                    break;
                default:
                    MinTargetConverted = MaxTargetConverted;
                    break;
            }
            #endregion
            ushort actualPosition = jrk.getVariables().scaledFeedback;
            #region updateUI
            lblMin.Text = MinTargetConverted.ToString();
            lblMax.Text = MaxTargetConverted.ToString();
            lblActual.Text = actualPosition.ToString();
            #endregion

            if (actualPosition <= MinTargetConverted + ErrorMargin)
jrk.setTarget(MaxTargetConverted);//I switched these bc it was moving backwards ASM
```

```
            else if (actualPosition >= MaxTargetConverted - ErrorMargin)
            {
               if (!CycleAlreadyStarted)
               {
                  jrk.setTarget(MinTargetConverted);//Go back and forth (hopefully...)ASM
                  sequenceCounter = 0;
                  CycleAlreadyStarted = true;//start cycle and start counting ASM
               }
            }


            sequenceCounter++;
            if (CycleAlreadyStarted && sequenceCounter >=
Convert.ToInt32(cmbHz.SelectedItem) * second)//don't restart cycle until 1 sec ASM
            {
               sequenceCounter = 0;
               CycleAlreadyStarted = false;
                  jrk.setTarget(MaxTargetConverted);
            }
         }
         anothercounter++;
        if (anothercounter >= 6*60*60*second) anothercounter = 0; //changed for 6 hr//
         //if (anothercounter >= 6 * 60 * 60 * second) { anothercounter = 0; connect(); }//
      }

      #endregion

      //ashley trying to code rest time//
      int anothercounter = 0;



      #region updating

      /// <summary>
      /// This function will be called once every 100 ms to do an update.
      /// </summary>
      void UpdateTimer_Tick(object sender, EventArgs eventArgs)
      {
         if (jrk == null)
         {

            // Try connecting to a device.
            try
            {
               TryToReconnect();
```

```
            }
            catch (Exception e)
            {
                Log(e);
                Log("Failed connecting to #" + SerialNumberTextBox.Text + ".");
                jrk = null;
            }
        }
        else
        {
            // Update the GUI and the device.
            try
            {
                RunSequence();
            }
            catch (Exception e)
            {
                // If any exception occurs, log it, set jrk to null, and keep trying..
                Log(e);
                Log("Disconnected from #" + SerialNumberTextBox.Text + ".");
                jrk = null;
            }
        }
    }

    #endregion

    private void label2_Click(object sender, EventArgs e)
    {

    }

    private void MainWindow_Load(object sender, EventArgs e)
    {
        cmbHz.SelectedIndex = 0;
        cmbStrain.SelectedIndex = 0;
    }

    private void label3_Click(object sender, EventArgs e)
    {
    }



  }
}
```

A.13 Growth factor pulldown by CG scaffolds

Reference: (Hortensius and Harley 2013)

Reagents

- Bovine serum albumin (Sigma-Aldrich A7906)
- Sterile PBS
- Growth factors
    - Human TGF-β1 (ProSpec CYT-716)
    - Human BMP-2 (ProSpec CYT-261)

Equipment and Supplies

- 24-well plates (Fisher 08-772-1)
- Sterile filters
- Syringes
- MTS 2/4 digital microtiter shaker (IKA 3208001)

Procedure

1) Prepare 100 mL solution of 1% BSA (weight) in PBS.

2) Sterile filter BSA solution.

3) Add 5 ng/mL of desired growth factor to BSA solution.

4) Place 3 scaffolds (6 mm diameter4 5 mm height) per well into a 24-well plate.

5) Add 1 mL of growth factor/BSA solution to each well.

6) Place on shaker at room temperature for 1 hr.

A.14 Quantitative analysis of TGF-β pulldown by CG scaffolds

Reference: (Hortensius and Harley 2013)

Reagents

- 1 N HCl
- 1.2 N NaOH/0.5 M HEPES
- Stop Solution - 2N H_2SO_4
- PBS
- Tween 20
- Reagent Diluent 1 10x concentrate (R&D Systems DY997)
- Color Reagent A (R&D Systems DY007)
- Color Reagent B (R&D Systems DY007)

Equipment and Supplies

- Human TGF-β DuoSet ELISA Kit (R&D Systems DY240)
- ELISA Plate sealers (R&D Systems DY992)
- Sterile filters
- Syringes
- Microcentrifuge tubes
- Fluorescence spectrophotometer (Tecan, Room 100 RAL)

Plate set up procedure

1) Prepare Wash Buffer – 0.05% Tween 20 in PBS

2) Prepare Block Buffer – 5% Tween 20 in PBS – sterile filtered

3) Dilute the Capture Antibody (to the working concentration stated in the product datasheet) in PBS without carrier protein.

4) Immediately coat a 96-well microplate with 100 µL per well of the diluted Capture Antibody.

5) Seal the plate and incubate overnight at room temperature.

6) Aspirate each well and wash with Wash Buffer, repeating the process two times for a total of three washes. Wash by filling each well with Wash Buffer (400 µL) using a squirt bottle. After the last wash, remove any remaining Wash Buffer by aspirating or by inverting the plate and blotting it against clean paper towels.

7) Block plates by adding 300 µL Block Buffer.

8) Seal plate and incubate 1 hr at room temperature

9) Repeat wash step in Step 6.

Sample activation procedure

1) Add 20 µL of 1 N HCl to 100 µL of sample. Mix well.

2) Incubate 10 min at room temperature

3) Add 20 µL of 1.2 N NaoH/0.5M HEPES. Mix well.

4) Assay immediately.

Assay procedure

1) Add 100 µL of samples or standards provided in Human TGF-β DuoSet ELISA Kit in Reagent Diluent per well.

2) Cover with adhesive strip and incubate 2 hr at room temperature

3) Repeat wash step in Part 1, Step 6.

4) Add 100 µL of Detection Antibody provided in Human TGF-β DuoSet ELISA Kit, diluted in Reagent Diluent per well.

5) Cover with adhesive strip and incubate 2 hr at room temperature.

6) Repeat wash step in Part 1, Step 6.

7) Prepare substrate solution – 1:1 mixture of Color Reagent A and Color Reagent B.

8) Add 100 µL of Substrate Solution provided in Human TGF-β DuoSet ELISA Kit to each well.

9) Cover with adhesive strip and incubate 20 min at room temperature. Avoid placing in direct light.

10) Add 50 µL of Stop Solution to each well. Gently tap the plate to ensure thorough mixing.

11) Immediately use fluorescence spectrophotometer to determine optical density of each well at 450 nm.

APPENDIX B: CELL CULTURE, ASSAY, AND IMAGING PROTOCOLS

B.1 Incubator disinfection protocol

Reagents

- Steris staphene spray (Fisher 14-415-15)
- 70% ethanol

Procedure

1) Shut off the CO_2 tanks and turn off the incubator.

2) Prepare the sterile hood by covering the inside with bench-coat.

3) Cover the chemical fume hood with fresh bench-coat.

4) Disassemble all removable parts from the incubator chamber. Spray all pieces from the incubator inside the chemical fume hood with staphene. Spray the inside of the inside of the incubator with staphene. Let stand for 15 min with the incubator door cracked open ~2 in.

5) Spray the inside of the incubator with 70% ethanol. Wipe off the excess staphene with paper towels.

6) Spray all internal pieces of the incubator in the chemical fume hood with 70% ethanol and wipe off the excess staphene. Spray each part generously with ethanol again and place into the sterile hood to dry. Do not wipe anything down. Allow all parts to air dry for 15-30 min.

7) Spray the inside of the incubator with 70% ethanol and allow all parts to dry for 15-30 min; do not wipe anything down.

8) Reassemble all internal pieces of the incubator, taking care to move each piece from the sterile hood to the incubator as quickly as possible.

9) Spray the inside of incubator again with 70% ethanol. Shut the foot and allow all parts to dry; do not wipe anything down.

10) Turn on the incubator power and open the valves on the CO_2 tanks. Allow the incubator to ventilate with the CO_2 on for 24 h before using again.

B.2 Tenocyte culture protocol

Reference: (Kapoor, Caporali et al. 2010; Caliari and Harley 2011; Caliari, Ramirez et al. 2011)

Reagents

- Complete tenocyte media (500 mL); store at 4^{o}C
    - 445 mL high glucose DMEM (Based on Fisher SH30022.FS, order from Sandy at SCS Media Facility); store at 4^{o}C
    - 50 mL fetal bovine serum (Invitrogen 16140-071); store at -20^{o}C
    - 5 mL antibiotic-antimyotic (Invitrogen 15140-122); store at -20^{o}C
    - 25 mg ascorbic acid (Wako 014-04801)
    - Sterile filter before use
- Trypsin-EDTA (Invitrogen 25300-062); store at -20^{o}C
- Trypan blue (Sigma-Aldrich T8154)
- DMSO (Fisher D128-500)
- Sterile phosphate-buffered saline without Ca^{2+} or Mg^{2+} (PBS)

Supplies and equipment

- Hausser phase contrast hemacytometer (Fisher 02-671-5)
- Tabletop centrifuge (VWR 53513-812)
- Optical microscope (Leica Microsystems DMIL LED)
- Water bath (37^{o}C, Fisher 15-474-35)
- Sterile filters
- Sterile pipettes (5, 10, 25 mL)
- T75 tissue culture flasks

*Note: all steps should be performed in the laminar flow hood unless otherwise noted.

Tenocyte thawing procedure

1) Place complete tenocyte media in water bath and warm to 37^{o}C.

2) Thaw frozen cell vials in 37^{o}C water bath for about 2 min.

3) Transfer the thawed cells and freezing media to a 15 mL centrifuge tube. Add complete tenocyte media until the cerulean effect has dissipated, then bring the volume up to 9 mL.

4) Remove a 10 μL cell suspension aliquot for counting. Gently re-suspend the cells in the diluted media and pellet the cells at 1000 rpm for 7 min.

5) While cells are spinning down, mix the 10 μL cell suspension aliquot with 10 μL of Trypan blue. Pipette several times to mix the stain and cell suspension.

6) Place a cover slip on the hemacytometer and pipette 10 μL of the stain/cell suspension into the hemacytometer.

7) Cell counts are performed in as many of the nine separate regions of the hemacytometer as is feasible. Average number of cells per region is used to calculate the total cell population. For this calculation, the dilution factor is typically 2 (1:1 ratio of cell suspension to Trypan blue).

*Total Cell Population = (Mean Cells per Region) * Dilution * 10,000 * (Cell Suspension Volume)*

8) Seed the cells at the required density (usually 10,000 cells/cm^2). Use around 10-12 mL media for a 100 mm dish, 12-14 mL for a T75, or 7-8 mL for a T25.

9) Place the flask(s) into the incubator. Check the confluence every 24 h and feed cells twice a week. Cells are usually confluent after 5 days. Do not use past passage 4.

Tenocyte feeding procedure

1) Warm complete tenocyte media in water bath to 37^{o}C.

2) When the media is warm, wipe dry with paper towel and spray with 70% ethanol before placing in the sterile hood.

3) Remove all old media from each T75 flask, taking care not to scrape the cells with the pipette tip.

4) Add 12-14 mL of complete tenocyte media. Return the T75 flasks to the incubator and feed every twice a week. Adjust volume of media accordingly for different sized flasks.

Tenocyte passaging procedure

1) Warm complete tenocyte media, sterile PBS, and 3 mL trypsin-EDTA per T75 flask to be passaged in water bath to 37^{o}C.

2) When the media, PBS and trypsin are warm, wipe them dry with paper towel and spray with 70% ethanol before placing in the sterile hood.

3) Remove all old media from each T75 flask, taking care not to scrape the cells with the pipette tip.

4) Add 10 mL of PBS per T75 flask and leave the PBS in the flask to rinse the cells for 30 s. Swirl gently to remove any excess media from the cells. Adjust volumes of PBS, media, and trypsin accordingly for different sized flasks.

5) Remove the PBS and add 3 mL of trypsin per T75 flask. Return the flasks to the incubator for 6 min to allow for the cells to detach from the tissue culture plastic (allow the cells to sit for 3-4 additional min in the incubator if they do not detach after 6 min). Slap flasks a few times to detach cells.

6) Add 6 mL of complete tenocyte media to each flask to neutralize the trypsin and to flush cells off of the tissue culture plastic.

7) Remove the trypsin, additional media, and cells from the flask and put into a conical tube. Remove a 10 μL cell suspension aliquot for counting. Centrifuge the cells at 1000 rpm for 7 min.

8) While cells are spinning down, mix the 10 μL cell suspension aliquot with 10 μL of Trypan blue. Pipette several times to mix the stain and cell suspension.

9) Place a cover slip on the hemacytometer and pipette 10 μL of the stain/cell suspension into the hemacytometer.

10) Cell counts are performed in as many of the nine separate regions of the hemacytometer as is feasible. Average number of cells per region is used to calculate the total cell population. For this calculation, the dilution factor is typically 2 (1:1 ratio of cell suspension to Trypan blue).

*Total Cell Population = (Mean Cells per Region) * Dilution * 10,000 * (Cell Suspension Volume)*

11) Aspirate off the media supernatant and add new media to dilute cells to desired concentration.

12) Seed the cells at the required density (usually 10,000-50,000 cells/cm^2). Use around 10-12 mL media for a 100 mm dish, 12-14 mL for a T75, or 7-8 mL for a T25.

13) Place the flask(s) into the incubator. Check the confluence every 24 h and feed cells every 48-72 h.

Tenocyte freezing procedure

1) Grow cells to confluence and replace media the day before freezing.

2) Warm complete tenocyte media, sterile PBS, and 3 mL trypsin-EDTA per T75 flask to be passaged in water bath to 37ºC.

3) When the media, PBS and trypsin are warm, wipe them dry with paper towel and spray with 70% ethanol before placing in the sterile hood.

4) Remove all old media from each flask, taking care not to scrape the cells with the pipette tip.

5) Add 10 mL of PBS per T75 flask and leave the PBS in the flask to rinse the cells for 30 s. Swirl gently to remove any excess media from the cells. Adjust volumes of PBS, media , and trypsin accordingly for different sized flasks.

6) Remove the PBS and add 3 mL of trypsin per T75 flask. Return the flasks to the incubator for 6 min to allow for the cells to detach from the tissue culture plastic (allow the cells to sit for 3-4 additional min in the incubator if they do not detach after 6 min). Slap flasks a few times to detach cells.

7) Add 6 mL of complete tenocyte media to each flask to neutralize the trypsin and to flush cells off of the tissue culture plastic.

8) Remove the trypsin, additional media, and cells from the flask and put into a conical tube. Remove a 10 μL cell suspension aliquot for counting. Centrifuge the cells at 1000 rpm for 7 min.

9) While cells are spinning down, mix the 10 μL cell suspension aliquot with 10 μL of Trypan blue. Pipette several times to mix the stain and cell suspension.

10) Place a cover slip on the hemacytometer and pipette 10 μL of the stain/cell suspension into the hemacytometer.

11) Cell counts are performed in as many of the nine separate regions of the hemacytometer as is feasible. Average number of cells per region is used to calculate the total cell population. For this calculation, the dilution factor is typically 2 (1:1 ratio of cell suspension to Trypan blue).

*Total Cell Population = (Mean Cells per Region) * Dilution * 10,000 * (Cell Suspension Volume)*

12) Aspirate off the media supernatant and calculate volume of freezing media needed to re-suspend 1-10 x 10^6 cells per mL (freezing media: 50% complete tenocyte, 40% FBS, 10% DMSO).

13) Aliquot cells into 1 mL cryogenic tubes and place in -20^{o}C freezer for 1 h.

14) Place cryogenic tubes in -80^{o}C freezer. Cells can be stored here for up to 6 months. For longer-term storage, keep cells at -80^{o}C for at least 24 h and then carefully move to liquid nitrogen storage in IGB.

B.3 hMSC culture and differentiation protocol

Reference: Protocols from Matt Wheeler group and Jennie P. Mather

Reagents

- Complete hMSC media (500 mL); store at 4^{o}C
    - 445 mL low glucose DMEM (Based on Fisher SH30022.FS, order from Sandy at SCS Media Facility); store at 4^{o}C
    - 50 mL MSC-validated fetal bovine serum (Invitrogen 12662-029); store at -20^{o}C
    - 5 mL antibiotic-antimyotic (Invitrogen 15140-122); store at -20^{o}C
- Trypsin-EDTA (Invitrogen 25300-062); store at -20^{o}C
- Trypan blue (Sigma-Aldrich T8154)
- DMSO (Fisher D128-500)
- Sterile phosphate-buffered saline without Ca^{2+} or Mg^{2+} (PBS)

Supplies and equipment

- Hausser phase contrast hemacytometer (Fisher 02-671-5)
- Tabletop centrifuge (VWR 53513-812)
- Optical microscope (Leica Microsystems DMIL LED)
- Water bath (37^{o}C, Fisher 15-474-35)
- Sterile filters
- Sterile pipettes (5, 10, 25 mL)
- T75 tissue culture flasks

*Note: all steps should be performed in the laminar flow hood unless otherwise noted.

MSC thawing procedure

1) Place complete MSC media in water bath and warm to 37^{o}C.

2) Thaw frozen cell vials in 37^{o}C water bath for about 2 min.

3) Transfer the thawed cells and freezing media to a 15 mL centrifuge tube. Add complete MSC media until the cerulean effect has dissipated, then bring the volume up to 9 mL.

4) Remove a 10 μL cell suspension aliquot for counting. Gently re-suspend the cells in the diluted media and pellet the cells at 600 g for 5 min.

5) While cells are spinning down, mix the 10 μL cell suspension aliquot with 10 μL of Trypan blue. Pipette several times to mix the stain and cell suspension.

6) Place a cover slip on the hemacytometer and pipette 10 μL of the stain/cell suspension into the hemacytometer.

7) Cell counts are performed in as many of the nine separate regions of the hemacytometer as is feasible. Average number of cells per region is used to calculate the total cell population. For this calculation, the dilution factor is typically 2 (1:1 ratio of cell suspension to Trypan blue).

*Total Cell Population = (Mean Cells per Region) * Dilution * 10,000 * (Cell Suspension Volume)*

8) Seed the cells at the required density (usually 5,000-6,000 cells/cm^2). Use around 10-12 mL media for a 100 mm dish, 12-14 mL for a T75, or 7-8 mL for a T25.

9) Place the flask(s) into the incubator. Check the confluence every 24 h and feed cells twice a week. Cells are usually confluent after 7-9 days. Do not use past passage 6.

MSC feeding procedure

1) Warm complete MSC or lineage-specific induction media in water bath to 37^{o}C.

2) When the media is warm, wipe dry with paper towel and spray with 70% ethanol before placing in the sterile hood.

3) Remove all old media from each flask or well plate, taking care not to scrape the cells with the pipette tip.

4) Add appropriate volume of media. Return the flasks or well plates to the incubator and feed every twice a week. Adjust volume of media accordingly for different sized containers.

MSC passaging procedure

1) Warm complete MSC media, sterile PBS, and 3 mL trypsin-EDTA per T75 flask to be passaged in water bath to 37^{o}C.

2) When the media, PBS and trypsin are warm, wipe them dry with paper towel and spray with 70% ethanol before placing in the sterile hood.

3) Remove all old media from each T75 flask, taking care not to scrape the cells with the pipette tip.

4) Add 10 mL of PBS per T75 flask and leave the PBS in the flask to rinse the cells for 30 s. Swirl gently to remove any excess media from the cells. Adjust volumes of PBS, media, and trypsin accordingly for different sized flasks.

5) Remove the PBS and add 3 mL of trypsin per T75 flask. Return the flasks to the incubator for 8 min to allow for the cells to detach from the tissue culture plastic (allow the cells to sit for 3-4 additional min in the incubator if they do not detach after 6 min). Slap flasks a few times to detach cells.

6) Add 6 mL of complete MSC media to each flask to neutralize the trypsin and to flush cells off of the tissue culture plastic.

7) Remove the trypsin, additional media, and cells from the flask and put into a conical tube. Remove a 10 μL cell suspension aliquot for counting. Centrifuge the cells at 600 g for 5 min.

8) While cells are spinning down, mix the 10 μL cell suspension aliquot with 10 μL of Trypan blue. Pipette several times to mix the stain and cell suspension.

9) Place a cover slip on the hemacytometer and pipette 10 μL of the stain/cell suspension into the hemacytometer.

10) Cell counts are performed in as many of the nine separate regions of the hemacytometer as is feasible. Average number of cells per region is used to calculate the total cell population. For this calculation, the dilution factor is typically 2 (1:1 ratio of cell suspension to Trypan blue).

*Total Cell Population = (Mean Cells per Region) * Dilution * 10,000 * (Cell Suspension Volume)*

11) Aspirate off the media supernatant and add new media to dilute cells to desired concentration.

12) Seed the cells at the required density (usually 5,000-6,000 cells/cm^2). Use around 10-12 mL media for a 100 mm dish, 12-14 mL for a T75, or 7-8 mL for a T25.

13) Place the flask(s) into the incubator. Check the confluence every 24 h and feed cells twice a week.

MSC freezing procedure

1) Grow cells to confluence and replace media the day before freezing.

2) Warm complete MSC media, sterile PBS, and 3 mL trypsin-EDTA per T75 flask to be passaged in water bath to 37^{o}C.

3) When the media, PBS and trypsin are warm, wipe them dry with paper towel and spray with 70% ethanol before placing in the sterile hood.

4) Remove all old media from each flask, taking care not to scrape the cells with the pipette tip.

5) Add 10 mL of PBS per T75 flask and leave the PBS in the flask to rinse the cells for 30 s. Swirl gently to remove any excess media from the cells. Adjust volumes of PBS, media , and trypsin accordingly for different sized flasks.

6) Remove the PBS and add 3 mL of trypsin per T75 flask. Return the flasks to the incubator for 8 min to allow for the cells to detach from the tissue culture plastic (allow the cells to sit for 3-4 additional min in the incubator if they do not detach after 6 min). Slap flasks a few times to detach cells.

7) Add 6 mL of complete tenocyte media to each flask to neutralize the trypsin and to flush cells off of the tissue culture plastic.

8) Remove the trypsin, additional media, and cells from the flask and put into a conical tube. Remove a 10 μL cell suspension aliquot for counting. Centrifuge the cells at 600 g for 5 min.

9) While cells are spinning down, mix the 10 μL cell suspension aliquot with 10 μL of Trypan blue. Pipette several times to mix the stain and cell suspension.

10) Place a cover slip on the hemacytometer and pipette 10 μL of the stain/cell suspension into the hemacytometer.

11) Cell counts are performed in as many of the nine separate regions of the hemacytometer as is feasible. Average number of cells per region is used to calculate the total cell population. For this calculation, the dilution factor is typically 2 (1:1 ratio of cell suspension to Trypan blue).

*Total Cell Population = (Mean Cells per Region) * Dilution * 10,000 * (Cell Suspension Volume)*

12) Aspirate off the media supernatant and calculate volume of freezing media needed to re-suspend 1-10 x 10^6 cells per mL (freezing media: 50% complete MSC media, 40% FBS, 10% DMSO).

13) Aliquot cells into 1 mL cryogenic tubes and place in -20^{o}C freezer for 1 h.

14) Place cryogenic tubes in -80^{o}C freezer. Cells can be stored here for up to 6 months. For longer-term storage, keep cells at -80^{o}C for at least 24 h and then carefully move to liquid nitrogen storage in IGB.

B.4 Cell seeding on CG scaffolds protocol

Reference: (Caliari and Harley 2011; Caliari, Ramirez et al. 2011)

Reagents

- Complete media (see E.2 and E.3 protocols for cell recipes); store at 4°C
- Trypsin-EDTA (Invitrogen 25300-062); store at -20°C
- Trypan blue (Sigma-Aldrich T8154)
- Human recombinant PDGF-BB (R&D Systems 220-BB-010); store at -20°C
- Human recombinant IGF-1 (R&D Systems 291-G1-050); store at -20°C
- Human recombinant SDF-1α (R&D Systems 350-NS-050); store at -20°C
- Human recombinant bFGF (R&D Systems 233-FB-025); store at -20°C
- Human recombinant GDF-5 (Peprotech 120-01); store at -20°C
- Human recombinant GDF-6 (Peprotech 120-04); store at -20°C
- Human recombinant GDF-7 (Peprotech 120-37); store at -20°C
- Human recombinant BMP-2 (ProSpec CYT-261); store at -20°C
- Human recombinant BMP-7 (ProSpec CYT-333); store at -20°C
- Human recombinant TGF-β1 (ProSpec CYT-761); store at -20°C
- Human recombinant TGF-β3 (ProSpec CYT-368); store at -20°C
- Sterile phosphate-buffered saline without Ca^{2+} or Mg^{2+} (PBS)

Supplies and equipment

- Ultra-low attachment 6-well plates (Fisher 07-200-601)
- Hausser phase contrast hemacytometer (Fisher 02-671-5)
- Tabletop centrifuge (VWR 53513-812)
- Optical microscope (Leica Microsystems DMIL LED)
- Water bath (37°C, Fisher 15-474-35)
- Sterile pipettes (5, 10, 25 mL)
- Kimwipes

*Note: all steps should be performed in the laminar flow hood unless otherwise noted. For growth factor supplemented studies, use tendon cell media without serum.

Procedure

1) Warm complete media, sterile PBS, and 3 mL trypsin-EDTA per T75 flask to be passaged in water bath to 37°C.

2) Place hydrated scaffold pieces in fresh media for at least 30 min.

3) Carefully remove excess media from scaffolds with a Kimwipe and place 3-4 scaffold pieces in each well of Ultra-low attachment 6-well plates. Do not overdry scaffolds (especially CGCaP scaffolds) as this will lead to reduced viability.

4) When the media, PBS and trypsin are warm, wipe them dry with paper towel and spray with 70% ethanol before placing in the sterile hood.

5) Remove all old media from each flask, taking care not to scrape the cells with the pipette tip.

6) Add 10 mL of PBS per T75 flask and leave the PBS in the flask to rinse the cells for 30 s. Swirl gently to remove any excess media from the cells. Adjust volumes of PBS, media, and trypsin accordingly for different sized flasks.

7) Remove the PBS and add 3 mL of trypsin per flask. Return the flasks to the incubator for 6-8 min to allow for the cells to detach from the tissue culture plastic (allow the cells to sit for 3-4 additional min in the incubator if they do not detach after 6 min). Slap flasks a few times to detach cells.

8) Add 6 mL of complete tendon cell media to each flask to neutralize the trypsin and to flush cells off of the tissue culture plastic.

9) Remove the trypsin, additional media, and cells from the flask and put into a conical tube. Remove a 10 μL cell suspension aliquot for counting. Centrifuge the cells at appropriate speed and time.

10) While cells are spinning down, mix the 10 μL cell suspension aliquot with 10 μL of Trypan blue. Pipette several times to mix the stain and cell suspension.

11) Place a cover slip on the hemacytometer and pipette 10 μL of the stain/cell suspension into the hemacytometer.

12) Cell counts are performed in as many of the nine separate regions of the hemacytometer as is feasible. Average number of cells per region is used to calculate the total cell population. For this calculation, the dilution factor is typically 2 (1:1 ratio of cell suspension to Trypan blue).

*Total Cell Population = (Mean Cells per Region) * Dilution * 10,000 * (Cell Suspension Volume)*

13) Aspirate off the media supernatant and add new media to dilute cells to desired concentration. For 8 mm diameter, 5 mm thick scaffold pieces dilute to 1-5 x 10^5 cells per 20-40 μL media.

14) Add 10-20 μL of cell suspension to each scaffold piece. Place scaffolds in incubator for 15-30 min.

15) Remove scaffolds from incubator, flip over, add additional 10-20 μL of cell suspension to the other side of each scaffold, and return to incubate for additional 2-3 h.

16) Carefully add 6 mL complete media (or media with growth factors but without serum) to each well. Change media every 3 days over the course of the experiment.

B.5 AlamarBlue metabolic activity protocol

Reference: (Tierney, Jaasma et al. 2009; Caliari and Harley 2011; Caliari, Ramirez et al. 2011)

Reagents

- Complete media (see E.2 and E.3 for recipes); store at 4ºC
- AlamarBlue (Invitrogen DAL1100); store at 4ºC

Supplies and equipment

- 24-well plates (Fisher 08-772-1)
- 96-well plates (Fisher 12-565-369)
- MTS 2/4 digital microtiter shaker (IKA 3208001)
- Water bath (37ºC, Fisher 15-474-35)
- Fluorescence spectrophotometer (Tecan, Room 299 RAL)

*Note: all steps should be performed in the laminar flow hood unless otherwise noted. The volumes of reagents used are correct for 8 mm diameter, 5 mm thick scaffold pieces. Use identical media to that being used for experiment.

Generating standard curve procedure

1) Warm media and alamarBlue in water bath to 37ºC.

2) Before starting an experiment, generate a standard curve with a known number of cells. The standard should have at least eight sample points: one well with just media, one well with media and alamarBlue, and six wells with media, alamarBlue, and a different number of cells. An example standard setup is shown:

	Well 1	**Well 2**	**Well 3**	**Well 4**	**Well 5**	**Well 6**	**Well 7**	**Well 8**
Media	1000 μL	900 μL	895 μL	890 μL	885 μL	880 μL	860 μL	840 μL
Cell suspension	0 μL	0 μL	5 μL	10 μL	15 μL	20 μL	40 μL	60 μL
AlamarBlue	0 μL	100 μL	100 μL	100 μL	100 μL	100 μL	100 μL	100 μL

Well 1 is a negative control, well 2 is a background control, and the other wells are used to make the standard curve.

3) Incubate at 37ºC under gentle (~50 rpm) shaking for 1.5-5.5 h. During this time healthy cells convert the active ingredient in alamarBlue (resazurin) to the highly fluorescent resorufin. Longer incubation times are necessary for smaller cell concentrations, but make sure not to incubate cells too long or all of the resazurin will be reduced to resorufin.

4) After incubation, pipette 100 μL in triplicate from each sample well into a clear 96-well plate.

5) Measure fluorescence (excitation: 540 nm, emission: 580 nm) on the spectrophotometer in RAL 299 using the program 'AlamarBlue F200'. Remember to reserve the F200 machine on the Google Calendar prior to use. For each data point, adjust the fluorescence reading by subtracting the reading from well 2 (background control). The standard curve is created by plotting cell number as a function of adjusted fluorescent intensity.

Quantifying metabolic activity on scaffolds procedure

1) For measuring cell metabolic activity on scaffolds, pipette 900 μL media into each well (one well for each scaffold piece plus the two control wells). Add 100 μL alamarBlue to each well except for one negative control well. Adjust volumes for smaller/larger materials accordingly, keeping the 9:1 media: alamarBlue® ratio constant.

2) Remove scaffolds to be assayed and rinse in sterile PBS to remove excess media and unattached/dead cells. Add scaffolds to experimental wells and incubate at 37^{o}C under gentle (~50 rpm) shaking for 1.5-5.5 h. The incubation time should be identical to the time used to make the standard curve.

3) After incubation, pipette 100 μL in triplicate from each sample well into a 96-well plate.

4) Measure fluorescence (excitation: 540 nm, emission: 580 nm) on the spectrophotometer in RAL 299 using the program 'AlamarBlue F200'. Remember to reserve the F200 machine on the Google Calendar prior to use. Subtract the background control from the data points and extrapolate adjusted fluorescent intensity on the standard curve to give metabolic activity.

5) This assay is non-destructive, so scaffolds can continue to be cultured and analyzed at later time points.

B.6 Hoechst DNA quantification protocol

Reference: (Kim, Sah et al. 1988; Caliari and Harley 2011; Caliari, Ramirez et al. 2011)

Reagents

- Hoechst dye buffer (500 mL); store at 4°C for up to 3 months
  - 400 mL deionized water
  - 58.44 g sodium chloride (RAL storeroom)
  - 0.605 g Tris base (RAL storeroom)
  - 0.185 g disodium EDTA (Sigma-Aldrich E5134)
  - Adjust pH to 7.4, bring total volume to 500 mL, sterile filter before use
- Papain buffer (100 mL); store at 4°C
  - 100 mL PBS
  - 1 mL 0.5 M EDTA (pH = 8.0, Sigma-Aldrich EDS); store at 4°C
  - 79 mg cysteine-HCl (Sigma-Aldrich 00320)
- Hoechst 33258 dye solution (1 mL); store at 4°C for up to 6 months
  - 1 mL sterile water
  - 1 mg Hoechst 33258 dye (Invitrogen H1398); store at 4°C
- Papain from Carica papaya (Sigma-Aldrich 76218); store at -20°C
- Sterile phosphate-buffered saline without Ca^{2+} or Mg^{2+} (PBS)

Supplies and equipment

- 96-well plates (Fisher 12-565-369)
- Vortex (Fisher 02-215-365)
- Water bath (60°C, Fisher 15-460-2SQ)
- Fluorescence spectrophotometer (Tecan, Room 299 RAL)
- Microcentrifuge tubes (1.5 mL)

Generating standard curve procedure

*Note: steps 1-2 should be performed in the laminar flow hood.

1) At the beginning of each experiment, a standard curve should be generated with a known number of cells. To make a standard curve spanning 5 x 10^3 to 1.5 x 10^6 million cells, make up active papain enzyme solution by dissolving 18-20 mg papain in 15 mL papain buffer in the 60°C water bath.

2) Spin down two aliquots of 2 million cells each. Remove supernatant and add 12 mL papain enzyme solution to one tube and 400 μL to the other tube. Allow to digest for 24 h in the 60°C water bath.

3) After 24 h, vortex tubes thoroughly. For the 12 mL tube, add cell lysate to labeled microcentrifuge tubes in 30 μL intervals (starting from a blank control) up to 300 μL. Bring all volumes to 300 μL with blank papain buffer. For the 400 μL tube, add cell lysate to labeled microcentrifuge tubes in 2 μL intervals (starting from a blank control) up to 30 μL. Bring all volumes to 30 μL with blank papain buffer.

4) Prepare Hoechst working dye solution by adding 1 μL dye solution to 10 mL Hoechst dye buffer. Vortex thoroughly. Add working dye solution to each tube to bring total volume to 630 μL. Vortex thoroughly. The Hoechst dye fluorescently binds to double-stranded DNA from the lysed cells, allowing quantification of DNA and thus cell number.

5) Pipette 200 μL from each tube in triplicate into a black 96-well plate.

6) Measure fluorescence (excitation: 360 nm, emission: 465 nm) on the spectrophotometer in RAL 299. Use the 'DNA F200' program and remember to reserve the F200 machine on the Google Calendar prior to use. For each data point, adjust the fluorescence reading by subtracting the reading from the blank control. The standard curve is created by plotting cell number as a function of adjusted fluorescent intensity.

Quantifying cell number on scaffolds procedure
*Note: step 2 should be performed in the laminar flow hood.

1) For measuring cell number on scaffolds, pipette 300 μL of papain enzyme solution into microcentrifuge tubes (one for each scaffold plus two controls: one tube with just papain enzyme solution as a negative control and one tube containing a blank scaffold with no seeded cells as a background control).

2) Remove scaffolds to be assayed and rinse in sterile PBS to remove excess media and unattached/dead cells. Add scaffolds to microcentrifuge tubes and incubate in 60^{o}C water bath for 24 h. Vortex occasionally to facilitate digestion of scaffold.

3) After incubation, pipette 600 μL Hoechst working dye solution in microcentrifuge tubes.

4) Remove samples from water bath and vortex thoroughly. Add 30 μL from each tube to its corresponding tube containing working dye solution. Vortex thoroughly.

5) Pipette 200 μL from each tube in triplicate from each sample well into a 96-well plate.

6) Measure fluorescence (excitation: 360 nm, emission: 465 nm) on the spectrophotometer in RAL 299. Use the 'DNA F200' program and remember to reserve the F200 machine on the Google Calendar prior to use. For each data point, adjust the fluorescence reading by subtracting the reading from the background control. Adjusted fluorescent intensity can be extrapolated on the standard curve to give a cell number.

B.7 Scaffold contraction protocol

References: (Spilker, Asano et al. 2001; Caliari and Harley 2011)

Supplies and equipment

- Drafting template

Procedure

* Note: all steps should be performed in the laminar flow hood unless otherwise noted.

1) On day 0, measure the diameter of the fully hydrated scaffolds before cell seeding. This can be done several ways:

- Place drafting template over well plate containing scaffolds and move template until finding the hole that most closely approximates the diameter of the scaffold.
- Remove scaffolds from solution and measure using template as before.

Scaffolds can be measured either in or out of solution, but the key is consistency; the same method should be used for all samples and time points.

2) Repeat step 1 for subsequent time points in experiment. Normalize measurements to results from day 0.

B.8 RNA isolation protocol

Reference: (Duffy, McFadden et al. 2011; Caliari, Weisgerber et al. 2012)

Reagents

- RNeasy Plant Mini Kit (Qiagen 74904)
- β-mercaptoethanol (Sigma M7522-100ML)
- 70% ethanol (use RNase free water when making solution)
- Sterile phosphate-buffered saline without Ca^{2+} or Mg^{2+} (PBS)
- RNase-free water
- Ice

Supplies and equipment

- 2 mL RNase free non-graduated microcentrifuge tubes
- RNase free pipette tips
- Ice bucket
- Kimwipes
- Microcentrifuge

Procedure

Reagent prep (before starting)

1) Lysis buffer: Add 10 µL β-mercaptoethanol (14.3 M) per 1 mL of Buffer RLT supplied with Qiagen kit. This solution can be stored at room temperature for 1 month.

2) Buffer RPE: Add 4 volumes of 100% ethanol to the bottle of Buffer RPE supplied with Qiagen kit.

RNA Extraction

*All steps are performed at room temperature. Work quickly; limit the number of samples for RNA extraction to 18-24 in each sitting. RNase free tips should be used throughout.

1) Label one microcentrifuge tube for each sample.

2) Put some ice (2^{nd} floor RAL) in an ice bucket.

3) Wash scaffolds in PBS three times, cut in half with razor blade, and then place in labeled tubes.

4) Add ~ 500 µL of ice-cold lysis buffer to each tube and keep on ice for ~ 5 min, shaking tubes periodically to help the buffer infiltrate the scaffolds. Scale amount of lysis buffer appropriately.

5) Pipette lysate into a labeled QIAShredder column. Place scaffold pieces in column as well. Spin at 14,000 rpm for 2.5 min.

6) Add equal volume of 70% ethanol to each sample and mix by pipetting up and down.

7) Add half of the lysate + ethanol to labeled RNeasy column (with 2-mL collection tube).

8) Centrifuge at 12,000 rpm for 30 s. Discard flow-through and replace column.

9) Add the remaining lysate + ethanol to the column.

10) Centrifuge at 12,000 rpm for 30 s. Discard flow-through and replace column.

11) Add 700 μL Buffer RW1 to the column.

12) Centrifuge at 12,000 rpm for 30 s. Discard flow-through and replace column.

13) Pipet 500 μL Buffer RPE into the column.

14) Centrifuge at 12,000 rpm for 30 s. Discard flow-through and replace column.

15) Add another 500 μL Buffer RPE into the column.

16) Centrifuge at 12,000 rpm for 2.5 min. Discard flow-through and place the column in a new 2 mL collection tube (supplied with kit).

17) Centrifuge at 12,000 rpm for 2.0 min.

18) Transfer the column to a new labeled, 1.5-mL collection tube.

19) Pipet 30 μL RNase-free water into the column and wait 5 min.

20) Centrifuge the RNeasy column at 12,000 rpm for 1.5 min.

21) Store RNA at -80°C for later use or put on ice if directly proceeding to quantification, reverse transcription, and RT-PCR.

B.9 Quantification of RNA and reverse transcription protocol

Reference: (Duffy, McFadden et al. 2011; Caliari, Weisgerber et al. 2012)

Reagents

- QuantiTect Reverse Transcription Kit (Qiagen 205313); store at -20°C although individual kit aliquots may be stored at 4°C once opened.
- TE buffer (pH = 8.0)
- DTT (100 mM stock); store at -20°C
- RNase-free water
- RNase H; store at -20°C
- Ice

Supplies and equipment

- Cuvettes
- Thermocycler (BioRad **185-2196)**
- RNase-free pipette tips
- RNase-free PCR tubes (100 µL, CLSL stockroom)
- Ice bucket
- Kimwipes
- Ambion DNase I removal kit
- Vortex (Fisher 02-215-365)

Procedure

<u>RNA quantification</u>

1) Gather pipettes, RNase-free tips, TE buffer, cuvettes, and samples in an ice bucket.

2) Proceed to the spectrophotometer in the IGB 2nd floor (shared equipment).

3) Remove piece of tape covering the cuvette opening and turn the machine on. Make sure it is in 'RNA' mode (button 9).

4) Pipet 50 µL TE buffer into a clean cuvette and blank the machine.

5) For each RNA sample, pipet 10 µL of RNA into 40 µL of TE buffer in cuvette. Lightly flick the cuvette several times to mix and then read absorbance. Record the A260 and A260/280 ratio readings.

6) Empty the cuvette on a pile of Kimwipes, getting the cuvette relatively dry. Repeat step 5 for subsequent samples.

7) RNA amount (µg) can be calculated using the following equation:

$$[RNA] = A_{260} * \left(40\ \frac{\mu g}{mL}\right) * dilution\ factor * \ RNA\ volume\ (mL)$$ (**Equation E.1**)

Normal procedure for reverse transcription with hexameric primers

1) Label PCR tubes for number of reactions needed and defrost reverse transcription kit components on ice if needed. Keep kit components and RNA samples on ice. Turn on thermocycler so it can warm up.

2) Calculate the amount of RNA needed for each reaction. Typically, > 10 ng of cDNA will be desired per well for subsequent RT-PCR experiment.

3) For 10 µL reactions, add 1 µL gDNA wipeout buffer (orange tubes) to each PCR tube.

4) Add RNase-free water to each PCR tube so that the total reaction volume (when RNA is added) will be 7 µL. If RNA quantification was low do not add water.

5) Add RNA to each tube. Add up to 10 µL per tube if RNA amount is very low.

6) Close tubes and place in thermocycler. Close lid with extra quarter turn of tightness.

7) Run the 'CAV1' program. This will begin by incubating the samples at 42°C for 2 min.

8) While the first step is running, prepare reaction buffer. Note that the RT buffer (green tubes) and the Primer Mix (purple tubes) can be combined in one tube. If you do this, place a check mark on the lid of the green tube. Combine 2.5 µL of RT buffer/primer mix plus 0.33-0.5 µL reverse transcriptase (red tubes) per sample into a single tube and vortex well.

9) Pipet 2.83-3 µL of reaction buffer mix into each PCR tube once the 2 min initial incubation is complete. Close tubes, lid, and then press enter to skip to the next step, which is a 15 min incubation at 42°C followed by 95°C incubation for 3 min.

10) Once the cycle is complete, place samples in a labeled box or Petri dish and put on ice if proceeding directly to RT-PCR, or store at -20°C (short term) or -80°C (long term).

Procedure for generating gene-specific cDNA

1) Label PCR tubes for number of reactions needed and defrost reverse transcription kit components on ice if needed. Keep kit components and RNA samples on ice. Turn on thermocycler so it can warm up.

2) DNA removal 1: incubate 1 µL gDNA wipeout buffer (orange tubes) with up to 100 ng RNA. Bring total volume to 7 µL with RNase-free water.

3) Run the 'ScxGFP' program, which begins by incubating mix at 42°C for 2 min.

4) DNA removal 2: add 1 µL of 10x DNase I buffer, 1 µL DNase I, and 1 µL RNase-free water to bring total volume to 10 µL. Incubate at RT for 15 min.

5) Inactivate DNase I by adding 1 µL of EDTA solution. Heat at 65°C for 10 min.

6) Add 1 µL of reverse primer (20 µM stock), 1 µL reverse transcriptase (red tubes), 1 µL DTT (100 mM stock), 2 µL RNase-free water, and 4 µL RT buffer (green tube WITHOUT primers added) to each tube to bring total volume to 20 µL.

7) Set up a reverse transcriptase-free control to test for the presence of genomic DNA contamination.

8) Incubate mix at 42°C for 15 min.

9) Incubate mix at 95°C for 3 min to inactivate reverse transcriptase.

10) Dilute RNase H so that 2 U are added to each reaction and then add 1 µL of the diluted RNase H to mix and incubate at 37°C for 20 min.

11) Freeze down cDNA for later use or dilute reaction 10 times in 179 µL RNase-free water to perform regular PCR using primers specific to the coding sequence of the scleraxis gene and encoding restriction sites to facilitate cloning in pEGFP-N1 and pEGFP-C1.

B.10 PCR protocol

Reference: (Duffy, McFadden et al. 2011; Caliari, Weisgerber et al. 2012)

Reagents

- QuantiTect SYBR Green Kit (Qiagen 204145); store at -20°C although individual kit aliquots may be stored at 4°C once opened.
- Primers (Integrated DNA Technologies)
    - Dilute to 30 µM in TE buffer (pH = 8.0)
    - Aliquot and store at -20°C or keep at 4°C
- Ice
- DNase removal buffer

Supplies and equipment

- Rainier multi-pipettes
- 384-well plates (Invitrogen 4309849)
- Plate covers (Invitrogen 4311971)
- Sealing tool
- Rainier pipette tips (VWR)
- RNase-free PCR tubes (500 µL, CLSL stockroom)
- Ice bucket
- Vortex (Fisher 02-215-365)
- Applied Biosystems 7900HT Fast Real-Time PCR system (Applied Biosystems)
- Sequence Detection Systems software v2.4 (Applied Biosystems)

Procedure

*Note: keep PCR area as clean as possible and remember to wipe down area with DNase removal buffer following each plate prep. Remember to reserve time on the PCR system on the IGB website (each plate takes 1 h 55 min to run).

1) Diagram plate layout and determine the amount of water, SYBR green, and primers you will need. Master mix 1 consists of SYBR green and primers, and is added at 5.2 µL per well for 10 µL reactions. Master mix 2 is RNase-free water and cDNA, and is added at 4.8 µL per well for 10 µL reactions. Make up ~ 10% excess reagent for each mix.

2) Make up master mixes. Vortex each tube of master mix 1 thoroughly and pipet into wells.

3) Vortex each tube of master mix 2 thoroughly and pipet into wells.

4) Place cover on plate. Make sure the plate is sealed tightly on all edges with the sealing tool.

5) Keep plate protected from light at 4°C until ready to analyze.

6) Transport to IGB 124A and set up plate on PCR machine. Follow instructions obtained during training on machine, making sure to add extra stage to determining product melting point. SYBR

green dye non-specifically binds to all DNA, so the melting curve must be obtained to confirm the presence of a single product.

7) Analyze results using the Sequence Detection Systems software to obtain Ct values. For multiple plates, make sure the threshold is set at the same number for each primer pair. Calculate fold changes in expression using the delta-delta Ct method.

B.11 Protein isolation protocol

Reference: (Caliari and Harley 2014)

Reagents

- RIPA buffer (500 mL)
    - 495 mL deionized water
    - 4.38 g sodium chloride (150 mM, RAL storeroom)
    - 5 mL Triton X-100 (1%, Sigma 93443-100ML)
    - 2.5 g sodium deoxycholate (0.5%, Sigma D6750-10G)
    - 0.5 g SDS (0.1%, Sigma L3771-25G)
    - 3.03 g Tris base (50 mM, RAL storeroom)
    - Adjust pH to 8.0 and store at 4°C
- Protease inhibitor cocktail (Sigma P8340-1ML)
- Phosphatase inhibitor cocktail 2 (Sigma P5726-1ML)
- Phosphatase inhibitor cocktail 3 (Sigma P0044-1ML)
- Ice
- Sterile phosphate-buffered saline without Ca^{2+} or Mg^{2+} (PBS)

Supplies and equipment

- Ice bucket
- Microcentrifuge tubes
- Vortex (Fisher 02-215-365)

Procedure

*Note: steps 2-3 should be performed in the laminar flow hood.

1) Label microcentrifuge tubes for each sample. Prepare ~ 200 µL of ice-cold RIPA buffer per sample and add protease and phosphatase inhibitors (100x stocks) fresh to the buffer.

2) Rinse scaffold pieces in PBS to remove dead and unattached cells. Place scaffolds in empty, labeled microcentrifuge tubes.

3) Pipet 150-200 µL complete RIPA buffer onto each scaffold piece.

4) Keep scaffolds on ice for 30 min, agitating with a pipet tip occasionally to aid buffer infiltration.

5) After 30 min, remove scaffold from tubes, squeeze out excess liquid, and store lysates at -80°C until use.

B.12 Western blotting protocol

Reference: (Caliari and Harley 2014)

Reagents

- Running buffer (1L, 10x); store at 4°C
    - 30.3 g Tris base (0.25 M, RAL storeroom)
    - 144 g glycine (1.92 M, RAL storeroom)
    - 10 g SDS (1%, Sigma L3771-25G)
    - Bring volume to 1 L in deionized water, sterile filter
- Running buffer: Need ~700 mL per gel (when running 1-2 gels), can re-use several times
    - 10% 10x running buffer
    - 90% deionized water
    - Final concentrations:25 mM Tris base, 192 mM glycine, 0.1% SDS. pH will be ~ 8.3.Store at 4°C.
- Towbin's electrotransfer buffer (1 L, 10x); store at 4°C
    - 30.3 g Tris base (0.25 M, RAL storeroom)
    - 144 g glycine (1.92 M, RAL storeroom)
    - Bring volume to 1 L in deionized water, sterile filter
- Transfer buffer: Need ~1 L per gel, can re-use several times
    - 20% Methanol (RAL storeroom)
    - 10% 10x Towbin's electrotransfer buffer
    - 70% Water
    - Store at 4°C
- TBS-T (1 L, 10x); store at 4°C
    - 24.2 g Tris base (0.2 M, RAL storeroom)
    - 80 g NaCl (RAL storeroom)
    - 10 mL Tween 20 (1% v/v, RAL storeroom)
- TBS-T (1x); store at 4°C
    - 10% 10x TBS-T
    - 90% deionized water
    - Final concentrations:20 mM Tris base, 0.8% w/v NaCl, 0.1 % v/v Tween 20, pH will be ~ 7.5
- 4x Laemlii buffer (CLSL stockroom): Need ~ 12 µL per sample
- Blocking Buffer (TBS-T + 5% non-fat milk)
    - 100 mL TBS-T
    - 5 g non-fat milk powder
    - Mix for ~ 15 min before use
- Ponceau S stain (Fisher Scientific, K793-500mL)
- Ice
- Deionized water
- β-mercaptoethanol (Sigma M7522-100ML)
- Stripping buffer (CLSL stockroom)

Supplies and equipment

- IGB shared equipment

    - Glass container
    - Biorad Mini-Protein apparatus
- Rainbow ladder (GE Healthcare, CLSL stockroom); store at -20°C
- Microcentrifuge tubes
- Gel-loading pipet tips
- Nitrocellulose membrane (Fisher Scientific, RPN303E)
- Whatman paper
- SuperSignal West Pico Chemiluminescence substrate (ECL reagents, CLSL stockroom); store at 4°C
- 10% polyacrylamide gels (CLSL stockroom); store at 4°C
- Plastic forceps
- Ice bucket
- Kimwipes
- Image Quant gel reader (GE Healthcare, IGB 124A)

Procedure

<u>Day 1: Protein lysate gel electrophoresis, transfer, primary antibody</u>

1) Have buffers and gels ready.

2) Thaw lysates on ice while walking to IGB.

3) Upon arrival, turn on heating block to 95°C on Schook's bench.

4) Label microcentrifuge tubes and prepare 4x Laemlii buffer by adding 0.5 µL β-mercaptoethanol for every 12 µL of buffer.

5) Add 37.5µL of lysate and 12.5 µL of Laemlii + β-mercaptoethanol per tube,

6) Heat tubes at 95°C in heating block for 5-10 min.

7) While tubes are heating, remove gels from fridge and rinse with water.

8) Take strip off bottom and place it to the front of electrophoresis apparatus.

9) Place a blank plastic cassette or another gel on the back side. Make sure everything is clamped in properly. (Red-red; black-black).

10) Pour running buffer between cassettes until gel is immersed. Fill container with running buffer to 2-gallon mark.

11) Take sample tubes. Spin down for a few seconds if you have solid pieces from hydrogels/scaffolds.

12) Carefully load 50 µL lysate/Laemlii mix into each lane (behind plate) using gel-loading tips.

Don’t use first or last lane. Load 5 µL rainbow ladder to one lane for reference.

13) Run at 80 V for 5-10 min until lysates become thin bands in stacking gel. This step can be run at RT but running at 4°C may reduce “smiley face effect.” There is a power supply available in the back 4°C cold room.

14) Run gel at 100 V for ~ 1.5 h until all lysates (blue line) arrive at the bottom black line. Check progress after 1 h to make sure proteins don’t run off the gel.

15) Prepare nitrocellulose membranes, filter papers, and transfer buffer ~ 15 min before gel is finished running. Cut membranes to match gel size.

16) Kill power and rinse gel cartridge thoroughly with DI water. Carefully open gel cartridge using opening lever by cracking open at 4 sides marked by arrowheads.

17) Remove stacking gel and rinse with water. Cut lane borders on top with green cutting tool.

18) Pour transfer buffer to the glass container. Then, prepare the transfer cassette assembly by stacking in the following order then soak it in transfer buffer in the glass container.

- Case (clear side)
- Sponge
- Whatman paper
- Membrane
- Gel
- Whatman paper
- Sponge
- Case (black side; negative terminal)

19) Use plastic forceps and/or green cutting tool to carefully maneuver the gel so that the entire area lays on the membrane.

20) Remove air bubbles by rolling with plastic pipet and then close cassette.

21) Place assembly in plastic module then into electrophoresis apparatus. Remember to match colors (e.g. black faces black).

22) Fill apparatus completely with transfer buffer, using big beaker to transfer buffer from glass container to the apparatus.

23) Place cooling unit (stored in far -20°C freezer) in buffer and transfer at 300 mA for 2 h at 4°C in far cold room.

24) After 2 h, take apart assembly. Discard filter paper and gel (nothing should be left in the gel, indicating the transfer was successful). Nick membrane edge (top left corner) with scissors so you know which side the protein is on (this is the side of the membrane that faced the gel!)

25) Stain with Ponceau S (1x) to check protein bands. Bands may not appear. Ponceau stain can be re-used. Cut bands according to molecular weight of desired targets while Ponceau stain is still visible. Rinse with TBS-T to remove stain.

26) Place membrane in mini plastic container (old microscope slide boxes) and pour in 10-15 mL blocking buffer. Incubate for 30 min on a shaker (~ 50 rpm).

27) While waiting, prepare primary antibody solution in ~ 5mL blocking buffer. Typical dilution is 1:2000, but optimize for each antibody. Note that primary antibodies diluted in blocking buffer can be used again. Store at -20°C or at 4°C for short times (< 2 weeks).

28) Incubate membranes in primary antibody solution overnight at 4°C on shaker.

Day 2 Secondary antibody, read blot using ECL reagents (enhanced chemiluminescence)

1) Wash membranes with TBS-T for 5 min on shaker at RT (3x).

2) While waiting, prepare 5 mL secondary antibody solution (1:2500 dilution) in blocking buffer from fridge. Make sure you use matching (anti-rabbit; anti-mouse, etc) secondary antibody.

3) Incubate in secondary antibody solution for 1 hr at RT under gentle shaking.

4) Wash membranes with TBS-T for 5 min on shaker at RT (3x).

5) While waiting, gather supplies for ECL detection: gloves, 15 mL conical tube, 1 mL pipette with tips, plastic forceps, and ECL reagents. Once membranes are finished rinsing add them to box of supplies.

6) Go down to IGB 124A. There should already be Kimwipes and saran wrap in this room.

7) Once in basement, log onto computer and start up the ImageQuant program.

8) Mix ECL reagents (1:1; make ~ 2 mL per full membrane).

9) Place saran wrap on a flat surface. Pick up your membrane with forceps then gently blot using Kimwipes. Quickly do this for all membranes and pipette mixed ECL solution onto the membranes.

10) Wrap membranes in saran wrap and keep in drawer for 2 min.

11) Take membranes from the drawer, blot, and place on clean saran wrap with forceps.

12) Place membranes in the detection chamber and focus to ensure membrane is in viewing window. Make sure the black tray is in the chamber and set at level 2 for chemiluminescence. Expose for 1 min first then adjust according to the output intensity.

13) Save image and perform post-analysis of band intensity using Gel Image Analyzer or ImageJ.

Stripping for re-probing

1) It may be desirable to strip the antibodies and re-probe for another protein that is close in molecular weight. To do this, begin by washing the membranes in TBS-T for 5 min (1x).

2) Cover membranes in stripping buffer and incubate under gentle shaking for 15 min.

3) Wash membranes in TBS-T for 5 min (3x).

4) Re-block membranes in blocking buffer for 30 min at RT under gentle shaking (see day 1 step 26). Repeat steps from here to completion.

B.13 Western Blot quantification protocol

Reference: http://www.lukemiller.org/ImageJ_gel_analysis.pdf

Procedure
1) Open the image file in ImageJ.

2) If the image isn't already in 8-bit grayscale, convert to grayscale is to go to Image>Type>8-bit.

3) If the bands are slanted, level them by selecting Image →Rotate→Arbitrarily…

4) Choose the rectangular selection option from the toolbar and draw a rectangle around the band in the first lane. Click Ctrl+1 to set the first lane.
Note: If your rectangle is taller than it is wide, ImageJ will assume your lanes run up and down, but if your rectangle is wider than it is tall, Image J will assume your lanes run up and down. The width of the selection is fixed for all lanes. It is important to get the shape and position of the first lane correct prior to setting it.

5) Place the mouse over the "1" inside the rectangle, clicking and holding down while dragging the box to the second lane. Click Ctrl+2 (or Analyze→Gels→Select Next Lane)

6) Place the mouse over the next rectangle band, clicking and holding down while dragging the box to the next lane. Again, click Ctrl+2. Repeat for any additional lanes.

7) Upon dragging the rectangle over the last lane, click Ctrl+3 (or Analyze→Gels→Plot Lanes). The plots will open in a new window.

8) Use the straight line tool to close the bottom of the first peak.

9) Using the plot window, scroll down to the next peak (the hand tool is good for scrolling). Use the straight line tool to again close off the peak. Repeat for any additional peaks.

10) Scroll back to the top and selecting the wand tool, click inside the peak. A new window will open with the value for the lane

11) Scroll to the next peak and use the wand tool. The new value will be added to the table in the new window. Repeat until all peaks are measured.

12) Peaks can be normalized to GAPDH bands. In the case of phosphorylated measurements, the peaks can be normalized to the unphosphorylated measurements.

13) Copy the data from the table and paste into excel for further analysis.

REFERENCES

Allen, J. L., M. E. Cooke, et al. (2012). "ECM stiffness primes the TGF pathway to promote chondrocyte differentiation." Molecular Biology of the Cell **23**(18): 3731-3742.

Andalib, M. N., J. S. Lee, et al. (2013). "The role of RhoA kinase (ROCK) in cell alignment on nanofibers." Acta Biomaterialia.

Arnoczky, S. P., T. Tian, et al. (2002). "Activation of stress-activated protein kinases (SAPK) in tendon cells following cyclic strain: the effects of strain frequency, strain magnitude, and cytosolic calcium." J Orthop Res **20**(5): 947-952.

Banes, A. J., M. Tsuzaki, et al. (1995). "Mechanoreception at the cellular level: the detection, interpretation, and diversity of responses to mechanical signals." Biochem Cell Biol **73**(7-8): 349-365.

Banks, J. M., L. C. Mozdzen, et al. (2014). "The combined effects of matrix stiffness and growth factor immobilization on the bioactivity and differentiation capabilities of adipose-derived stem cells." Biomaterials **35**(32): 8951-8959.

Baselga, J., M. L. Rothenberg, et al. (2008). "TGF-beta signalling-related markers in cancer patients with bone metastasis." Biomarkers : biochemical indicators of exposure, response, and susceptibility to chemicals **13**(2): 217-236.

Beederman, M., J. D. Lamplot, et al. (2013). "BMP signaling in mesenchymal stem cell differentiation and bone formation." Journal of biomedical science and engineering **6**(8A): 32-52.

Beredjiklian, P. K., M. Favata, et al. (2003). "Regenerative versus reparative healing in tendon: a study of biomechanical and histological properties in fetal sheep." Annals of biomedical engineering **31**(10): 1143-1152.

Berthet, E., C. Chen, et al. (2013). "Smad3 Binds Scleraxis and Mohawk and Regulates Tendon Matrix Organization." Journal of Orthopaedic Research: n/a-n/a.

Bibby, D. C., N. M. Davies, et al. (2000). "Mechanisms by which cyclodextrins modify drug release from polymeric drug delivery systems." International journal of pharmaceutics **197**(1-2): 1-11.

Blevins, F. T., M. Djurasovic, et al. (1997). "Biology of the rotator cuff tendon." The Orthopedic clinics of North America **28**(1): 1-16.

Blitz, E., A. Sharir, et al. (2013). "Tendon-bone attachment unit is formed modularly by a distinct pool of Scx- and Sox9-positive progenitors." Development **140**(13): 2680-2690.

Blitz, E., S. Viukov, et al. (2009). "Bone ridge patterning during musculoskeletal assembly is mediated through SCX regulation of Bmp4 at the tendon-skeleton junction." Dev Cell **17**(6): 861-873.

Bosworth, L. A., S. R. Rathbone, et al. (2014). "Dynamic loading of electrospun yarns guides mesenchymal stem cells towards a tendon lineage." Journal of the Mechanical Behavior of Biomedical Materials **39**(0): 175-183.

Breidenbach, A. P., S. D. Gilday, et al. (2013). "Functional tissue engineering of tendon: Establishing biological success criteria for improving tendon repair." Journal of biomechanics.

Burk, J., A. Plenge, et al. (2016). "Induction of Tenogenic Differentiation Mediated by Extracellular Tendon Matrix and Short-Term Cyclic Stretching." Stem Cells International **2016**: 7342379.

Butler, D. L., N. Juncosa-Melvin, et al. (2008). "Functional tissue engineering for tendon repair: A multidisciplinary strategy using mesenchymal stem cells, bioscaffolds, and mechanical stimulation." J Orthop Res **26**(1): 1-9.
Caliari, S. R., E. A. Gonnerman, et al. (2015). "Collagen scaffold arrays for combinatorial screening of biophysical and biochemical regulators of cell behavior." Advanced Healthcare Materials **4**(1): 58-64.
Caliari, S. R. and B. A. Harley (2013). "Composite Growth Factor Supplementation Strategies to Enhance Tenocyte Bioactivity in Aligned Collagen-GAG Scaffolds." Tissue Eng Part A.
Caliari, S. R. and B. A. Harley (2014). "Collagen-GAG scaffold biophysical properties bias MSC lineage choice in the presence of mixed soluble signals." Tissue Engineering. Part A **20**(17-18): 2463-2472.
Caliari, S. R. and B. A. C. Harley (2011). "The effect of anisotropic collagen-GAG scaffolds and growth factor supplementation on tendon cell recruitment, alignment, and metabolic activity." Biomaterials **32**(23): 5330-5340.
Caliari, S. R. and B. A. C. Harley (2014). "Structural and biochemical modification of a collagen scaffold to selectively enhance MSC tenogenic, chondrogenic, and osteogenic differentiation." Adv Healthc Mater **3**(7): 1086-1096.
Caliari, S. R., M. A. Ramirez, et al. (2011). "The development of collagen-GAG scaffold-membrane composites for tendon tissue engineering." Biomaterials **32**(34): 8990-8998.
Caliari, S. R., D. W. Weisgerber, et al. (2015). "Collagen Scaffolds Incorporating Coincident Gradations of Instructive Structural and Biochemical Cues for Osteotendinous Junction Engineering." Advanced Healthcare Materials **4**(6): 831-837.
Caliari, S. R., D. W. Weisgerber, et al. (2012). "The influence of collagen–glycosaminoglycan scaffold relative density and microstructural anisotropy on tenocyte bioactivity and transcriptomic stability." Journal of the Mechanical Behavior of Biomedical Materials **11**: 27-40.
Caporali, E., A. Kapoor, et al. (2009). TGF-b and microtopographical cues promote expression of tenogenic marker genes and tenocyte alignment. Proceedings of the 36th Annual Conference of the Veterinary Orthopedic Society.
Chamberlain, L. J., I. V. Yannas, et al. (2000). "Near-terminus axonal structure and function following rat sciatic nerve regeneration through a collagen-GAG matrix in a ten-millimeter gap." Journal of neuroscience research **60**(5): 666-677.
Chan, B. P., K. M. Chan, et al. (1997). "Effect of basic fibroblast growth factor. An in vitro study of tendon healing." Clinical Orthopaedics and Related Research(342): 239-247.
Chen, C., H. Uludag, et al. (2012). "Noggin suppression decreases BMP-2-induced osteogenesis of human bone marrow-derived mesenchymal stem cells in vitro." Journal of Cellular Biochemistry **113**(12): 3672-3680.
Chen, X., Z. Yin, et al. (2012). "Force and scleraxis synergistically promote the commitment of human ES cells derived MSCs to tenocytes." Scientific Reports **2**.
Clegg, P. D., S. Strassburg, et al. (2007). "Cell phenotypic variation in normal and damaged tendons." International Journal of Experimental Pathology **88**(4): 227-235.
Colvin, A. C., N. Egorova, et al. (2012). "National Trends in Rotator Cuff Repair." The Journal of Bone and Joint Surgery. American volume. **94**(3): 227-233.
Connelly, J. T., E. J. Vanderploeg, et al. (2010). "Tensile Loading Modulates Bone Marrow Stromal Cell Differentiation and the Development of Engineered Fibrocartilage Constructs." Tissue engineering. Part A **16**(6): 1913-1923.

Dalby, M. J., N. Gadegaard, et al. (2014). "Harnessing nanotopography and integrin-matrix interactions to influence stem cell fate." Nat Mater **13**(6): 558-569.
Dickerson, D. A., T. N. Misk, et al. (2013). "In vitro and in vivo evaluation of orthopedic interface repair using a tissue scaffold with a continuous hard tissue-soft tissue transition." J Orthop Surg Res **8**: 18.
Doroski, D. M., M. E. Levenston, et al. (2010). "Cyclic tensile culture promotes fibroblastic differentiation of marrow stromal cells encapsulated in poly(ethylene glycol)-based hydrogels." Tissue Eng Part A **16**(11): 3457-3466.
Duance, V. C., D. J. Restall, et al. (1977). "The location of three collagen types in skeletal muscle." FEBS Lett **79**(2): 248-252.
Duffy, G. P., T. M. McFadden, et al. (2011). "Towards in vitro vascularisation of collagen-GAG scaffolds." European cells & materials **21**: 15-30.
Engler, A., L. Bacakova, et al. (2004). "Substrate compliance versus ligand density in cell on gel responses." Biophys J **86**(1 Pt 1): 617-628.
Farnebo, S., C. Y. Woon, et al. (2014). "Reconstruction of the Tendon–Bone Insertion With Decellularized Tendon–Bone Composite Grafts: Comparison With Conventional Repair." The Journal of Hand Surgery **39**(1): 65-74.
Farrell, E., F. J. O'Brien, et al. (2006). "A collagen-glycosaminoglycan scaffold supports adult rat mesenchymal stem cell differentiation along osteogenic and chondrogenic routes." Tissue engineering **12**(3): 459-468.
Font Tellado, S., E. R. Balmayor, et al. (2015). "Strategies to engineer tendon/ligament-to-bone interface: Biomaterials, cells and growth factors." Advanced Drug Delivery Reviews **94**: 126-140.
Font Tellado, S., W. Bonani, et al. (2017). "Fabrication and Characterization of Biphasic Silk Fibroin Scaffolds for Tendon/Ligament-to-Bone Tissue Engineering." Tissue Engineering Part A.
Fox, A. J., A. Bedi, et al. (2011). "Diabetes mellitus alters the mechanical properties of the native tendon in an experimental rat model." J Orthop Res **29**(6): 880-885.
Frank, O., M. Heim, et al. (2002). "Real-time quantitative RT-PCR analysis of human bone marrow stromal cells during osteogenic differentiation in vitro." Journal of Cellular Biochemistry **85**(4): 737-746.
Freyman, T. M., I. V. Yannas, et al. (2001). "Fibroblast contraction of a collagen–GAG matrix." Biomaterials **22**(21): 2883-2891.
Fukunaga, T., T. Yamashiro, et al. (2003). "Connective tissue growth factor mRNA expression pattern in cartilages is associated with their type I collagen expression." Bone **33**(6): 911-918.
Galatz, L. M., L. J. Sandell, et al. (2006). "Characteristics of the rat supraspinatus tendon during tendon-to-bone healing after acute injury." J Orthop Res **24**(3): 541-550.
Galloway, M. T., A. L. Lalley, et al. (2013). "The role of mechanical loading in tendon development, maintenance, injury, and repair." J Bone Joint Surg Am **95**(17): 1620-1628.
Garvican, E. R., A. Vaughan-Thomas, et al. (2008). "Chondrocytes harvested from osteochondritis dissecans cartilage are able to undergo limited in vitro chondrogenesis despite having perturbations of cell phenotype in vivo." Journal of Orthopaedic Research **26**(8): 1133-1140.
Genin, G. M., A. Kent, et al. (2009). "Functional Grading of Mineral and Collagen in the Attachment of Tendon to Bone." Biophysical Journal **97**(4): 976-985.

Genin, G. M. and S. Thomopoulos (2017). "The tendon-to-bone attachment: Unification through disarray." Nat Mater **16**(6): 607-608.
Gibson, L. J. and M. F. Ashby (1997). Cellular solids: structure and properties. Cambridge, U.K., Cambridge University Press.
Gibson, L. J., M. F. Ashby, et al. (2010). Cellular materials in nature and medicine. Cambridge ; New York, Cambridge University Press.
Gotoh, M., K. Hamada, et al. (1997). "Significance of granulation tissue in torn supraspinatus insertions: An immunohistochemical study with antibodies against interleukin-1β, cathepsin D, and matrix metalloprotease-1." Journal of Orthopaedic Research **15**(1): 33-39.
Govoni, M., C. Muscari, et al. (2016). "Mechanical Actuation Systems for the Phenotype Commitment of Stem Cell-Based Tendon and Ligament Tissue Substitutes." Stem Cell Reviews and Reports **12**(2): 189-201.
Grier, W. G., A. S. Moy, et al. (2017). "Cyclic tensile strain enhances human mesenchymal stem cell Smad 2/3 activation and tenogenic differentiation in anisotropic collagen-glycosaminoglycan scaffolds." European cells & materials **33**: 227-239.
Grier, W. K., E. M. Iyoha, et al. (2017). "The influence of pore size and stiffness on tenocyte bioactivity and transcriptomic stability in collagen-GAG scaffolds." Journal of the Mechanical Behavior of Biomedical Materials **65**: 295-305.
Grinnell, F., C. H. Ho, et al. (2003). "Dendritic fibroblasts in three-dimensional collagen matrices." Mol Biol Cell **14**(2): 384-395.
Gross, G. and A. Hoffmann (2013). "Therapeutic strategies for tendon healing based on novel biomaterials, factors and cells." Pathobiology **80**(4): 203-210.
Guo, X. and X. F. Wang (2009). "Signaling cross-talk between TGF-beta/BMP and other pathways." Cell research **19**(1): 71-88.
Hao, J., Y. Zhang, et al. (2013). "Mechanotransduction in cancer stem cells." Cell Biol Int **37**(9): 888-891.
Harley, B. A., T. M. Freyman, et al. (2007). "A new technique for calculating individual dermal fibroblast contractile forces generated within collagen-GAG scaffolds." Biophys J **93**(8): 2911-2922.
Harley, B. A., H. D. Kim, et al. (2008). "Microarchitecture of three-dimensional scaffolds influences cell migration behavior via junction interactions." Biophys J **95**(8): 4013-4024.
Harley, B. A., J. H. Leung, et al. (2007). "Mechanical characterization of collagen–glycosaminoglycan scaffolds." Acta Biomaterialia **3**(4): 463-474.
Harley, B. A., A. K. Lynn, et al. (2010). "Design of a multiphase osteochondral scaffold III: Fabrication of layered scaffolds with continuous interfaces." J Biomed Mater Res A **92**(3): 1078-1093.
Harley, B. A., A. K. Lynn, et al. (2010). "Design of a multiphase osteochondral scaffold. II. Fabrication of a mineralized collagen-glycosaminoglycan scaffold." J Biomed Mater Res A **92**(3): 1066-1077.
Harley, B. A., M. H. Spilker, et al. (2004). "Optimal degradation rate for collagen chambers used for regeneration of peripheral nerves over long gaps." Cells Tissues Organs **176**(1-3).
Hayashida, T., M. Decaestecker, et al. (2003). "Cross-talk between ERK MAP kinase and Smad signaling pathways enhances TGF-beta-dependent responses in human mesangial cells." FASEB J **17**(11): 1576-1578.

He, P., K. S. Ng, et al. (2012). "In Vitro Ligament–Bone Interface Regeneration Using a Trilineage Coculture System on a Hybrid Silk Scaffold." Biomacromolecules **13**(9): 2692-2703.
Hinck, A. P. (2012). "Structural studies of the TGF-betas and their receptors - insights into evolution of the TGF-beta superfamily." FEBS letters **586**(14): 1860-1870.
Hoganson, D. M., E. M. O'Doherty, et al. (2010). "The retention of extracellular matrix proteins and angiogenic and mitogenic cytokines in a decellularized porcine dermis." Biomaterials **31**(26): 6730-6737.
Holladay, C., S.-A. Abbah, et al. (2014). "Preferential tendon stem cell response to growth factor supplementation." Journal of Tissue Engineering and Regenerative Medicine: n/a-n/a.
Hortensius, R. A., J. R. Becraft, et al. (2015). "The effect of glycosaminoglycan content on polyethylenimine-based gene delivery within three-dimensional collagen-GAG scaffolds." Biomater Sci **3**(4): 645-654.
Hortensius, R. A., J. H. Ebens, et al. (2016). "Immunomodulatory effects of amniotic membrane matrix incorporated into collagen scaffolds." J Biomed Mater Res A **104**(6): 1332-1342.
Hortensius, R. A. and B. A. C. Harley (2013). "The use of bioinspired alterations in the glycosaminoglycan content of collagen–GAG scaffolds to regulate cell activity." Biomaterials **34**(31): 7645-7652.
Hudalla, G. A., N. A. Kouris, et al. (2011). "Harnessing endogenous growth factor activity modulates stem cell behavior." Integr Biol (Camb) **3**(8): 832-842.
James, R., G. Kesturu, et al. (2008). "Tendon: biology, biomechanics, repair, growth factors, and evolving treatment options." J Hand Surg Am **33**(1): 102-112.
Janmey, P. A. and C. A. McCulloch (2007). "Cell mechanics: integrating cell responses to mechanical stimuli." Annu Rev Biomed Eng **9**: 1-34.
Jiang, D., P. Gao, et al. (2016). "Combined effects of engineered tendon matrix and GDF-6 on bone marrow mesenchymal stem cell-based tendon regeneration." Biotechnology Letters **38**(5): 885-892.
Jiang, Y., Y. Wang, et al. (2016). "Cyclic tensile strain promotes the osteogenic differentiation of a bone marrow stromal cell and vascular endothelial cell co-culture system." Archives of Biochemistry and Biophysics **607**: 37-43.
Jones, G. C., A. N. Corps, et al. (2006). "Expression profiling of metalloproteinases and tissue inhibitors of metalloproteinases in normal and degenerate human achilles tendon." Arthritis & Rheumatism **54**(3): 832-842.
Kanazawa, T., T. Furumatsu, et al. (2014). "Role of Rho small GTPases in meniscus cells." Journal of Orthopaedic Research **32**(11): 1479-1486.
Kapoor, A., E. H. G. Caporali, et al. (2010). "Microtopographically patterned surfaces promote the alignment of tenocytes and extracellular collagen." Acta Biomaterialia **6**(7): 2580-2589.
Ker, E. D. F., B. Chu, et al. (2011). "Engineering spatial control of multiple differentiation fates within a stem cell population." Biomaterials **32**(13): 3413-3422.
Ker, E. D. F., A. S. Nain, et al. (2011). "Bioprinting of growth factors onto aligned sub-micron fibrous scaffolds for simultaneous control of cell differentiation and alignment." Biomaterials **32**(32): 8097-8107.
Killian, M. L., L. Cavinatto, et al. (2012). "The role of mechanobiology in tendon healing." Journal of Shoulder and Elbow Surgery **21**(2): 228-237.

Kim, Y.-J., R. L. Y. Sah, et al. (1988). "Fluorometric assay of DNA in cartilage explants using Hoechst 33258." Analytical Biochemistry **174**(1): 168-176.
Klatte-Schulz, F., S. Pauly, et al. (2013). "Characteristics and stimulation potential with BMP-2 and BMP-7 of tenocyte-like cells isolated from the rotator cuff of female donors." PLoS One **8**(6): e67209.
Kuo, C. K. and R. S. Tuan (2008). "Mechanoactive tenogenic differentiation of human mesenchymal stem cells." Tissue Engineering. Part A **14**(10): 1615-1627.
Laboureau, J., L. Dubertret, et al. (2004). "ERK activation by mechanical strain is regulated by the small G proteins rac-1 and rhoA." Experimental Dermatology **13**(2): 70-77.
Langer, R. and J. P. Vacanti (1993). "Tissue engineering." Science **260**(5110): 920-926.
Lee, C. H., B. Shah, et al. (2010). "CTGF directs fibroblast differentiation from human mesenchymal stem/stromal cells and defines connective tissue healing in a rodent injury model." The Journal of Clinical Investigation **120**(9): 3340-3349.
Lee, J. C., C. T. Pereira, et al. (2015). "Optimizing Collagen Scaffolds for Bone Engineering: Effects of Cross-linking and Mineral Content on Structural Contraction and Osteogenesis." Journal of Craniofacial Surgery **26**(6): 1992-1996.
Lee, N., J. Robinson, et al. (2016). "Biomimetic strategies for engineering composite tissues." Current opinion in biotechnology **40**: 64-74.
Li, X., J. Xie, et al. (2009). "Nanofiber Scaffolds with Gradations in Mineral Content for Mimicking the Tendon-to-Bone Insertion Site." Nano Letters **9**(7): 2763-2768.
Lipner, J., W. Liu, et al. (2014). "The mechanics of PLGA nanofiber scaffolds with biomimetic gradients in mineral for tendon-to-bone repair." Journal of the Mechanical Behavior of Biomedical Materials **40**(0): 59-68.
Lipner, J., H. Shen, et al. (2015). "In Vivo Evaluation of Adipose-Derived Stromal Cells Delivered with a Nanofiber Scaffold for Tendon-to-Bone Repair." Tissue engineering. Part A **21**(21-22): 2766-2774.
Liu, C., Z. Zhang, et al. (2013). "Gelatin-based hydrogels with [small beta]-cyclodextrin as a dual functional component for enhanced drug loading and controlled release." RSC Advances **3**(47): 25041-25049.
Liu, H., L. Yang, et al. "Biomimetic tendon extracellular matrix composite gradient scaffold enhances ligament-to-bone junction reconstruction." Acta Biomaterialia.
Liu, J., X. Tao, et al. (2015). "CTGF Positively Regulates BMP12 Induced Tenogenic Differentiation of Tendon Stem Cells and Signaling." Cellular Physiology and Biochemistry **35(**5): 1831-1845.
Liu, K. L., Z. Zhang, et al. (2011). "Supramolecular hydrogels based on cyclodextrin-polymer polypseudorotaxanes: materials design and hydrogel properties." Soft Matter **7**(24): 11290-11297.
Liu, S. H., R. S. Yang, et al. (1995). "Collagen in tendon, ligament, and bone healing. A current review." Clin Orthop Relat Res(318): 265-278.
Liu, Y., H. S. Ramanath, et al. (2008). "Tendon tissue engineering using scaffold enhancing strategies." Trends Biotechnol **26**(4): 201-209.
Lo, I. K. Y., L. L. Marchuk, et al. (2004). "Matrix Metalloproteinase and Tissue Inhibitor of Matrix Metalloproteinase mRNA Levels Are Specifically Altered in Torn Rotator Cuff Tendons." The American Journal of Sports Medicine **32**(5): 1223-1229.
Lorbach, O., M. Baums, et al. (2015). "Advances in biology and mechanics of rotator cuff repair." Knee Surgery, Sports Traumatology, Arthroscopy: 1-12.

Lorda-Diez, C. I., A. Canga-Villegas, et al. (2013). "Comparative transcriptional analysis of three human ligaments with distinct biomechanical properties." Journal of Anatomy **223**(6): 593-602.
Lorda-Diez, C. I., J. A. Montero, et al. (2009). "Transforming Growth Factors β Coordinate Cartilage and Tendon Differentiation in the Developing Limb Mesenchyme." Journal of Biological Chemistry **284**(43): 29988-29996.
Lu, H. H. and S. Thomopoulos (2013). "Functional Attachment of Soft Tissues to Bone: Development, Healing, and Tissue Engineering." Annual Review of Biomedical Engineering **15**(1): null.
Lui, P. P. Y., Y. F. Rui, et al. (2011). "Tenogenic differentiation of stem cells for tendon repair-what is the current evidence?" Journal of Tissue Engineering and Regenerative Medicine **5**(8): e144-e163.
Lynn, A. K., S. M. Best, et al. (2010). "Design of a multiphase osteochondral scaffold. I. Control of chemical composition." J Biomed Mater Res A **92**(3): 1057-1065.
Lyons, F. G., J. P. Gleeson, et al. (2014). "Novel Microhydroxyapatite Particles in a Collagen Scaffold: A Bioactive Bone Void Filler?" Clinical Orthopaedics and Related Research **472**(4): 1318-1328.
Lysdahl, H., A. Baatrup, et al. (2014). "Preconditioning Human Mesenchymal Stem Cells with a Low Concentration of BMP2 Stimulates Proliferation and Osteogenic Differentiation In Vitro." BioResearch open access **3**(6): 278-285.
Machín, R., J. R. Isasi, et al. (2012). "β-Cyclodextrin hydrogels as potential drug delivery systems." Carbohydrate polymers **87**(3): 2024-2030.
Madaghiele, M., A. Sannino, et al. (2008). "Collagen-based matrices with axially oriented pores." Journal of Biomedical Materials Research Part A **85A**(3): 757-767.
Maeda, E., J. C. Shelton, et al. (2009). "Differential regulation of gene expression in isolated tendon fascicles exposed to cyclic tensile strain in vitro." J Appl Physiol **106**(2): 506-512.
Maeda, T., T. Sakabe, et al. (2011). "Conversion of mechanical force into TGF-beta-mediated biochemical signals." Curr Biol **21**(11): 933-941.
Malaval, L., F. Liu, et al. (1999). "Kinetics of osteoprogenitor proliferation and osteoblast differentiation in vitro." Journal of Cellular Biochemistry **74**(4): 616-627.
Manning, C. N., A. G. Schwartz, et al. (2013). "Controlled delivery of mesenchymal stem cells and growth factors using a nanofiber scaffold for tendon repair." Acta Biomaterialia.
Martin, R. B., D. B. Burr, et al., Eds. (1998). Skeletal Tissue Mechanics. New York, Springer.
Martin, T. A., S. R. Caliari, et al. (2011). "The generation of biomolecular patterns in highly porous collagen-GAG scaffolds using direct photolithography." Biomaterials **32**(16): 3949-3957.
Massague, J. and Y. G. Chen (2000). "Controlling TGF-beta signaling." Genes & development **14**(6): 627-644.
Massague, J. and D. Wotton (2000). "Transcriptional control by the TGF-beta/Smad signaling system." The EMBO journal **19**(8): 1745-1754.
Mei, L., J. Nguyen, et al. (2013). "Load Regulates Bone Formation and Sclerostin Expression through a TGFβ-Dependent Mechanism." PLoS One **8**(1): e53813.
Miller, E. D., J. A. Phillippi, et al. (2009). "Inkjet printing of growth factor concentration gradients and combinatorial arrays immobilized on biologically-relevant substrates." Combinatorial chemistry & high throughput screening **12**(6): 604-618.

Miyazono, K. (2000). "TGF-beta signaling by Smad proteins." Cytokine & Growth Factor Reviews **11**(1-2): 15-22.
Moffat, K. L., I. N. E. Wang, et al. (2009). "Orthopedic Interface Tissue Engineering for the Biological Fixation of Soft Tissue Grafts." Clinics in Sports Medicine **28**(1): 157-176.
Mozdzen, L. C., R. Rodgers, et al. (2016). "Increasing the strength and bioactivity of collagen scaffolds using customizable arrays of 3D-printed polymer fibers." Acta Biomater **15**(33): 25-33.
Mozdzen, L. C., A. Vucetic, et al. (2017). "Modifying the strength and strain concentration profile within collagen scaffolds using customizable arrays of poly-lactic acid fibers." Journal of the Mechanical Behavior of Biomedical Materials **66**: 28-36.
Mura, P. (2014). "Analytical techniques for characterization of cyclodextrin complexes in aqueous solution: a review." Journal of pharmaceutical and biomedical analysis **101**: 238-250.
Murchison, N. D., B. A. Price, et al. (2007). "Regulation of tendon differentiation by scleraxis distinguishes force-transmitting tendons from muscle-anchoring tendons." Development **134**(14): 2697-2708.
O'Brien, F. J., B. A. Harley, et al. (2004). "Influence of freezing rate on pore structure in freeze-dried collagen-GAG scaffolds." Biomaterials **25**(6): 1077-1086.
O'Brien, F. J., B. A. Harley, et al. (2005). "The effect of pore size on cell adhesion in collagen-GAG scaffolds." Biomaterials **26**(4): 433-441.
Okech, W. and C. K. Kuo (2016). Informing Stem Cell-Based Tendon Tissue Engineering Approaches with Embryonic Tendon Development. Metabolic Influences on Risk for Tendon Disorders. P. W. Ackermann and D. A. Hart. Cham, Springer International Publishing**:** 63-77.
Olde Damink, L. H. H., P. J. Dijkstra, et al. (1996). "Cross-linking of dermal sheep collagen using a water-soluble carbodiimide." Biomaterials **17**(8): 765-773.
Osman, S. K., G. M. Soliman, et al. (2015). "Physically cross-linked hydrogels of beta - cyclodextrin polymer and poly(ethylene glycol)-cholesterol as delivery systems for macromolecules and small drug molecules." Current drug delivery **12**(4): 415-424.
Papakrivopoulou, J., G. E. Lindahl, et al. (2004). Differential roles of extracellular signal-regulated kinase 1/2 and p38MAPK in mechanical load-induced procollagen α1(I) gene expression in cardiac fibroblasts.
Pauly, S., F. Klatte, et al. (2010). "Characterization of tendon cell cultures of the human rotator cuff." European cells & materials **20**: 84-97.
Paxton, J. Z., P. Hagerty, et al. (2011). "Optimizing an Intermittent Stretch Paradigm Using ERK1/2 Phosphorylation Results in Increased Collagen Synthesis in Engineered Ligaments." Tissue Eng Part A.
Paxton, J. Z., P. Hagerty, et al. (2012). "Optimizing an Intermittent Stretch Paradigm Using ERK1/2 Phosphorylation Results in Increased Collagen Synthesis in Engineered Ligaments." Tissue Engineering Part A **18**(3-4): 277-284.
Pedowitz, D. and G. Kirwan (2013). "Achilles tendon ruptures." Curr Rev Musculoskelet Med **6**(4): 285-293.
Pelham, R. J. and Y.-l. Wang (1997). "Cell locomotion and focal adhesions are regulated by substrate flexibility." Proceedings of the National Academy of Sciences **94**(25): 13661-13665.

Peyton, S. R. and A. J. Putnam (2005). "Extracellular matrix rigidity governs smooth muscle cell motility in a biphasic fashion." Journal of Cellular Physiology **204**(1): 198-209.
Phillips, J. E., K. L. Burns, et al. (2008). "Engineering graded tissue interfaces." Proceedings of the National Academy of Sciences **105**(34): 12170-12175.
Porter, J. R., T. T. Ruckh, et al. (2009). "Bone tissue engineering: A review in bone biomimetics and drug delivery strategies." Biotechnology Progress **25**(6): 1539-1560.
Prabaharan, M. and R. Jayakumar (2009). "Chitosan-graft-β-cyclodextrin scaffolds with controlled drug release capability for tissue engineering applications." International journal of biological macromolecules **44**(4): 320-325.
Pryce, B. A., S. S. Watson, et al. (2009). "Recruitment and maintenance of tendon progenitors by TGFbeta signaling are essential for tendon formation." Development **136**(8): 1351-1361.
Qiu, Y., J. Lei, et al. (2014). "Cyclic tension promotes fibroblastic differentiation of human MSCs cultured on collagen-fibre scaffolds." Journal of Tissue Engineering and Regenerative Medicine: n/a-n/a.
Quapp, K. M. and J. A. Weiss (1998). "Material characterization of human medial collateral ligament." J Biomech Eng **120**(6): 757-763.
Quinlan, E., A. Lopez-Noriega, et al. (2015). "Development of collagen-hydroxyapatite scaffolds incorporating PLGA and alginate microparticles for the controlled delivery of rhBMP-2 for bone tissue engineering." J Control Release **198**: 71-79.
Quinlan, E., E. M. Thompson, et al. (2015). "Long-term controlled delivery of rhBMP-2 from collagen-hydroxyapatite scaffolds for superior bone tissue regeneration." Journal of controlled release : official journal of the Controlled Release Society **207**: 112-119.
Radu, C. D., O. Parteni, et al. (2016). "Applications of cyclodextrins in medical textiles - review." Journal of controlled release : official journal of the Controlled Release Society **224**: 146-157.
Ren, X., D. Bischoff, et al. (2015). "Osteogenesis on nanoparticulate mineralized collagen scaffolds via autogenous activation of the canonical BMP receptor signaling pathway." Biomaterials **50**(0): 107-114.
Ren, X., V. Tu, et al. (2016). "Nanoparticulate mineralized collagen scaffolds induce in vivo bone regeneration independent of progenitor cell loading or exogenous growth factor stimulation." Biomaterials **89**: 67-78.
Ren, X., D. W. Weisgerber, et al. (2016). "Nanoparticulate Mineralized Collagen Scaffolds and BMP-9 Induce a Long-Term Bone Cartilage Construct in Human Mesenchymal Stem Cells." Advanced Healthcare Materials **5**(14): 1821-1830.
Rhett, J. M., G. S. Ghatnekar, et al. (2008). "Novel therapies for scar reduction and regenerative healing of skin wounds." Trends in Biotechnology **26**(4): 173-180.
Rodell, C. B., C. B. Highley, et al. (2016). "Evolution of hierarchical porous structures in supramolecular guest-host hydrogels." Soft Matter **12**(37): 7839-7847.
Rys, J. P., D. A. Monteiro, et al. (2016). "Mechanobiology of TGFβ signaling in the skeleton." Matrix Biology **52–54**: 413-425.
Saadat, F., A. C. Deymier, et al. (2016). "The concentration of stress at the rotator cuff tendon-to-bone attachment site is conserved across species." Journal of the Mechanical Behavior of Biomedical Materials **62**: 24-32.
Sakiyama-Elbert, S. E. and J. A. Hubbell (2000). "Controlled release of nerve growth factor from a heparin-containing fibrin-based cell ingrowth matrix." J Control Release **69**(1): 149-158.

Sarasa-Renedo, A., V. Tunç-Civelek, et al. (2006). "Role of RhoA/ROCK-dependent actin contractility in the induction of tenascin-C by cyclic tensile strain." Experimental Cell Research **312**(8): 1361-1370.
Scheufler, C., W. Sebald, et al. (1999). "Crystal structure of human bone morphogenetic protein-2 at 2.7 A resolution." Journal of molecular biology **287**(1): 103-115.
Schulz Torres, D., T. M. Freyman, et al. (2000). "Tendon cell contraction of collagen–GAG matrices in vitro: effect of cross-linking." Biomaterials **21**(15): 1607-1619.
Schulze-Tanzil, G., O. Al-Sadi, et al. (2012). "Decellularized Tendon Extracellular Matrix—A Valuable Approach for Tendon Reconstruction?" Cells **1**(4): 1010.
Schwartz, A. G., J. H. Lipner, et al. (2013). "Muscle loading is necessary for the formation of a functional tendon enthesis." Bone **55**(1): 44-51.
Schwartz, A. G., J. D. Pasteris, et al. (2012). "Mineral Distributions at the Developing Tendon Enthesis." PloS one **7**(11): e48630.
Schweitzer, R., J. H. Chyung, et al. (2001). "Analysis of the tendon cell fate using Scleraxis, a specific marker for tendons and ligaments." Development **128**(19): 3855-3866.
Schweitzer, R., E. Zelzer, et al. (2010). "Connecting muscles to tendons: tendons and musculoskeletal development in flies and vertebrates." Development **137**(17): 2807-2817.
Shaw, H. M. and M. Benjamin (2007). "Structure–function relationships of entheses in relation to mechanical load and exercise." Scandinavian Journal of Medicine & Science in Sports **17**(4): 303-315.
Shen, H., R. H. Gelberman, et al. (2013). "BMP12 induces tenogenic differentiation of adipose-derived stromal cells." PLoS One **8**(10): e77613.
Shi, M., J. Zhu, et al. (2011). "Latent TGF-beta structure and activation." Nature **474**(7351): 343-349.
Shi, Y. and J. Massague (2003). "Mechanisms of TGF-beta signaling from cell membrane to the nucleus." Cell **113**(6): 685-700.
Skutek, M., M. van Griensven, et al. (2001). "Cyclic mechanical stretching modulates secretion pattern of growth factors in human tendon fibroblasts." Eur J Appl Physiol **86**(1): 48-52.
Soheilmoghaddam, M., G. Sharifzadeh, et al. (2014). "Regenerated cellulose/β-cyclodextrin scaffold prepared using ionic liquid." Materials Letters **135**: 210-213.
Soller, E. C., D. S. Tzeranis, et al. (2012). "Common features of optimal collagen scaffolds that disrupt wound contraction and enhance regeneration both in peripheral nerves and in skin." Biomaterials **33**(19): 4783-4791.
Soltanoff, C. S., S. Yang, et al. (2009). "Signaling networks that control the lineage commitment and differentiation of bone cells." Critical reviews in eukaryotic gene expression **19**(1): 1-46.
Song, F., D. Jiang, et al. (2017). "Mechanical Loading Improves Tendon-Bone Healing in a Rabbit Anterior Cruciate Ligament Reconstruction Model by Promoting Proliferation and Matrix Formation of Mesenchymal Stem Cells and Tendon Cells." Cellular Physiology and Biochemistry **41**(3): 875-889.
Spalazzi, J. P., E. Dagher, et al. (2008). "In vivo evaluation of a multiphased scaffold designed for orthopaedic interface tissue engineering and soft tissue-to-bone integration." Journal of Biomedical Materials Research Part A **86A**(1): 1-12.
Spilker, M. H., K. Asano, et al. (2001). "Contraction of collagen–glycosaminoglycan matrices by peripheral nerve cells in vitro." Biomaterials **22**(10): 1085-1093.

Taylor, S. E., A. Vaughan-Thomas, et al. (2009). "Gene expression markers of tendon fibroblasts in normal and diseased tissue compared to monolayer and three dimensional culture systems." BMC musculoskeletal disorders **10**: 27.
Thomopoulos, S., R. Das, et al. (2011). "Fibrocartilage Tissue Engineering: The Role of the Stress Environment on Cell Morphology and Matrix Expression." Tissue engineering. Part A **17**(7-8): 1039-1053.
Thomopoulos, S., R. Das, et al. (2010). "bFGF and PDGF-BB for Tendon Repair: Controlled Release and Biologic Activity by Tendon Fibroblasts In Vitro." Annals of biomedical engineering **38**(2): 225-234.
Thomopoulos, S., R. Das, et al. (2009). "Enhanced flexor tendon healing through controlled delivery of PDGF-BB." Journal of orthopaedic research : official publication of the Orthopaedic Research Society **27**(9): 1209-1215.
Thomopoulos, S., H.-M. Kim, et al. (2007). "Decreased muscle loading delays maturation of the tendon enthesis during postnatal development." Journal of Orthopaedic Research **25**(9): 1154-1163.
Thomopoulos, S., H. M. Kim, et al. (2010). "The Effects of Exogenous Basic Fibroblast Growth Factor on Intrasynovial Flexor Tendon Healing in a Canine Model." The Journal of Bone and Joint Surgery. American volume. **92**(13): 2285-2293.
Thomopoulos, S., M. Zaegel, et al. (2007). "PDGF-BB released in tendon repair using a novel delivery system promotes cell proliferation and collagen remodeling." Journal of Orthopaedic Research **25**(10): 1358-1368.
Thomopoulos, S., E. Zampiakis, et al. (2008). "The effect of muscle loading on flexor tendon-to-bone healing in a canine model." J Orthop Res **26**(12): 1611-1617.
Tierney, C. M., M. J. Jaasma, et al. (2009). "Osteoblast activity on collagen-GAG scaffolds is affected by collagen and GAG concentrations." Journal of Biomedical Materials Research Part A **91A**(1): 92-101.
Tierney, E. G., G. P. Duffy, et al. (2013). "Non-viral gene-activated matrices-next generation constructs for bone repair." Organogenesis **9**(1).
Towler, D. A. and R. H. Gelberman (2006). "The alchemy of tendon repair: a primer for the (S)mad scientist." J Clin Invest **116**(4): 863-866.
Vanderploeg, E. J., C. G. Wilson, et al. (2008). "Articular chondrocytes derived from distinct tissue zones differentially respond to in vitro oscillatory tensile loading." Osteoarthritis Cartilage **16**(10): 1228-1236.
Vickers, S. M., T. Gotterbarm, et al. (2010). "Cross-linking affects cellular condensation and chondrogenesis in type II collagen-GAG scaffolds seeded with bone marrow-derived mesenchymal stem cells." Journal of Orthopaedic Research **28**(9): 1184-1192.
Vitale, M. A., M. G. Vitale, et al. (2007). "Rotator cuff repair: an analysis of utility scores and cost-effectiveness." J Shoulder Elbow Surg **16**(2): 181-187.
Voleti, P. B., M. R. Buckley, et al. (2012). "Tendon Healing: Repair and Regeneration." Annual Review of Biomedical Engineering **14**(1): 47-71.
Wang, J. G., M. Miyazu, et al. (2001). "Uniaxial cyclic stretch induces focal adhesion kinase (FAK) tyrosine phosphorylation followed by mitogen-activated protein kinase (MAPK) activation." Biochem Biophys Res Commun **288**(2): 356-361.
Wang, J. H. C. (2006). "Mechanobiology of tendon." Journal of Biomechanics **39**(9): 1563-1582.

Weinbaum, J., J. Schmidt, et al. (2013). "Combating Adaptation to Cyclic Stretching by Prolonging Activation of Extracellular Signal-Regulated Kinase." Cellular and Molecular Bioengineering **6**(3): 279-286.
Weisgerber, D. W., S. R. Caliari, et al. (2015). "Mineralized collagen scaffolds induce hMSC osteogenesis and matrix remodeling." Biomaterials Science **3**(3): 533-542.
Weisgerber, D. W., D. O. Kelkhoff, et al. (2013). "The impact of discrete compartments of a multi-compartment collagen–GAG scaffold on overall construct biophysical properties." Journal of the Mechanical Behavior of Biomedical Materials **28**: 26-36.
Westhrin, M., M. Xie, et al. (2015). "Osteogenic differentiation of human mesenchymal stem cells in mineralized alginate matrices." PloS one **10**(3): e0120374.
Wolfman, N. M., G. Hattersley, et al. (1997). "Ectopic induction of tendon and ligament in rats by growth and differentiation factors 5, 6, and 7, members of the TGF-beta gene family." Journal of Clinical Investigation **100**(2): 321-330.
Xie, J., X. Li, et al. (2010). ""Aligned-to-random" nanofiber scaffolds for mimicking the structure of the tendon-to-bone insertion site." Nanoscale **2**(6): 923-926.
Xin, X., X. H. Li, et al. (2013). "Pentamethylquercetin ameliorates fibrosis in diabetic Goto-Kakizaki rat kidneys and mesangial cells with suppression of TGF-beta/Smads signaling." European journal of pharmacology **713**(1-3): 6-15.
Xu, B., G. Song, et al. (2011). "Effect of focal adhesion kinase on the regulation of realignment and tenogenic differentiation of human mesenchymal stem cells by mechanical stretch." Connect Tissue Res **52**(5): 373-379.
Xu, B., G. Song, et al. (2012). "RhoA/ROCK, cytoskeletal dynamics, and focal adhesion kinase are required for mechanical stretch-induced tenogenic differentiation of human mesenchymal stem cells." Journal of Cellular Physiology **227**(6): 2722-2729.
Xu, Y. and G. A. Murrell (2008). "The basic science of tendinopathy." Clin Orthop Relat Res **466**(7): 1528-1538.
Xu, Y., Q. Wang, et al. (2015). "Cyclic Tensile Strain Induces Tenogenic Differentiation of Tendon-Derived Stem Cells in Bioreactor Culture." BioMed research international **2015**: 790804.
Yang, G., B. B. Rothrauff, et al. (2016). "Tendon-Derived Extracellular Matrix Enhances Transforming Growth Factor-β3-Induced Tenogenic Differentiation of Human Adipose-Derived Stem Cells." Tissue Engineering Part A **23**(3-4): 166-176.
Yang, P. J. and J. S. Temenoff (2009). "Engineering orthopedic tissue interfaces." Tissue engineering. Part B, Reviews **15**(2): 127-141.
Yannas, I. V. (2001). Tissue and organ regeneration in adults. New York, Springer.
Yannas, I. V., E. Lee, et al. (1989). "Synthesis and characterization of a model extracellular matrix that induces partial regeneration of adult mammalian skin." Proc Natl Acad Sci U S A **86**(3): 933-937.
Yao, L., C. S. Bestwick, et al. (2006). "Phenotypic drift in human tenocyte culture." Tissue engineering **12**(7): 1843-1849.
Yeung, T., P. C. Georges, et al. (2005). "Effects of substrate stiffness on cell morphology, cytoskeletal structure, and adhesion." Cell Motility and the Cytoskeleton **60**(1): 24-34.
Yin, J. P., P. Fu, et al. (2008). "[Effects of piperazine ferulate on connective tissue growth factor and extracellular matrix in TGF-beta1 induced mesangial cells]." Sichuan da xue xue bao. Yi xue ban = Journal of Sichuan University. Medical science edition **39**(5): 732-735.

Yourek, G., S. M. McCormick, et al. (2010). "Shear stress induces osteogenic differentiation of human mesenchymal stem cells." Regenerative medicine **5**(5): 713-724.
Yuen, S. N., J. Folkman, et al. (1990). "Affinity of fibroblast growth factors for beta-cyclodextrin tetradecasulfate." Analytical biochemistry **185**(1): 108-111.
Zaman, M. H., L. M. Trapani, et al. (2006). "Migration of tumor cells in 3D matrices is governed by matrix stiffness along with cell-matrix adhesion and proteolysis." Proceedings of the National Academy of Sciences **103**(29): 10889-10894.
Zelzer, E., E. Blitz, et al. (2014). "Tendon-to-bone attachment: from development to maturity." Birth Defects Res C Embryo Today **102**(1): 101-112.
Zhang, F. and M. Laiho (2003). "On and off: proteasome and TGF-beta signaling." Experimental cell research **291**(2): 275-281.
Zhang, G., Y. Ezura, et al. (2006). "Decorin regulates assembly of collagen fibrils and acquisition of biomechanical properties during tendon development." J Cell Biochem **98**(6): 1436-1449.
Zhang, J., B. Li, et al. (2011). "The role of engineered tendon matrix in the stemness of tendon stem cells in vitro and the promotion of tendon-like tissue formation in vivo." Biomaterials **32**(29): 6972-6981.
Zhou, J., C. Xu, et al. (2011). "In vitro generation of osteochondral differentiation of human marrow mesenchymal stem cells in novel collagen–hydroxyapatite layered scaffolds." Acta Biomaterialia **7**(11): 3999-4006.
Zou, B., Y. Liu, et al. (2012). "Electrospun fibrous scaffolds with continuous gradations in mineral contents and biological cues for manipulating cellular behaviors." Acta Biomaterialia **8**(4): 1576-1585.